The Development of Novel Tools for the Metabolic Labelling of Glycans in Cancer

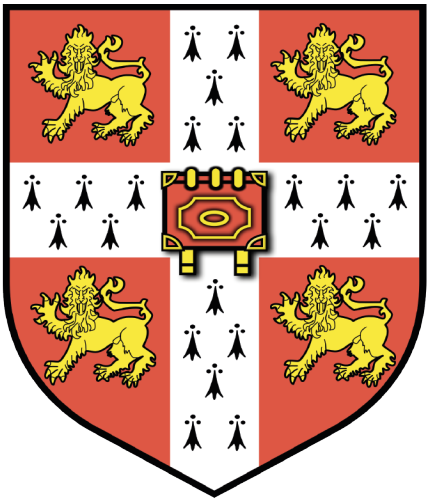

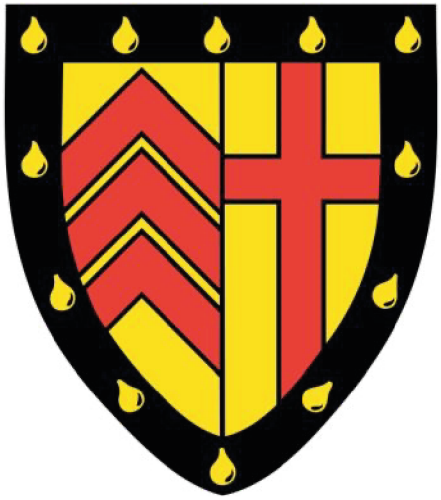

Daniel Ryan Parle

Clare College

University of Cambridge

March 2022

Supervisor: Professor Finian Leeper

This dissertation is submitted for the degree of

Doctor of Philosophy

UNIVERSITY OF CAMBRIDGE
Yusuf Hamied Department of Chemistry

EPSRC

CANCER RESEARCH UK

Declaration

This thesis is submitted for the degree of Doctor of Philosophy.

I hereby declare that:

This thesis is the result of my own work and includes nothing which is the outcome of work done in collaboration except as declared in the preface and specified in the text. It is not substantially the same as any work that has already been submitted before for any degree or other qualification except as declared in the preface and specified in the text. It does not exceed the prescribed word limit of 60,000 words set by the Physics and Chemistry Degree Committee.

Daniel Ryan Parle
March 2022

Abstract: The Development of Novel Tools for the Metabolic Labelling of Glycans in Cancer

Daniel Ryan Parle - 2022

Aberrant cell surface glycosylation is key in tumour proliferation, metastasis, and immune evasion, with hypersialylation one of the alterations most observed in tumour cells. Changes in the glycome can be monitored by incorporating unnatural sugars bearing bioorthogonal chemical reporters. Methylcyclopropenes are one such reporter with good incorporation and kinetics of the subsequent inverse-electron-demand Diels-Alder reaction (IED-DA) with tetrazines.

The methylcyclopropene tagged monosaccharide most often used *in vitro* (Ac_4ManCyoc) has yet to be used for *in vivo* applications. This is believed to be due to its lack of aqueous solubility. Herein a method is described for variable acetylation of tagged monosaccharides. Enhanced *in vitro* glycan-labelling was observed using Ac_3ManCyoc or Ac_2ManCyoc relative to Ac_4ManCyoc. This enhancement was consistent across multiple cell lines. Other tagged sugars showed reduced labelling with decreased acetylation, presumably due to decreased cell permeability. Initial attempts at *in vivo* labelling of hypersialylation using Ac_3ManCyoc are also described.

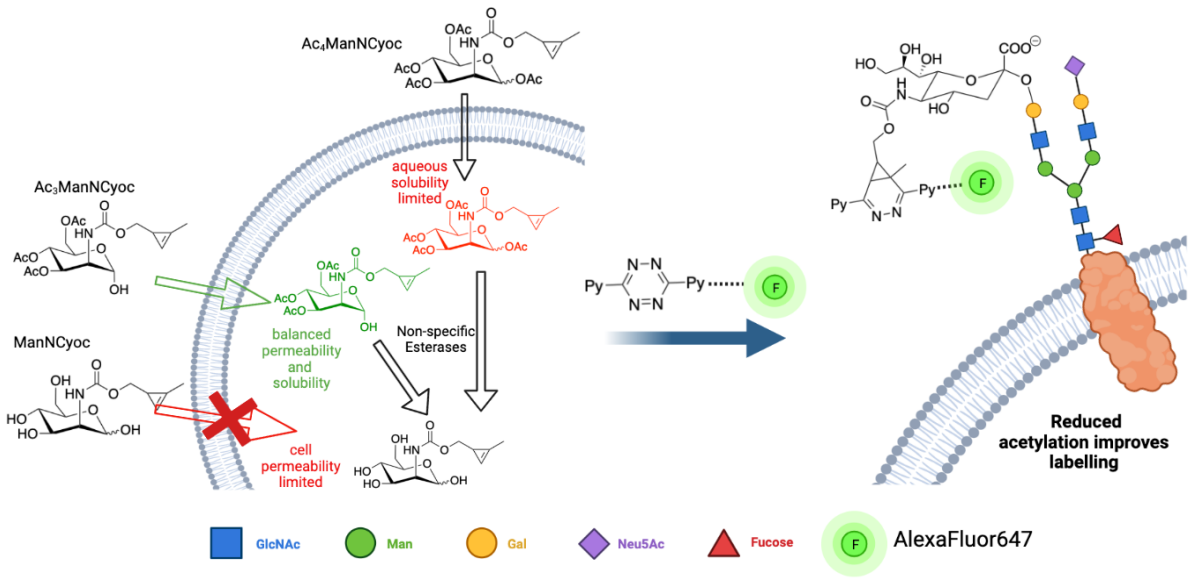

Graphical Abstract - The effect of Acetylation on Ac_XManNCyoc labelling

Ac_3ManCyoc and another tagged sugar Ac_4GalNAz were then used for dual-sugar labelling. The ratio of incorporation of the different monosaccharides was compared across multiple cell lines. In general, a higher Ac_3ManCyoc:Ac_4GalNAz ratio was observed in faster growing cell lines. Thus, this could be a useful tool in assessing tumour aggressiveness.

ODIBO, a strained dibenzocyclooctyne with an enhanced rate of cycloaddition with azides was synthesised, but attempts to reduce its hydrophobicity had limited success; reduced *in vitro* glycan-labelling relative to TMDIBO (another dibenzocyclooctyne) was observed.

The synthesis is reported of the first (*E,Z*)-cyclooctadiene. Its rate of IED-DA with tetrazines proved to be amongst the fastest reported under the same conditions.

Finally, synthesis of some novel tagged fucose analogues is described. Glycan-labelling using these analogues is studied, targeting the well-known enhanced fucosylation in cancer.

Dedication

This work is dedicated to my family, and in particular to my parents Jane and Tim, my sister Jessica, and my grandparents Mary and Terry. They have always encouraged me in everything I have done, and their hard work and unwavering support has allowed me to learn and grow in such amazing places as St. Andrews and Cambridge. All I can say is thank you for everything you have done for me and for teaching me the true meaning of:

"You'll Never Walk Alone"

Acknowledgments

First and foremost, I would like to thank my supervisor Professor Finian Leeper, for his guidance and support and for allowing me to be a part of this exciting work. His ideas and challenges have enabled me to develop into a better scientist and is a key reason this work has been possible. I would also like to thank Professor Kevin Brindle for allowing me to be part of his group, and for his stimulating and insightful input. Dr André Neves has been crucial for this work and for the project in general, providing a deep understanding and innovative ways to apply our chemistries. His contributions to the *in vitro* experiments were vital and alongside Dr Flaviu Bulat, they performed the *in vivo* studies contained herein. Particular thanks go to Dr Flaviu Bulat, his help and encouragement has been integral for every part of this thesis, constantly pushing the projects forward and listening to all my ideas, no matter how optimistic they may be. He has taught me many of the biological skills and been vital for this work in so many ways.

I would also like to pay thanks to the many members of both the Leeper and Brindle labs who have provided advice and support as well as humour and friendship. In chemistry Alex Chan, Matt Corney and Maxime Couturier provided vital help and laughs in the lab. To the three part III students who I have been fortunate to supervise; Seymá Sever, Sam Thomson and Georgia Edmonds, who have not just provided important results, but also been an integral part of the group.

Much appreciated is the support of the NMR and mass spectrometry services, as well as the technical staff in the Department of Chemistry. In CRUK the flow cytometry core for their training and support and the microscopy core who helped greatly with the florescent microscopy experiments, in particular Heather Zecchini.

Next, I would like to thank the people who have not been directly involved in this work, but who have supported me in many other ways, and made this such an enjoyable experience. The friends I have been fortunate enough to make in my time Cambridge, in particular; Calum Aschroft, Matt De Brett, Thomas Espaas, Sam Hodder, Luke Jenkins, Dan Muthukrishna, Andrea Paterlini, Audrey Plyler, and Nick Taylor. To my friends from further North, Anthony Morley, Danny O'neill, Joe Woods and Jordan Ratcliffe for their humour and perspective. Also, to my partner Eve, for her faith in my ability and unwavering support in helping me get through any challenge I faced. Finally, this thesis would not have been possible without the support of my family.

Table of Contents

List of Abbreviations

Abbreviation	Definition
ACN	Acetonitrile
ADC	Antibody-drug conjugate
BARAC	Biarylazacyclooctynone
BCN	Bicyclo[6.1.0]nonyne
Boc	*tert*-butyloxycarbonyl
CAR-T	Chimeric antigen receptor therapy
CD8+	Cluster of differentiation 8
CMP	Cytidine-monophospho
COSY	Homonuclear correlation spectroscopy
CRUK	Cancer research UK
CuAAC	Copper-catalysed azide alkyne cycloaddition
DAPI	4',6-diamidino-2-phenylindole
DCM	Dichloromethane
DIBAC	Dibenzoazacyclooctyne
DIBO	Dibenzoannulated cyclooctyne
DIFO	Difluorinated cyclooctyne
DMB	1,2-diamino-4,5-methylenedioxybenzene
DIPEA	*N,N*-Diisopropylethylamine
DMF	Dimethylformamide
DMSO	Dimethyl sulfoxide
***E,E*-COD**	*trans,trans*-cyclooctadiene
***E,Z*-COD**	*cis,trans*-cyclooctadiene
EDC	1-Ethyl-3-(3-dimethylaminopropyl)carbodiimide
EDG	Electron-donating group
EtOAc	Ethyl acetate
EWG	Electron-withdrawing group
Fmoc	Fluorenylmethoxycarbonyl
FRET	Förster (or fluorescence) resonance energy transfer
FSC	Forward scatter
Fuc	Fucose

FUT	Fucosyltransferase
Gal	Galactose
GalNAc	*N*-acetylgalactosamine
GDP	Guanosine diphosphate
GFP	Green florescent protein
Glc	Glucose
GlcNAc	*N*-acetylglucosamine
HOBT	Hydroxybenzotriazole
HOMO	Highest occupied molecular orbital
HPLC	High-performance liquid chromatography
HRMS	High resolution mass spectroscopy
i.p.	Intraperitoneal injection
IE	Incorporation efficiency
IED-DA	Inverse-electron demand Diels-Alder
LCMS	Liquid chromatography mass spectroscopy
LUMO	Lowest unoccupied molecular orbital
Lys	Lysine
Man	Mannose
ManNAc	*N*-acetylmannosamine
mCPBA	*meta*-Chloroperoxybenzoic acid
MeOH	Methanol
MFI	Mean (median) fluorescent intensity
MM2	Molecular mechanics 2
MO	Molecular orbital
MOE	Metabolic oligosaccharide engineering
MRI	Magnetic resonance imaging
NHS	*N*-Hydroxysuccinimide
NMR	Nuclear magnetic resonance
OCT	Cyclooctyne
ODIBO	Oxo-dibenzocyclooctyne
PBS	Phosphate-buffered saline
PEG	Polyethylene glycol
PET	Positron emission tomography

PMSA	Prostatic specific membrane antigen
PNP	*para*-Nitrophenol
POFUT	Protein *O*-fucosyltransferase
ppm	Parts per million
RuAAC	Ruthenium-catalysed azide alkyne cycloaddition
SBR	Signal to background ratio
sLe	Silyl-Lewis antigen
SPAAC	Strain promoted azide alkyne cycloaddition
SPECT	Single-photon emission computed tomography
SSC	Side scatter
ST6GalI	Beta-galactoside alpha 2,6-sialyltransferase
TBAF	Tetra-*n*-butylammonium fluoride
TCO	*Trans*-cyclooctene
TFA	Trifluoroacetic acid
THF	Tetrahydrofuran
TLC	Thin-layer chromatography
TMDIBO	Tetramethoxydibenzocyclooctyne
UDP	Uridine diphosphate
Xyl	Xylose

1. Introduction

1.1. Glycobiology

1.1.1. Introduction to the Importance of Cell Surface Glycosylation

Glycans are complex biomacromolecules formed via glycosidic *O*-linkage of monosaccharides (sugars). Unlike many biologically important polysaccharides, glycans are heteropolymeric structures.[1] Due to the branching and variable anomeric linkage possibilities of monosaccharides, glycans are more diverse than polypeptides and nucleic acids.[2, 3] Glycans can exist in the free form or covalently attached to a protein or lipid as a glycoconjugate. Glycoconjugates can then be categorised by the nature of this linkage, with glycoproteins subdivided into two main categories in Eukaryotes, *N*-linked glycans (glycosidic bond is with the nitrogen of an asparagine residue) or *O*-linked (bond is formed with oxygen on serine/threonine) (Figure 1).[4]

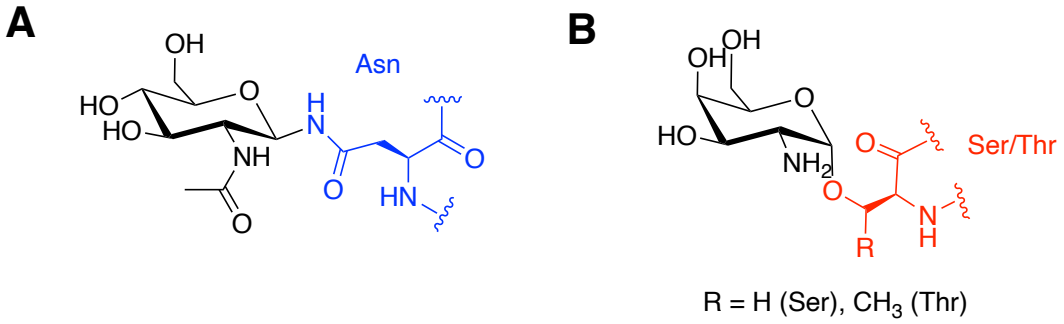

Figure 1 – Glycosidic linkage for A) N-glycans and B) O-glycans.

There are 9 common monosaccharides which upon activation can act as sugar donors for glycans in eukaryotes (Figure 2). These are: Glucose (Glc), Galactose (Gal), Mannose (Man), Fucose (Fuc), Xylose (Xyl), Glucuronic acid (GlcA), *N*-acetylglucosamine (GlcNAc), *N*-acetylgalactosamine (GalNAc) and sialic acids (of which N-acetylneuraminic acid (Neu5Ac) is the most common member in humans).[5] Often the terminal monosaccharide, sialic acid is biosynthesised in the cell from N-acetylmannosamine (further discussion of this is seen in section 1.1.3).[6]

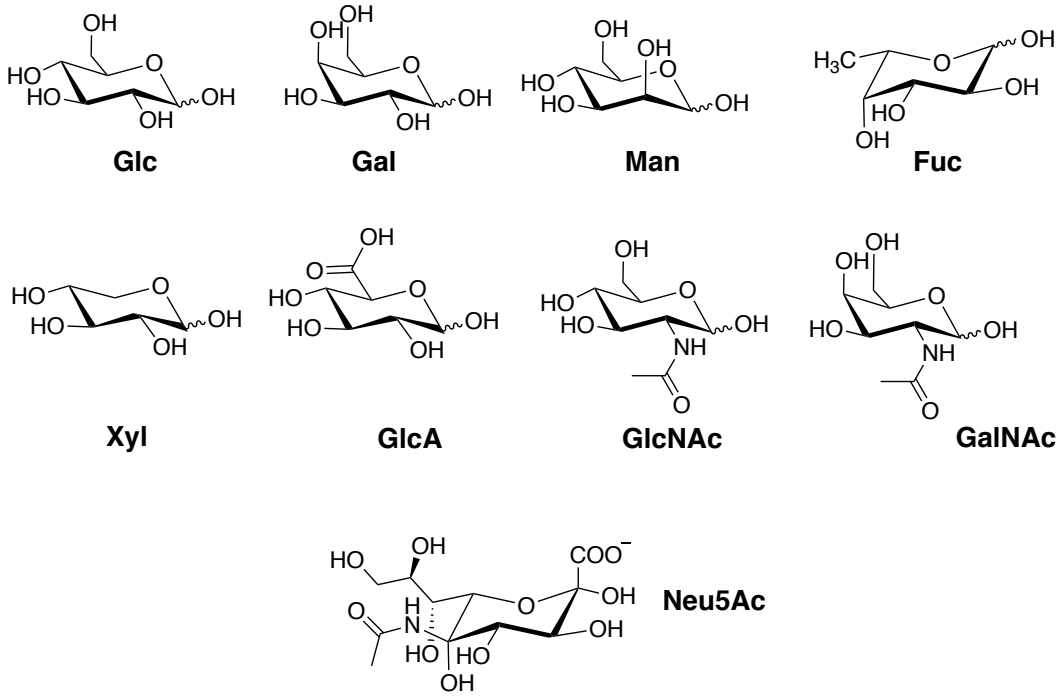

Figure 2 - The common monosaccharide building blocks of glycans in eukaryotes.

Glycoconjugates are located throughout the cell and outside the membrane. It was originally believed that these conjugates were only found attached to cell membranes, intracellular organelles, or secreted molecules. It has since been shown that they also exist freely in the cytosol and nucleus.[7]

The structural diversity of glycans generated from the number of monomers, the branching and the variable linkage is key due to the divergent functions of glycan structures. This is highlighted by the fact that glycosylation is the most prevalent post-translational modification with between 50-70% of human proteins being glycosylated.[8] The vital importance of glycans is demonstrated by the fact that no living cell has ever been found without a complex array of glycans on the cell surface.[9]

This importance comes as a result of the vital roles in which glycans play in all cellular processes including many intrinsic and extrinsic interactions such as differentiation, cell-cell adhesion (Figure 3) and cell growth.[10] This incolves glycan interactions with receptors and with carbohydrate binding proteins such as galcetins. Glycan expression is not exclusively linked to genomic behaviour, as it is not template driven.[11] Instead, glycan structures depend on the activity of glycosyltransferases and associated enzymes and by the intracellular concentration of the activated monosaccharides.[12]

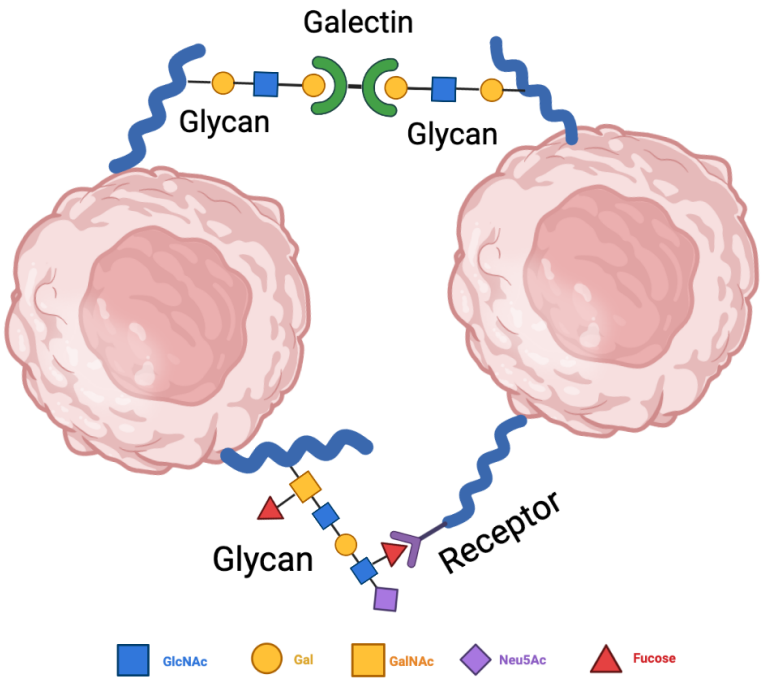

Figure 3 – Glycans play an important role in many intracellular behaviours such as cell signalling and cell-cell adhesion. This occurs via numerous mechanisms such as glycan-receptor interactions and interactions with carbohydrate binding proteins such as galectins.

1.1.2. Aberrant Glycosylation in Cancer

It is no surprise, given the variety of biological functions that glycans are associated with, that abnormal glycosylation is observed in many diseases. This includes physical and mental development deficiencies, muscular dystrophy, and chronic inflammatory diseases.[10, 11, 13] This importance is further highlighted by the fact that genetic defects in glycosylation are often lethal at the embryonic stage.[13]

Abnormal glycosylation also plays an important role in cancer. Changes in glycosylation involve up- and downregulation of naturally occurring glycans as well as neo-expression of glycans normally only found in embryonic tissues.[11] These changes allow for characteristic behaviour of tumours including proliferation, immune evasion, metastasis and reduced cell-cell adhesion.[14, 15] The structural variation in glycans required for these altered cellular properties comes via changes in the monosaccharides (Figure 4). This includes changes in the composition of the glycans (e.g., replacing one monosaccharide with another), variation in linkage of monosaccharides and altered branching/truncation.[15,16] These changes are usually due to changes in the expression levels of various enzymes in the glycan biosynthetic pathway (glycosyltransferases and glycosidases).[11]

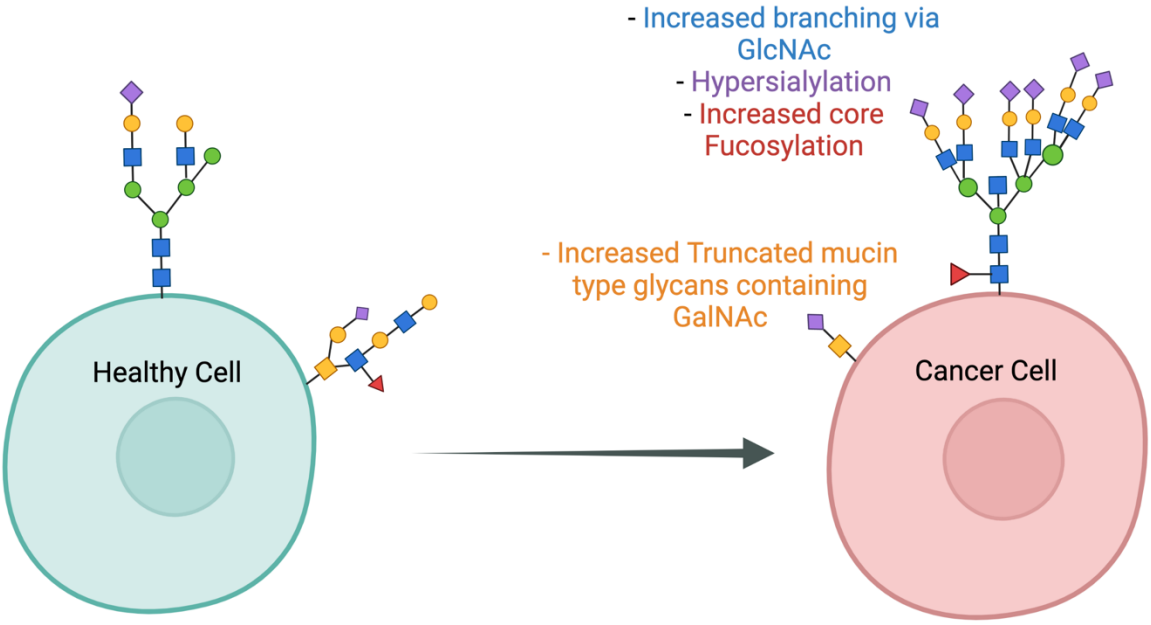

Figure 4 -Altered cell surface glycosylation between healthy and tumour cells. This occurs via several mechanisms including increased sialylation, increased branching (via GlcNAc) and increased truncated mucin types glycans containing GalNAc.

GlcNAc levels can be varied by increased expression of *N*-acetylglucosaminyltransferase-V (GnT-V). The increased levels of GlcNAc can lead to increased β1,6-GlcNAc branching, modifying the *N*-glycans of E-cadherin a glycoprotein cell-cell adhesion molecule, disrupting its function, and enabling metastatic behaviour. The importance of this is highlighted by this disruption being found in 70% of invasive carcinomas.[17,18]

Changes in glycosylation in cancer are not exclusive to extracellular proteins. *O*-GlcNAcylation is a common post translational modification of proteins important for signalling and regulation.[19] *O*-GlcNAcylation is analogous to phosphorylation and, as it is important in the regulation of many cellular processes, increased levels of *O*-GlcNAcylation are seen in many tumours.[20, 21] It is thought that hyper *O*-GlcNAcylation stems from cancer cells shifting to their metabolism towards anaerobic glycolysis (the Warburg effect).[20, 22, 23] The increased glucose uptake required for elevated glycolysis also leads to an upregulation other glucose-dependent pathways. In particular, the hexosamine biosynthetic pathway is upregulated by increased glucose flux, elevating levels of the product of the pathway, the activated sugar for *O*-GlcNAcylation, UDP-GlcNAc.[21, 24]

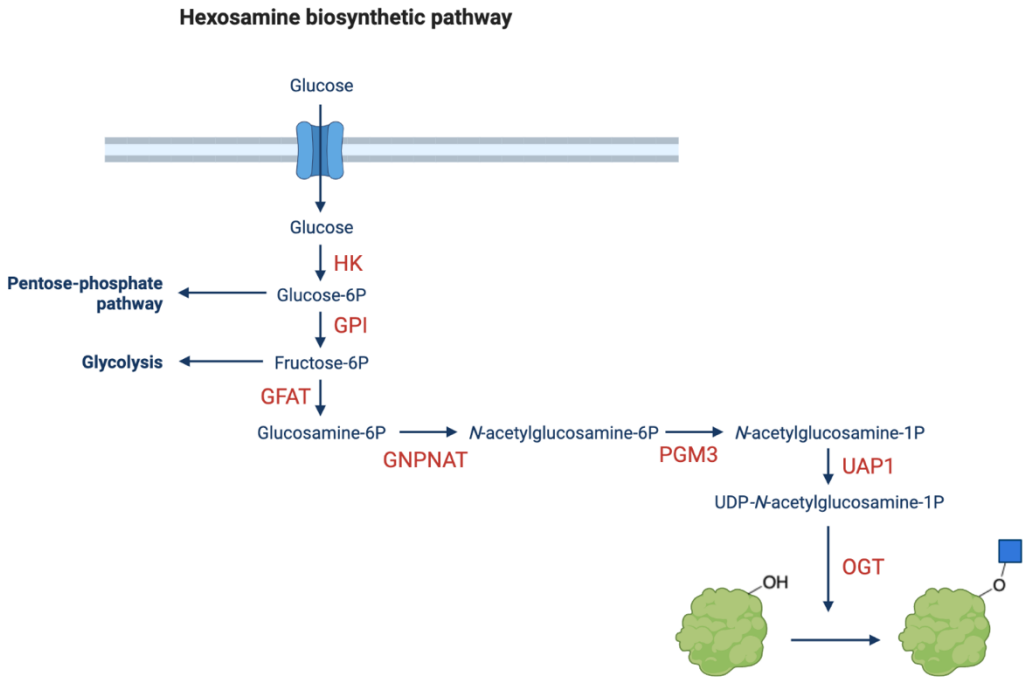

Figure 5 -Increased glucose flux due to the Warburg effect also leads to upregulation of the hexosamine biosynthetic pathway, producing UDP-GlcNAc for O-GlcNAcylation.

Cell surface glycosylation modification in cancer also occurs via GalNAc, including the over expression of truncated *O*-Glycans.[15] Mucins are glycoproteins which contain a large number of glycans initiated via glycosidic linkage of GalNAc to a Ser/Thr residues (mucin-type glycans).[25] Truncation of these mucin type glycans is highly prevalent in cancer and is associated with poor prognosis.[26] Overexpression of the mucins themselves is known to have a significant effect on cell signalling and is a therapeutic target for vaccines and immunotherapies.[27, 28]

1.1.3. Sialyl Lewis Antigens and Hypersialylation

Cell adhesion is also well known to be affected by Lewis-type antigens on the cell surface and their interaction with selectins.[29] Expression of these carbohydrates can be massively upregulated in cancer and is strongly associated with metastatic potential of tumours.[30,31] As can be seen in Figure 6, sialyl Lewis antigens (SLe) are capped with sialic acid residues (specifically N-acetylneuraminic acid).

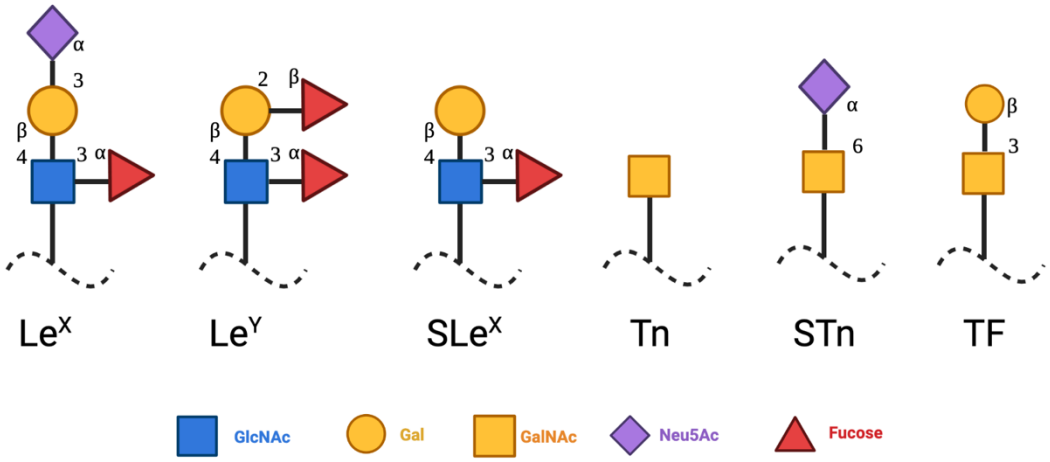

Figure 6 – The biosynthesis and monosaccharide composition of cancer-associated Lewis antigens and in particular SLe antigens. The terminal monosaccharide of SLe antigens is N-acetylneuraminic acid.

The role of sialylation in cancer is not limited to sialyl Lewis antigens, with hypersialylation (increased levels of sialic acid) especially as the terminal monosaccharide being a consistent feature of altered glycosylation in cancer.[32] Normal levels of sialylation are vital for cellular function,[32] but the enhanced levels seen in tumours lead to tumour progression and metastasis.[33] Blocking sialic acid expression *in vivo*, has been shown to suppress tumour growth by enhancing susceptibility of tumours to immune response, increasing CD8+ natural killer cells and reducing regulatory T-cells.[34]

Sialic acids have also been shown to have a role in avoiding cell death in tumours. One mechanism this occurs is via upregulation of the glycosyltransferase beta-galactoside alpha 2,6-sialyltransferase (ST6GalI) which hypersialylates N-glycans, including on the cell death receptor Fas, with hypersialylation protecting against Fas-dependant apoptosis.[35] There is also work to suggest that hypersialylation, and in particular upregulation of ST6GalI confers resistance to treatment in cancer. Overexpression of ST6GalI in ovarian cancer cells led to resistance to chemotherapeutic agent *cis*-platin. Whereas an ST6GalI knockout sensitised the cancer cells to the treatment.[33, 36]

Three key mechanisms have been described which lead to the hypersialylation of cancerous cell surfaces. These are increased expression of sialyltransferases, diminished neuraminidase expression, and increased availability of CMP-sialic acid (the activated sugar that acts as the donor), or some combination of all three.[33, 37, 38]

As previously mentioned, sialic acid is biosynthesised intracellularly. The precursor ManNAc can either be produced via epimerisation of GlcNAc or UDP-GlcNAc, or via ManNAc itself perfusing into the cell

from the extracellular environment.[39-41] The ManAc is then phosphorylated, before a further two modifications generate sialic acid. The sialic acid is then activated by CMP-sialic acid synthases to produce the CMP-Sialic acid, which is then transferred to the golgi. Here the activated sugar acts as a donor, adding sialyl groups to the glycan chain *via* a sialyltransferase, before the glycan is transported to the cell surface.[41]

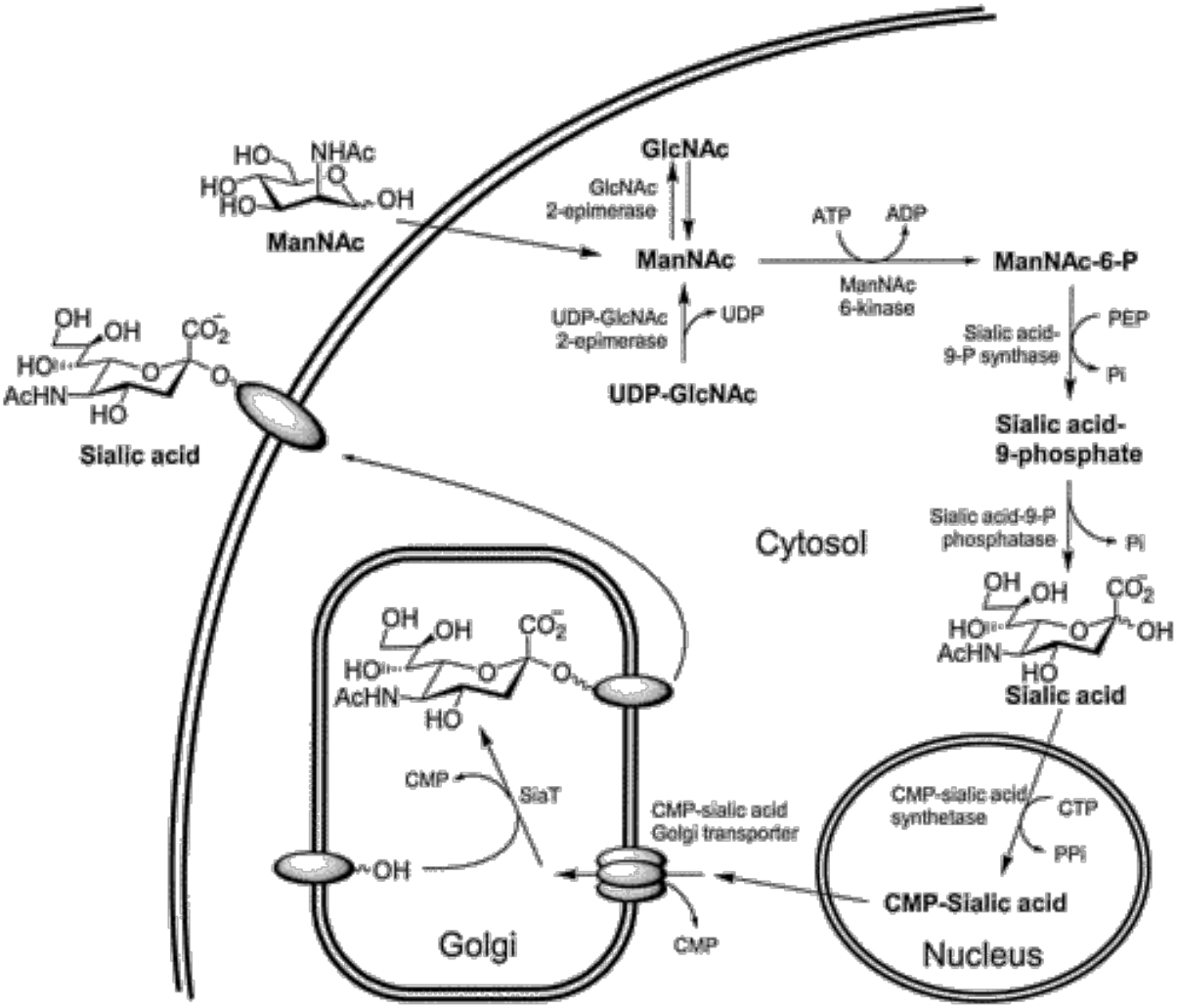

Figure 7 - Sialic acid biosynthesis and subsequent addition of CMP-sialic acid to the glycan, which is then transported and displayed on the cell surface. Figure taken from Jacobs et al.[41]

1.2. Bioorthogonal Chemistry and The Chemical Reporter Strategy

1.2.1. General Principles and Historical development

Bioorthogonal chemistry was first used to describe a chemical reaction that could occur inside a living system by the Bertozzi group in 2003.[42] This pioneering work demonstrated the biorthogonality of the Staudinger ligation between an azide tagged galactosamine (GalNAz) and a phosphine oxide probe. Conducting chemistry in an active biological medium is a challenge due to the obvious constraints. Perhaps the most important consideration is selectivity. Ensuring that the two reagents only react with each other and not any of the other reactive species, which are generally in much larger excess, is a difficulty. This usually requires reactive groups which are abiotic. The resulting ligation product must also be inert to the same environment, including enzymatic degradation. The reaction conditions need to be accessible under the constraints of living systems. This means the reaction being feasible at physiological temperature and pH. To overcome the dilute concentration of the two reagents, the reaction kinetics must be fast at physiological temperature. Also of vital importance is that the reagents and the products must not be cytotoxic, at the concentrations they are used at.[43-45]

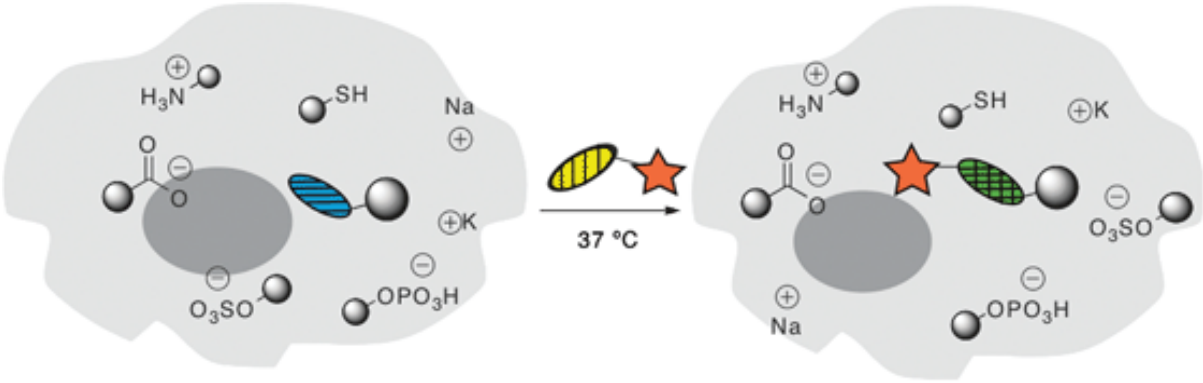

Figure 8 – Selectivity is a key requirement for a bioorthogonal reaction. In this example the blue and yellow handles must react exclusively with each other, and the resulting product also must be unreactive to the biologically reactive species. Figure taken from Jewett and Bertozzi.[46]

While the term "bioorthogonal" was first coined in 2003, it was work by Tsien and co-workers in 1998[47, 48] that really sparked the field. They developed a biarsenical fluorophore probe which could react with a genetically introduced tetracysteine set of residues which is almost absent from the mammalian proteome. This allowed them to fluorescently label the proteins of interest *in vitro*.[47] This sparked interest in bioorthogonal chemistry and in particular the chemical reporter strategy.

The chemical reporter strategy involves incorporation of an unnatural bioorthogonal handle into a target biomolecule. This handle can then undergo a bioorthogonal reaction to attach a functional motif (*e.g.* imaging agent or drug) to the biomolecule. Key is that this handle minimally disrupts the native function of the biomolecule of interest, instead the unnatural substrate is tolerated by the cell biosynthetic machinery and incorporated just as its natural analogue would be.[49, 50] An advantage to this strategy, in particular for proteins, is that it avoids the sterically cumbersome nature of, for example, affinity agents and green fluorescent protein (gfp).[47, 50]

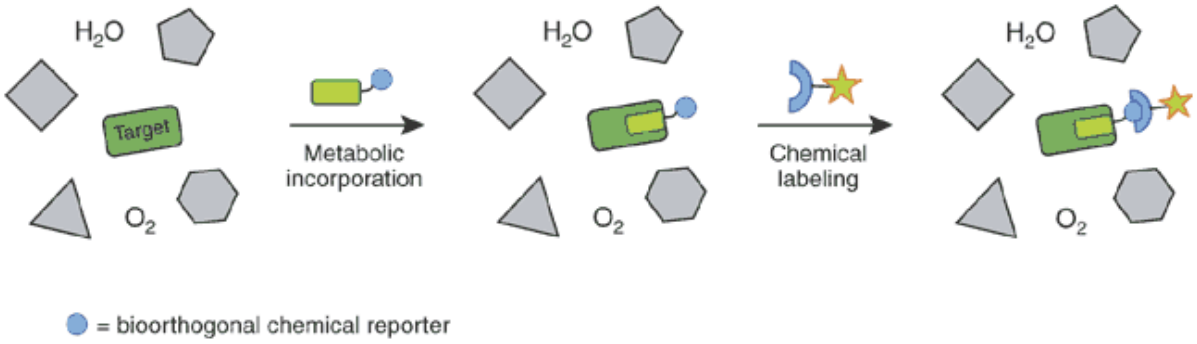

Figure 9 - The chemical reporter strategy. Figure taken from Prescher and Bertozzi.[49]

1.2.2. Azides as Chemical Reporters

One of the first and most widely used chemical reporters is the azide group. The broad application of the azide stems from it being abiotic in mammals (and absent from nearly all other species)[51], aiding selectivity for the bioorthogonal reaction. The small size of the azide also means that it minimally perturbs the overall structure of the biomolecule, particularly for large substrates like proteins, where the change is negligible.[43] Further to this azides are stable at physiological temperature and pH, do not photodecompose in ambient light (aryl azides do but alkyl azides used more widely as reporters do not), and organic azides are not cytotoxic. They are also resistant to oxidation and do not react with water. Despite being mild electrophiles, they do not react with biological nucleophiles such as amines due to their 'hard' nature. Alkyl azides do react with thiols but the reaction with monothiols requires heating to 100 °C or catalysis.[51, 52]

Azides are also advantageous due to the multiple possible reactive partners. One of the first developed bioorthogonal reactions was the Staudinger ligation. As previously mentioned, this was utilised to ligate azide tagged glycans with phosphine-containing reagents.[53] In the reaction the azide handle reacts with the phosphine, liberating nitrogen, and, *via* an aza-ylide, forms a stable amide (Scheme 1). This was then developed into the traceless Staudinger ligation, which enables cleavage of the

phosphine oxide to give an amide cross-linked product.[54] Aerobic oxidation of the electron-rich phosphine reactive partner to the phosphine oxide, diminishes the yield and produces unwanted byproducts.[55] When first reported, the kinetics were seen as an advantage (with second order rate in the 10^{-3} M^{-1} s^{-1} range[56]), but with many subsequent reactions showing much enhanced kinetics the Staudinger ligation has largely been surpassed.

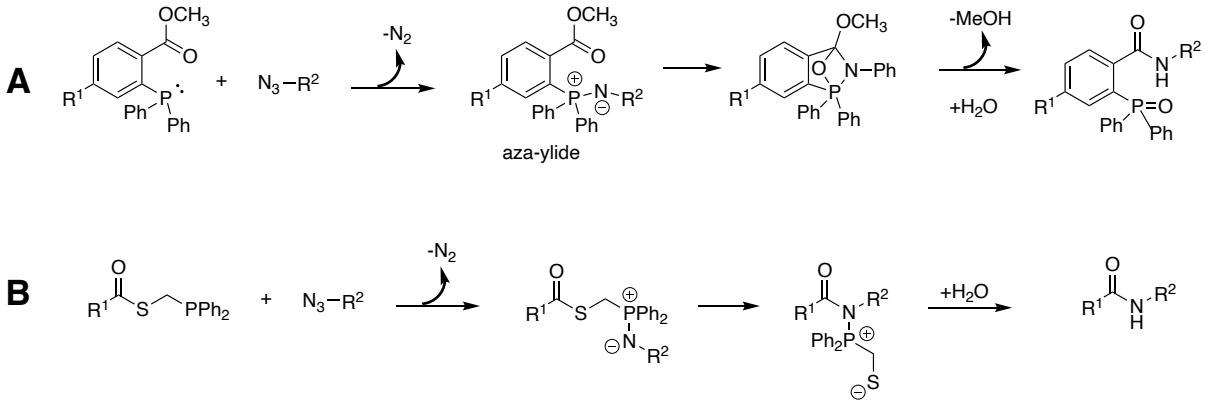

Scheme 1 - A) The first report of the Staudinger ligation, with the aza-ylide crucial in preventing hydrolysis. B) An example of the traceless Staudinger ligation.

Azides can also act as 1,3-dipoles to undergo Huisgen [3+2] cycloadditions with alkynes, which are also extremely rare in nature, aiding orthogonality.[57] This "click" reaction yields a triazole product but requires activation of the alkyne (dipolarophile) or very high temperatures. To make this reaction compatible with biological environments the Sharpless and Meldal groups both independently reported use of catalytic Cu(I), which allowed the reaction with terminal alkynes to proceed under physiological conditions, due to it being up to 10^7 times fast than the uncatalysed version.[58-60] The copper-catalysed azide-alkyne cycloaddition (CuAAC) also shows enhanced kinetics relative to the Staudinger ligation, with *in vitro* rate constants at least 25 times higher.[61] The catalysed method is also advantageous due to the regioselectivity, with the 1,4-disubsituted triazoles being formed almost exclusively (Scheme 2).[62] Despite its many uses, the major limitation of CuAAC bioorthogonal chemistry is the cytotoxicity of the copper catalyst[63], which has limited its *in vivo* applications, in particular.[64] Attempts to mediate the toxicity have been made with biocompatible copper ligands, but toxicity remains a concern.[62, 63] Ruthenium-catalysed azide-alkyne cycloaddition (RuAAC) has also been developed, which selectively forms the 1.5-disubsituted triazole[65], but has not shown promise in bioorthogonal reactions.[66]

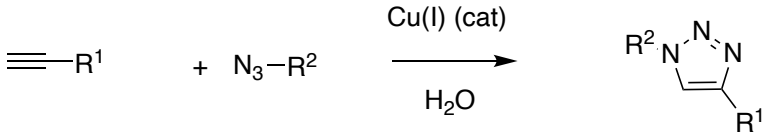

Scheme 2 – General scheme for CuAAC reactions.

To eliminate the need for potentially cytotoxic metal catalysis, the Bertozzi group employed ring-strained cyclooctynes as the dipolarophile).[67] The 18 kcal mol^{-1} of strain released upon cycloaddition leads to the reaction proceeding without elevated temperatures or heavy metal catalysis.[49] Enhancement of the rates of strain-promoted azide-alkyne cycloaddition (SPAAC) via new cyclooctyne probes has allowed both *in vitro* and *in vivo* applications.[68] This is discussed further in section 3.1.

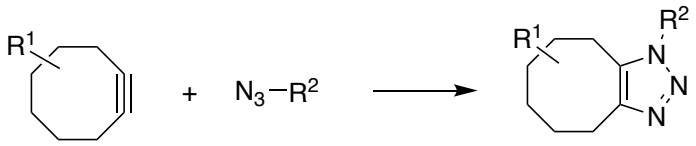

Scheme 3 - General Scheme for SPAAC reactions.

1.2.3. IED-DA Bioorthogonal Reactions

One of the recurring themes in bioorthogonal chemistry is the use of strain to promote cycloaddition reactions.[45] This is utilised in a second common class of bioorthogonal reactions, inverse electron-demand Diels-Alder (IED-DA) reactions. In this reaction class an electron rich dienophile undergoes a cycloaddition with an electron poor diene. The reaction of strained dienes, particularly with a tetrazine reactive partner, are among the fastest reported bioorthogonal reactions.[69] Over a decade ago, the Fox group reported the bioorthogonal IED-DA reaction between *trans*-cyclooctene (TCO) and tetrazine. The reaction kinetics (k_2 2000 M^{-1} s^{-1}) enabled rapid conjugation at low concentration, with the rates far in excess of those seen for SPAAC and CuAAC.[70] There is some isomerisation to the unreactive *cis*-isomer over time, with the rate of isomerisation increased in the presence of thiols, limiting the long-term stability of TCO to an in-serum half-life of 3.26 hours. However, there is limited isomerisation in some aqueous solvents, with no isomerisation to the *cis*-isomer observed in PBS after 7 days.[71,72]

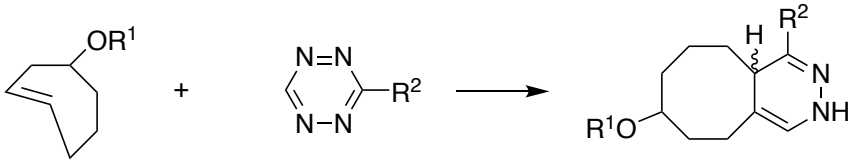

Scheme 4 - General scheme for TCO IDE-DA reaction.

Other IED-DA chemical handles have been developed, including norbornene[73] and vinyl boronic acids[74]. The problem with these handles is their relative size. Compared to the azide handles these motifs are much larger and this can prevent efficient incorporation, via the native biosynthetic route, of a chemical reporter. As such, smaller (albeit less reactive) handles such as methyl cyclopropenes have been developed to strike a balance between kinetics and incorporation.[75] Further discussion of TCO related IED-DA reactions is contained in 3.3.1 and the use of methyl cyclopropenes is discussed in section 2.1.

1.3. Metabolic Oligosaccharide Engineering

1.3.1. Metabolic Oligosaccharide Engineering *In Vitro*

As glycan biosynthesis is not template driven, genetic manipulation methods widely used for protein imaging are often challenging.[76] As such alternative methods to image glycans *in vitro* have been introduced including lectins[77] and antibodies[78] for affinity-based detection of glycoconjugates. While these are useful for imaging the glycome *in vitro*, their relatively weak binding affinity, and poor tissue permeability, severely reduce their use *in vivo*.[76, 79] Modulation of the key enzymes on the glycosylation biosynthetic pathway has also been widely attempted (including glycosyltransferases and glycosidases). The disadvantage to perturbing the natural function by mutation is that, especially *in vivo,* a change in phenotype can be hard to detect. Also, because of the essential nature of many glycosylation pathways, their alteration can be lethal.[80]

So, metabolic incorporation of unnatural monosaccharides has been developed as an alternative method to image the glycome. Mutant enzymes can be developed and produced to tolerate unnatural substrates[81], but this is a challenging and pain-staking process, especially to produce the concentrations of enzymes required to be useful practically.[80] However, it has been found that in some cases the native enzymes on the biosynthetic pathway of glycosylation are somewhat substrate-promiscuous. Small chemical perturbations from the native substrate are sometimes tolerated, and analogues bearing small chemical tags, can be incorporated and aid understanding of biological processes.[80, 82]

Tetracetylated monosaccharides are generally used as they have much increased cell permeability relative to unacetylated derivatives.[83] After perfusion across the membrane, non-specific cytosolic esterases deprotect the sugars (Figure 10). The sugar analogue then passed along the native

biosynthetic pathway and the activated sugar is attached to the growing glycan chain in the Golgi. The tagged glycoconjugate is then transferred to the extracellular matrix, where the tag can be used for imaging or even drug delivery purposes via a bioorthogonal reaction.

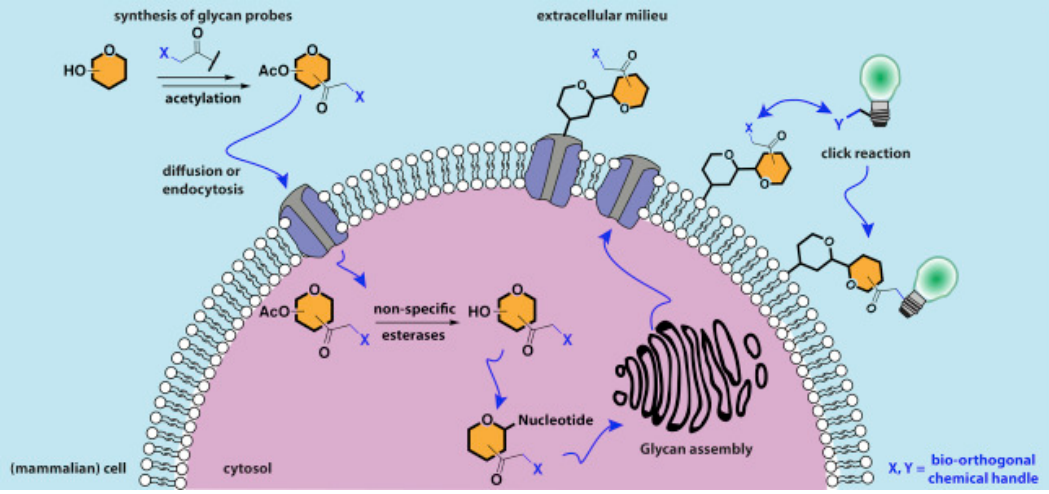

Figure 10 – General approach for MOE. Ac_4 analogues are used for cell diffusion with the first intracellular step being deacetylation by non-specific esterases. The tagged sugar is treated as the native substrate would be, with the tagged sugar eventually being expressed as part of a glycan on the cell surface. A subsequent bioorthogonal reaction with the tag can be used to attach an imaging motif (as shown in this case) or potentially a drug delivery system. Figure taken from Sminia et al.[84]

Early attempts at this metabolic oligosaccharide engineering (MOE) involved the use of halogenated and deoxy sugars, but this was cytotoxic.[85, 86] Cytotoxicity is a general concern in MOE, as analogues, with the structural similarity to the native substrate sometimes act as competitive inhibitors of normal glycosylation pathways.[84] However, this has its own potential application as therapeutic treatments for certain overexpression related disorders, including cancer.[84]

The first real success of a tagged monosaccharide as an MOE analogue was again developed by the Bertozzi group, in 1997.[87] They reported the use of an unnatural ManNAc analogue, with a ketone reactive handle linked to the amide on the sugar (ManNLev, Figure 11). They were then able to covalently ligate the analogue on the cell surface via reaction of the ketone with a hydrazide-biotin conjugate. The biotin could then react with a fluorescent avidin to generate a large increase in fluorescent intensity of Jurkat, HL-60, and HeLa cells relative to treatment with phosphate-buffered saline (PBS) or the natural ManNAc analogue.[87] This first *in vitro* example of MOE has sparked research spanning four decades, with many different unnatural sugars synthesised and used.

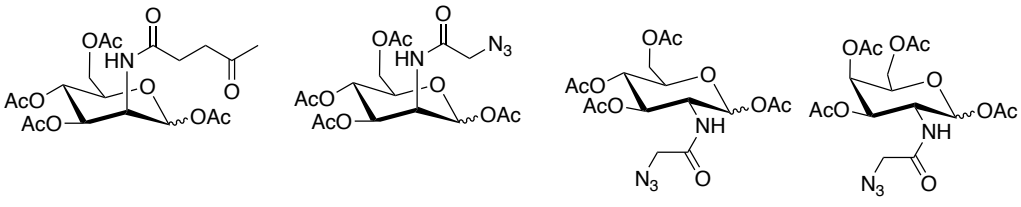

Figure 11 – Some of the first MOE monosaccharides.

Whilst the first example used ketones, it is arguably the use of azides as chemical tags for MOE that really sparked interest. Again, via amide linkage an azide-tagged ManNAc analogue N-acetylazidomannosamine (ManNAz) was synthesised. This analogue was first incorporated and imaged using the previously discussed Staudinger ligation.[53] Using a biotin/avidin combination, contrast was observed between tagged sugar and control treated HeLa and Jurkat cells. Notably, the azide, phosphine and the resulting ligation product had no effect on cell growth or viability.[54]

This seminal work was then expanded to include similar azide tagged analogues of GalNAc and GlcNAc. *N*-Azidoacetylgalactosamine (GalNAz)[42] and *N*-azidoacetylglucosamine (GlcNAz)[88] were synthesised and showed labelling under the same Staudinger ligation conditions previously used for ManNAz. However, GlcNAz labelling was much lower than the other azide analogues. GalNAz gives higher cell surface labelling than GlcNAz under the same conditions.[89] This work by Boyce *et al*.[89] showed GalNAz is converted to UDP-GalNAz and can then be epimerised to UDP-GlcNAz, allowing cross-talk of the pathways, and going some way to explaining the increased labelling with GalNAz, especially given the weak tolerance of the native GlcNAc pyrophosphorylase enzymes to modified substrates. Just as the same cell line shows variable labelling with the different tagged sugars, the same tagged sugar shows variable labelling in different cell lines.[90] The variability of labelling between different sugars bearing the same tag is seen for a variety of chemical reporters including methylcyclopropenes,[91] and isonitriles[92] which are used for IED-DA based labelling. Mannosamine analogues generally show the highest labelling due to the tolerance of the sialic acid pathway to unnatural substrates[41], and hence most tags are developed on mannosamine derivatives.

There is a large quantity of research focused on the development of tagged monosaccharides for MOE and their use *in vitro* is well reviewed.[82, 84, 93-96]

1.3.2. Metabolic Oligosaccharide Engineering *In Vivo*

MOE was first used in animals in 2004, when the Bertozzi group used the Staudinger ligation to image ManNAz labelled glycans of mice.[97] This example was however not truly *in vivo*, as the mice were euthanised and splenocytes (cells rich in sialosides) isolated. This was done in different examples, one where the phosphine probe was added post euthanisation and another where it was added 90 minutes pre euthanisation (and hence the Staudinger ligation conducted *in vivo* before euthanisation and subsequent splenocyte isolation). In both examples the splenocytes were imaged *ex vivo via* flow cytometry and showed enhanced fluorescence compared to those from the untreated mice.[97]

The first application of MOE *in vivo* was demonstrated by the Bertozzi group in 2008 imaging Zebrafish embryos using Ac_4GalNAz and a strained cyclooctyne probe (DIFO) (Figure 12).[98] Zebrafish embryos are widely used in studies, and in particular for imaging, due to their *ex utero* development (during which they are mostly translucent) as well as their disease models being well understood.[76] Staudinger and CuAAC ligation were thought to be either too slow or cytotoxic for *in vivo* applications and hence SPAAC was used. Ac_4GalNAz was used, as opposed to Ac_4ManNAz, perhaps due to the known abundance of mucin type O-glycans in zebrafish embryonic development.[99]

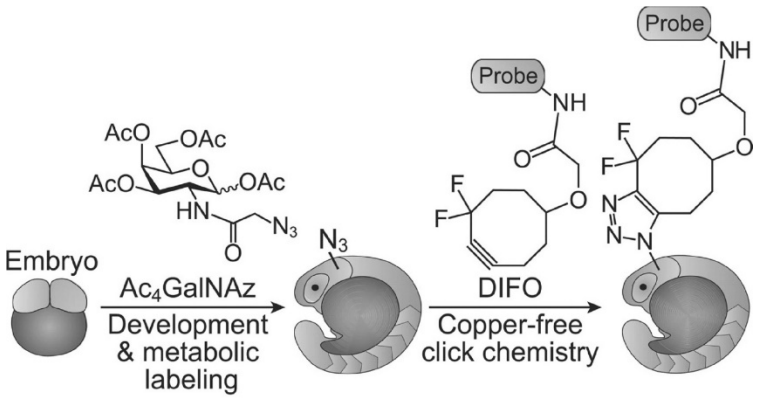

Figure 12 - In vivo labelling of zebrafish using Ac4GalNAz and DIFO. Taken from Laughlin et al.[98]

The Brindle and Leeper groups were the first to report the imaging of sialylated glycans i*n vivo.*[100] LL2 tumour-bearing mice were treated with Ac_4ManNAz and subsequently labelled glycans were reacted via Staudinger ligation with a biotinylated phosphine. The mice were left for two hours post phosphine addition to allow time for the Staudinger ligation. Subsequently, the mice were treated with neutravidin (to react with the biotin) bearing a fluorophore or ^{111}Indium and imaged via optical imaging or single-photon-emission computed tomography (SPECT), respectively (Figure 13). There was a significant increase (53%) between sugar and non-sugar treated tumour to tissue ratio.

However, it was noted that for clinical translation, lower concentrations of the reagents would be needed, and this could be possible via enhanced kinetics such as that seen with SPAAC.[100]

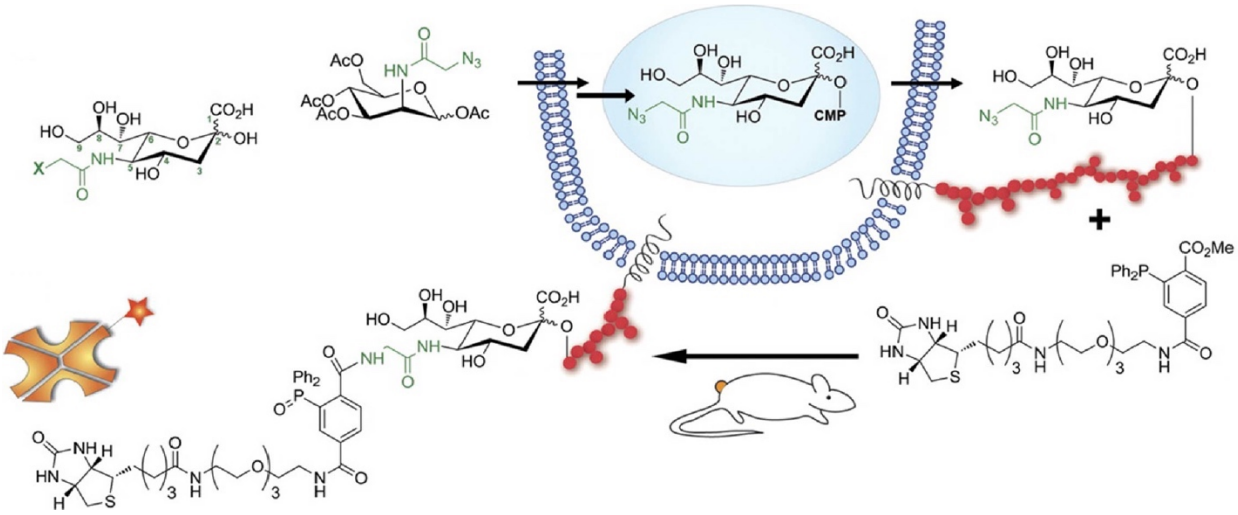

Figure 13 - In vivo labelling of sialylated glycans in LL2 implanted mice. Mice were treated with Ac_4ManNAz for 4 days (i.p.), which is subsequently expressed on the cell surface as sialic acid. Biotinylated phosphine was added and then the neutravidin imaging agent (either bearing a fluorophore or ^{111}In) added 2 hours post phosphine. Mice were imaged by optical imaging or SPECT. Figure taken from Neves et al.[100]

Applying the enhanced kinetics of SPAAC the Leeper and Brindle groups were able to use Ac_4GalNAz to again label LL2 tumour glycans *in vivo*.[101] Following metabolic labelling with the sugar a gadolinium bearing strained cyclooctyne (TMDIBO-Lys-Gd) showed sugar-dependent contrast two hours post injection as measured by magnetic resonance imaging (MRI) (Figure 14). There were however higher levels of non-specific accumulation of TMDIBO-Lys-Gd in the tumour than in other tissues, reducing the ratio of gadolinium concentration in sugar-treated tumours to those which were solvent treated.[101]

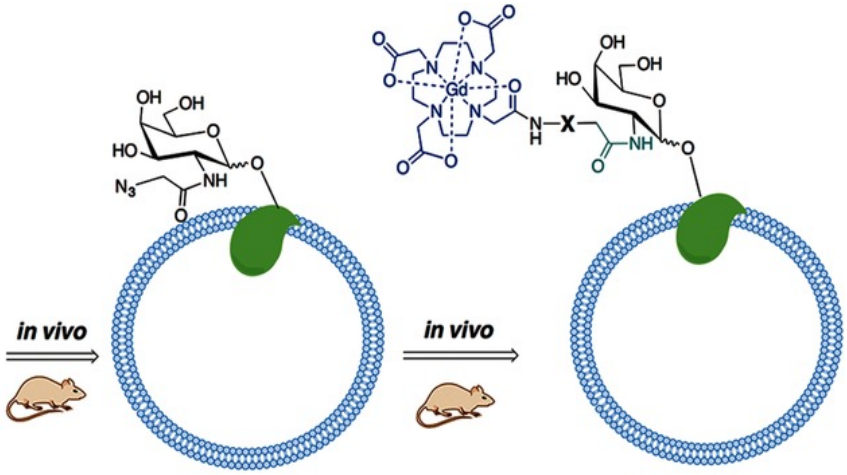

Figure 14 – In vivo imaging of Ac_4GalNAz labelled glycans in LL2 tumours using a TMDIBO-Lys-Gd and imaging by MRI. Figure taken from Neves et al.[101]

Further enhanced kinetics were developed by using a "double click" labelling approach.[102] Using the same tumour model and sugar (LL2 and $Ac_4GalNAz$), labelled glycans were first reacted with TMDIBO. However, rather than this cyclooctyne being directly linked to the imaging agent, it was instead linked to a reactive TCO group. After 24 hours (when this was done after 3 hours contrast was lower) the TCO reactive handle was reacted with a fluorescently labelled tetrazine. Due to the enhanced kinetics of the second click, lower concentrations of the tetrazine imaging probe could be used, reducing background signal, and therefore enhancing contrast. A comparable strategy for Staudinger ligation-based double click (phosphine linked-TCO), showed reduced double click contrast probably due to the slower kinetics and increase hydrophobicity of the phosphine probe.[102]

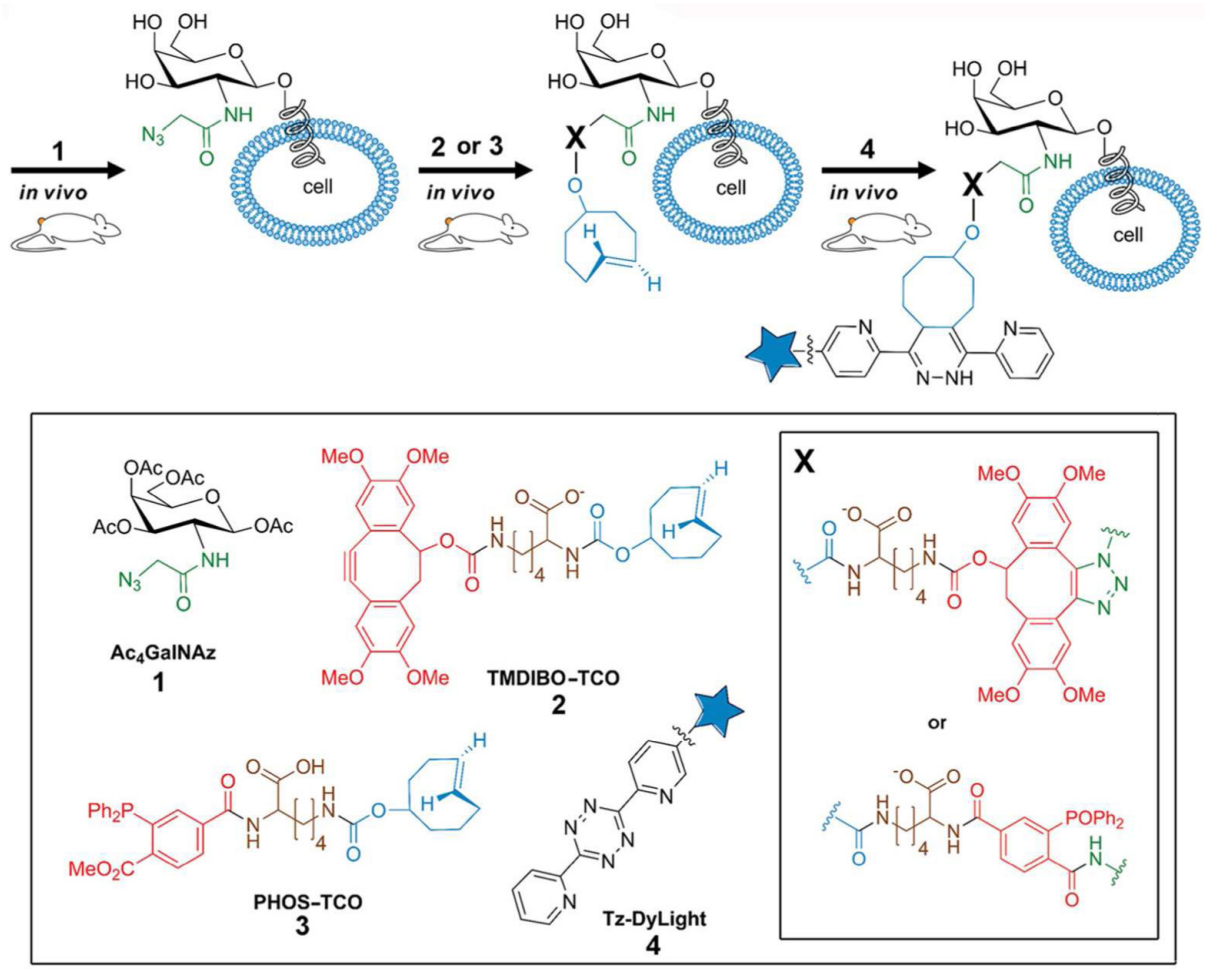

Figure 15 – Double click labelling of $Ac_4GalNAz$ labelled glycans in vivo. Figure taken from Neves et al.[102]

2. Metabolic Labelling with Variably Acetylated sugars

2.1. An introduction into Methyl Cyclopropenes for MOE

As previously discussed IED-DA based chemical reporters are particularly useful due to their enhanced rate of reaction with tetrazine reactive partners. TCO based chemical handles show rapid kinetics, but their size makes metabolic incorporation difficult, with the large perturbation from the native substrate meaning the enzymes on the biosynthetic pathway are not very tolerant towards TCO tagged monosaccharides.[103] Despite this a TCO tagged monosaccharide has been reported for use in MOE, Ac_4ManNTCO was synthesised and imaged tumours *in vitro* and *in vivo* using a bioorthogonal turn-on nanoprobe, with the advanced nature of the probe allowing for imaging despite the expected very low inccoporation.[104] Other bulky chemical reporters for IED-DA based ligation have been developed such as a bicyclononyne-tagged sialic acid (BCNSia)[105] and norbornene tagged mannosamine derivatives,[106] but their use has been limited due to their low incooporation.[69] Linear terminal alkenes have also been used to tag monosaccharides, but slow kinetics of the tagged sugars with tetrazines, k_2 = 0.01-0.1 M^{-1} s^{-1}, limit their use, despite rates increasing with increasing chain length (but this decreases incorporation).[69, 107, 108]

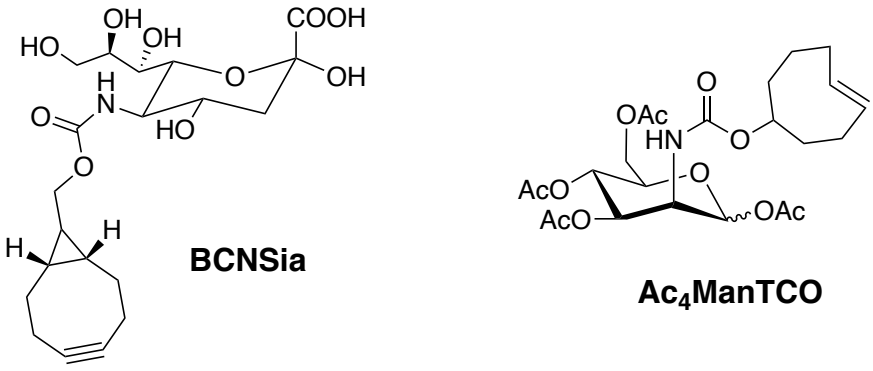

Figure 16 - A timeline of some IED-DA based MOE monosaccharides developed.

One type of IED-DA based chemical reporter which aims to balance the kinetics and incorporation are cyclopropenes. Their small size means incorporation as tags on unnatural monosaccharides is much more tolerated than larger motifs like TCO.[75] Unsubstituted cyclopropenes are generally unstable as they are prone to dimerisation and polymerisation.[109] Despite this, unsubsituted cyclopropenes have been use for MOE in the form of Ac_4ManNCp.[110] Using Ac_4ManNCp, Xiong *et al.* were able to label several tumour cell lines *in vitro*. They also labelled sialylated glycans with Ac_4ManNCp *in vivo* but

imaging was carried out by isolation and treated of splenocytes with a fluorescein tetrazine probe *ex vivo*.[110]

Substitution of the cyclopropene alkene has been shown to improve stability, in particular using methyl cyclopropenes.[109] One methyl group enhances stability, and does not decrease the rate of IED-DA markedly, but dimethylation has been shown to decrease the rate of IED-DA significantly (from $3.0x10^{-2}$ M^{-1} s^{-1} to $0.037x10^{-2}$ M^{-1} s^{-1} on comparable cyclopropenes).[75] As such, methyl cyclopropenes have been shown to be well tolerated and incorporated as MOE tagged monosaccharides.[75, 91, 111-113] The electron withdrawing character at C-1 (position shown by the red arrow in Figure 17) is also crucial for the labelling, with the linkage again aiming to strike the balance between incorporation and kinetics. Ac_4ManNCp and amide linked methyl cyclopropene Ac_4ManNCyc both have a carbonyl group directly attached to the cyclopropene. This electron-withdrawing effect reduces the rate of the IED-DA, as demonstrated by carbamate linked cyclopropenes having an approximately 100-fold rate enhancement over the similar electron-withdrawing amide linked cyclopropenes.[109, 113] This is highlighted in work by Hassenrück and Wittmann[91] who compared the kinetics of the reaction of Ac_4ManNCp, Ac_4ManNCyc and the carbamate linked derivative Ac_4ManNCyoc with a tetrazine derivative. This showed the rate enhancement for Ac_4ManNCyoc to be tenfold over the amide derivative. They also showed a 3-fold reduction in rate with methyl substitution (rate difference between Ac_4ManNCp and Ac_4ManNCyc).

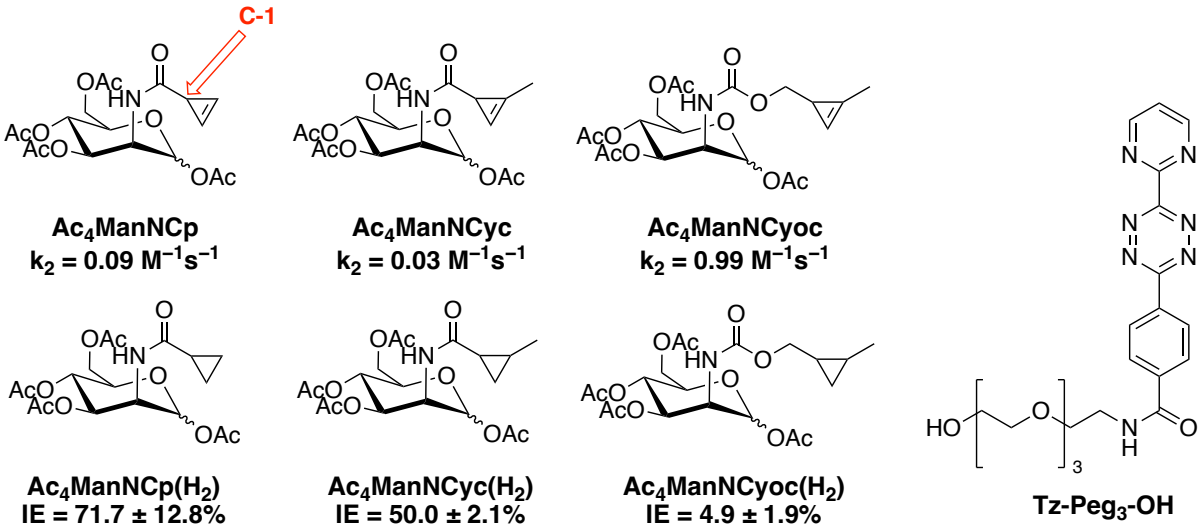

Figure 17 - Comparison of the rate constant of various cyclopropene handles for the IED-DA with Tz-Peg_3-OH. IE determined using the cyclopropane analogues. Data taken from Hassenrück and Wittmann.[91]

The same work by Hassenrück and Wittmann[91] went on to demonstrate the difference in incorporation efficiency (IE) between the analogues. In this case the incorporation efficiency us a

measure of the quantity of cellular sialic acid residues which are labelled with the chemical reporter (R) after incubation with the tagged monosaccharide. This is commonly measured by 1,2-diamino-4,5-methylenedioxybenzene (DMB) derivatisation. Cells are first heated under acidic conditions to release sialic acids and then reacted with DMB which selectively reacts with α-keto acids Neu5Ac to form a fluorophore. HPLC followed by fluorescent detection can allow separation and quantification (via integration of the fluorescent signals) of the levels of natural (Neu5Ac) and tagged (Neu5AcR) sialic acids. The IE can then be calculated by the following equation:

$$IE(\%) = \left(\frac{\text{Neu5AcR}}{\text{Neu5Ac} + \text{Neu5AcR}}\right) \times 100$$

Cyclopropane mimics were needed as cyclopropenes are unstable under the elevated temperature and acidic conditions required. Ac_4ManNCyoc showed a much-reduced IE compared to the amide derivatives, suggesting the tag is much less tolerated by the enzymes of the native substrate compared to the amide analogues. Despite this the highest MOE-induced labelling was observed with Ac_4ManNCyoc, suggesting that the rapid kinetics is the dominant factor, compensating for the reduced level of incorporation.[91]

Tetra-acetylated monosaccharides are generally used for *in vitro* and *in vivo* studies as this protects the polar hydroxyl groups, with fully unacetylated sugars too polar for efficient passive diffusion across the cell membrane. After cellular uptake the monosaccharides are then deacetylated by non-specific esterases in the cytosol (Figure 18).[83]

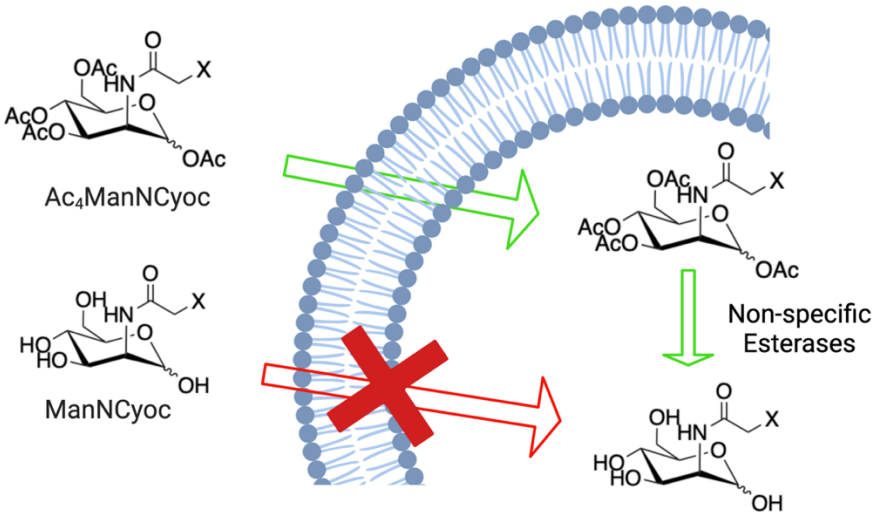

Figure 18 -Cell uptake of tagged monosaccharides. Tetra-acetated derivatives can diffuse across the membrane and then be enzymatically deacetylated in the cytosol. Unacetylated monosaccharides are too polar for efficient cell uptake.

Despite the promising *in vitro* labelling potential of the cyclopropene tagged monosaccharides only a single report of *in vivo* work has been reported. As previously mentioned, this work by Xiong *et al.* using Ac_4ManNCp used *ex vivo* labelling of splenocytes.[110] We believe the reason why the most promising *in vitro* candidate Ac_4ManNCyoc has not been used in any *in vivo* applications is due to its poor aqueous solubility. Initial attempts to carry out *in vivo* work using the compound within the group were unsuccessful due to the inability to sufficiently dissolve the compound in the required solvent vehicle for *in vivo* studies (up to 10% DMSO in PBS). When a solution was first prepared in DMSO and then diluted to the required concentration with PBS, immediate precipitation occurred. This highlights the hydrophobicity of the compound, with a cLogP of 2.20, which means at the relatively high concentrations of sugar required (due to the low maximum injection volume) the compound is not sufficiently dissolved. Higher concentrations of DMSO (or greater volumes of 10% DMSO in PBS) are not permitted in the animal protocol.

2.1.1. Project Aims

The aim of this project is to overcome the aqueous insolubility of ManNCyoc sugars by varying the level of acetylation of the monosaccharide. The unacetylated sugar is too polar for efficient cell uptake, whereas the tetra-acetylated sugar is too nonpolar for aqueous dissolution. It was believed an intermediary level of acetylation (e.g., mono-, di- or triacetylated monosaccharide) may strike a balance between the two extremes.

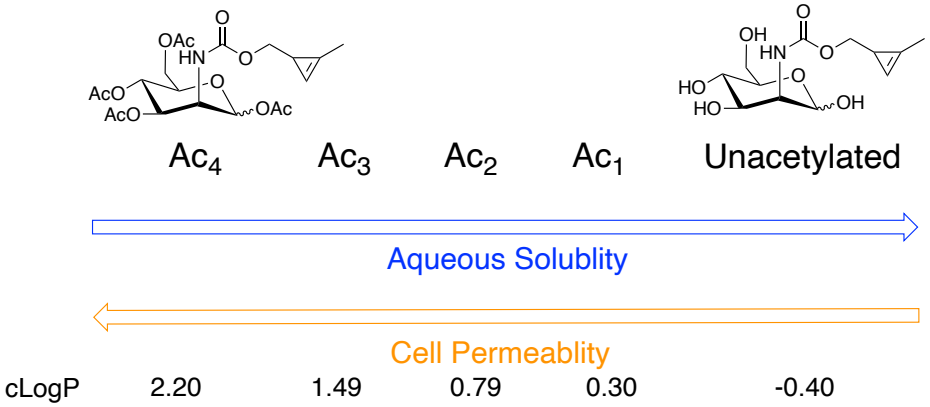

Figure 19 - cLogP of Ac_xManNCyoc. Aiming to strike a balance between cell permeability and aqueous solubility. cLogP calculated using molinspiration.[114]

We therefore aimed to synthesise Ac_1, Ac_2, Ac_3 and Ac_4ManNCyoc. Previous work by Shahd Fouad and Falviu Bulat[115], had shown enhanced labelling with Ac_3ManNCyoc relative to the tetracetylated derivative but the different levels of acetylation had proved difficult to separate and so the sugars

were used as complex mixtures. We therefore aimed to synthesise Ac_1 to Ac_4 ManNCyoc in high degree of purity, and discrete levels of acetylation. We then would test incorporation of the different degrees of acetylation, via incubation of cells with each level of acetylated precursor, followed by IED-DA reaction with a fluorescent tetrazine, and analysis by flow cytometry. We also wanted to investigate what effect acetylation had on other Cyoc-labelled sugars and so aimed to synthesise and test the acetylation panel (Ac_1-Ac_4) of GalNCyoc and GlcNCyoc as well. To compare these results with other chemical tags, we aimed to synthesise Ac_1-Ac_4 ManNAz, GalNAz, and GlcNAz, the Ac_4 versions of which have been widely used *in vitro* and *in vivo* and do not seem to suffer from the same aqueous insolubility.

2.2. Variable Acetylation

2.2.1. Synthesis of Tagged Sugars with Variable Acetylation

ManNAz, GalNAz and GlcNAz were synthesised as previously described in literature.[116] This involved first synthesising azidoacetic acid, and subsequent amide coupling using EDC/HOBT to give the *N*-azidoacetyl sugar (Scheme 5).

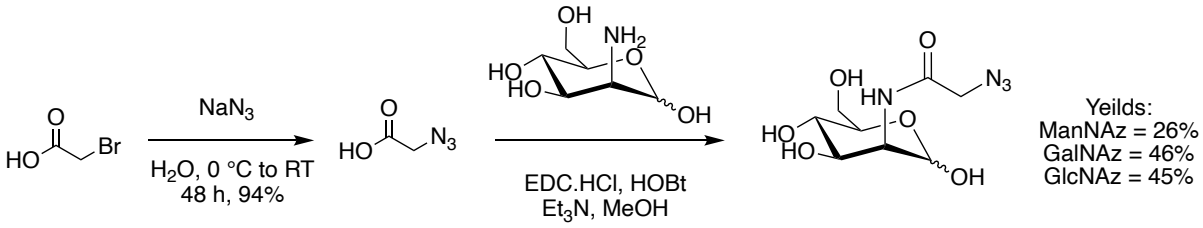

Scheme 5 - Synthesis of azido tagged sugars (ManNAz is used as an example).

Carbamate-linked methyl cyclopropene tagged derivatives of the same sugars (ManNCyoc, GalNCyoc and GlcNCyoc) were prepared as described by Patterson *et al*. (Scheme 6) via reaction of the corresponding amino sugar and Cyoc-PNP **1**.[113] Purification of the unacetylated sugars for both azide and cyclopropene tags was difficult due to their high polarity, requiring chromatography with a high polarity eluent (10-20% MeOH in DCM), which resulted in co-elution with DIPEA and other impurities. This has previously been reported with azide tags and is usually not a problem as the impurities can be removed after the tetra-acetylation step and the only purpose of the chromatography is to remove unreacted ManN.HCl and EDC.[116] However, as the target here was lower levels of acetylation, attempts were made to improve the separation at this stage, to remove excess triethylamine and HOBT. Use of an acidic modifier (0.5 % acetic acid) in the eluting solvent was attempted, with protonation of amines aiding chromatographic seperation[117, 118], but this had limited success in removing the polar impurities more than the unmodified solvent system.

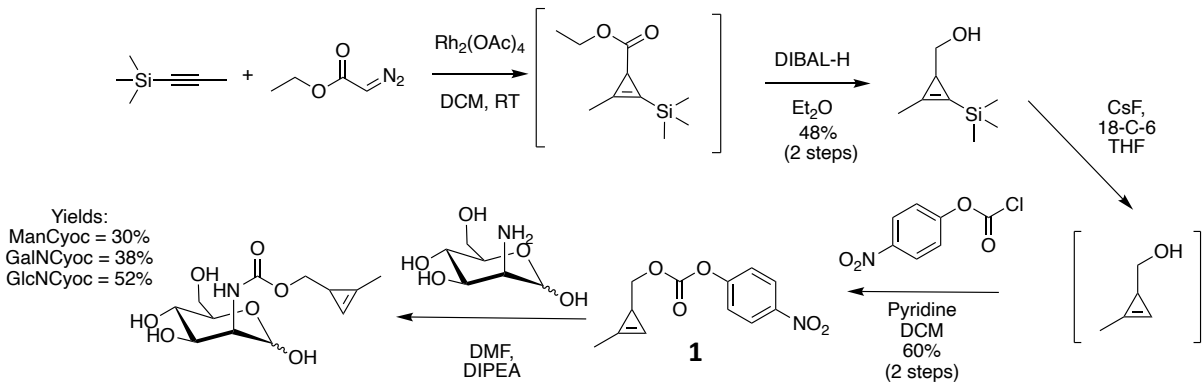

Scheme 6 - Cyclopropene tagged sugar synthesis (ManNCyoc used as an example).

To synthesise the tetra-acetylated derivatives, the unacetylated sugar was dissolved in excess pyridine and acetic anhydride and stirred overnight (Scheme 7). This was applied to all the sugars and gave the respective products as a mixture of anomers.

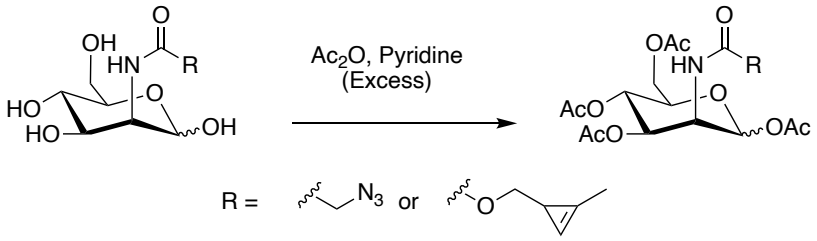

Scheme 7 - General procedure for synthesis of tetracetylated sugars (Man used as an example).

To synthesise the analogues with intermediate levels of acetylation (Ac_1 to Ac_3) the unacetylated sugar was reacted with the corresponding stochiometric equivalents of acetic anhydride, using pyridine as a solvent (Scheme 8). For example, to give a mono-acetylated sugar, the substrate was dissolved in pyridine and 1 equiv. of acetic anhydride added.

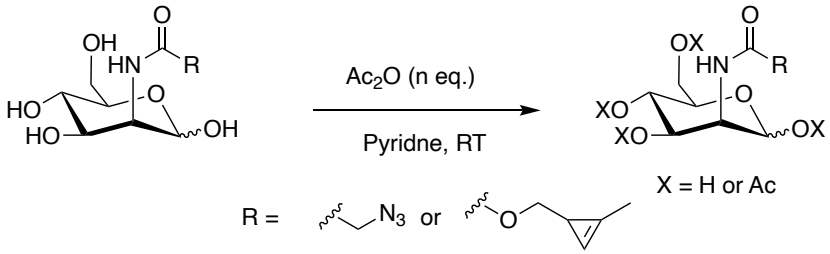

Scheme 8 - Synthesis of variably acetylated sugars via stochiometric addition of acetic anhydride (Man used as an example).

The reaction with stochiometric Ac_2O produces products a mixture of products, in terms of the degree of acetylation (e.g., mono-, di- *etc*.), the regiochemistry of the acetylation and the anomer produced. This makes separation difficult via normal phase chromatography, due to the overlap of products. To minimise the formation of over acetylated products (*e.g*., di- when synthesising mono-) the protocol was adjusted, and the acetic anhydride was added in slowly and pre-diluted in pyridine. This helped to control the degree of acetylation to some extent, but a mixture of products remained. High-performance liquid chromatography (HPLC) of the crude reaction mixtures was attempted but a lack of a strong UV signal, as well as a failure to find a gradient that gave efficient separation, meant this method was unsuccessful.

The mixture of anomers, as well as degree and position of acetylation made the ^{1}H and ^{13}C NMR difficult to interpret, particularly in the crude samples. This was further complicated for the

cyclopropene tagged sugars due to the use of racemic (2-methylcycloprop-2-en-1-yl)methanol to prepare the sugar.

For the more polar/lower degree of acetylation sugars (mono- and di-acetylated) normal phase chromatography gradients and conditions were optimised to access the desired product with good control of the degree of acetylation. However, there was no control of the position of acetylation. The degree of acetylation was confirmed by ^{1}H NMR and high resolution mass spectroscopy (HRMS). For Cyoc sugars, ^{1}H NMR was used for determination of the degree of acetylation by comparison of the integration of the acetyl peaks (~2.1 ppm) relative to the alkene proton of the cyclopropene (~6.7 ppm) – note that the peak at ca. 2.17 ppm is the methyl group on the cyclopropene. For the azido sugars, the level of acetylation was assigned by comparison of the integral of the main anomeric signal with the acetyl peaks. Further details can be found in section 5.2.

For the less polar tri-acetylated products the above methods were unsuccessful. This is because the tri-and tetra-acetylated derivatives co-eluted under all the gradients/conditions attempted. In preliminary *in vitro* experiments conducted by Flaviu Bulat, Shahd Fouad and myself, this mixture of products was used as is. However, due to the promising nature of the results with crude Ac_3ManNCyoc, alternative routes were sought for a more selective synthesis of the triacetylated derivatives.

One route which was envisioned involved selective protection of the anomeric position (Scheme 9). The anomerically protected sugar could then be reacted with excess pyridine and acetic acid (the same conditions as used for the tetra-acetylated derivatives) to acetylate the remaining free hydroxyl groups. Finally, the anomeric protecting group could be cleaved to give the triacetylated sugar. This was attempted using *N*-methylhydroxylamine as the anomeric protecting group, based on previous reports by Dasgupta et al.[119] The *N*-methylhydroxylamine forms the β-anomer selectively, and the subsequent hydrolysis causes interconversion to the α-anomer.

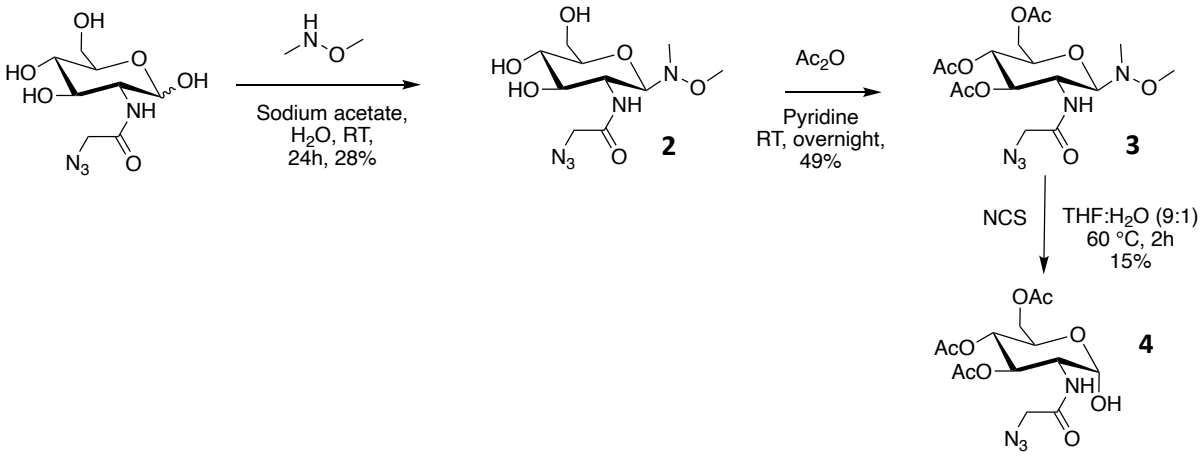

Scheme 9 - Selective anomeric protection route. The route was successful for synthesis of GlcNAz but deprotection conditions were incompatible with the cyclopropene handle.

The selective anomeric protection route was successfully carried out on GalNAz, to give the triacetylated sugar selectively, in terms of both degree and position of acetylation. The reaction proceeds with anomeric selectivity from the first step, with *N*-methylhydroxylamine forming the β-anomer of **2** selectively. The stereochemistry is retained in the conversion to **3,** with the final deprotection hydrolysis causing interconversion to the α-anomer of **4**.[119] Only the α-anomer was observed by ^{1}H NMR, but due to the small amount of material recovered and hence dilute NMR it is possible there was some small degree of β-anomer that was not detected (formed in the synthesis or via mutarotation). Separating the resulting Ac_3GalNAz product from residual NCS or by-product succinimide proved challenging, with succinimide signals found in the product ^{1}H NMR. The instability of the cyclopropene was also a concern. An analytical sample of Ac_4ManCyoc was reacted with NCS at 60 °C and followed by TLC. Degradation of the sugar was observed, this is understandable given the instability of the cyclopropene under similar conditions in the literature.[91, 110] instability to acid in particular was noted, and so the potential liberation of HCl in the reaction mixture, as well as chlorination of the cyclopropene are likely causes of the degradation.

Because of these issues, an alternative route was designed. Instead of selective protection/deprotection, selective deacetylation was attempted. Numerous reports in the literature exist for conditions to selectively deacetylate the anomeric position of mono-, di- and polysaccharides, including the use of hydrazine hydrate[120], ammonium carbonate[121] and zinc acetate.[122] It was found that that addition of ammonia (7M in MeOH) to a solution of the monosaccharide in THF, as described by Fiandor *et al*.[123], selectively deacetylated at the anomeric position and, crucially, was compatible with both the methyl cyclopropene and azide motifs (Scheme 10). The procedure is selective for the α-anomer as reported[123], with small amounts of the β-anomer present in the ^{1}H NMR seen over time,

perhaps as a consequence of mutarotation. The stereoselectivity of the reaction is not believed to be due to reaction of only one anomer, as complete starting material consumption was observed, and in the initial report by Fiandor *et al*[123] 100% α and 100% β solutions both fully reacted, deacetylating selectively, and only forming only the α anomer. Despite this the deacetylation reactions conducted in this report all had yields of 50% or lower. Complete consumption of starting material and earlier reports[123] suggest this is not due to only one anomer reacting, and no other byproducts were observed by TLC. However, we believe the basic or nucleophilic properties of ammonia could have reacted at the anomeric position or with the cyclopropene to form a byproduct, which due to the polar amine formed remained on the baseline of the TLC (and hence would not elute in the column). However, no analytical data was collected to support this hypothesis.

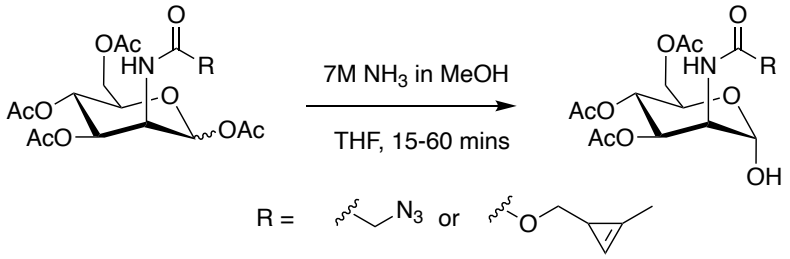

Scheme 10 - Selective deacetylation using 7M ammonia in MeOH

The selective deacetylation procedure was applied to all 6 sugars, and in conjunction with the tetra-acetylation and unselective mono/di-acetylation methods led to the complete panel of sugars being produced (Ac_1 to Ac_4 ManNCyoc, GalNCyoc, GlcNCyoc, ManNAz, GalNAz and GlcNAz).

The corresponding probes for the tagged sugars were synthesised, with TMDIBO-Lys-AlexaFluor647 acting as the strained cyclooctyne for SPAAC (further discussion on SPAAC probes can be found in 3.1) to react with the azide tag, and the PEG-linked tetrazine (Tz-PEG_{11}-AlexaFluor647) to react with the methylcyclopropene tag via IED-DA. The probes were synthesised in 10 and 5 steps respectively. synthesis of both probes is detailed in Scheme 11 and Scheme 12 below but has been discussed in more detail in other reports.[124-128] The tetrazine probe synthesis started from a precursor (dipyridyl tetrazine) synthesised by Yelena Wainman, the TMDBIO-Lys synthesis was carried out from the commercially sourced 4-Allyl-1,2-dimethoxybenzene.

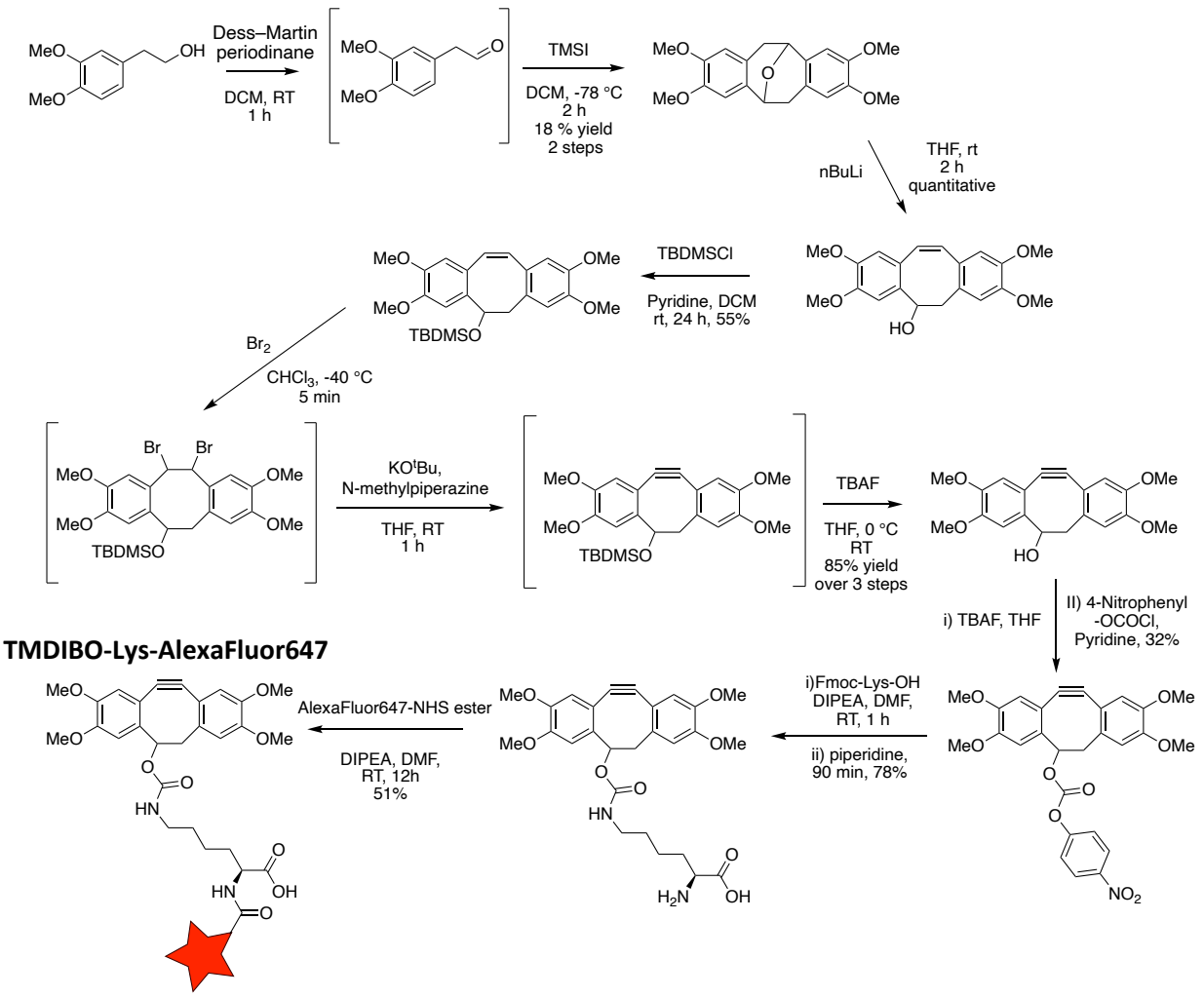

Scheme 11 - Synthesis of TMDIBO-Lys-AlexaFluor647.

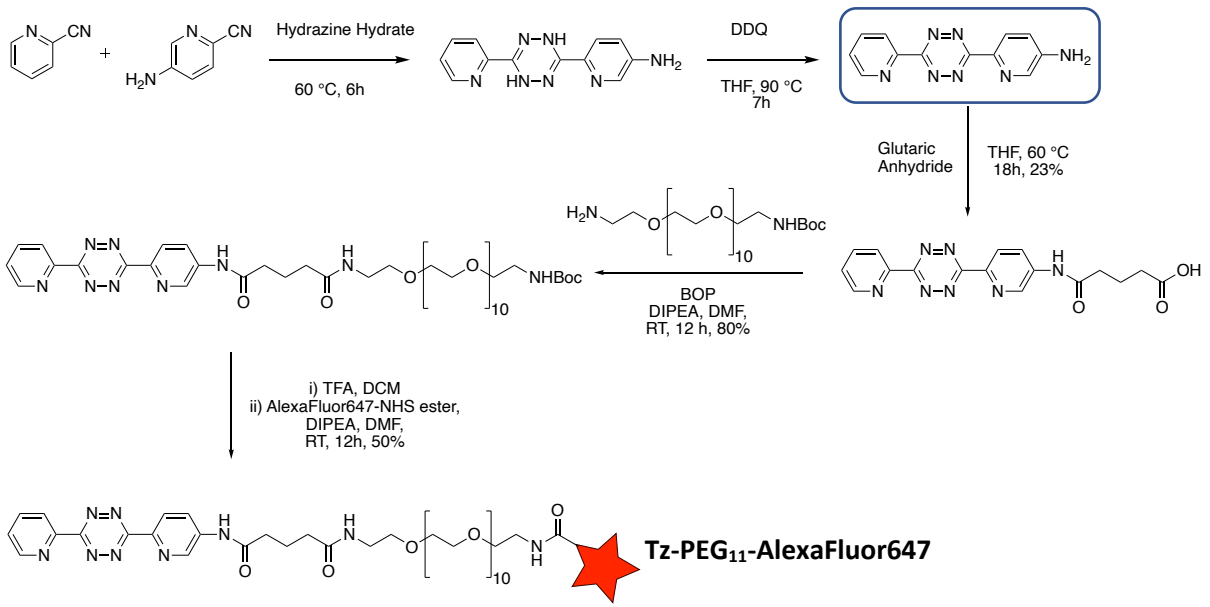

Scheme 12 - Synthesis of Tz-PEG$_{11}$-AlexaFluor647. Synthesis up to dipyridyl tetrazine (highlighted in blue box) was carried out by Yelena Wainman.

2.2.2. In Vitro Labelling

The complete acetylation panel was then taken forward to be tested *in vitro*. The initial cell line chosen for our *in vitro* studies was COLO205, a human cell line derived from the colon of a 70-year-old patient with a colorectal adenocarcinoma by Semple *et al*.[129] The rationale for the selection of this cell line was multi factorial. Firstly, the cell line was readily accessible due to ongoing projects within the Brindle group, which also meant there was expertise in handling the cell line. Further to this, early detection of colorectal cancer has been sought due to the importance of early diagnosis.[130] This is highlighted by the decrease in 5-year survival rates from 92% with stage I colon cancer (in the US) to only 12% with stage IV/metastatic colon cancer.[130]

The *in vitro* labelling strategy is shown in Figure 20. Previous labelling experiments carried out within the group (in particular by Flaviu Bulat) had optimised the conditions for the most efficient labelling *in vitro*, which could then be directly translated *in vivo*. Cells treated with azido tagged sugars were incubated with the TMDIBO-Lys-AlexaFluor647 probe and cells treated with cyclopropene tagged sugars were labelled with a tetrazine-PEG_{11}-AlexaFluor647 dye.

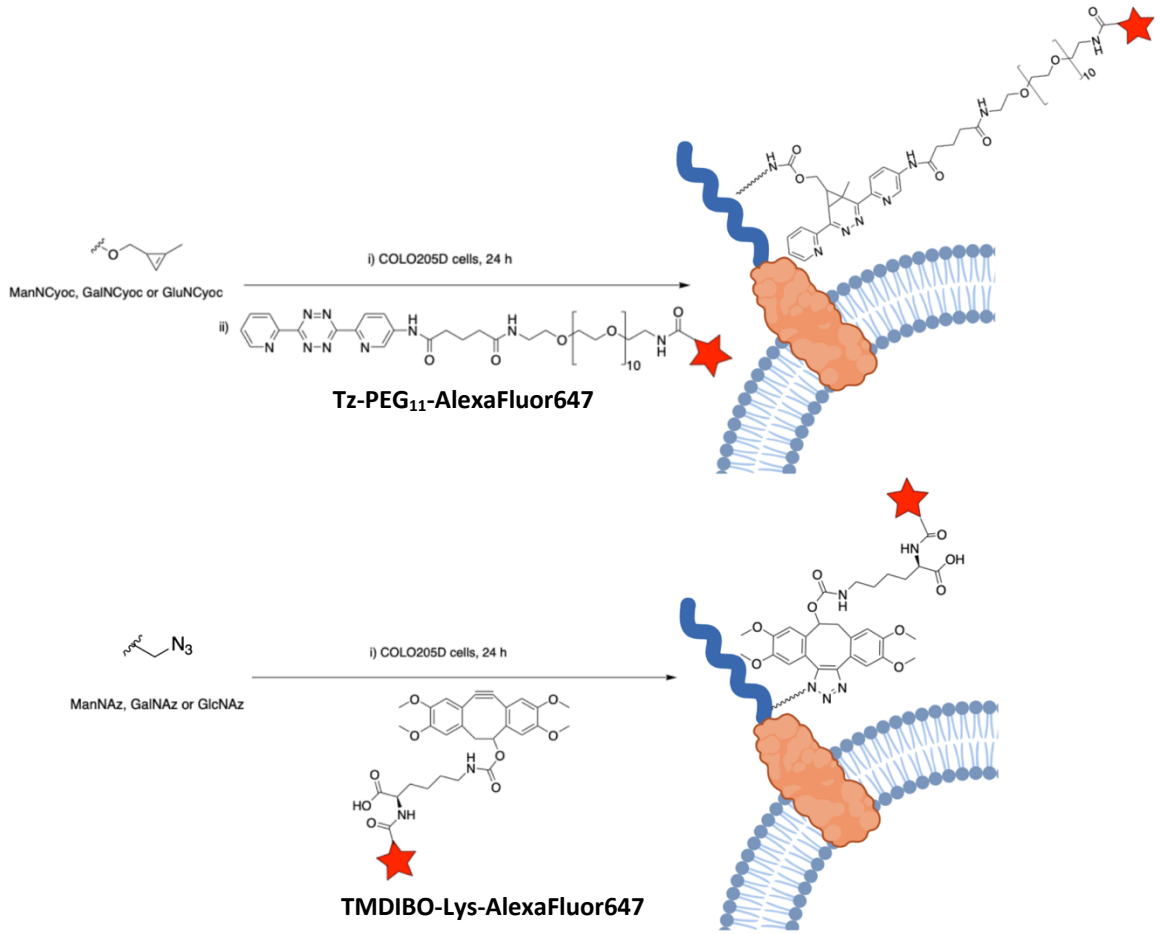

Figure 20 - In vitro labelling strategy.

A two-step labelling approach (*e.g.*, first reacting the cells with Tz-biotin and then labelling with a fluorescently labelled neutravidin) is widely used in literature. This often results in improved contrast due to a reduction in the background signal, resulting from the neutravidin exhibiting less nonspecific binding.[100] However, this was not used for our studies as it would not be possible to use this method *in vivo.* Instead, a dipyridyl tetrazine directly PEG-linked to a fluorescent motif was used. The PEG linker is important for reducing the overall hydrophobicity of the probe and therefore reducing the nonspecific binding and hence lowering background signal. For the data contained in this thesis AlexaFluor647 was used as the fluorophore, unless otherwise stipulated. The *in vitro* labelling protocol was carried out as illustrated in Figure 21.

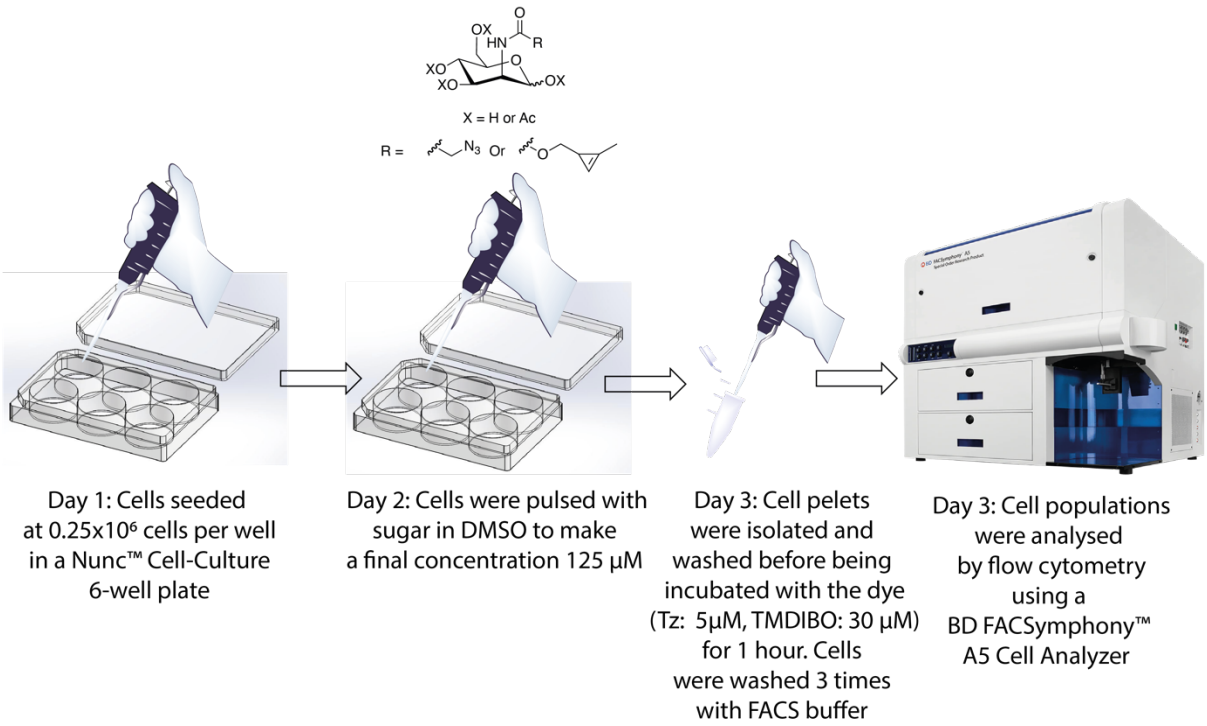

Figure 21 - In vitro labelling protocol description.

The poor aqueous solubility of Ac_4ManNCyoc was immediately apparent upon addition of the sugar in DMSO (stock solution of 110 mM) to the cell media, with visible turbidity. This was not observed with the other degrees of acetylation. Quantification of the cell-labelling by flow cytometry is shown in Figure 22. The MFI (median fluorescent intensity) is a measure of the fluorescent intensity of a population. The distribution of this intensity for each population can be visualised by histograms for (Appendix section 7.1 for this experiment and other acetylation experiments). There was a large increase in contrast (signal-to-background ratio, SBR) between the widely used Ac_4ManNCyoc (5.2 ± 0.5) monosaccharide and the tri- and diacetylated derivatives (16.6 ± 0.8 and 17.4 ± 0.4 respectively). The SBR in this case, is the ratio of fluorescent intensity of the desired population (e.g., cells treated with a certain level of acetylation) relative to the fluorescent intensity of the cell population treated with the dye alone (the background signal). Higher ratios indicate good incorporation of the chemically tagged sugar and subsequent bioorthogonal reaction. Increased non-specific binding can result in increased background signal, decreasing the SBR. The high SBR with Ac_3/Ac_2ManNCyoc presumably comes because the decreased hydrophobicity of the Ac_3 and Ac_2, makes the substrates more water-soluble. This overcomes the solubility limitation of Ac_4ManNCyoc, which reduces the availability of the tetra-acetylated substrate to the cells. In contrast, Ac_3ManNCyoc and Ac_2ManNCyoc strike a balance between being hydrophilic enough to be suitably aqueous soluble, without compromising too much their ability to perfuse the cell membrane. Ac_1ManNCyoc tends to the other extreme - while the aqueous solubility is good, the substrate is now so polar that cell perfusion is reduced, limiting the

substrate availability in the cell for the native glycosylation processes and resulting in decreased SBR (3.8 ± 0.3). Histograms for this experiment (and other acetylation experiments) can be found in Appendix section 7.1.

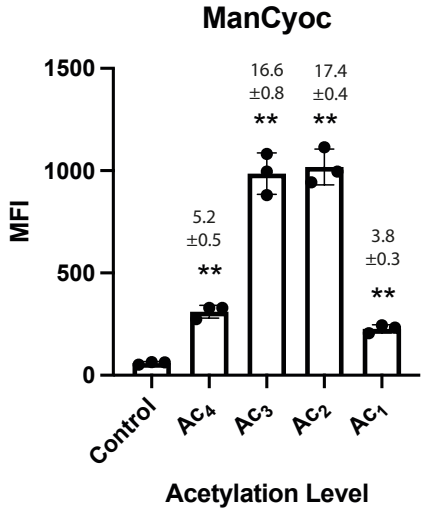

*Figure 22 – Treatment of COLO205 cells with ManNCyoc acetylation panel. COLO205 cells were incubated in the presence or absence (control) of the indicated Ac_xManNCyoc sugar at 125 μM (Ac_1, Ac_2, Ac_3 or Ac_4) for 24 h. They were then incubated with dyes (Tz- PEG_{11}-AlexaFluor647 (5 μM); + Sytox green cell death stain, (50 nM) for 1 h at 37 °C, then washed and analysed by flow cytometry. Median fluorescence intensity (MFI) is shown as mean ± SD. Signal-to-background ratios (SBR) relative to the control (PBS) are shown above each bar; n=3 technical replicates. Statistical analysis was performed using an unpaired t test with Welch correction (**** P≤0.0001,*** P≤0.001,** P≤0.01,* P≤0.05). 2 independent replicates conducted on different days produced comparable results*

Following the promising results displayed with the Ac_xManNCyoc panel, Ac_xGalNCyoc and Ac_xGlcNCyoc panels were labelled as previously described and analysed by flow cytometry (Figure 23). Overall, there is a large decrease in contrast when Ac_xGalNCyoc and Ac_xGlcNCyoc are used for labelling as opposed to their corresponding Ac_xManNCyoc equivalents. This decrease in contrast with Ac_xGalNCyoc and Ac_xGlcNCyoc has also previously been observed in human embryonic kidney[91] (HEK293T), HeLa[131] and Jurkat[113] cells. More widely, the decreased labelling with GalN and GlcN analogues relative to their ManN counterparts has been widely demonstrated with other of chemical tags in a variety of cell lines.[83, 88] The relative decrease comes as a result of a decrease in labelling efficiency with these sugars, due to a lower tolerance of the relevant native enzymes on the biosynthetic pathways towards unnatural analogues.[83] With these sugars the tetra-acetylated sugar was incorporated as well as or better than the sugars with three or fewer acetyl groups. It seems that aqueous solubility is not a limiting factor for Ac_xGalNCyoc and Ac_xGlcNCyoc, and rather the lack of efficient incorporation is what limits the level of labelling. This may explain why the same acetylation profile as with Ac_xManNCyoc is not seen; if the labelling is not limited by the solubility of the sugar,

then the only change upon decreasing the level of acetylation is a decrease in cell permeability, which further decreases the labelling.

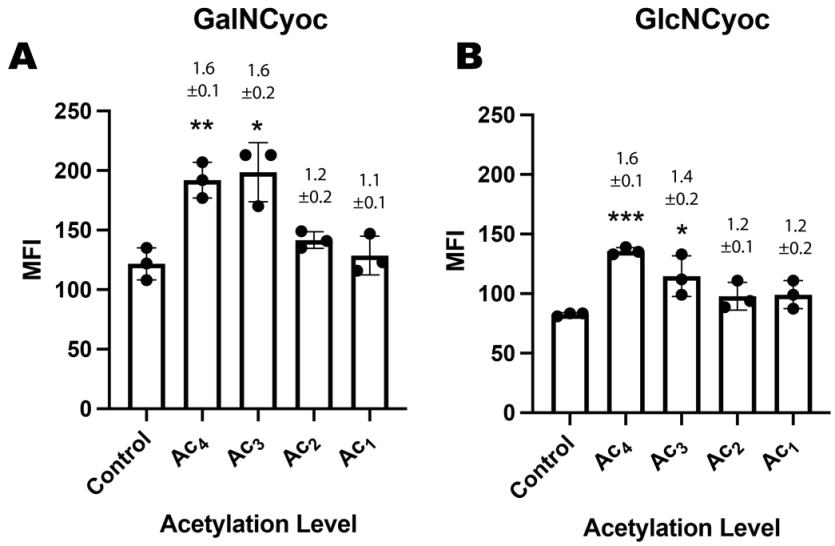

*Figure 23 - Treatment of COLO205 cells with GalNCyoc and GlcNCyoc acetylation panels. COLO205 cells were incubated in the presence or absence of the indicated sugar A) GalNCyoc B) GlcNCyoc 125 µM (Ac1, Ac2, Ac3 or Ac4) for 24 h. They were then incubated with dyes (Tz- PEG_{11}-AlexaFluor647 (5 µM) + Sytox green cell death stain (50 nM)) for 1 h at 37 °C and analysed by flow cytometry. Median fluorescence intensity (MFI) is shown as mean ± SD. Signal-to-background ratios (SBR) relative to the control (PBS) are above each bar; n=3 technical replicates. Statistical analysis was performed using an unpaired t test with Welch correction (**** P≤0.0001,*** P≤0.001,** P≤0.01,* P≤0.05). Independent replicates with each sugar panel, conducted on different days produced comparable results*

It is worth noting that due to the complex biosynthetic pathways and the network of enzymes involved, especially epimerases, monosaccharides can be interconverted. As such a tagged sugar may end up on the cell surface via interconversion. This is particularly known for GlcN analogues which can be epimerised and ultimately expressed as a sialic acid residue, which is known to be possible with GlcNCyoc.[132]

Having completed the *in vitro* panel for the methyl cyclopropene tagged sugars the effect of variable acetylation on azido-tagged sugars was studied. Tetra-acetylated azido sugars do not suffer from the same aqueous solubility limitations due to their reduced hydrophobicity (Figure 24).

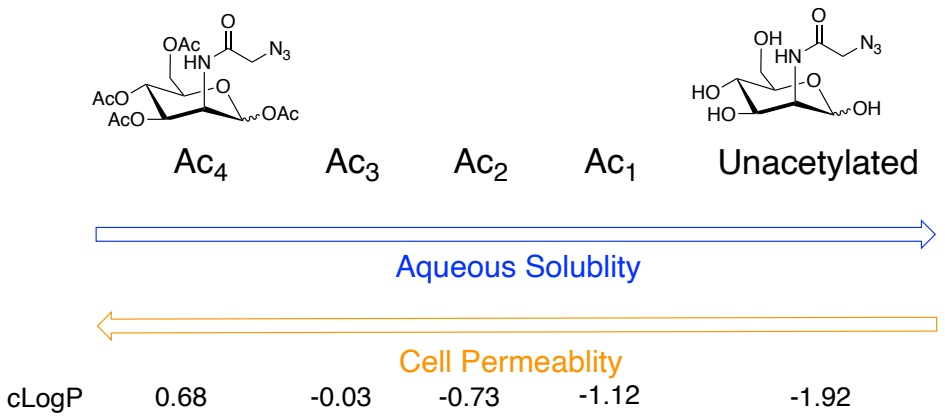

Figure 24 - cLogP of Ac_xManNAz.

As can be seen in Figure 25, decreasing the level of acetylation for Ac_xManNAz below tetra-acetylated, decreased the extent of the subsequent cell surface labelling. This is presumably because aqueous solubility is no longer a concern and is not limiting the substrate availability. Therefore, decreasing the level of acetylation simply decreases cell permeability, reducing intracellular concentration and reducing cell surface labelling. For Ac_xGalNAz and Ac_xGlcNAz this same profile was not as prevalent. This again is believed to be due to the decrease in promiscuity of the native biosynthetic pathways towards unnatural substrates, as previously discussed.

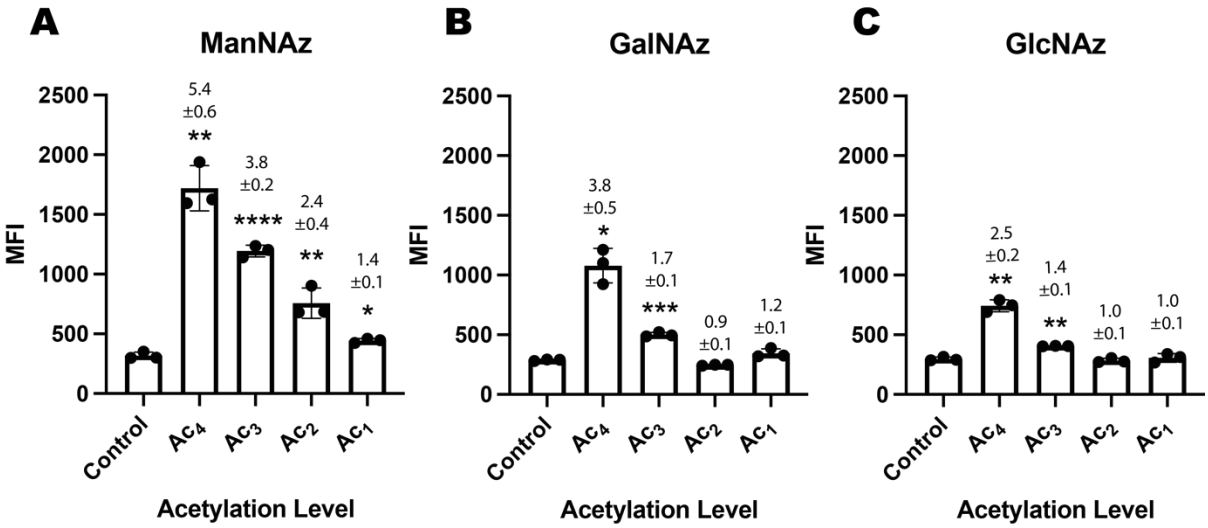

*Figure 25 - Treatment of COLO205 cells with ManNAz, GalNAz and GlcNAz acetylation panels. COLO205 cells were incubated in the presence or absence of the appropriate sugar, A) ManNAz, B) GalNAz and C) GlcNAz 125μM (Ac_1, Ac_2, Ac_3 or Ac_4), for 24 h. They were then incubated with dyes (TMDIBO-Lys-AlexaFluor647 (30 μM) + Sytox green cell death stain (50 nM) for 1 h at 37 °C and analysed by flow cytometry. Median fluorescence intensity (MFI) is shown as mean ± SD. Signal-to-background ratios (SBR) relative to the control (PBS) are above each bar; n=3 technical replicates. Statistical analysis was performed using an unpaired t test with Welch correction (**** P≤0.0001, *** P≤0.001, ** P≤0.01, * P≤0.05).*

The *in vitro* results clearly show that acetylation has a marked effect on the incorporation of unnatural monosaccharides, and their subsequent cell surface labelling. While for the azido tagged sugars,

decreased acetylation led to decreased labelling, for Ac_xManNCyoc this was not the case. Ac_3ManNCyoc and Ac_2ManNCyoc, were shown to have increased labelling compared to the Ac_4ManNCyoc derivative, and importantly were less hydrophobic. These two compounds, therefore, offer potential as novel agents for imaging tumour hypersialylation *in vivo*.

Recent reports[133,134] of non-enzymic *S*-glyco modification of proteins by anomerically deacetylated monosaccharides are not thought to explain the increase in labelling with Ac_3ManNCyoc and Ac_2ManNCyoc (relative to Ac_4ManNCyoc). If the labelling increase seen with Ac_3ManNCyoc and Ac_2ManNCyoc was due to *S*-glyco modification the same effect would have been expected in other di- and triacetylated Cyoc sugars (e.g. GalNCyoc and GlcNCyoc) as GalN and GlcN derivatives have also been described as substrates for *S*-glyco modification. All three azido-tagged sugars have been shown to participate in this modification,[133,134] and in this study none of the lower degrees of acetylation of the azido sugars showed enhanced labelling. Since only Ac_3ManNCyoc and Ac_2ManNCyoc show increased labelling relative to the tetracetylated derivative, this non-enzymatic reaction is unlikely to be responsible for the enhanced labelling.

To experimentally confirm our belief that *S*-glyco modification was not playing a part in the increased labelling with Ac_3ManNCyoc and Ac_2ManNCyoc we aimed to confirm the cyclopropene tags were incorporated as modified sialic acids. Since earlier work had shown DMB derivatisation is incompatible with cyclopropenes, specifically due to the heat/acidic conditions required to cleave the sialic acids.[91] We aimed to find conditions to selectively cleave sialic acid residues from the cell surface post incubation with Ac_3ManNCyoc, cells would then be reacted with the tetrazine probe as usual, and the MFI compared with that of sugar treated (and tetrazine labelled) cells which were not exposed to the cleavage conditions. In this hypothesis it is expected that the MFI would be decreased in cells which had sialic acids cleaved as no cyclopropene tags should be left on the cell surface for the tetrazine to react with. We attempted to achieve this selective cleavage via enzymatic approaches first using neuraminidase from *Clostridium perfringens* (Figure 26). However, this proved unsuccessful with no cleavage of sialic acid residues observed detected and no decrease in signal between the enzyme treated and control samples. This is perhaps unsurprising given neuraminidases are known to be resistant towards similar alkyne handles.[135] Since the same work[135] had shown neuraminidases could tolerate azido tags we attempted to test our neuraminate protocol using Ac_4ManNAz treated cells (labelling with TMDIBO) but again found no decrease in signal between the enzyme treated and control samples. This suggests the protocol was not successfully cleaving sialic acids. We instead attempted to use PNGAse F, which should cleave all *N*-glycans, but again we found no decrease in MFI

between enzyme and non-enzyme treated cells (with both Ac_3ManNCyoc and Ac_4ManNAz). These commercial glycosidases are designed to work on cell lysates, with insufficient time remaining in these studies to find an optimised protocol for removal of tagged cell surface sialic acid residues.

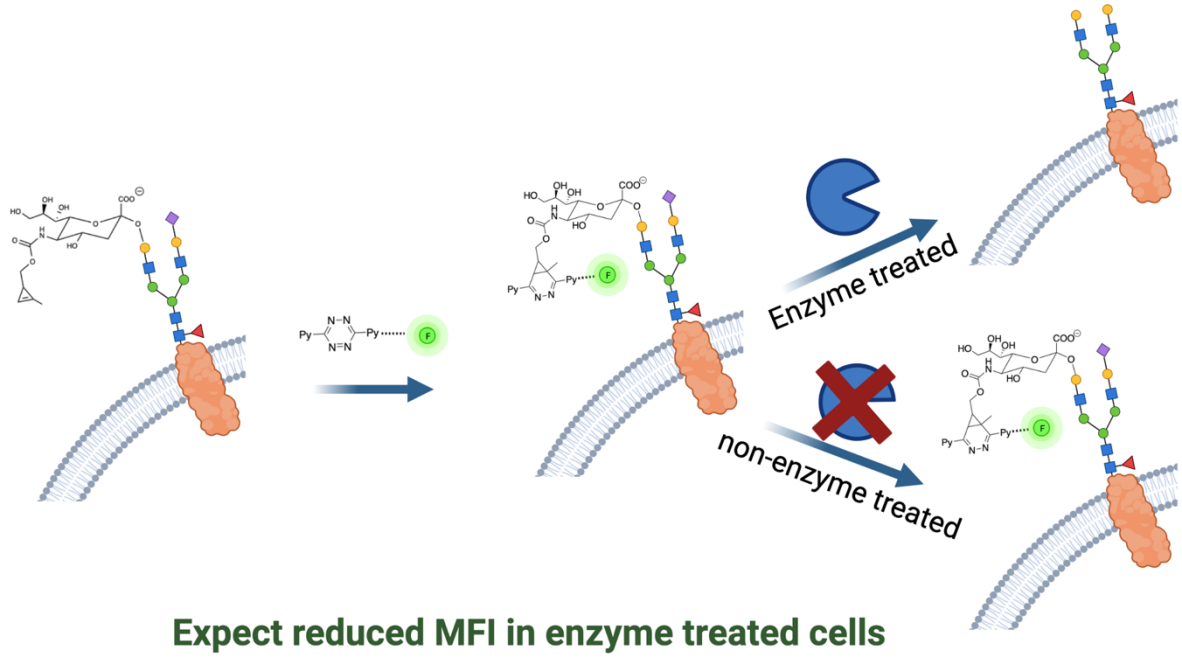

Figure 26 – Unsuccessful attempt to demonstrate incorporation of ManCyoc is via sialic acid pathway. We anticipated a decrease in MFI between cells treated with neuraminidase/PNGase F. No decrease was seen with a lack of enzyme cleavage believed to be the cause.

2.2.3. *In Vivo* Studies

In vivo studies were carried out by Flaviu Bulat and André Neves at CRUK Cambridge institute

For the *in vivo* studies it was decided that Ac_3ManNCyoc would be used. This was due to the greater control of the position and degree of acetylation, resulting in a more chemically defined compound. This, alongside the increased yield of the synthesis, also made the scale up of the synthesis required for the *in vivo* studies easier. The fluorophore on the tetrazine-PEG_{11} probe was changed from AlexaFluor647 to DyLight™ 800 dye (which when used to repeat the ManNCyoc panel *in vitro*, showed comparable SBR). A near-IR dye was sought due to the greater tissue penetration relative to dyes in the visible range Figure 27.[136]

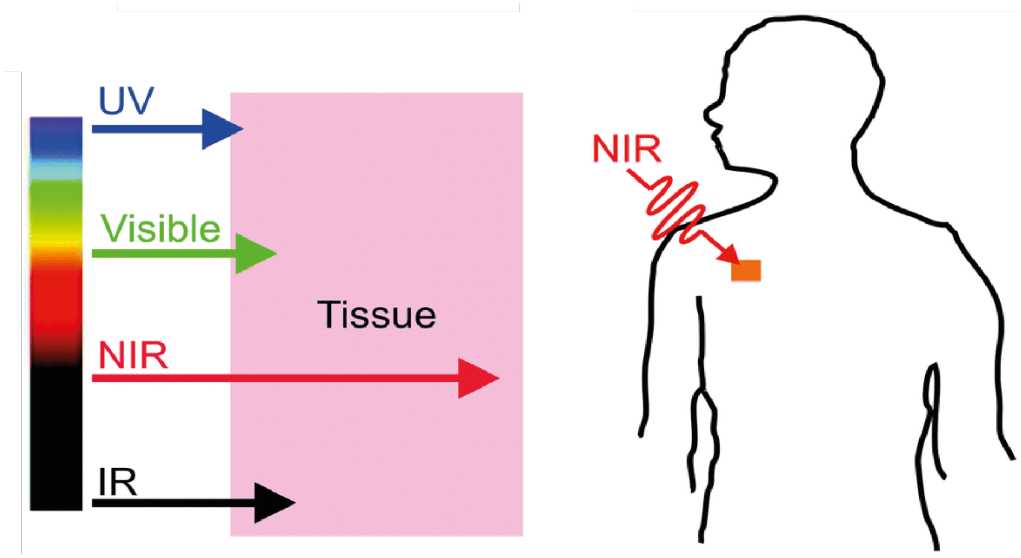

Figure 27 - Improved tissue penetration with near IR fluorophores. Figure taken from Wu et al.[136]

The COLO205 cells that were previously used for the *in vitro* studies were used and were implanted subcutaneously into nude mice. The dosing protocol was designed based on previous experience within the group for metabolic labelling of tumours *in vivo*.[100, 101] Ac_3ManNCyoc (150 mg kg^{-1}) was administered *via* intraperitoneal injection (i.p.) consecutively in a 3-day protocol (n=2, ++) or the mice were treated with solvent vehicle PBS/DMSO (n=2, -+). On day 4 all were treated with tetrazine-PEG_{11}-DyLight800 (0.02 µmol kg^{-1}). On day 5 *in vivo* fluorescence imaging was performed using an IVIS 200 imaging system (Figure 28A). Tumour fluorescence intensity was determined using automated ROI segmentation using Living Image® 4.5 software. (Figure 28B). *Ex vivo* analysis was performed after scanning (Figure 28C).

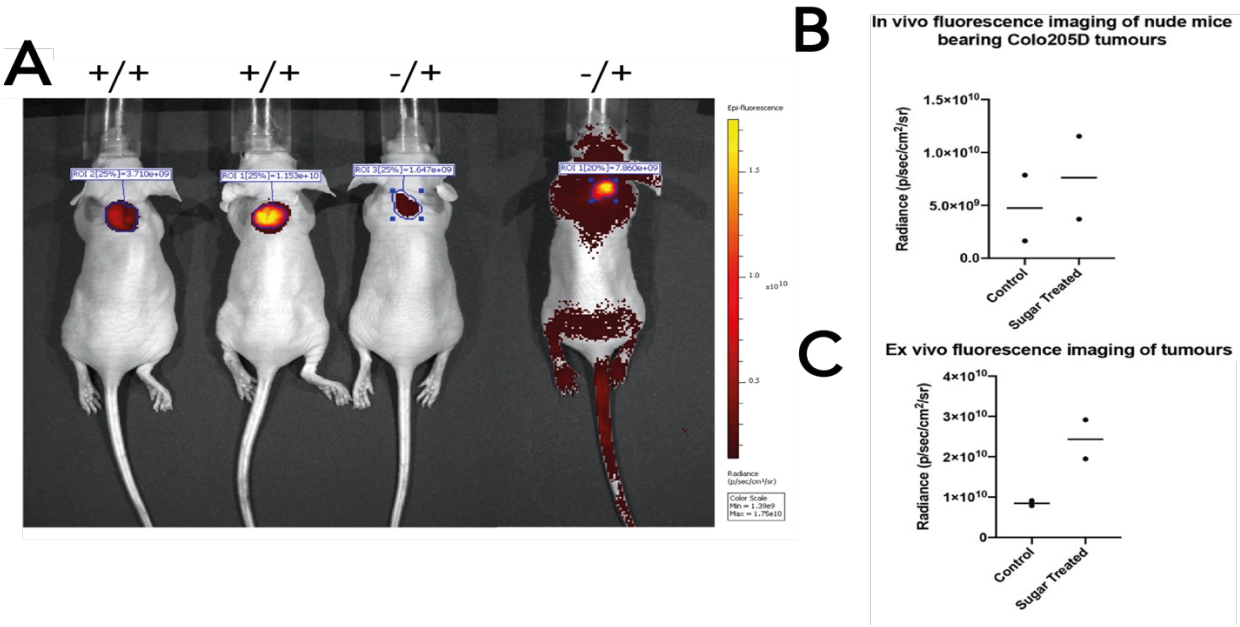

Figure 28 - In vivo imaging of Ac_3ManNCyoc treated mice. (A) Animals treated with Ac_3ManNCyoc and subsequently tetrazine-PEG_{11}-DyLight800 (+/+) and control mice (-/+) treated with fluorescent probe only. (B) Tumour fluorescence intensity (radiance levels) obtained by in vivo fluorescence imaging. (C) Ex vivo tumour imaging.

The initial *in vivo* results were promising with suggestion that there was some difference in fluorescence levels in the tumour, between the mice treated with Ac_3ManNCyoc and those treated with the tetrazine dye alone. Interestingly, the rapid clearance of the tetrazine-PEG_{11}-DyLight800 is highlighted in Figure 28A by a lack of fluorescence in the clearance routes such as the renal system. This led us to believe that this system could be used *in vivo* tool for imaging tumour hypersialylation and we wanted to expand our *in vivo* studies to larger cohorts.

However, due to the Covid-19 pandemic *in vivo* studies were paused. When we were able to return to the lab the tetrazine-PEG_{11}-DyLight800 had visibly degraded, and this was confirmed by unsuccessful labelling *in vitro*. Therefore, for the larger cohort *in vivo* study of tumour hypersialylation in COLO205 tumours, the tetrazine-PEG_{11}-AlexaFluor647 used in the previous *in vitro* studies was used.

The same protocol was then applied to the larger cohorts, with n=6 for the sugar treated cohort and n=5 for the dye alone. The resulting fluorescent imaging and data analysis is shown in Figure 29 below, as well as the *ex vivo* imaging.

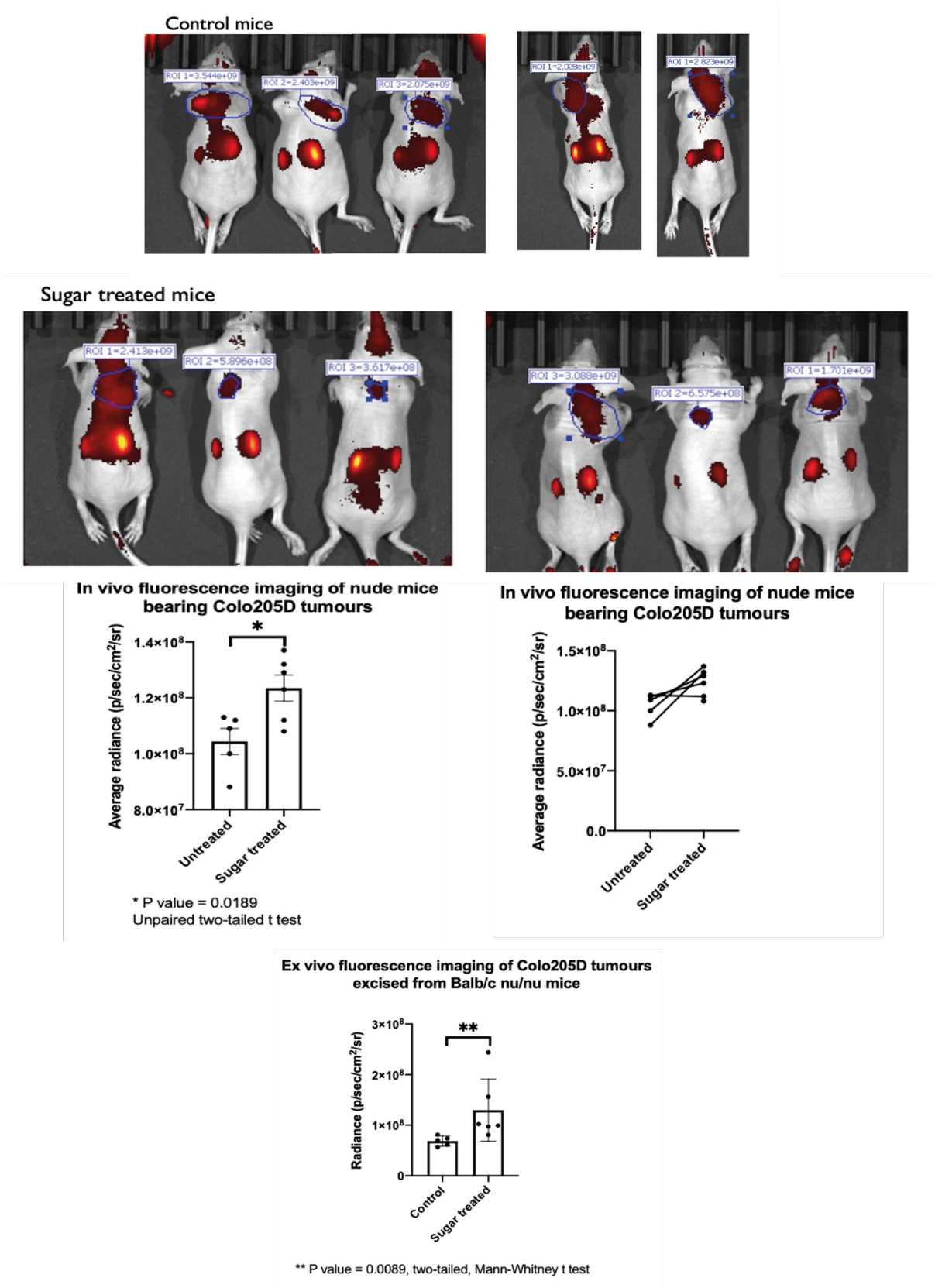

*Figure 29 - Treatment of MDA-MB-231 and PANC-1 cells with ManNCyoc acetylation panel. In vivo imaging with larger cohorts. Sugar treated mice were treated with Ac_3ManNCyoc (150 mg/kg) for 3 consecutive days, untreated mice were injected with solvent vehicle only (PBS:DMSO). On day 3 all mice were treated with tetrazine-PEG_{11}-AlexaFluor647 (0.02 µmol kg^{-1}) and imaged on day 5. (**** P≤0.0001,*** P≤0.001,** P≤0.01,* P≤0.05).*

The larger cohorts demonstrated only a modest contrast between sugar treated and untreated mice, with an overall SBR of 1.2, when the average fluorescent intensity of both populations is compared. This is somewhat enhanced *ex vivo* (SBR = 1.5). This enhancement could be explained by the decreased tissue penetration of the 647 dye (which is somewhat compensated for *ex vivo*). Notably, the clearance of the tetrazine-PEG_{11}-AlexaFluor647, is less efficient. This can clearly be seen in the images taken, with the kidneys clearly highlighted, unlike with the near IR dye. The chemical structures of fluorescent and near IR fluorophores are often significantly different, both between brands and between different emission wavelengths. As such, a return to a near-IR fluorophore, with a similarly good (if not improved) clearance should be used for further studies.

In both Figure 28 and Figure 29 non-specific tumour accumulation of the tetrazine-PEG_{11}-Dylight800 or tetrazine-PEG_{11}-AlexaFluor647 probe is seen. In the non-sugar treated mice there is clearly tetrazine localising in the tumour, and as such this must be via a mechanism independent of the click chemistry reaction. Non-specific uptake of fluorescent probes by tumours is known, and could be minimised by using some more recent clinically approved dyes.[137]

Whilst the use of the 647 fluorophore is one possible reason for the lower than anticipated *in vivo* contrast, it was suggested that the main issue may be the tumour model itself. It has been noted in literature that COLO205 tumour bulks can be heterogeneous *in vivo*.[138] Potentially, this could result in divergent behaviour within the tumour, leading to uneven distribution of labelling.[139] Further to this, it was suggested that COLO205 may not be the best model for monitoring tumour hypersialylation given there are inconsistent levels of tumour hypersialylation in colon cancers,[140] and as sialylation is strongly associated with metastasis,[141] perhaps an alternative cell line, which is more metastatic could demonstrate improved SBR, *in vitro* and *in vivo*.

2.2.4. *In Vitro* Studies with Alternative Cell Lines

The Ac_xManNCyoc panel was tested in two alternative cell lines, MDA-MB-231[142] and PANC-1.[143] These were selected for several strategic reasons, primarily existing expertise within the Brindle group in growing these tumours *in vitro and in vivo,* and their homogeneity *in vivo*. The acetylation panel using Ac_xManNCyoc was carried out in identical fashion to that with COLO205. The resulting flow cytometry analysis is shown in Figure 30.

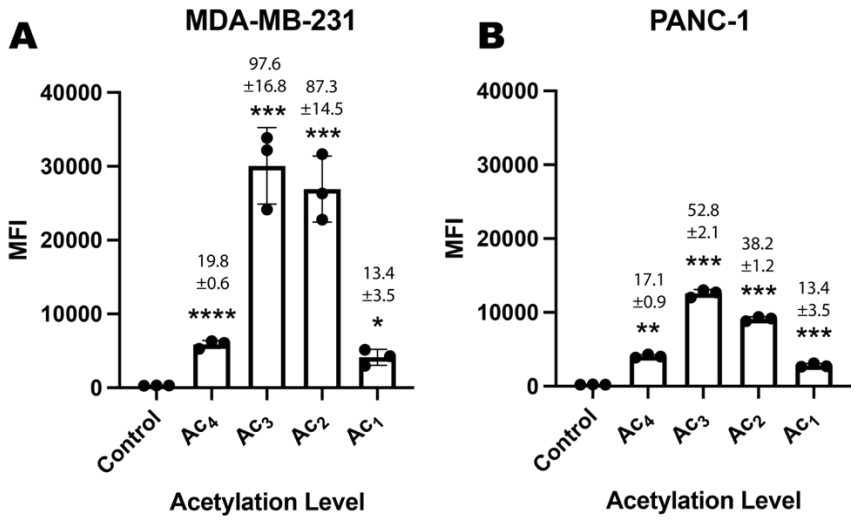

*Figure 30 - (A) MDA-MB-321 and (B) PANC-1 cells were incubated in the presence or absence (control) of the appropriate $Ac_xManNCyoc$ sugar 125μM (Ac_1, Ac_2, Ac_3 or Ac_4) for 24 h. They were then incubated with dyes ($Tz\text{-}PEG_{11}$-AlexaFluor647 (5 μM) + Sytox green cell death stain (50 nM)) for 1 h at 37 °C, then washed and analysed by flow cytometry. Median fluorescence intensity (MFI) is shown as mean ± SD. Signal-to-background ratios (SBR) relative to the control (PBS) are above each bar; n=3 technical replicates. Statistical analysis was performed using an unpaired t test with Welch correction (**** P≤0.0001,*** P≤0.001,** P≤0.01,* P≤0.05).*

Enhanced labelling was demonstrated in both new cell lines for all levels of acetylation, relative to the previous COLO205 model. Our best candidates from the previous *in vitro* studies (Ac_3ManNCyoc and Ac_2ManNCyoc) showed much greater contrast, with Ac_3ManNCyoc enhancing from 16.6 ± 0.8 in COLO205 cells to 52.8 ± 2.1 in PANC-1 cells and 97.6 ± 16.8 in MDA-MB-321 cells. Similarly, with Ac_2ManNCyoc the contrast increased from 17.4 ± 0.4 to 38.2 ± 1.2 and 87.3 ± 14.5, respectively. Even the solubility limited Ac_4ManCyoc and cell perfusion limited Ac_1ManNCyoc showed enhanced contrast.

As such, the MDA-MB-231 and PANC-1 cell lines have promising potential to improve the *in vivo* contrast previously demonstrated with the COLO205 model. The increased level of labelling *in vitro*, is probably a consequence of an increased level of sialylation in these tumour lines, with the result that more ManNCyoc is expressed on the surface of the cell (because of upregulation of enzymes in the sialylation pathway) which can subsequently react with the tetrazine probe. There could also be a potential increase in tumour homogeneity *in vivo* using the MDA or PANC-1 models, which could help increased *in vivo* contrast.

Unfortunately, due to the ongoing financial constraints at CRUK caused by COVID, and difficulties with Home Office licensing, further *in vivo* work is yet to be completed. Further discussion of the planned work and potential applications is contained in the future work section 2.4.2.

2.2.5. Fluorescent Microscopy

The scanning of the fluorescent microscopy plates was carried out by Heather Zecchini at CRUK Cambridge

To better visualise the labelling on a cellular level, fluorescent microscopy experiments were conducted. The protocol previously used within the group[92] was adapted. Instead of a cover slip approach, the experiment was simplified using ibidi's µ-Slide 8 well (Figure 31). This meant the cells could be grown in the plates, the sugars added, and the labelling procedure carried out all in the wells. The plates are then imaged (from underneath) using fluorescent microscopy.

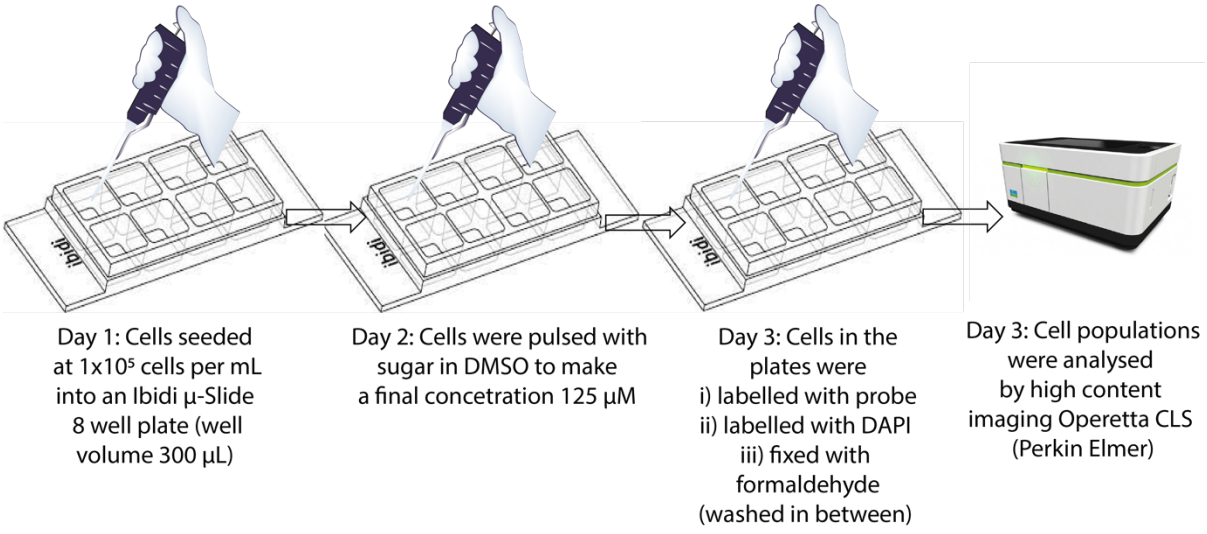

Figure 31 - Adapted fluorescent microscopy protocol.

The first cell line studied via this method was PANC-1 cells. This is due to their strong adhesive behaviour in culture, meaning the protocol is easier to conduct as the cells are less perturbed during the labelling and washing procedure. Despite this, a lot of cells were lost during the process and on some occasions, images with high cell density were hard to obtain.

First the labelling of Ac_3ManNCyoc treated PANC-1 cells with Tz-PEG_{11}-AlexaFluor647 was compared to PANC-1 cells treated with the tetrazine probe alone (Figure 32). As expected, there was clear difference between the two populations, with sugar treated samples showing a strong red staining around the cell, which corresponds to our tetrazine-PEG_{11}-AlexaFluor647 probe. In the non-sugar treated sample, there was minimal non-specific accumulation of the dye across the cell.

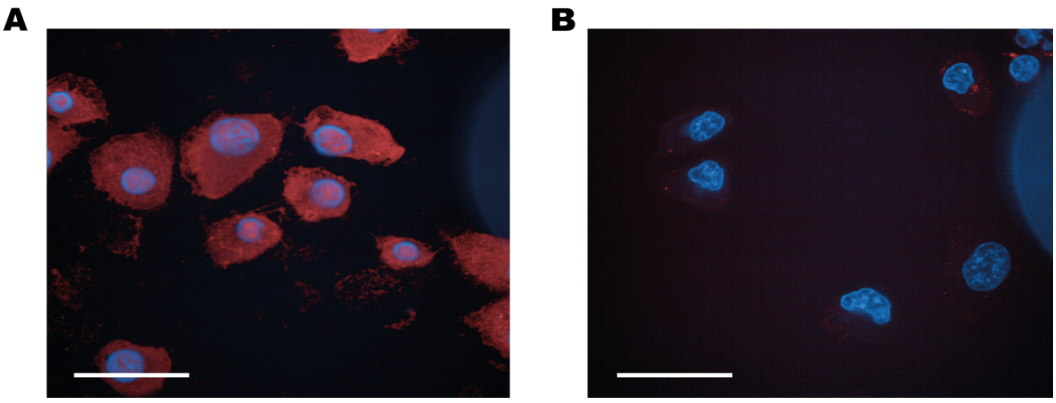

Figure 32 - Fluorescence microscopy of PANC-1 cell glycans. Cells were cultured with (A) or without (B) $Ac_3ManNCyoc$ (125 µM) for 24 h and then incubated with solution of Tz-PEG_{11}-AF647 (5 µM) and DAPI (100 nM), Red: AF647, Blue: DAPI nuclear stain, scale bar 50 µm.

However, there was an unexpected irregularity with the staining. Staining was observed across the cell, including in the centre where the DAPI indicates this is an intracellular/nuclear environment. It was anticipated that if the DAPI overlay is removed you would only see extracellular labelling forming a "halo" like effect with no signal in the cell cytoplasm. This was not believed to be due to intracellular labelling as the charged dye on the tetrazine probe makes it unlikely to be able to efficiently diffuse into the cell (especially given the 1-hour incubation). The instrument scanning parameters were then varied with the suggestion that the problem was in some way caused by the image plane that was taken with the hypothesis that the staining seen across the cell, which looked like intracellular labelling was due to the spherical nature of the cell and was staining on the top/bottom of the cell surface. However, despite attempts at optimisation including running a large z stack with multiple planes (Figure 33) no correction was found.

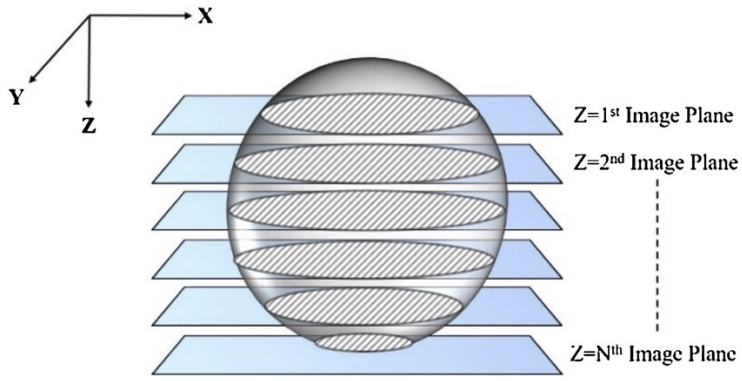

Figure 33 - Visual explanation of Z stack. Figure taken from Trivedi and Mills.[144]

The sugar used was next studied as a possible cause. To do this the experiment was repeated but additional wells were used to treat cells with $Ac_4ManNAz$, which were then labelled with TMDIBO, a

combination previously shown to produce the halo effect expected.[124] As can be seen in Figure 34 the labelling across the cell was seen with both sugar/dye combinations. As this had not been seen in the previously TMDIBO publication this suggested there was something wrong with the experimental set-up as opposed to the compounds used. The protocol was altered to fix the cells with formaldehyde before staining with the dye and DAPI, but this led to no improvement (unsurprising given fixation often leads to permeabilisation). Cells were also treated with Ac_3ManNAz, with the same labelling profile seen, confirming this was not due to the tri-acetylated nature of the sugar.

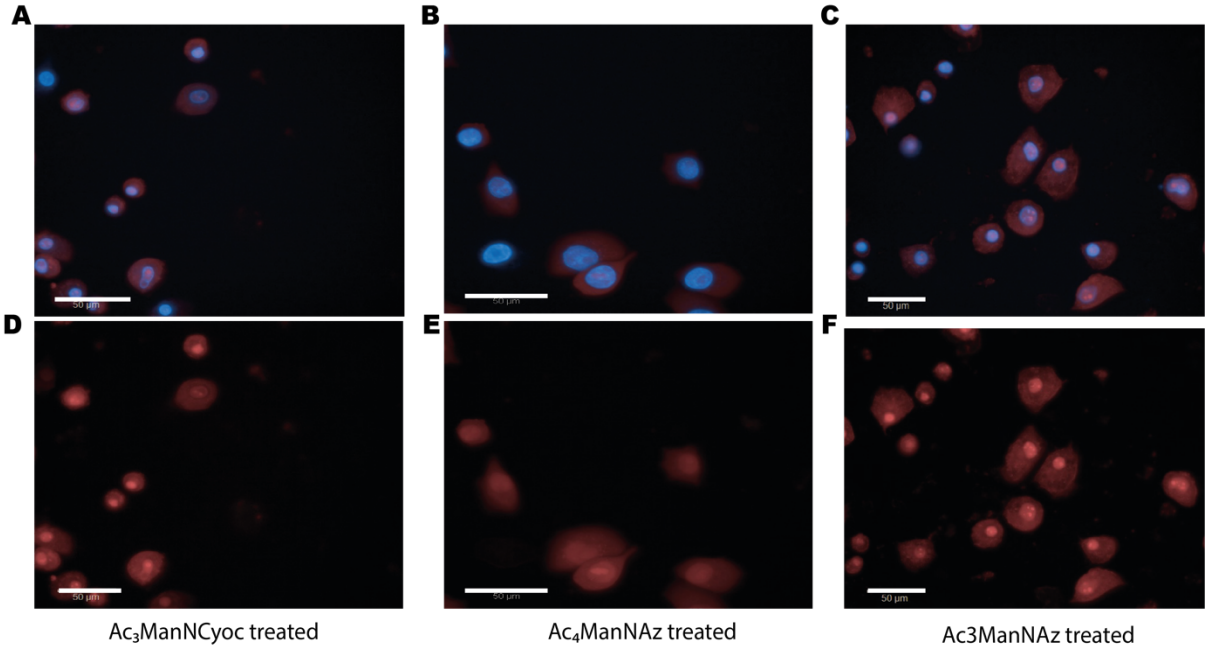

Figure 34 - Fluorescence microscopy of PANC-1 cell glycans. Cells were cultured with Ac_3ManNCyoc (125 µM) (A and D), Ac_4ManNAz (125 µM) (B and E) or Ac_3ManNAz (125 µM) (C and F) for 24 h. Wells were then incubated with a dye solution containing DAPI (100 nM) and either Tz-PEG_{11}-AlexaFluor647 (5 µM) (A and D) or TMDIBO-Lys-AlexaFluor647 (50 µM) (B, C, E and F)), Red: AF647, Blue: DAPI nuclear stain, scale bar 50 µm. Top row of images (A-C) is overlay of both 647 and DAPI channels, the bottom row (D-F) have the DAPI overlay removed.

The cell line treated was varied, with suggestion the unusual labelling distribution could be in part due to the "leaky" nature of the pancreatic duct cells.[145] MDA-MB-231 were used, again due to their adherent culture growth meaning they would not be washed away during the many washes with FACS buffer post-staining. A further small modification was made to the protocol. In previous experiments when cells were washed, the supernatant was removed via aspiration. As this is quite an aggressive motion, it was believed a lot of cells were removed because of the aspiration. The new method involved instead simply removing the supernatant via a Gilson pipette (the same pipette as was used to add the washing solution). This new method was seen to visually increase cell density during imaging.

The images collected for the MDA-MB-231 stained cells are shown in Figure 35 below. The effect of the different levels of acetylation of $Ac_xManNCyoc$, which had previously demonstrated to show variable labelling, was studied to see if it affected the positioning of the labelling in relation to the cell. The use of MDA-MB-231 cells helped reduce the problem with the lack of clear membrane staining. The clear membrane staining is further supported by the intensity plots to the right of the images collected for each acetylation level in Figure 35. In the sugar treated cells there is a clear maximum in intensity as the line passes across the membrane, which then dips across the cell before maximising again as it hits the other side of the cell membrane, showing the clear membrane staining. In the dye alone treated sample there is a maximum across the entire cell, with no difference between the membrane and intracellular environments. It is believed this is due to some autofluorescence from the cell in the 647 channel, hence its constituency across the cell and its low intensity relative to the membranes of sugar-treated cells (this also explains why the intensity does not tend to zero in the middle of the sugar treated cells). There was no significant difference noticed in the distribution of labelling between the levels of acetylation of $Ac_xManNCyoc$.

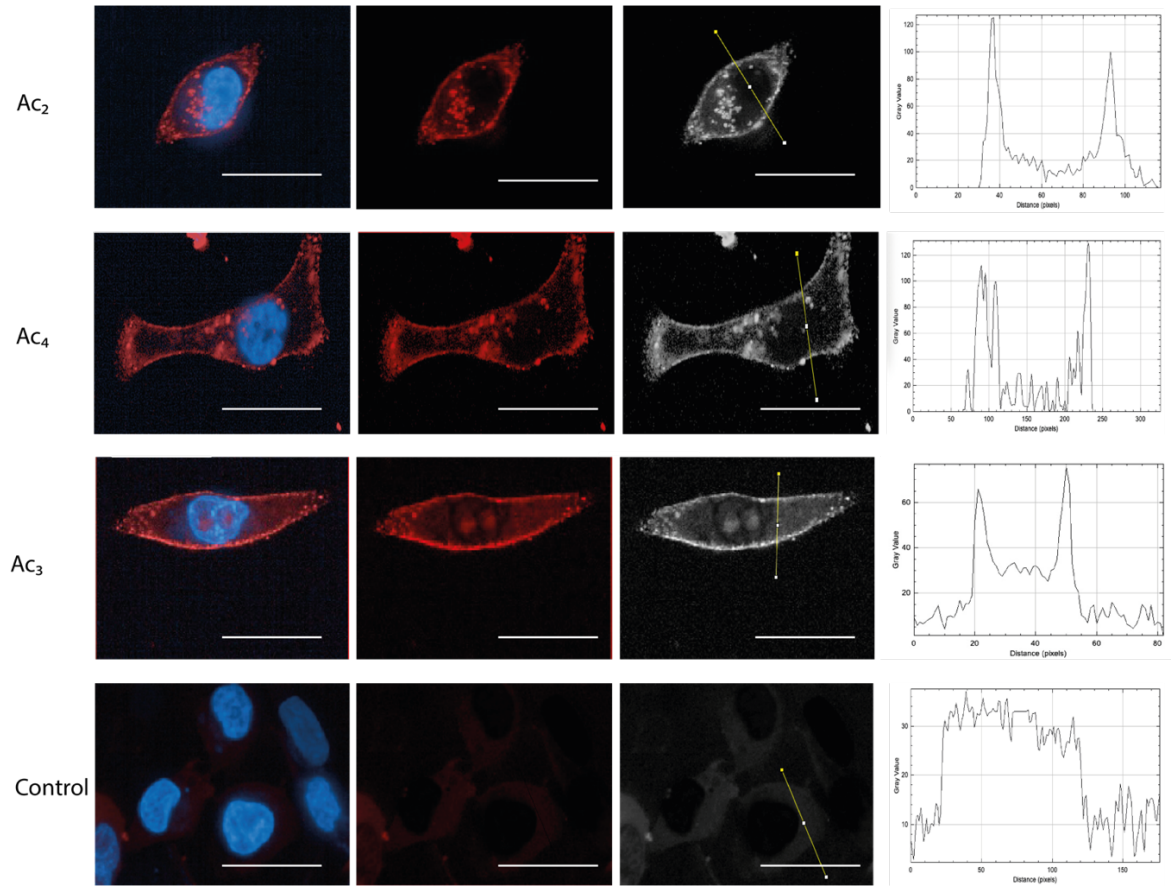

Figure 35 - Fluorescence microscopy of MDA-MB-231 cells. Cells were cultured with appropriate $Ac_xManNCyoc$ sugar (125 µM) (as indicated on left of panel) for 24 h. Wells were then incubated with a dye solution containing DAPI (100 nM) and Tz-AlexaFluor647 (5 µM). Red: AF647, Blue: DAPI nuclear stain, scale bar 50 µm. Images on furthest left show 647 and DAPI channels, the next images have the DAPI overlay removed, images on the furthest right are plots of 647 intensity across the line drawn in the image to the left.

With further *in vivo* studies paused, we wanted to investigate how the level of sialylation varied across cell lines, using metabolic labelling with Ac_3ManNCyoc as a tool to do this. We also wanted to correlate the Ac_3ManNCyoc induced labelling with the labelling of another tagged sugar and see how the two varied relative to each other, across cell lines (*e.g.*, would an increase in Ac_3ManCyoc labelling correlate with a similar increase in Ac_4GalNAz labelling or are the pathways up/down-regulated to different extents). As such, a dual-labelling approach was sought.

2.3. Dual sugar Labelling

Bioorthogonal reactions which can occur simultaneously in the presence of other bioorthogonal ligations, with little or no-cross reaction are well known and have been used in biological systems.[146] This allows for the possibility of dual metabolic labelling, where two different chemical tags can be metabolically incorporated and subsequently bioorthogonally ligated using different and orthogonal chemistries. It is hoped that dual sugar labelling will allow for greater understanding of the dynamics of glycosylation and comparison of the relative levels of incorporation and subsequent labelling.[147]

This was first demonstrated by Cole et al[148] who when reporting the MOE potential of Ac_4ManNCyc, also showed its orthogonality. They demonstrated that Ac_4ManNCyc and Ac_4GalNAz could be co-cultured and subsequently labelled with a fluorescent tetrazine and strained cyclooctyne respectively. They were then able to visualise this dual labelling using fluorescent microscopy, but no quantification of the labelling was given.[148]

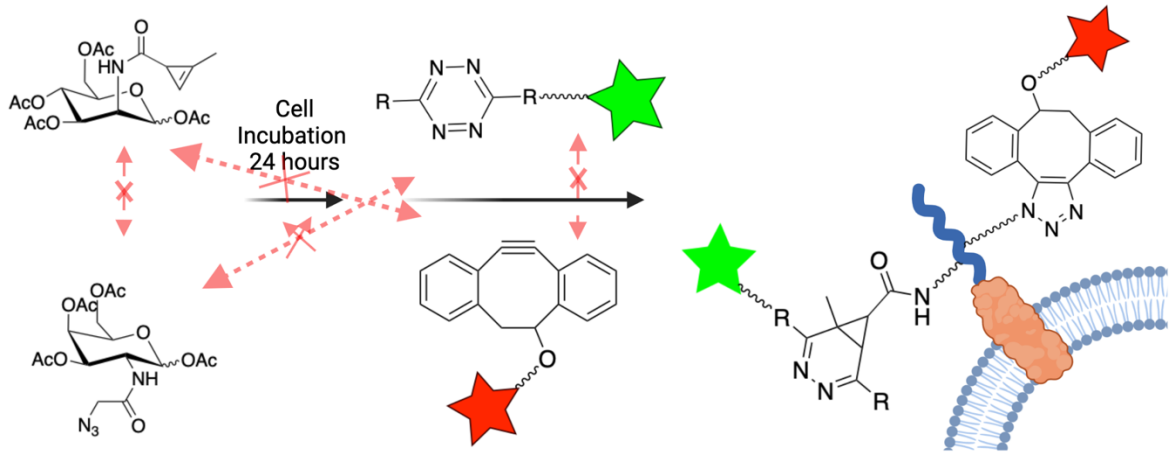

Figure 36 – Dual labelling described by Cole et al.[148] They were able to dual-label using Ac_4ManNCyc and Ac_4GalNAz with corresponding fluorescent tetrazine and strained cyclooctyne.

Further uses of the orthogonality of IED-DA and SPAAC in dual sugar MOE include the use of terminal alkene and azide labelled sugars.[149] The Leeper and Brindle groups also demonstrated the orthogonality of isonitrile and azido tagged sugars.[147]

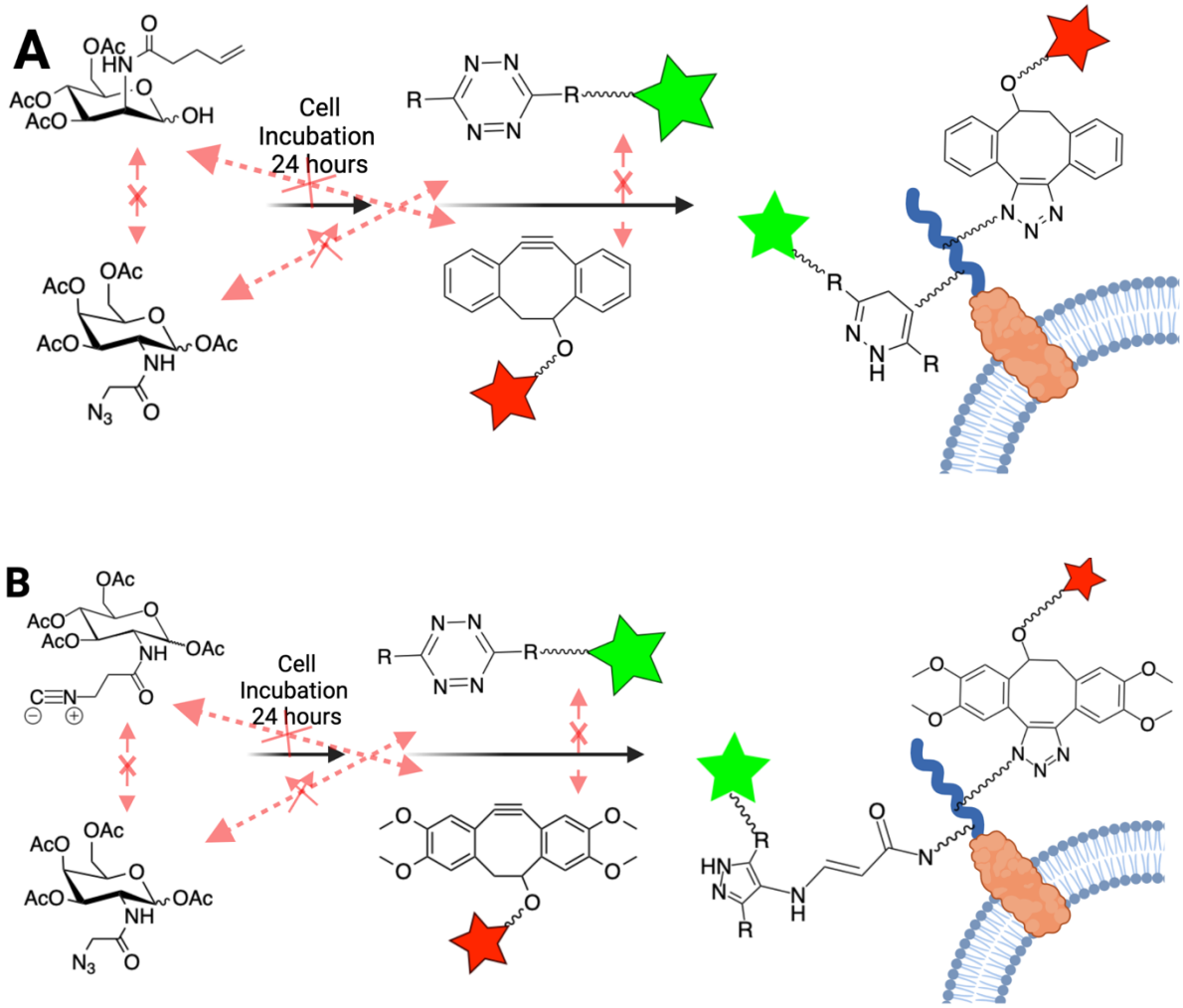

Figure 37 - A) Dual labelling described by Niederwieser et al.[148] MOE dual label using Ac_4ManNPtl and Ac_4GalNAz with corresponding fluorescent tetrazine and strained cyclooctyne. B) Dual labelling described by Wainman et al.[147] MOE dual label using Ac_4Glc-n-Iso and Ac_4GalNAz with corresponding fluorescent tetrazine and strained cyclooctyne.

We aimed to use a similar system to Cole *et al*.[148] but using our Ac_3ManCyoc in place of Ac_4ManCyc and using the probes we had synthesised for our earlier *in vitro* work. The dual sugar labelling abilities of this system was to be tested, and then applied to multiple cell lines. We then wanted to look at how the ratio of the labelling from the different sugar/dye combinations varied across multiple cell lines and if it would correlate with any physiological properties off the cell line *e.g*. growth.

2.3.1. Dual sugar *In Vitro* Labelling Protocol

The *in vitro* labelling protocol was adjusted to include coincubation of Ac_3ManNCyoc and Ac_4GalNAz at 125 µM final concentration of each sugar (from a 110 mM stock in DMSO) (Figure 38). Tz-PEG_{11}-AlexaFluor647 was replaced with Tz- PEG_{11}-AlexaFluor488, which was synthesised according to the previously described protocol.[128] This allowed for concurrent use of the previously described TMDIBO-Lys-AlexaFluor647. Due to the separation between the excitation/emission wavelengths of the 488 and 647 dyes these could be used concurrently, with minimal overlap of the signals. Tz- PEG_{11}-AlexaFluor488 was used as previously at 5 µM, but the TMDIBO-Lys-AlexaFluor647 concentration was increased to 50 µM, to enhance the signal and hence make it easier to see any changes in the contrast. The cell death stain Sytox green was not used with these experiments, due to signal overlap with AlexaFluor488. Gating was only carried out to select single cells via a forward scatter (FSC) vs side scatter (SSC) plot, and cell viability was analysed separately in a subsequent experiment (Figure 43). The seeding density was increased from $0.25x10^6$ to $0.5x10^6$ to make the protocol/handling easier and faster.

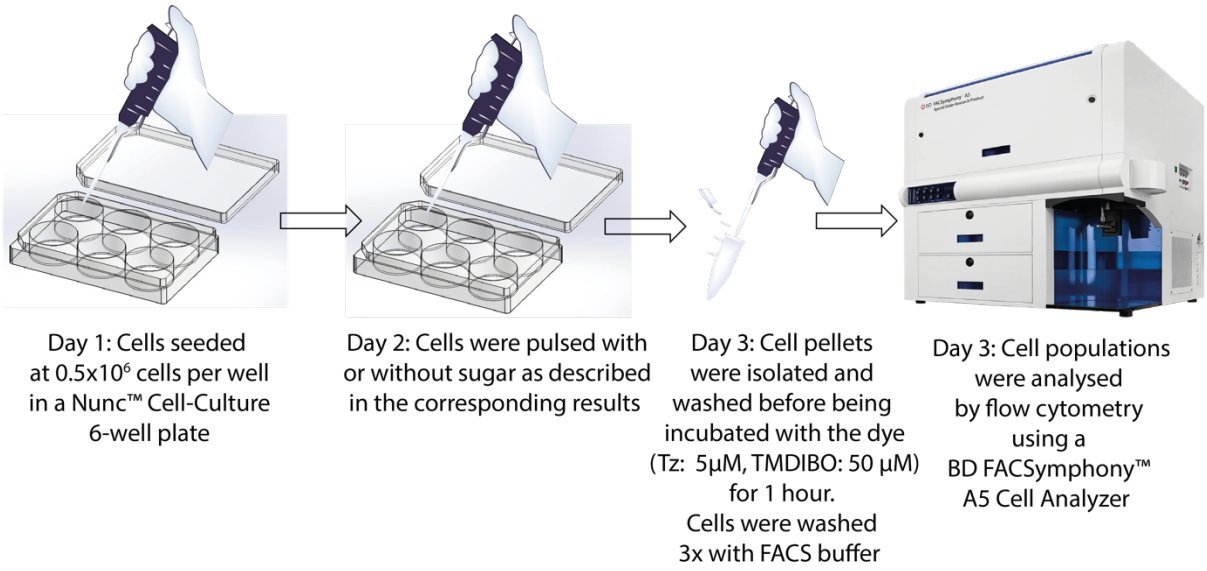

Figure 38 - Dual sugar labelling in vitro protocol.

The orthogonality of IED-DA and SPAAC reactions, and specifically tetrazine-cyclopropene and dibenzocyclooctyne-azide reactions (Figure 39) has previously been shown.[148-150]

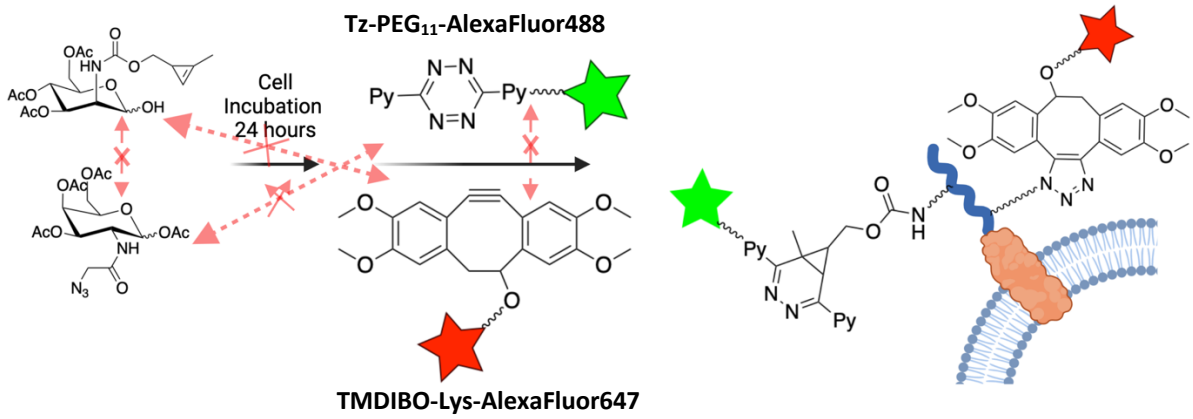

Figure 39 – In vitro dual sugar labelling strategy.

Numerous controls were also set up including single sugar controls and single dye controls. Due to the manually intensive nature of the protocol and the number of factors to control for, most of the controls were only carried out on the first cell line studied, COLO205. This would allow us to show there was no cross reactivity and subsequent cell lines required only dual-sugar treated, single-sugar treated and dye alone treated samples. This is displayed in Figure 40.

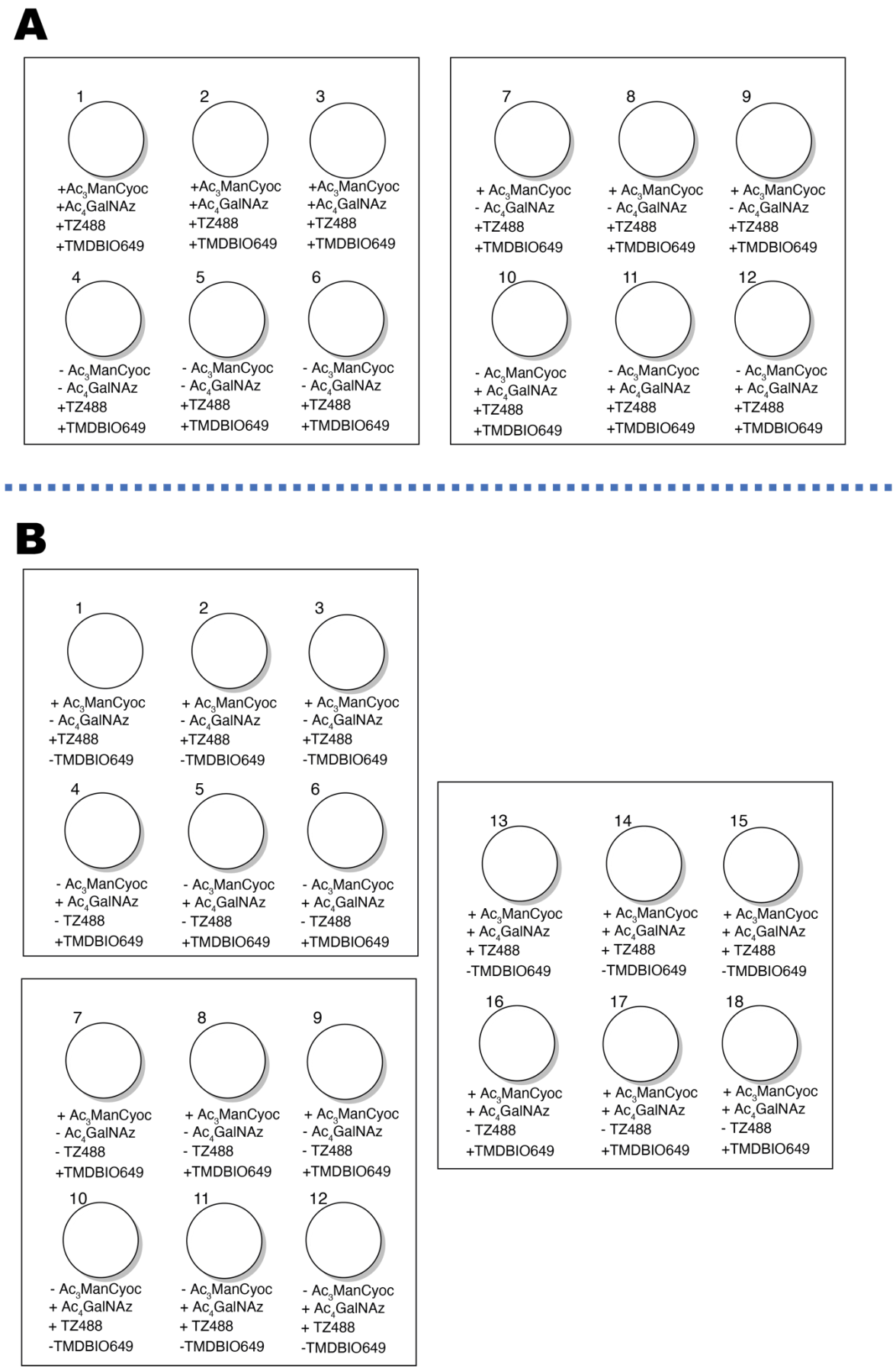

Figure 40 - A) Layout of Nunc™ wells used for all cell lines. B) Controls used only on COLO205 to prove no cross-reactivity.

2.3.2. Dual Sugar *In Vitro* Labelling Results

Due to equipment limitations and to ease time management, the experiments illustrated in Figure 40 were carried out on separate days. The results of the first set of experiments Figure 40(A) are shown in Figure 41. In the dual treated samples, there is contrast/significant SBR relative to the untreated samples. However, the SBR with Ac_3ManNCyoc in the 488 channel is significantly lower than that previously observed in the single sugar treated acetylation panel for COLO205 cells using a Tz-AlexaFluor647 dye (Figure 22). This is likely due to autofluorescence decreasing the SBR due to increased background signal. This autofluorescence is particularly known in mammalian cells which contain many compounds excited by the 488 nm laser.[151, 152] For Ac_4GalNAz, as expected there is no significant difference in contrast between the dual and single treated samples (SBR 2.6 ± 0.1 and 2.8 ± 0.2 respectively). However, for Ac_3ManNCyoc there is a 2-fold increase in the SBR when the single sugar is used instead of both sugars.

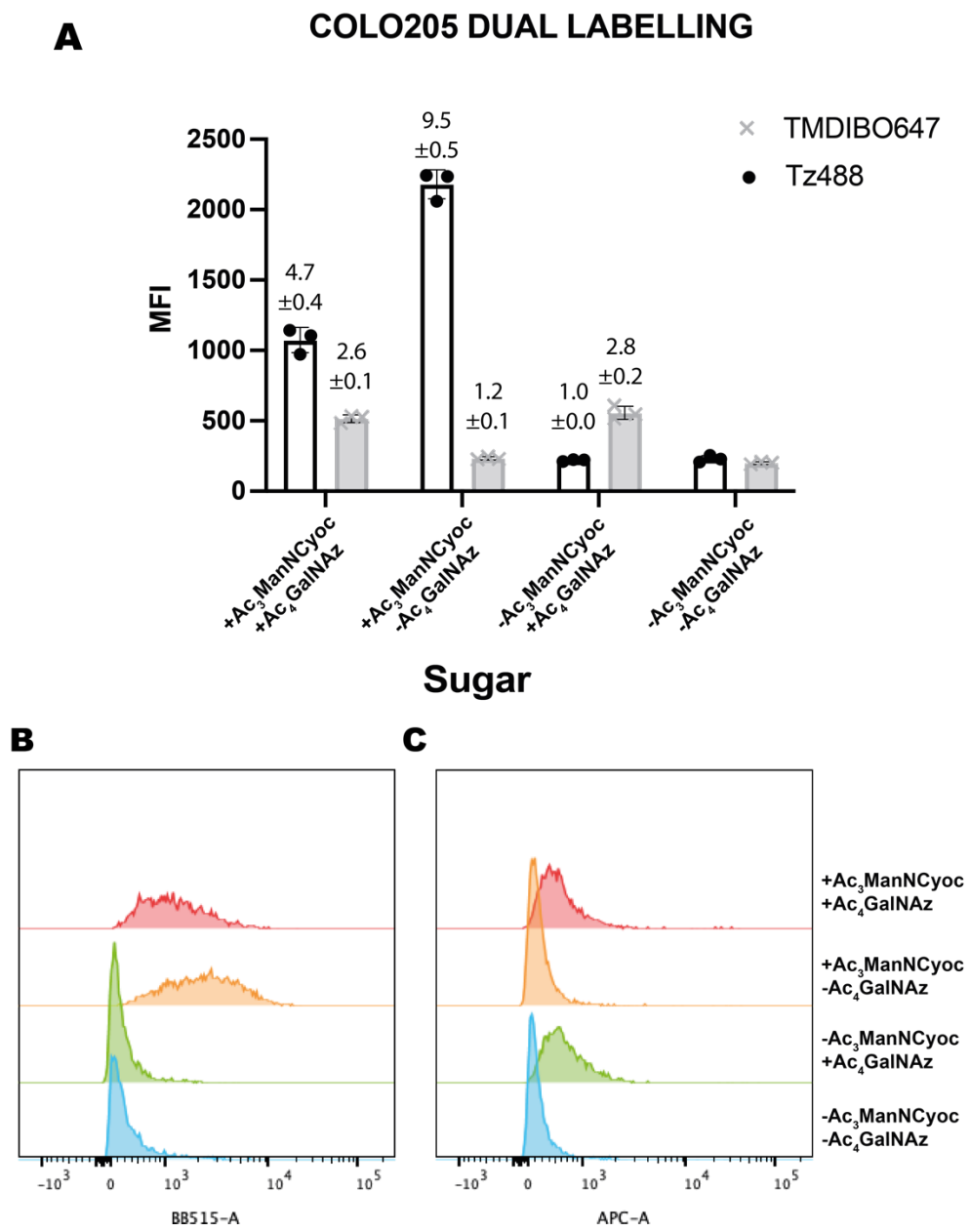

Figure 41 – Dual sugar treatment of COLO205 cells. A) COLO205 cells were incubated in the presence or absence of the indicated sugar 125 μM for 24 h. They were then incubated with the dye solution (Tz-AlexaFluor488 (5 μM) + TMDIBO-AlexaFluor647 (50 μM)) for 1 h at 37 °C, washed and analysed by flow cytometry. Median fluorescence intensity (MFI) is shown as mean ± SD. Signal-to-background ratios (SBR) relative to the control (-Man-Gal) are above each bar; n=3 technical replicates. B) and C) Histograms giving number of events (vertical axis) versus fluorescence intensity (horizontal axis) B) Tz-AlexaFluor488 and C) TMDIBO-AlexaFluor647. In each panel the sugars used, from top to bottom, are: +Man+Gal, +Man-Gal, -Man+Gal and then the no-sugar control.

Additional controls listed in Figure 40(B) were carried out to try and investigate if there were any cross reactivity or synergistic effects (Figure 42). Use of the incorrect sugar and probe partners (ManNCyoc with TMDIBO or GalNAz with Tz) showed no increase in labelling in the corresponding emission profile over the fluorophore alone, thus proving that cyclopropene tagged sugars only react with the tetrazine probe and azide labelled sugars only react with the TMDIBO probe (as has been demonstrated before with other dibenzocyclooctynes and tetrazines[148]). Notably, a decrease in tetrazine labelling when

both sugars were added relative to when only ManNCyoc is added was observed, as seen previously but this time when only the tetrazine dye was used. This suggests that the decrease is not due to any cross reactivity of the probes (or any FRET/energy transfer) and is instead due to an effect related to the sugars. As before, the level of labelling with TMDIBO remained consistent when GalNAz was used on its own or dual fed with ManNCyoc.

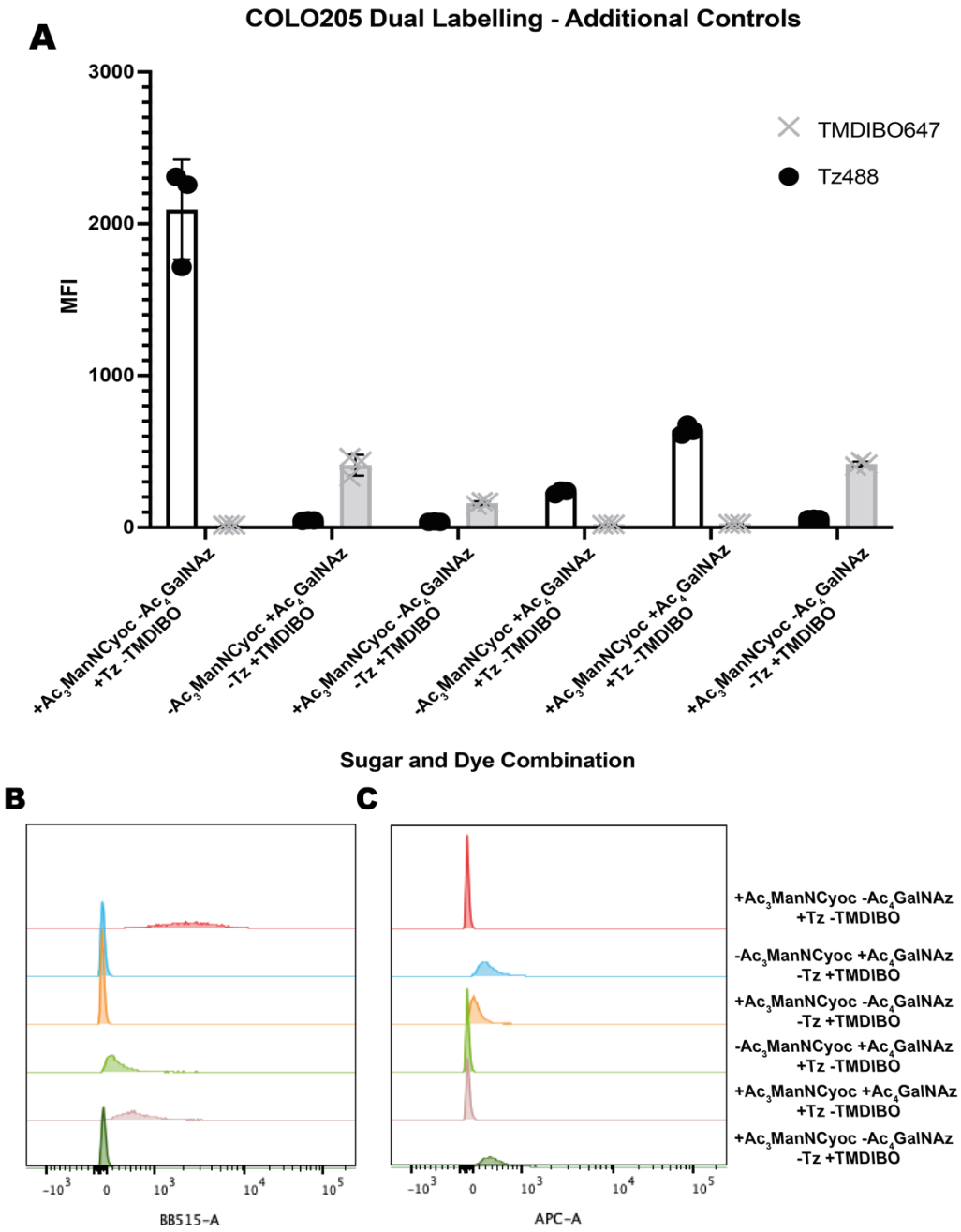

Figure 42 - Dual sugar control treatment of COLO205 cells. A) COLO205 cells were incubated in the presence or absence of the indicated sugar(s) (125 µM) for 24 h. They were then incubated with the dye solution described in the figure (Tz-AlexaFluor488 (5 µM) and/or TMDIBO-AlexaFluor647 (50 µM) for 1 h at 37 °C, then washed and analysed by flow cytometry. Median fluorescence intensity (MFI) is shown as mean ± SD. n=3 technical replicates. B) and C) Histograms giving number of events (vertical axis) versus fluorescence intensity (horizontal axis) B) Tz-AlexaFluor488 and C) TMDIBO-AlexaFluor647. In each panel the sugars used, from top to bottom, are: +Man-Gal+Tz-TMDIBO, -Man+Gal-Tz+TMDIBO, +Man-Gal-Tz+TMDIBO, -Man+Gal+Tz-TMDIBO, +Man+Gal+Tz-TMDIBO, +Man+Gal-Tz+TMDIBO.

Following this, cell viability was probed as a potential explanation for this unusual decrease in tetrazine labelling with dual sugar treated samples. In the previous dual-labelling experiments published by the Leeper and Brindle groups, the decrease in dual treated samples was observed, believed to be due to sugar induced growth inhibition or competition between the sugars.[147] As previously mentioned, no cell-viability stain was used to gate the flow experiments in this dual labelling study, due to potential bleed over of the signals between Sytox green and the AlexaFluor488. As such, the concern was that dual feeding was decreasing cell viability, and this was somehow decreasing the labelling (although the labelling of individual still-viable cells should not be affected by this).

To probe the cell viability, COLO205 cells were seeded in Nunc™ wells and treated as described in Figure 40A, except that DMSO was added to control wells in the same volume as added to the treated ones. 24 hours post incubation the cell pellet from each well was collected, resuspended in 5 mL RPMI media, and analysed on a Vi-CELL XR cell viability analyser. The resulting cell viability, viable cells per mL and total cells per mL for each sample are shown in Figure 43. The only statistically significant variation was in the cell viability of the dual treated samples. There was a small but significant decrease in viability from an average of 93.2% in the control to 86.9% in the dual treated samples. All other samples showed no significant variation from the control treated cells, in any of the metrics analysed. Whilst there is a decrease in viability, it was not believed this is sufficient to cause the decrease in tetrazine labelling in dual treated samples.

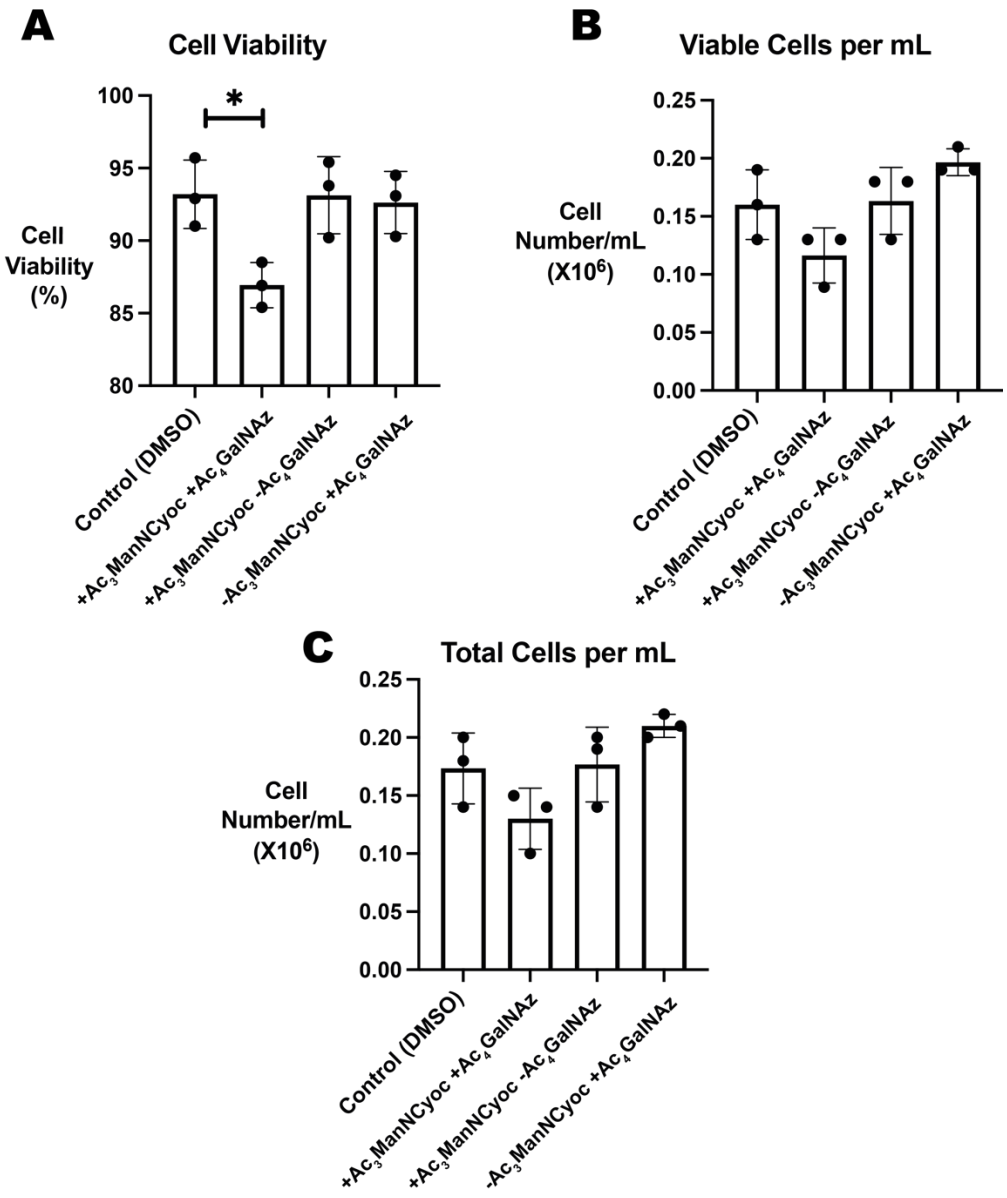

*Figure 43 – The effect of dual sugar treatment on the viability and growth of COLO205 cells. COLO205 cells were incubated in the presence or absence of the indicated sugar(s) (125 μM) for 24 h. The cells pellet was collected and resuspended before being analysed on a Vi-CELL XR cell viability analyser. A) Shows the cell viability of each sample B) the number of viable cells per mL and C) the total cells per mL. ; n=3 technical replicates. Statistical analysis was performed using an unpaired t test with Welch correction (**** P≤0.0001,*** P≤0.001,** P≤0.01,* P≤0.05).*

The same methodology developed was then applied to other cell lines, to see if the decrease in tetrazine labelling in dual treated samples was consistent across all cell lines, or some artefact of COLO205 behaviour/physiology. This also enabled us to carry out our earlier objective of comparing the ratio of mannosamine to galactosamine labelling as a way of probing hypersialylation.

The next cell line to be dual labelled was the previously used MDA-MB-231. In the acetylation studies this had shown the greatest contrast with ManNCyoc sugars. As previously discussed just the dual treated, single treated and untreated (all incubated with both dyes) were studied. As shown in Figure 44 there is a significant increase in SBR relative to the COLO205 model. This is most pronounced in the

IED-DA induced SBR's. The single sugar ManNCyoc SBR increased from 9.5 ± 0.5 to 41.3 ± 1.3, and the dual from 4.7 ± 0.4 to 22.9 ± 3.9. Once again, there was a decreased MFI of the tetrazine488 channel in the dual treated sample, with a near 2-fold decrease similar to that previously observed in COLO205 cells.

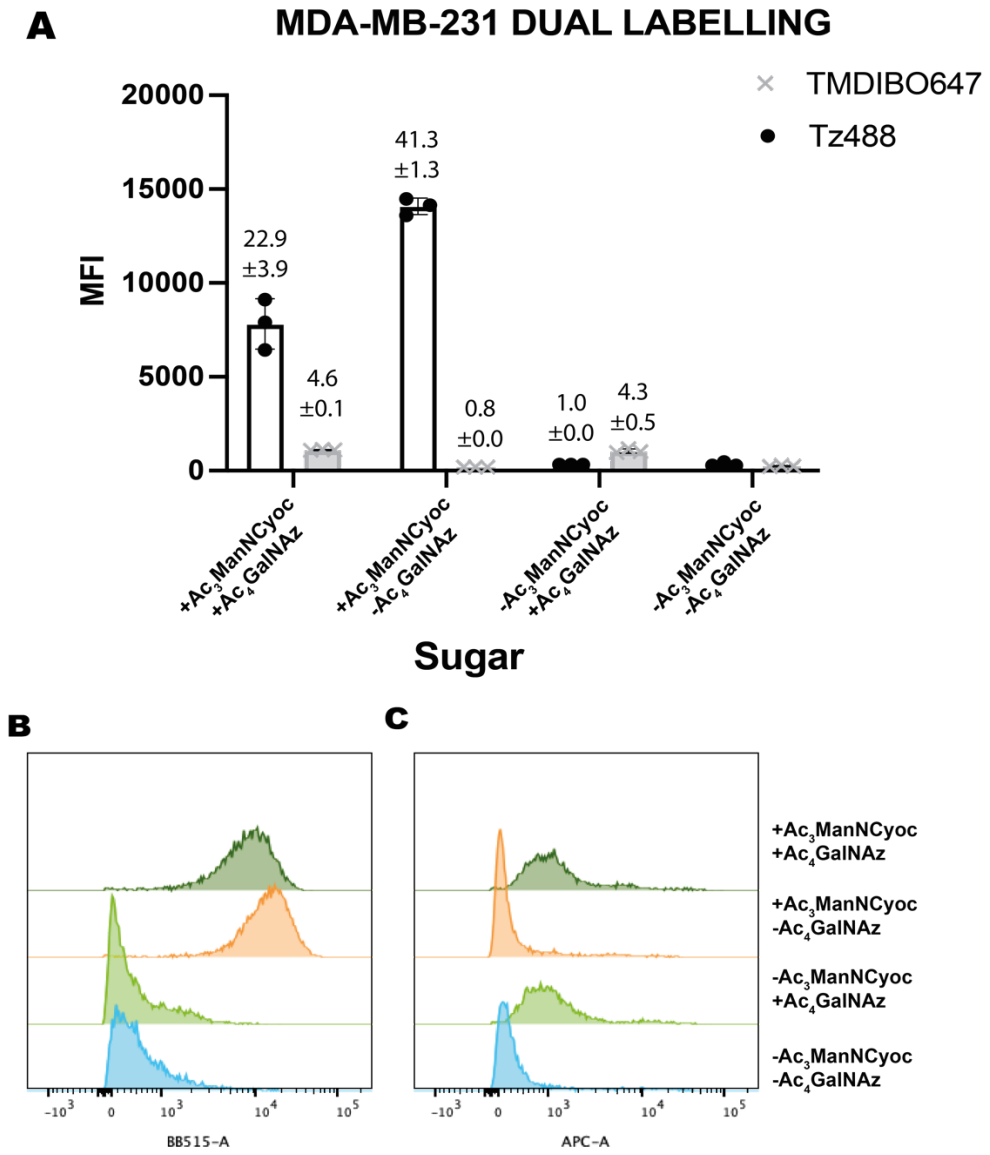

Figure 44 - Dual sugar treatment of MDA-MB-231 cells. A) MDA-MB-231 cells were incubated in the presence or absence of the indicated sugar (125 μM) for 24 h. They were then incubated with the dye solution (Tz-PEG$_{11}$-AlexaFluor488 (5 μM) + TMDIBO-Lys-AlexaFluor647 (50 μM)) for 1 h at 37 °C and analysed by flow cytometry. Median fluorescence intensity (MFI) is shown as mean ± SD. Signal-to-background ratios (SBR) relative to the control (-Man-Gal) are above each bar; n=3 technical replicates. B) and C) Histograms giving number of events (vertical axis) versus fluorescence intensity (horizontal axis) B) Tz-PEG$_{11}$-AlexaFluor488 and C) TMDIBO-Lys-AlexaFluor647. In each panel the sugars used, from top to bottom, are: +Man+Gal, +Man-Gal, -Man+Gal and then the no-sugar control.

Next, two more cancer cell lines were studied. The previously used pancreatic cancer cell line PANC-1 and Jurkat cells, a widely used cancer cell line, immortalised from an acute T cell leukemia.[153] Hypersialylation had previously been demonstrated in PANC-1 cells (Figure 30) and so dual labelling was of interest here. Jurkat cells as well as being widely used in the literature, are also an important

cell line in a potential collaborative project at CRUK, involving imaging the distribution of cells in chimeric antigen receptor therapy (CAR-T). As such, the dual-sugar labelling profile in these cell lines was measured. Figure 45 and Figure 46 show the dual labelling of PANC-1 and HEK cells respectively. In both, there is a clear difference in labelling between the dual fed and single ManCyoc treated cells, but this has now increased to an approximately 3-fold difference. Also of note is the increased labelling of GalNAz relative to ManNCyoc in these two cell lines; this is discussed in detail later in Table 1. Again, no significant difference was seen in the labelling with GalNAz in the dual-fed and single-sugar fed cells.

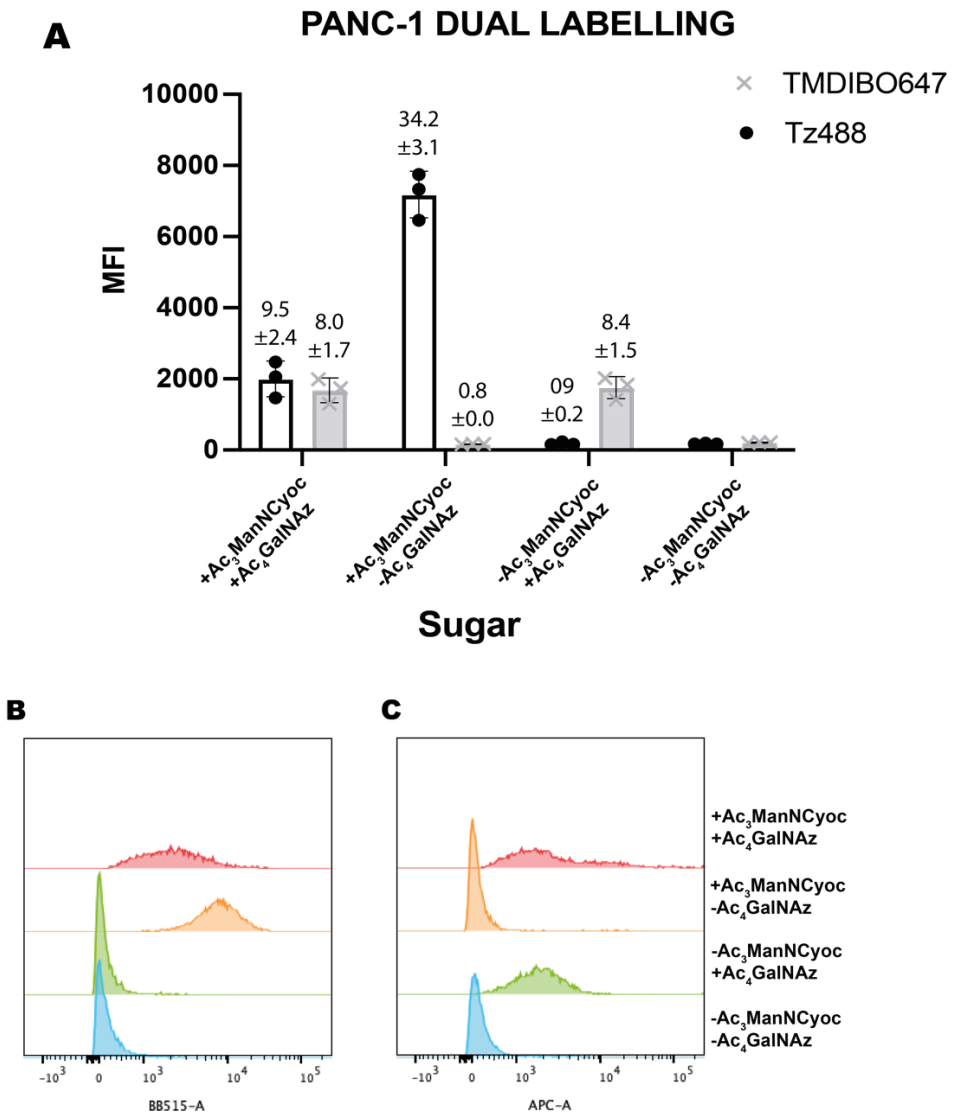

Figure 45 - Dual sugar treatment of PANC-1 cells. A) PANC-1 cells were incubated in the presence or absence of the indicated sugar (125 µM) for 24 h. They were then incubated with the dye solution (Tz-PEG$_{11}$-AlexaFluor488 (5 µM) + TMDIBO-Lys-AlexaFluor647 (50 µM)) for 1 h at 37 °C and analysed by flow cytometry. Median fluorescence intensity (MFI) is shown as mean ± SD. Signal-to-background ratios (SBR) relative to the control (-Man-Gal) are above each bar; n=3 technical replicates. B) and C) Histograms giving number of events (vertical axis) versus fluorescence intensity (horizontal axis) B) Tz-PEG$_{11}$-AlexaFluor488 and C) TMDIBO-Lys-AlexaFluor647. In each panel the sugars used, from top to bottom, are: +Man+Gal, +Man-Gal, -Man+Gal and then the no-sugar control.

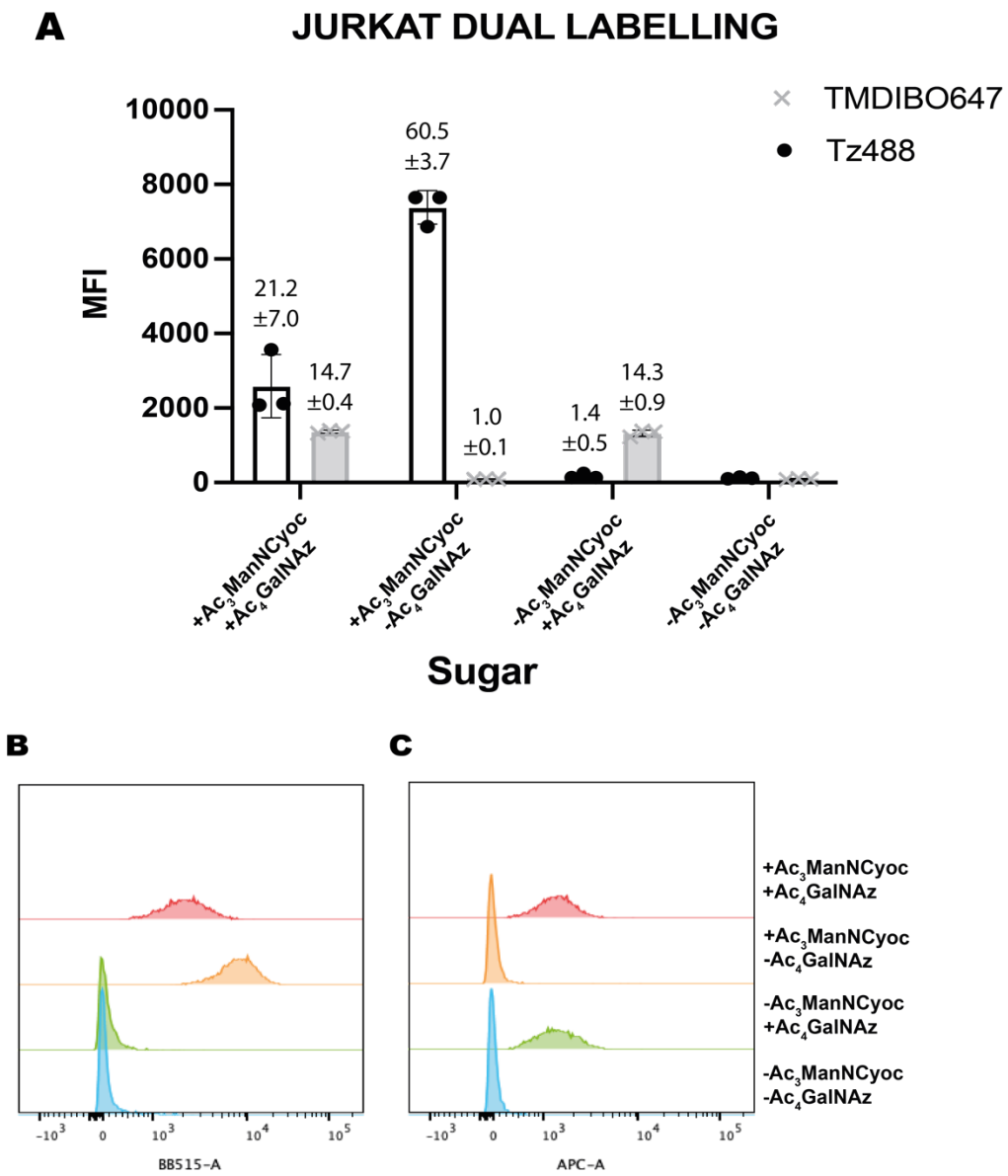

Figure 46 - Dual sugar treatment of Jurkat cells. A) Jurkat cells were incubated in the presence or absence of the indicated sugar (125 µM) for 24 h. They were then incubated with the dye solution (Tz-PEG$_{11}$-AlexaFluor488 (5 µM) + TMDIBO-Lys-AlexaFluor647 (50 µM)) for 1 h at 37 °C and analysed by flow cytometry. Median fluorescence intensity (MFI) is shown as mean ± SD. Signal-to-background ratios (SBR) relative to the control (-Man-Gal) are above each bar; n=3 technical replicates. B) and C) Histograms giving number of events (vertical axis) versus fluorescence intensity (horizontal axis) B) Tz-PEG$_{11}$-AlexaFluor488 and C) TMDIBO-Lys-AlexaFluor647. In each panel the sugars used, from top to bottom, are: +Man+Gal, +Man-Gal, -Man+Gal and then the no-sugar control.

Comparison of the dual labelling in a non-cancerous cell line was also carried out. The difficulty with this was finding a model with could be easily cultured *in vitro*. Since the previous cell lines, used were cancerous and hence fast growing, they are relatively easy to culture. This is often not the case for non-cancerous mammalian cell lines, which can be difficult to culture. However, some models do exist, particularly in fast growing/dividing cell lines. Once such model is human embryonic kidney (HEK293)[154] which are fast growing and a robust model. Exposed to the same dual labelling conditions used for the cancerous cell lines, the resulting labelling is shown in Figure 47. The 3-fold decrease in

tetrazine labelling in dual treated samples relative to the single ManNCyoc treated samples, was again demonstrated. Significant levels of sialylation are measured, with single treated SBR of 30.6 ± 3.1, comparable with the hypersialylated tumour cell lines. This is believed to be due to the intrinsic properties of the cell line, notably as an embryonic cell line rapid growth is expected. This rapid growth may in part be induced or aided by hypersialylation and make the cell line behave "tumour like". This behaviour is what allows efficient cell culture and so it may be difficult to find a suitable non-cancerous mammalian cell model which does not rapidly proliferate.

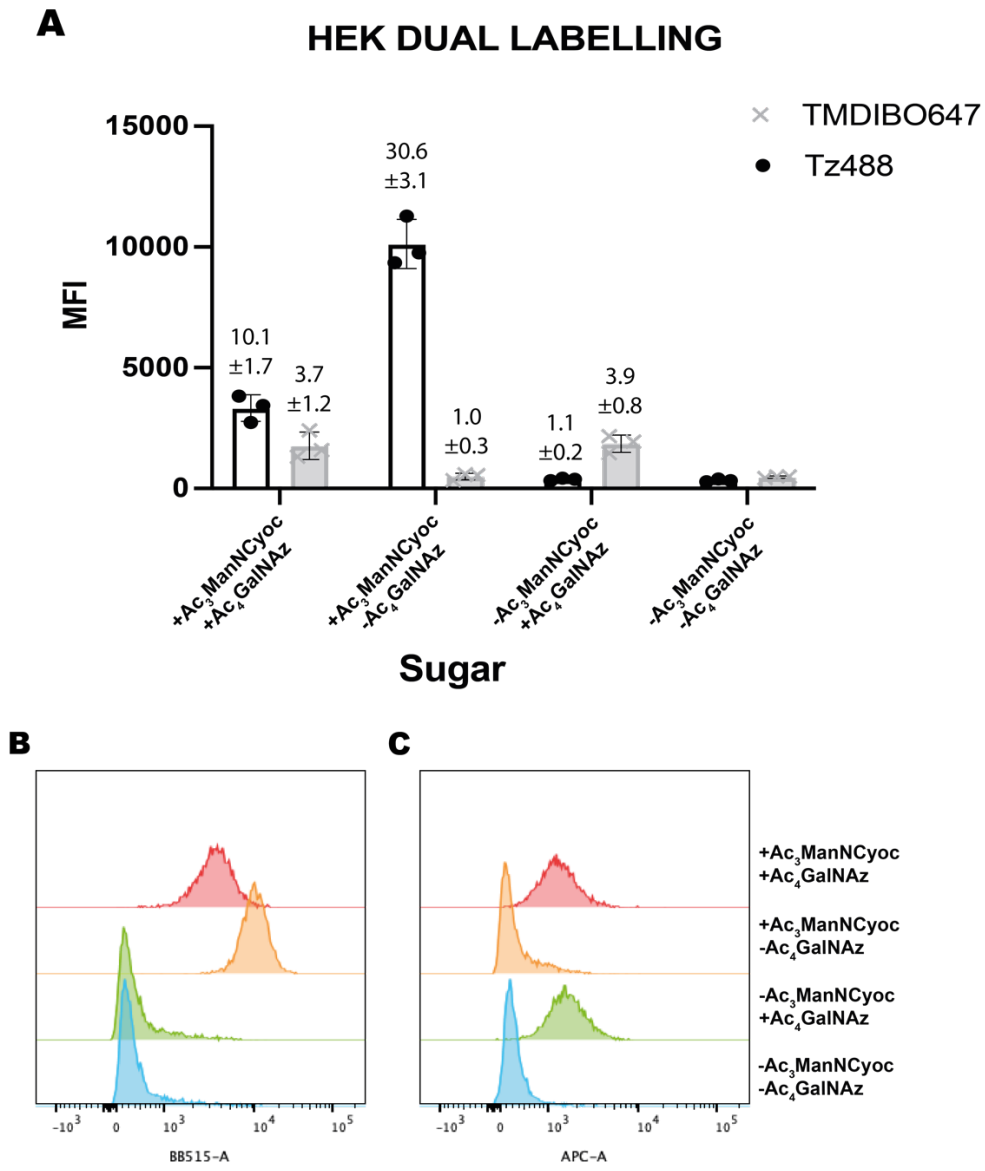

Figure 47 - Dual sugar treatment of HEK293 cells. A) HEK293 cells were incubated in the presence or absence of the indicated sugar (125 µM) for 24 h. They were then incubated with the dye solution (Tz-AlexaFluor488 (5 µM) + TMDIBO-AlexaFluor647 (50 µM)) for 1 h at 37 °C and analysed by flow cytometry. Median fluorescence intensity (MFI) is shown as mean ± SD. Signal-to-background ratios (SBR) relative to the control (-Man-Gal) are above each bar; n=3 technical replicates. B) and C) Histograms giving number of events (vertical axis) versus fluorescence intensity (horizontal axis) B) Tz-AlexaFluor488 and C) TMDIBO-AlexaFluor647. In each panel the sugars used, from top to bottom, are: +Man+Gal, +Man-Gal, -Man+Gal and then the no-sugar control.

2.3.3. Comparison of Dual Labelling SBR

Collated in Table 1 are the SBRs generated from the various dual labelling experiments. There are significant differences in the SBR across the different cell lines used. One consistent trend however is the increase in SBR in the single- versus the dual treated samples for Ac_3ManCyoc. In all cell lines studied there was a significant increase varying from 2-fold in COLO205 to 3.6-fold in PANC-1 cells. Since it has previously been demonstrated[155] that the reaction rate between TCO and strained cyclooctynes was minimally small, it therefore follows that the rate with the much less strained and reactive cyclopropenes would be even lower. Further to this, the single dye controls in Figure 42 show the same decrease in labelling between dual treated and single treated Ac_3ManCyoc samples, proving that the effect is not due to Ac_3ManCyoc reacting with TMDIBO. Also, no contrast was seen when Ac_4GalNAz was incubated with tetrazine, relative to the non-sugar treated tetrazine treated cells. Therefore, the only possible cross-reaction which could cause the decrease is a reaction between the sugars (between the cyclopropene and the azide). Previously, cross reaction between the more reactive TCO and an azide had been shown to be extremely slow, and beyond the timescale of our protocol.[155] Further to this, computational modelling[150] had calculated methylcyclopropenes should be mutually orthogonal to azides. This ultimately led to the dual labelling of cyclopropene and azide tagged sugars, with no reported cross reactivity.[148] In this example the methylcyclopropene used was amide linked to the sugar, as well as a different probe (but this was excluded as a cause). However, in this first example only fluorescent microscopy was used with no quantitative data, so it remains unclear if they saw the same decrease in labelling in dual combinations. This is further discussed in section 2.3.4

Table 1 - SBR collected for the sugar combinations across the multiple cell lines.

Cell line	Dual treated Ac_3ManCyoc SBR	Dual treated Ac_4GalNAz SBR	Single treated Ac_3ManCyoc SBR	Single treated Ac_4GalNAz SBR
COLO205	4.7 ± 0.4	2.6 ± 0.1	9.5 ± 0.5	2.8 ± 0.2
MDA-MB-231	22.9 ± 3.9	4.6 ± 0.1	41.3 ± 1.3	4.3 ± 0.5
PANC-1	9.5 ± 2.4	8.0 ± 1.7	34.2 ± 3.1	8.4 ± 1.5
Jurkat	21.2 ± 7.0	14.7 ± 0.4	60.5 ± 3.7	14.3 ± 0.9
HEK293	10.1 ± 1.7	3.7 ± 1.2	30.6 ± 3.1	3.9 ± 0.8

The ratio of the SBR induced by the Ac_3ManNCyoc and tetrazine-PEG_{11}-AlexaFluor488 ligation to that for the Ac_4GalNAz and TMDIBO-Lys-AlexaFluor647 ligation is shown in Table 2. The ratios not only vary

between dual- and single-sugar treated cells (due to the above-mentioned decrease in Ac_3ManCyoc dual labelling) but also across cell lines. This suggests that the relative incorporation of the monosaccharide is a function of the cellular behaviour as well as the nature of the chemical tag, supporting our belief that dual sugar strategies could help assess tumour properties. The biggest difference in dual and single treated SBR ratio was seen in HEK293 cells.

Table 2 – Ratio of SBR collected for the sugar combinations across the multiple cell lines.

Cell line	Dual treated ratio of SBR (Ac_3ManNCyoc:Ac_4GalNAz)	Single treated ratio of SBR (Ac_3ManNCyoc:Ac_4GalNAz)
COLO205	1.8	3.4
MDA-MB-231	5.0	9.6
PANC-1	1.2	4.1
Jurkat	1.4	4.2
HEK293	2.7	7.8

MDA-MB-231 cells show the highest dual and single treated SBR ratio of 5.0 and 9.6 respectively. MDA-MB-231 is a very aggressive cell line, being triple negative and categorised as basal B[156] (Figure 48). This fits well with our hypothesis that hypersialylation corresponds well with tumour aggressiveness, and that a relative increase in the level of sialylation (measured via increased Ac_3ManNCyoc:Ac_4GalNAz) corresponds with more aggressive tumour behaviour.

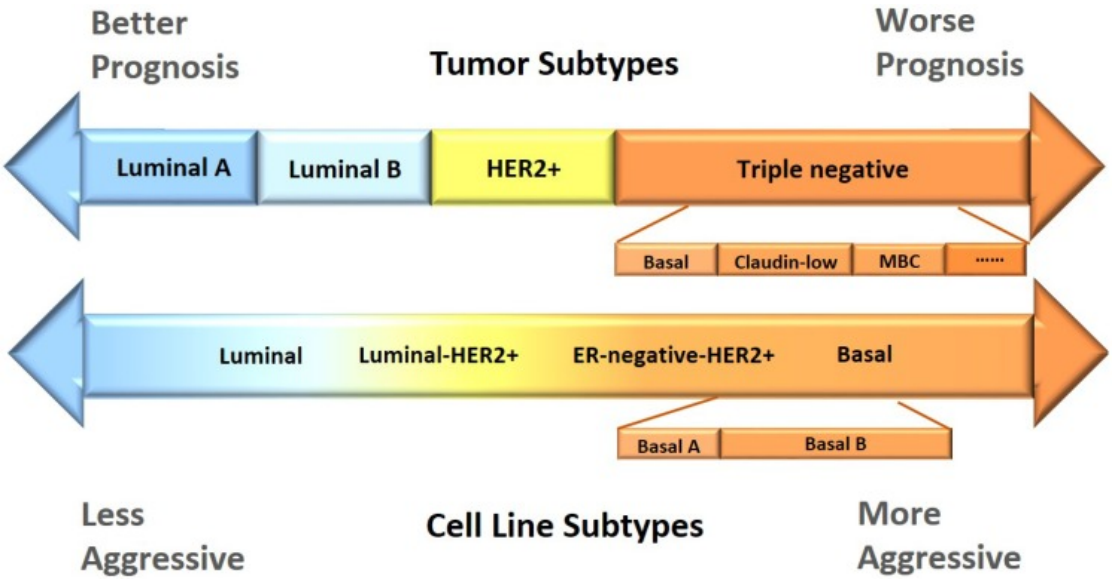

Figure 48 – Breast cancer categorisation as a function of aggression. MDA-MB-231 falls into the category with the worst progression due to its testing negative for all 3 estrogen receptors. This category is then further subdivided with MDA-MB-231 being in the most aggressive basal B category. Taken from Dai et al.[156]

To further test the hypothesis that the ratio of SBR could be in some way diagnostic, perhaps as a measure of tumour aggression, the growth rate of the various cell lines was compared to the SBR ratios. The *in vitro* cell growth profiles (taken from the PHE culture collections) for COLO205, MDA-MB-231, PANC-1 and HEK293, and are shown in Figure 49 (data was not available for Jurkat cells).[157] The two cell lines which have the fastest *in vitro* growth (confluency at around 60 hours) are MDA-MB-231 and HEK293 cells. These cell lines also show highest dual and single SBR ratio, showing the biggest difference in relative sialylation to the other cell lines (Ac_3ManCyoc:Ac_4GalNAz labelling). PANC-1 cells reach confluency after approximately 140 hours, with COLO205 cells only being confluent at around 200 hours. This again fits with our single sugar SBR ratios, but in the dual treated samples COLO205 has a higher SBR ratio.

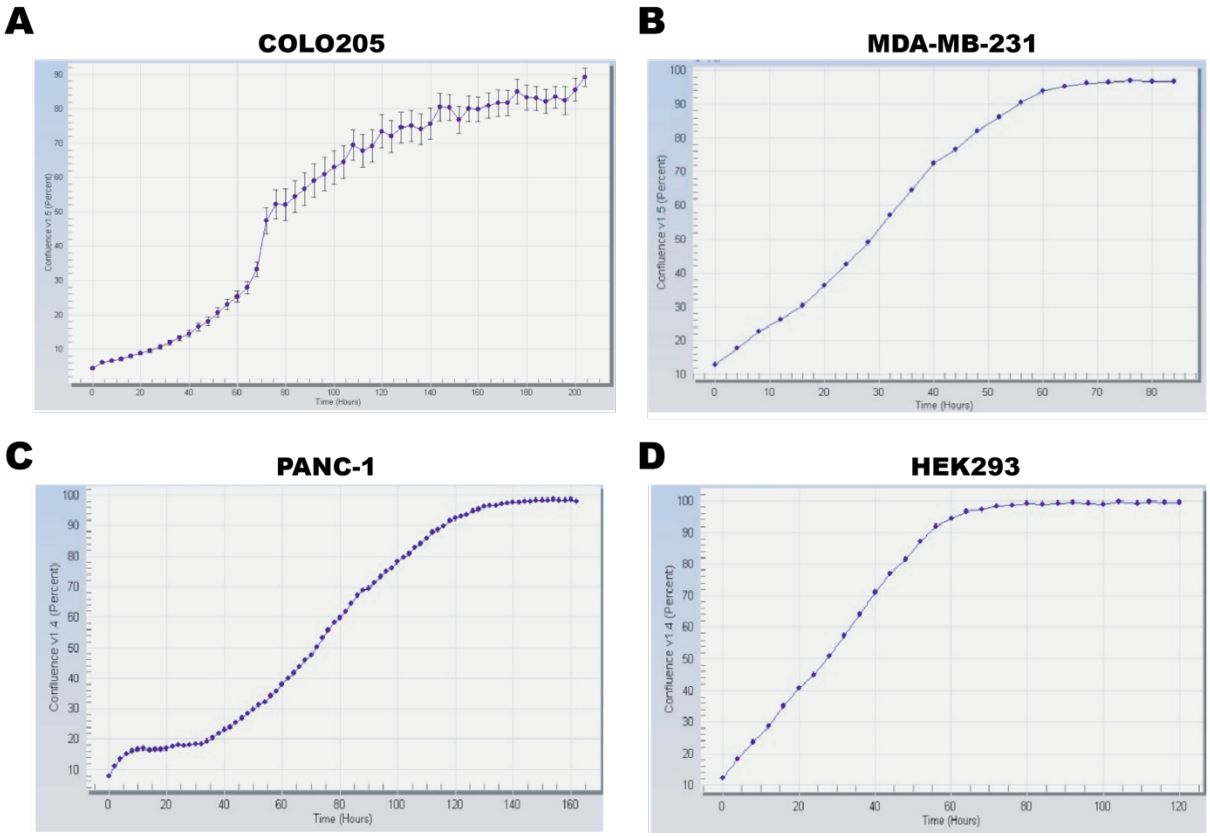

Figure 49 – Cell growth profile (time in hours vs percentage confluency). A) COLO205, B) MDA-MB-231, C) PANC-1, D) HEK293. Figures taken from PHE general cell collection (note the scaling of the X-axis varies across A-D).[157]

Figures provided by Labcorp Drug Development[158] also allowed us to correlate our SBR ratios with *in vivo* growth properties in 2 of the cell lines used: MDA-MB-231 and PANC-1. Shown in Figure 50 are plots of mean tumour burden vs days post implant. The MDA-MB-231 implanted exhibited a much larger tumour burden at earlier times, further supporting that this is a more aggressive/faster growing model.

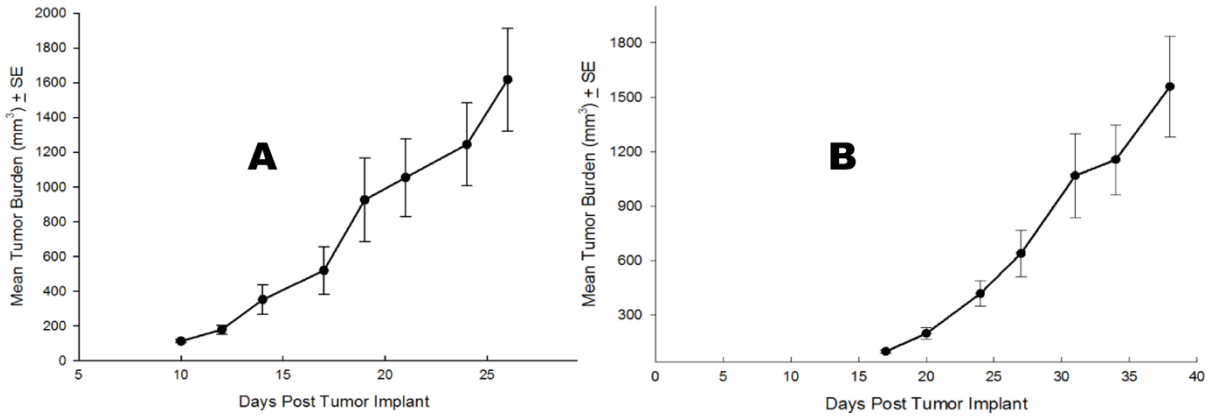

Figure 50 - Plots of tumour burden vs days post implant for A) MDA-MB-231 and B) PANC-1. Data provided by Labcorp Drug Development.[158]

Further comparison used various parameters of the *in vivo* growth. MDA-MB-231 which has a much higher dual- and single-treated SBR ratio is clearly a faster growing (and shorter doubling time) tumour, which also reaches staging at a much earlier timepoint. This again correlates with our hypothesis that a higher ratio of SBR correlates with tumour invasiveness, *in vitro* and *in vivo*.

Table 3 - Comparison of in vivo properties of MDA-MB-231 and PANC-1 cells with measured SBR ratios. In vivo data provided by Labcorp Drug Development.[158]

Parameters	MDA-MB-231	PANC-1
Strain	Nude	Nude
Implant Type	Fragments	Fragments
Implant Location	SC, High Axila	SC
Time to Staging	10 days	18 days
Time to 750mm^3	18 days	30.9 days
Td (doubling time)	3.4 days	5.2 days
Dual treated ratio of SBR (Ac_3ManNCyoc:Ac_4GalNAz)	5.0	1.2
Single treated ratio of SBR (Ac_3ManNCyoc:Ac_4GalNAz)	9.6	4.1

2.3.4. Probing the Decrease in Dual Labelling

With cross-probe reactivity and reaction between Ac_4GalNAz and the tetrazine probe (and the same for Cyoc/tetrazine) ruled out in the controls, the only remaining purely chemical cause for the decrease in ManNCyoc labelling in the dual-sugar experiment was *via* an unknown reaction between the sugars. If Ac_4GalNAz at 125 μM essentially saturated the cell, and the excess azide reacted with the Ac_3ManNCyoc to reduce the availability of the cyclopropene, this could reduce the cyclopropene labelling. To probe this, sugar controls were made up in PBS, and a 1:1 mixed sample, all at a final concentration of 11 μM. A more dilute concentration (closer to that used *in vitro*) was not used as it approached the detection limit of the HRMS system and made any potential reaction difficult to follow. The 3 samples were then incubated at 37 °C and analysed by HRMS at 0 h, 1 h, 24 h and 48 h.

The single sugar control for Ac_4GalNAz showed no change over the 48-hour time course (Figure 52). Multiple peaks are seen even in the single sugar controls due to the separation of anomers, rotamers and diastereoisomers. The single sugar control of Ac_3ManNCyoc indicated slow degradation of the compound with the emergence of new peaks which grew over the 48 hours (Figure 51). The degradation products could not be identified.

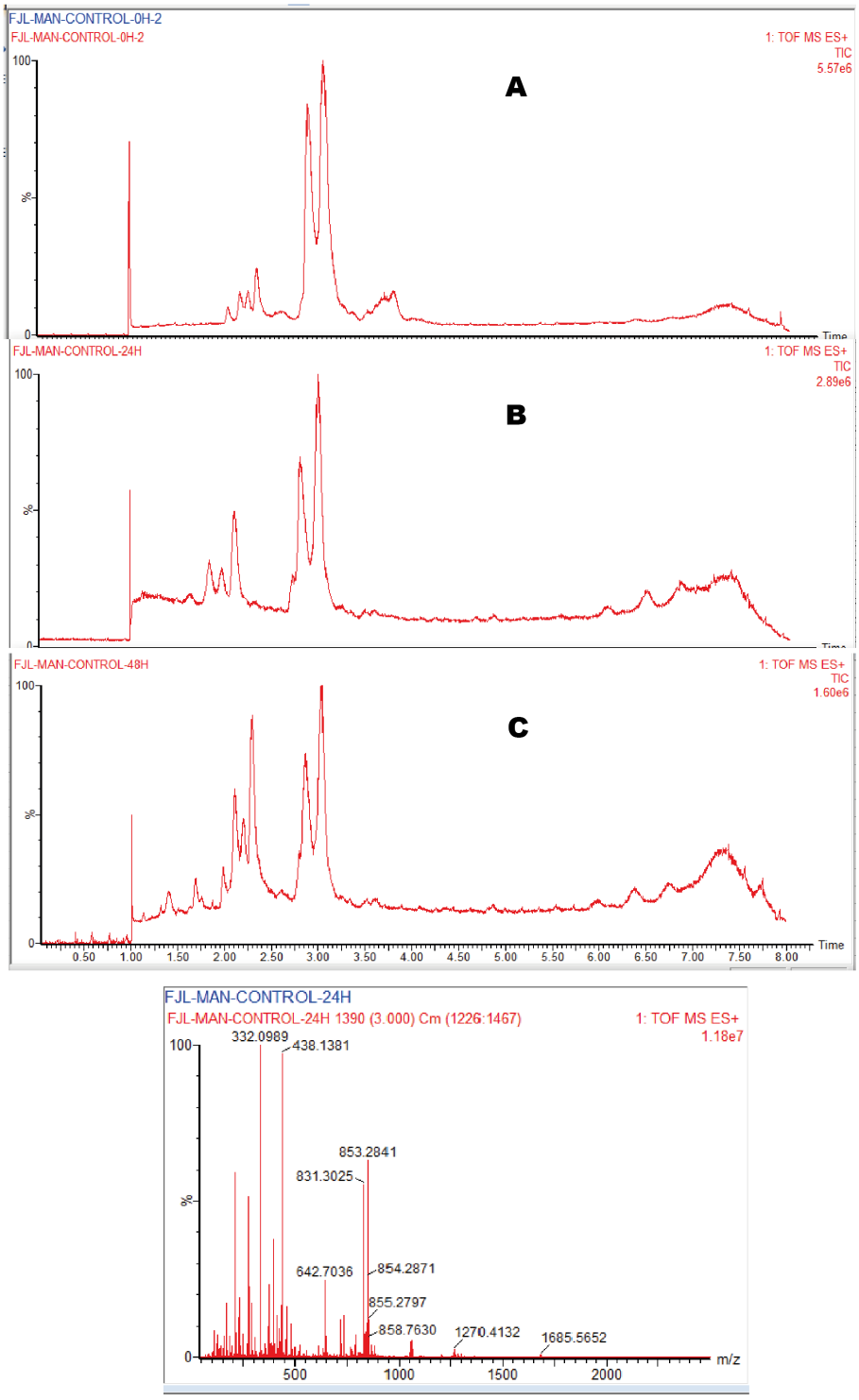

Figure 51 - Time course of HRMS of Ac_3ManNCyoc in PBS. A) 0h B) 24h C) 48h. Samples were heated to 37 °C between analysis runs. Aquired on a Waters Acquity UPLC system running in positive mode with an electrospray source. LC system: solvent A: 2 mM NH4OAc in H2O/MeCN (95:5); solvent B: MeCN; solvent C: 2% formic acid with a gradien oft: 5 – 95 % B with constant 5 % C.

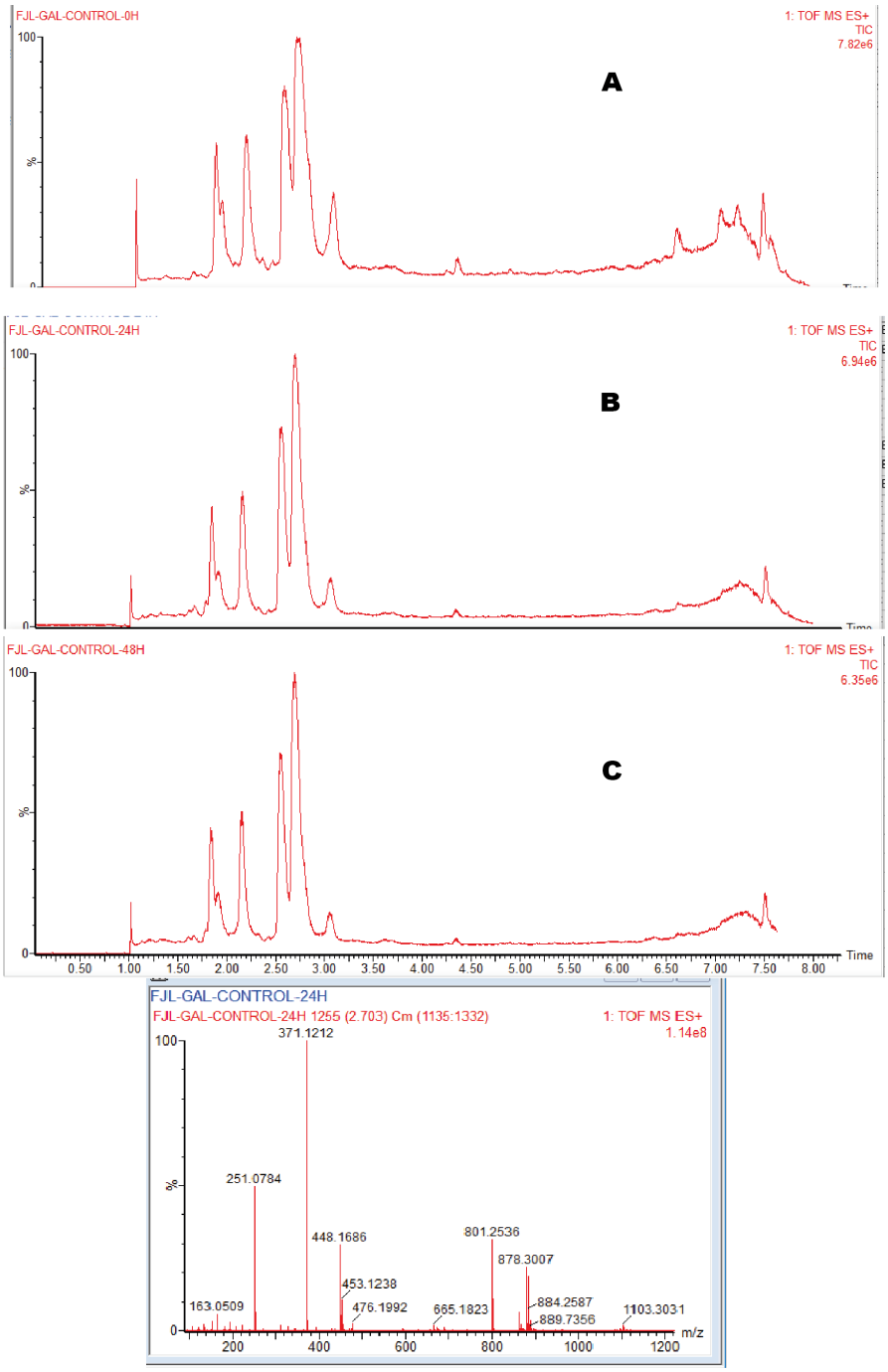

Figure 52 - Time course of HRMS of Ac_4GalNAz in PBS. A) 0h B) 24h C) 48h. Samples were heated to 37 °C between analysis runs. Aquired on a Waters Acquity UPLC system running in positive mode with an electrospray source. LC system: solvent A: 2 mM NH4OAc in H2O/MeCN (95:5); solvent B: MeCN; solvent C: 2% formic acid with a gradien oft: 5 – 95 % B with constant 5 % C.

In the 1:1 sugar mix sample after 48 hours there seemed to be little change in the sample. The only slight variation was the emergence/growth of a small peak around 3.5 minutes as highlighted in Figure 53. This was only a minor peak and no peak observed in the range you would expect for the bimolecular reaction (combined exact mass = 861.2764 AU, no anticipated added cation, NH_4^+, Na^+ or K^+, corresponded with the new peak at 937 m/z).

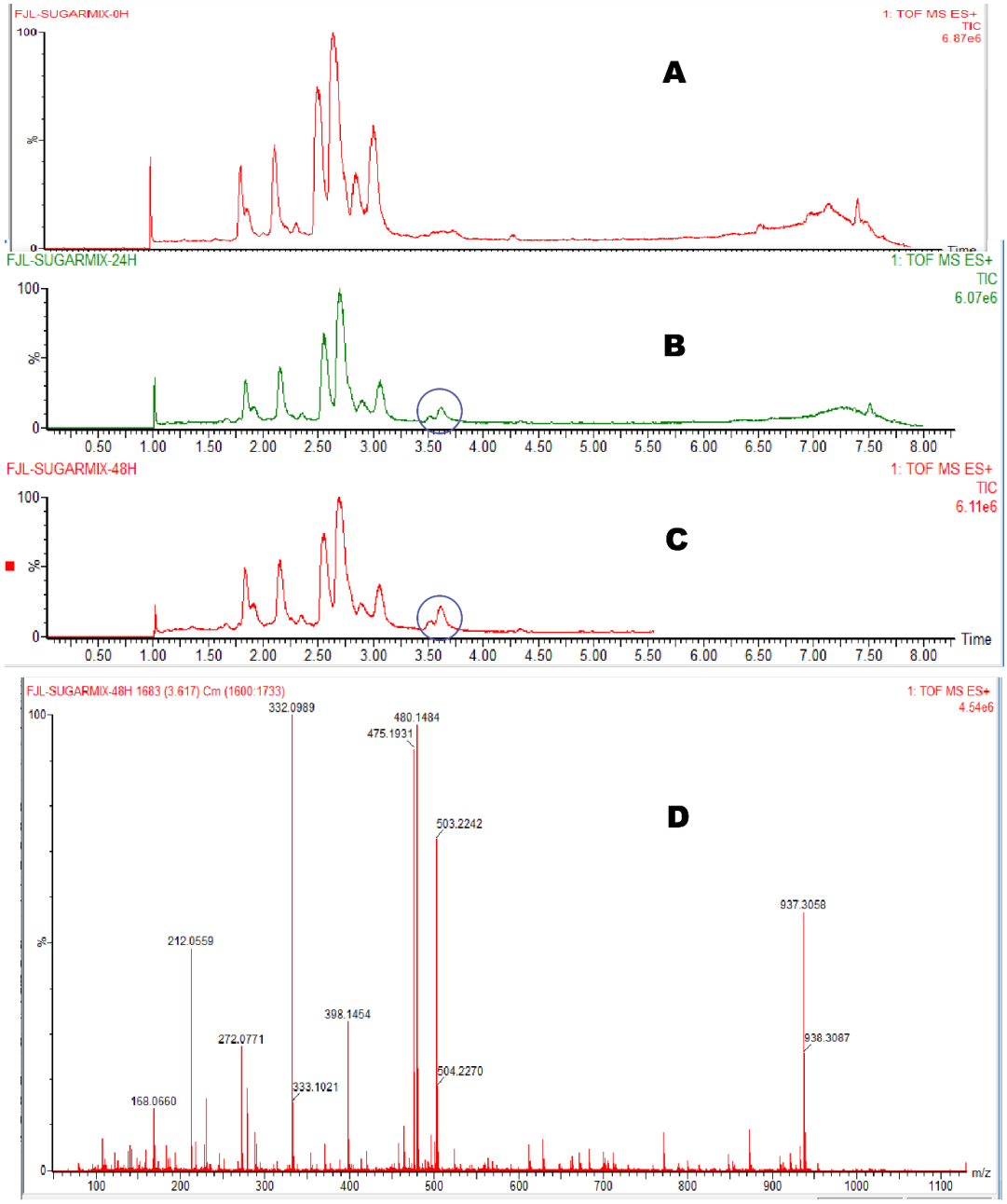

Figure 53 - Time course of HRMS of a 1:1 mix of Ac_3ManNCyoc:Ac_4GalNAz in PBS. A) 0h B) 24h C) 48h D) Mass trace of peak circled in 24h and 48h plots.

As the 1:1 mixed sample seems to remain largely consistent over the 48-hour time course, and over 24 hours (the incubation time *in vitro*), it seems unlikely this is the cause of the decrease in mannosamine induced labelling in dual treated samples. Even the small new peak which emerged, would not be sufficient to cause the decrease. The slow degradation of Ac_3ManNCyoc in the single sugar sample is also unlikely to be indicative of any cause, as degradation on its own would decrease labelling in the both the single treated and the dual treated samples.

Despite this we wanted to further probe to see if there is a potential cross reaction between the cyclopropene and azide motifs, even if this was not causing the decrease in labelling. To do this a model carbamate-linked methylcyclopropene (**5**) was synthesised and used to study the potential reaction with benzyl azide (Scheme 13). It was important to use a carbamate linked cyclopropene as previous studies had use amide linked approaches and did not note cross-reactivity.[148] First a HRMS experiment was carried out in a similar way to that used for the sugar compounds. Benzyl azide (**6**) and cyclopropene (**5**) single compound controls were run at 7.5 mM in MeOH, as well as a 1:1 mixture at the same concentration. Over 24 hours at 37 °C, no change was seen in the single treated samples.

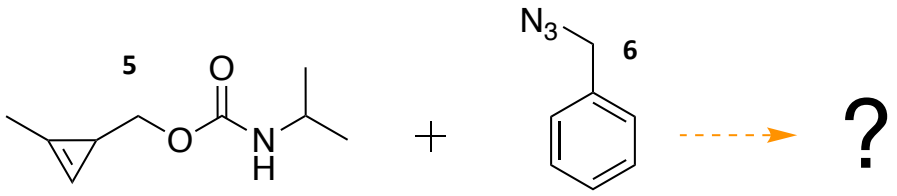

Scheme 13 – Model compounds used to study potential methylcyclopropene and azide cross reaction.

In the HRMS runs shown in Figure 54 the combined sample is simply an overlay of the single compound samples (the intensity is different due to the different ionisation potential of the compounds). Over 24 hours no reaction was observed, and the sample remained the same by HRMS. This indicated there was no reaction between the two species. The three peaks seen in the total ion count (TIC) chromatograph of benzyl azide are believed to be due to highly ionisable species present in the commercially sourced benzyl azide, which may be masking any benzyl azide ionisation.[159]

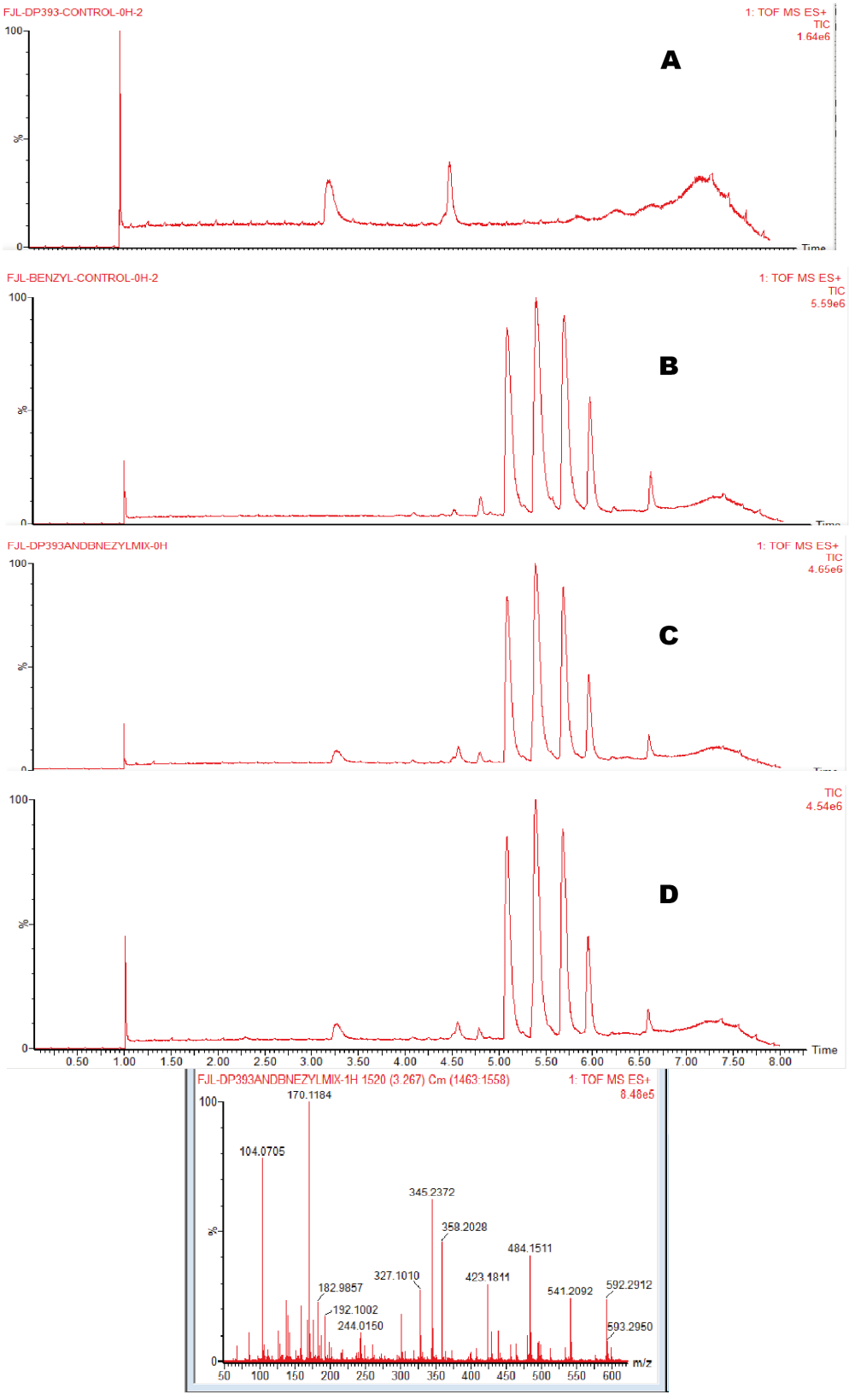

*Figure 54 - Time course of HRMS of a 1:1 mix of **5** and benzyl azide in MeOH. A) 5 alone at 0 h B) benzyl azide alone at 0 h C) 1:1 mix at 0 h D) 1:1 mix at 24 h.*

To further support this, similar experiments were run via ^{1}H NMR in deuterated acetone. Again, single sample controls were run as well as the 1:1 mix, at various time points after being heated to 37 °C. In these experiments the compounds were studied at 54 mM, in both the single and mixed samples. As can be seen in Figure 55, again the mixed sample is simply an overlay of the two reagents (the control samples). This does not change over the 24-hour time scale studied, indicating no reaction took place. Impurities are seen in the NMR spectra obtained for the commercially sourced benzyl azide, but these also had no effect.

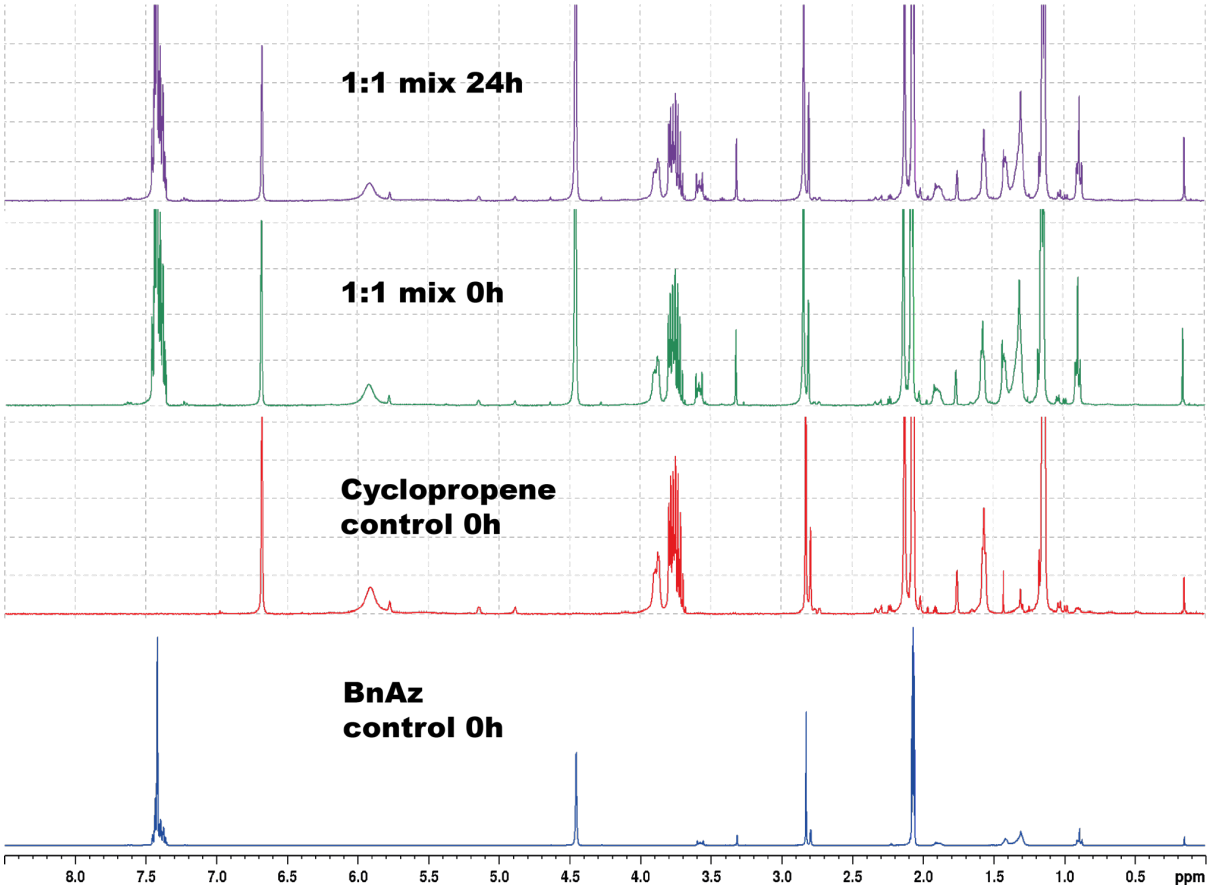

Figure 55 - ^{1}H NMR of 1:1 mix and control samples showing no reaction over 24 hours. Samples were heated to 37 °C between scans. ^{1}H NMR spectra were acquired at 400 MHz at room temperature in MeOD.

With all possible cross-reactivity combinations eliminated it remained unclear as to the cause in the decrease in ManNCyoc induced labelling in dual treated samples. With the chemical properties and reactions seemingly not the cause, it is likely to be a function of the complex cellular interactions associated with the sugars. For example, as interconversion of monosaccharides is documented[132] then perhaps the decrease could be due to interconversion of GalNAz into the sialic acid pathway. As the interconversion of GlcNAc to sialic acid ManNAc is known to occur via GlcNAc 2-epimerase[160] and

UDP-GalNAc can be epimerised to UDP-GlcNAc via UDP-glucose 4-epimerase.[161] However, this is unlikely due to the slow nature of these interconversions.[160]

Ongoing projects at CRUK had demonstrated that the tendency of COLO205 (and other cancerous cell lines) towards apoptosis as opposed to necrosis can result in inaccurate Vi-cell cell-viability measurements.[162] This is believed to be due to the lack of membrane degradation in apoptotic death, leading to a lack of uptake of the cell death marker (trypan blue), resulting in false positives (*e.g.*, apoptotic cells showing as viable). Therefore, we returned to the previous hypothesis (from earlier in this report and our previous publication[147]) that the dual sugar combination was resulting in growth inhibition or cell death, and this was causing the decrease in labelling.

To test this, cell viability was measured in an alternative cell line (MDA-MB-231) and as well as the original sugar concentrations used, lower sugar concentrations of single- and dual-sugar treated samples were analysed (Figure 56). There was no statistically significant effect on viability in the samples exposed to the previously used sugar concentrations (125 μM), although this may be due to one variant data point as the mean viability for the +Man +Gal (125 μM) sample does appear to be lower than the other treated and control samples. There is a significant difference in the viable and total cells per mL measurements, with only the +Man +Gal (125 μM) sample showing a much lower viable and total cells per mL. Cells were initially seeded at 0.25 x 10^6 cells After isolating the cell pellet the pellet was resuspended in 2 mL fresh media to analyse on the Vi-CELL. As such the +Man +Gal (125 μM) sample, at 0.11 x 10^6 viable cells mL^{-1}, means there were a total of 0.22 x 10^6 viable cells in the sample. This indicates the cell growth inhibition (and potentially cytostatic nature) of this sugar combination at that concentration. The single treated samples at 125 μM did not show the same effect. Also of importance are the +Man +Gal (50 μM) treated samples did not see any effect on cell growth. All samples except +Man +Gal (125 μM) approximately doubled in cell number in the 48 hours between seeding and measurement, which fits with the untreated growth shown in (Figure 49). Therefore, we believe the high sugar concentration of 125 μM of each sugar, and so essentially 250 μM of total tagged sugar concentration has a significant effect on cell growth. As cell growth is heavily interlinked with glycosylation, the reduction in cell growth is what we believe to be leading to the decrease in labelling in dual treated samples.

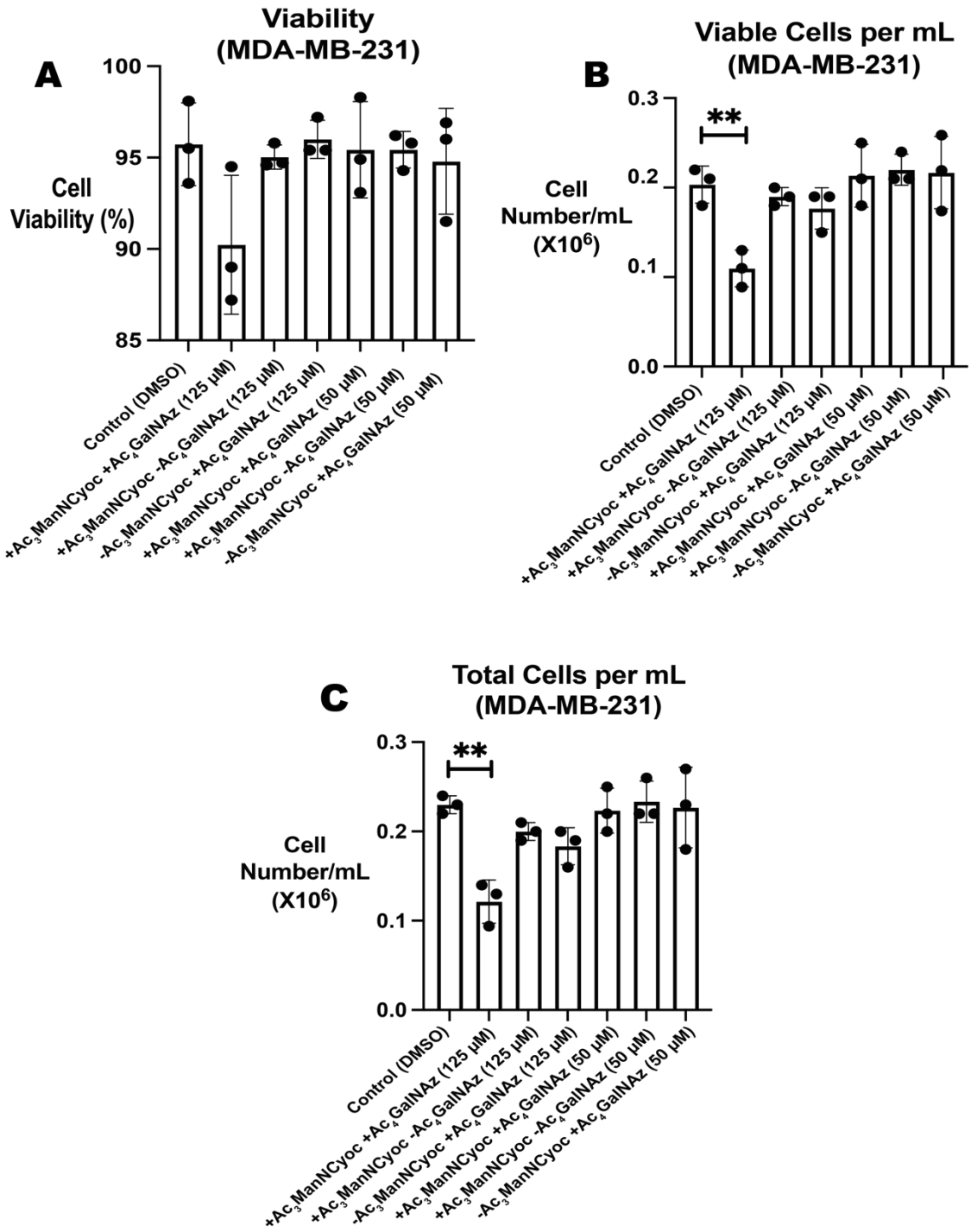

*Figure 56 – The effect of dual sugar treatment on the viability and growth of COLO205 cells. MDA-MB-231 cells were incubated in the presence or absence of the indicated sugar(s) (125 or 50 µM) for 24 h. The cells pellet was collected and resuspended before being analysed on a Vi-CELL XR cell viability analyser. A) Shows the cell viability of each sample B) the number of viable cells per mL and C) the total cells per mL; n=3 technical replicates. Statistical analysis was performed using an unpaired t test with Welch correction (**** P≤0.0001,*** P≤0.001,** P≤0.01,* P≤0.05).*

To test the hypothesis that the reduction in cell growth was causing the decrease, we conducted the same labelling experiments previously conducted, but incubating the cells with the lower sugar concentration which did not show any effect on viability (50 µM). The cells were collected and labelled

using identical conditions to the previous experiments, and the subsequent flow cytometry data is shown in Figure 57 below. In the dual treated sample the SBR from the Tz488 channel is actually larger (26.3 ± 3.1) than in the 125 μM experiment (22.9 ± 3.9) although this difference is not statistically significant, the fact labelling does not decrease at lower sugar concentrations does support the growth suppression hypothesis. The single Ac_3ManNCyoc treated sample does have a lower SBR from the Tz488 channel than the 125 μM experiments (33.9 ± 2.7 and 41.3 ± 1.3 respectively). There is still a difference between the dual and single Ac_3ManNCyoc treated samples in the Tz488 channel (unpaired Welsh t tests show a p value of 0.033) but this difference is now much lower than the 2-3-fold decrease we had previously seen. This further supports our belief that the reduction we see is due to the cell growth inhibitory behaviour of these tagged sugars, particularly at higher concentrations. In the dual- and single-treated Ac_4GalNAz samples the TMDBIO-647 channel SBR does decrease by almost a factor of 2 when the reduced sugar concentration is compared to the original experiments in Figure 44. As seen in the previous experiments there is no decrease in the TMDBIO-647 channel SBR between single and dual treated Ac_4GalNAz samples.

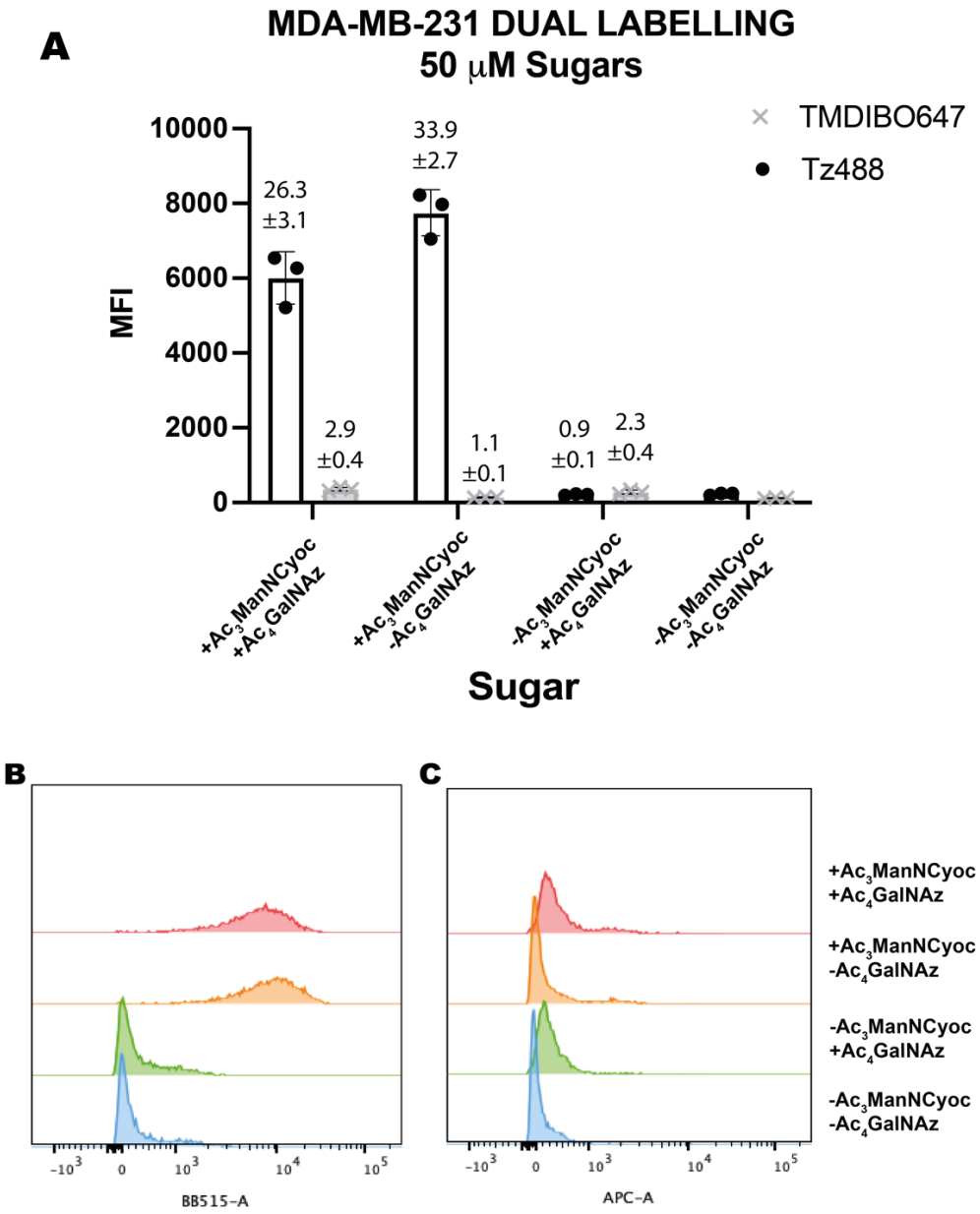

Figure 57 – Reduced concentration dual sugar treatment of HEK293 cells A) MDA-MB-231 cells were incubated in the presence or absence of the indicated sugar (50 μM) for 24 h. They were then incubated with the dye solution (Tz-PEG$_{11}$-AlexaFluor488 (5 μM) + TMDIBO-Lys-AlexaFluor647 (50 μM)) for 1 h at 37 °C and analysed by flow cytometry. Median fluorescence intensity (MFI) is shown as mean ± SD. Signal-to-background ratios (SBR) relative to the control (-Man-Gal) are above each bar; n=3 technical replicates. B) and C) Histograms giving number of events (vertical axis) versus fluorescence intensity (horizontal axis) B) Tz-PEG$_{11}$-AlexaFluor488 and C) TMDIBO-Lys-AlexaFluor647. In each panel the sugars used, from top to bottom, are: +Man+Gal, +Man-Gal, -Man+Gal and then the no-sugar control.

2.4. Summary and Future Work

2.4.1. Summary

Ac_3ManNCyoc (and Ac_2ManNCyoc) showed enhanced labelling relative to the widely used tetracetylated derivative. Other Cyoc-tagged monosaccharides did not show the same effect, and with azido tagged sugars, decreased acetylation led to decreased labelling. The decreased hydrophobicity of Ac_3ManNCyoc allowed for first-in-kind *in vivo* studies with COLO205 implanted mice. These initial *in vivo* experiments showed modest contrast between sugar treated and dye alone treated mice.

Further *in vitro* studies showed MDA-MB-231 and PANC-1 had much greater levels of sialylation relative to COLO205. All acetylation levels of Ac_xManNCyoc showed enhanced labelling but this was particularly pronounced for Ac_3ManNCyoc. We believe these models will show better contrast *in vivo*, due to the increased hypersialylation, as well as potentially being more homogenous *in vivo*.

Further *in vitro* work with our lead compound Ac_3ManNCyoc enabled us to visualise the labelling of MDA-MB-231 cells via fluorescent microscopy. This confirmed extracellular labelling, and a clear maximum of labelling at the edge of the cell.

Dual sugar labelling with Ac_3ManNCyoc and Ac_4GalNAz across multiple cell lines showed the ratio of incorporation of each of the monosaccharides. It was found that the fastest growing cell lines had the greatest relative ratio of sialylation, suggesting that hypersialylation is a vital part of enhanced cell growth and as such is an important tumour marker. Labelling from ManNCyoc-tetrazine bio-orthogonal ligation was significantly reduced in the presence of GalNAz. Various controls, HRMS and ^{1}H NMR experiments ruled out any chemical cross reactivity as a potential cause. Cell growth inhibition was seen in dual treated samples that was not seen in the single-treated samples. Reduced sugar concentration (50 μM instead of 125 μM) did not show the same growth inhibition effect. Labelling of cells treated at this reduced concentration still showed significant SBR but now with labelling from ManNCyoc-tetrazine bio-orthogonal ligation not much reduced by the presence of GalNAz.

2.4.2. Future Work

We believe Ac_3ManNCyoc is a novel candidate for labelling tumour hypersialylation *in vivo* and that further *in vivo* studies with MDA-MB-231 (or PANC-1) implanted mice would lead to enhanced contrast compared to the contrast seen with COLO205. As well as conducting this *in vivo* work with fluorescent imaging it is believe this approach can be adjusted to do first-in-kind PET studies. In collaboration with Flaviu Bulat a tetrazine probe which replaces the fluorescent dye with a NODAGA chelator has been synthesised (Scheme 14).

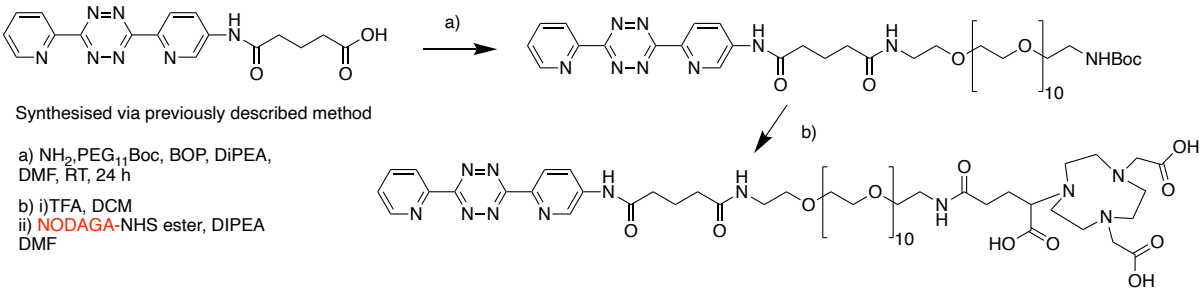

Scheme 14 – Synthesis of Tetrazine-PEG_{11}-NODAGA.

Flaviu has been able to radiolabel the Tetrazine-PEG_{11}-NODAGA with Ga^{68} and by adapting the *in vitro* labelling protocol has been able to demonstrate contrast *in vitro*. This is an exciting potential project which would be the first reported use of PET imaging with MOE. The advantages of PET imaging *in vivo* would make this a much more clinically applicable technology.

Response to treatment has been a key driver at CRUK in recent years. Rapid detection of whether a patient is responding to a particular treatment, allows clinicians to make better decisions, and potentially try more treatment options in the same timeframe. It would therefore be of interest if a change in sialylation (detected via single or dual labelling) resulted from treatment of cells with a potent cytotoxic compound. Ultimately demonstrating this response to treatment *in vivo* would make a potential clinical application for MOE.

Future dual sugar labelling experiments should be conducted with the lower concentrations of sugars (50 μM instead of 125 μM). A cell death marker with fluorescence at a wavelength different from the two probes used could be used to gate the cells and ensure that only viable cells are being used to measure cell surface fluorescent labelling. Targeting the close proximity of sialic acid and GalNAc residues in onco-foetal anitgen sTn, via dual sugar labelling, could allow for Förster resonance energy transfer (FRET) based detection of these antigens.

3. Improved Kinetics of Bioorthogonal Reactions

3.1. An introduction into Strained Cyclooctenes as Probes for SPAAC

As previously discussed, the enhanced kinetics of SPAAC reactions relative to Staudinger ligations and the lack of requirement for heavy metal catalysts seen in CuAAC/RuAAC means that SPAAC reactions are a better way to ligate the widely used azide reporter group. An important factor in SPAAC reactions is the nature of the strained cyclooctyne. Enhanced kinetics is a constant driving force behind the new development of cyclooctynes, but this has to often be balanced against stability, with the two often being a difficult balancing act.[46] The stability of cyclic alkynes increase with ring size, due to decreased distortion of the bond angle from the ideal linear 180° angle. Cyclooctynes are the smallest ring size isolatable for cyclic alkynes, with the alkyne bond angle of 163°, resulting in 18 kcal mol^{-1} of ring strain.[67]

The first reported cyclooctyne for SPAAC was cyclooctyne (OCT) (Figure 59) by the Bertozzi group in 2004.[67] The probe offered significant rate enhancement over uncatalysed reactions with linear alkynes, but the reaction kinetics were still considerably less than CuAAC reactions.[163] Rate enhancement was achieved by placing electron withdrawing groups at the propargylic position (Figure 58), as was done with two fluorine atoms in difluorocyclooctyne (DIFO).[164] The enhanced kinetics allowed for the first *in vivo* use of SPAAC.[98]

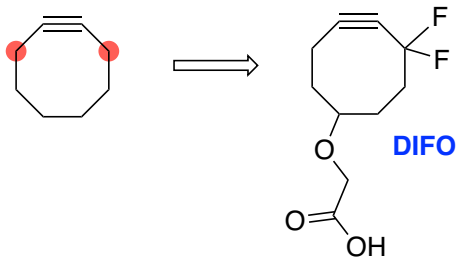

Figure 58 - The propargylic position on cyclooctyne highlighted in red. Substitution here led to the development of DIFO with electron-withdrawing fluorenes.

An alternative way to increase the reaction rate was found to be achieved by increasing the distortion through conformational constraints. This was achieved by fusing aromatic rings as first demonstrated by dibenzocyclooctyne (DIBO).[165] Further advantages of this strategy were enhanced ease of synthesis and the potential to use the aromatic rings for easy attachment of motifs such as fluorophores.[165]

However, DIBO was found to be unstable and decomposed within a few days when stored at room temperature. Further to this, the probe was also significantly hydrophobic. This led to the development of tetramethoxydibenzocyclooctyne (TMDIBO) by the Leeper and Brindle groups[124], which via addition of methoxy groups to the aromatic rings, increased the stability and decreased the hydrophobicity relative to DIBO (and showed a slight rate enhancement). Despite the improvement in hydrophobicity, these fused cyclooctynes all have high lipophilicity which can result in non-specific binding.[166] Alternatively strain was introduced by fusion of a cyclopropane ring in the example of bicyclo[6.1.0]non-4-yne (BCN)[167] but the lack of benzo-fusion leads to instability in biological settings.[168]

Addition of an sp^2-like centre into the cyclooctyne ring of the dibenzocyclooctyne has been shown to lead to further rate enhancement.[46, 169] This has been demonstrated by the introduction of an amide nitrogen into the ring first carried out by Debets *et al*. in the synthesis of dibenzoazacyclooctyne (DIBAC).[169] The rate of SPAAC was then further enhanced by the development of biarylazacyclooctynone (BARAC), with the amide now inside the ring as part of a lactam.[46, 170] A comparison of the rates of probes discussed in this section is seen in Figure 59. 3,3,6,6-Tetramethylthiaheptyne, a strained 7 membered sulfur containing hetrocycle does show kinetics SPAAC greater than BARAC but decomposes before it can be isolated.[68, 171]

One of the fastest SPAAC probes synthesised to date is oxa-dibenzocyclooctyne (ODIBO) with an ether linkage internal in the cyclooctyne and the alkyne installed via photochemical elimination of a cyclopropenone.[172] However, direct comparison is difficult as, while the SPAAC reaction with benzyl azide is faster than that measured for BARAC, they were measured in different solvents which has significant effect of the rate of SPAAC reactions and the kinetics of cycloadditions in general.[68, 173] Particularly prominent is the rate enhancement of SPAAC reactions in aqueous solvents, with this seemingly caused by higher polarity and/or donor-acceptor interactions with the solvent, as opposed to any aggregation/solubility effects.[172] Comparison of rates is also affected by the azide used, with benzyl azide perhaps the most widely used (but notably insoluble in water) and the structural and electronic properties of the azide also affects the rate.[68] An additional factor to consider when comparing measured reaction rates in general is the measurement technique used. ^{1}H NMR is a widely used but is very limited for fast reactions due to the time lapse between mixing and measurement, often leading to underestimates of the rate.[68, 124, 172] *In situ* techniques providing real-time measurement based on UV or IR absorptions are better at measuring the kinetics of fast reactions under pseudo-first order conditions.[68] All the kinetic measurements conducted in this report were

measured using a stopped-flow system which maximises rapid mixing and UV detection to capture the rapid kinetics of the reactions studied.

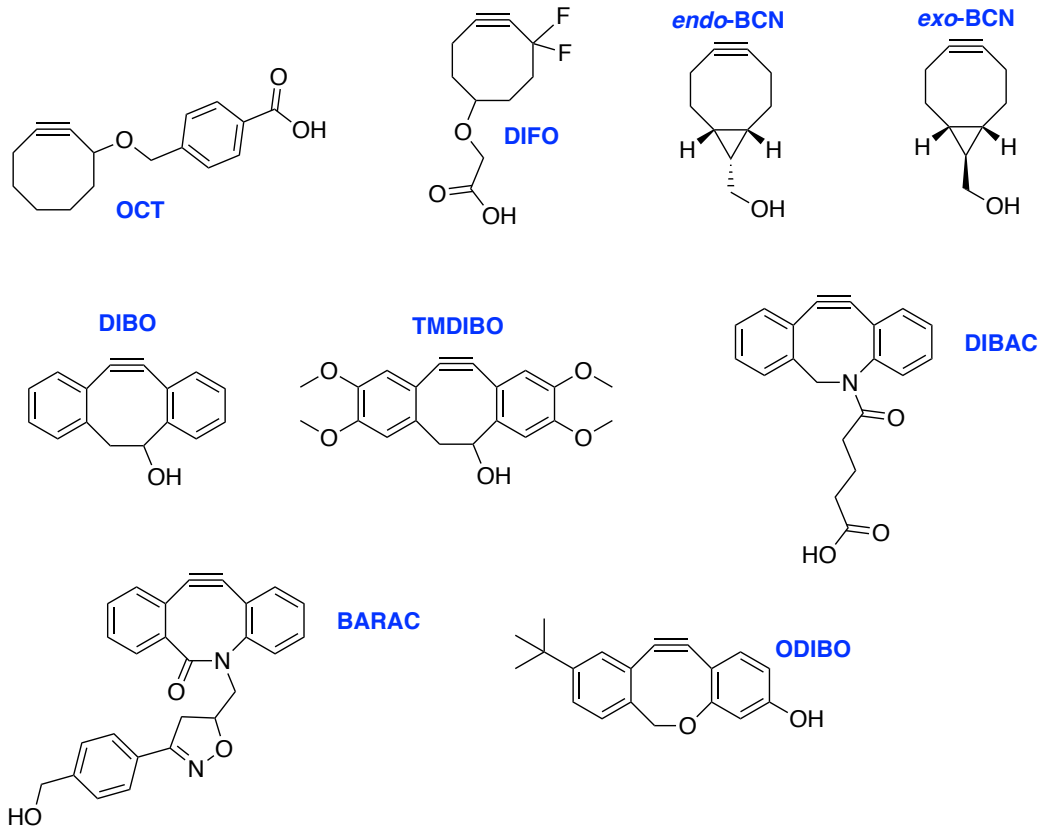

Figure 59 - A selection of strained cyclooctyne probes.

Table 4 - Kinetic properties of assorted SPAAC probes.

Probe	k_2 of SPAAC with BnAz (x 10^{-2} M^{-1} s^{-1})	Solvent used for kinetic measurement	Technique used
OCT	0.24[67]	CD_3CN	NMR
DIFO	7.6[164]	CD_3CN	NMR
BCN	14 (endo)[167] 11 (exo) [167]	CD_3CN:D_2O (3:1)	NMR
DIBO	5.67[163]	MeOH	UV
TMDIBO	9.4[124]	MeOH	UV
DIBAC	31[169]	MeOH	NMR
BARAC	96[170]	CD_3CN	NMR
ODIBO	166[172]	MeOH	UV

3.2. ODIBO scaffolds

3.2.1. Synthesis of Novel ODIBO Scaffolds

The reported kinetics of the SPAAC reaction of ODIBO with azides were promising. However, as is often the case with these highly strained probes, it is a very hydrophobic compound. This has perhaps limited its usage, particularly for *in vivo* imaging purposes, where hydrophobicity leads to non-specific accumulation, ultimately negating contrast. In fact, when a ^{18}F-labelled ODIBO-linked prostate specific membrane antigen (PSMA) ligand was synthesised from reaction of ^{18}F-ODIBO with an azide tagged PSMA ligand, negligible contrast was observed compared to a similar BCN-linked analogue.[174] This lack of contrast with the triazole PMSA ligand formed from reaction of ODIBO, was believed to stem from the hydrophobicity of the reagent negatively effecting the biodistribution.

Our aim was to harness the enhanced kinetics from ODIBO but reduce the hydrophobicity. Taking the core ODIBO scaffold shown in Figure 60 we envisioned 3 possible sites for modification. The most obvious modification was to replace the very hydrophobic ^{t}Bu group, with a more hydrophilic substituent. Alternatively, we envisioned building a handle from R^2 to attach on a hydrophilic (and potentially charged) motif. However, modification at R^1 and R^2 had the potential to be synthetically challenging, due to the key Friedel Crafts step in the synthesis. Conjugation at R^3 to attach a hydrophilic linker (which would also act as a handle to attach on the resulting imaging agent) was believed to be a possible alternative.

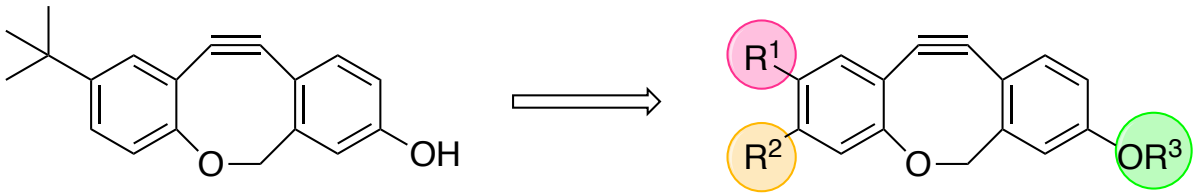

Figure 60 - Potential ways to reduce ODBIO hydrophobicity

First the original scaffold was synthesised to optimise and gain experience in the synthetic procedures (as well as potentially include the R^3 linker). The synthetic route used was based on an updated version of the route carried out initially by Popik et al.[172] This updated route, again by the Popik group[175], used silyl protection of the phenol instead of MOM (making the deprotection less harsh) and used a Mitsunobu reaction to form the ether, as opposed to using an S_N2 reaction between an alkyl bromide and a phenol. As shown in Scheme 15, below the multistep synthesis begins with silyl protection of 3-

hydroxybenzaldeyhde, which proceeded in near quantitative yield. Reduction of the aldehyde **8** with sodium borohydride successfully yielded the benzyl alcohol **9** in similarly high yield (94%). **9** was reacted with 4-tert-butylphenol using DIAD and triphenylphosphine via a Mitsunobu reaction. The resulting ether **10** was easily isolated despite the often difficult to remove by-product triphenylphosphine oxide. In this case the work up procedure and chromatography were sufficient to remove any Ph_3PO. Following the Mitsonobu reaction, the ether underwent an intramolecular Friedel Crafts cyclisation using tetrachlorocyclopropene and $AlCl_3$ to form the cyclopropenone. Following the cyclisation, the next step was removal of the *tert*-butyldimethylsilyl protecting group with TBAF. Finally, the photochemical step was tested using a newly acquired Rayonet reactor. Using the very dilute reaction concentration and short reaction times described in the previous literature,[172, 175] and following the reaction by liquid chromatography mass spectroscopy (LCMS), partial completion was observed (product formed but still some photo-ODBIO **12** left). After increasing the reaction times, there was no change in %completion. We believed this to be a consequence of the experimental set up, as in this batch Rayonet system the reaction mixture is not stirred. This meant a heterogenous solution in which the outer layers of the vessel were exposed to the UV radiation and could react, whereas the centre of the tube was not sufficiently penetrated by the UV light. A small magnetic stirrer plate could not be used due to the position of a metal fan to cool the system. Instead, it was found that stopping the reaction at 10-minute intervals, vigorously shaking, and restarting the reaction, for a total of 30 minutes, led to complete conversion of photo-ODBIO **12** to ODBIO **13**.

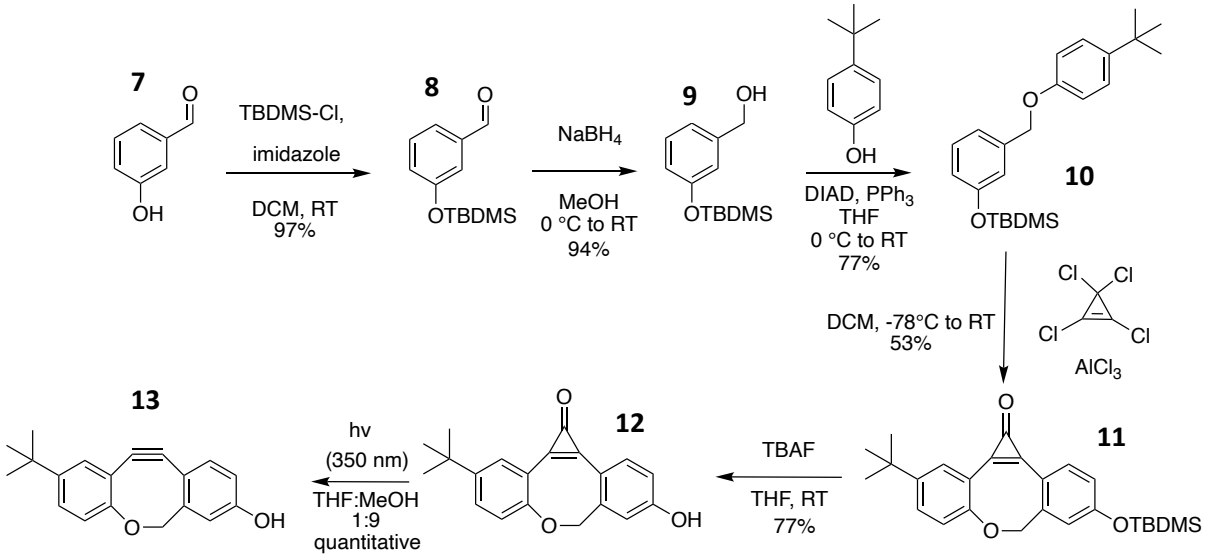

Scheme 15 - Synthesis of ODIBO.

With the core scaffold in place, potential substitution was attempted. Replacement of R^1 was an obvious way to do this, simply replacing the ^{t}Bu with a hydrogen reducing the cLog P of the photo-reacted product from 5.78 to 3.96 (Scheme 16). However, this implicitly simple way to reduce the

hydrophobicity, was perhaps too obvious - the ^{t}Bu may well be essential for the cyclisation reaction, in either a steric- or electronic-directing capacity. A ^{t}Bu is *ortho-para* directing in terms of its electronic properties, with the *para* position already substituted by the ether which is also *ortho-para* directing. The ether is the dominant directing effect, and with the ^{t}Bu blocking the *para* position the only likely site for substitution is *ortho* to the ether (*meta* to the ^{t}Bu). As such, we imagined replacing this ^{t}Bu group with another, less hydrophobic motif to block this *para* position would lead to efficient synthesis. Despite this in the initial report of ODIBO by Popik et al[172], replacement of the ^{t}Bu with a methyl substituent proved challenging, with the steric properties of the ^{t}Bu perhaps in some way important.

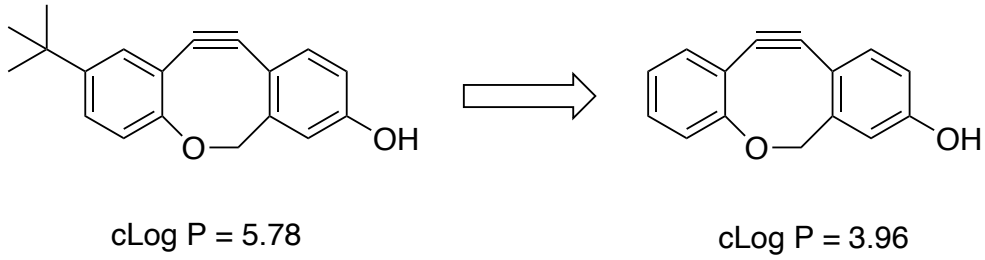

Scheme 16 - cLog P of ODIBO derivatives. Calculated using ChemDraw.

In terms of simply making the ODBIO derivative with the ^{t}Bu removed, the difficulty in this is highlighted by the Popik group themselves. In their original report[172] they were able to make a compound with the ^{t}Bu replaced by a proton, but a methoxy group is added in position R^2, and they report a very low yield for this synthesis relative to the ^{t}Bu derivative. When this synthesis was attempted (replacing 4-tert-butylphenol with phenol in the Mitsunobu reaction) no product was detected in the subsequent cyclisation by LCMS or ^{1}H NMR of the crude.

The cyclised product post-Friedel Crafts acylation can easily be identified in the crude ^{1}H NMR via the characteristic doublets corresponding to the CH_2 protons in the newly formed ring. These protons are placed into different environments by the slow interconversion between two mirror-image conformations of the product and are easily distinguished due to their large *J* values of around 12 Hz, with the doublets coming between 5.5 and 4 ppm (Figure 61).

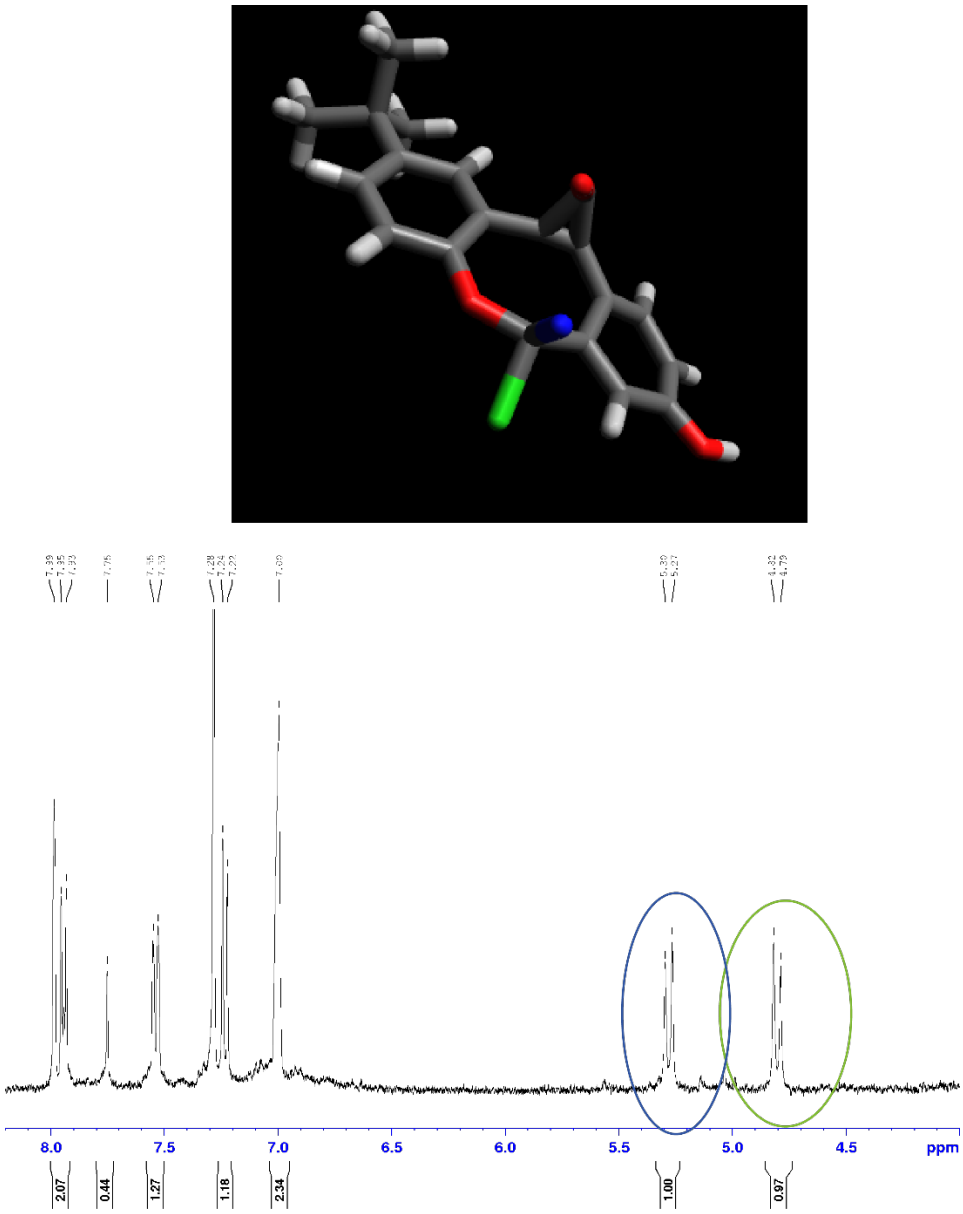

Figure 61 - Snapshot of NMR with characteristic doublets corresponding to the blue and green protons in the molecule above. 3D conformation using Avogadro molecular editor.

Further attempts to replace the ^{t}Bu were carried out by myself and two Part III students as part of their Masters projects, Şeyma Sever and Sam Thomson. Some of the compounds whose syntheses were attempted are shown below. For most of the compounds the synthesis failed at the Friedel Crafts cyclisation. It seemed that the ^{t}Bu was essential for this part of the synthesis, likely due to its steric directing properties. More detail on this can be found in their Part III reports.

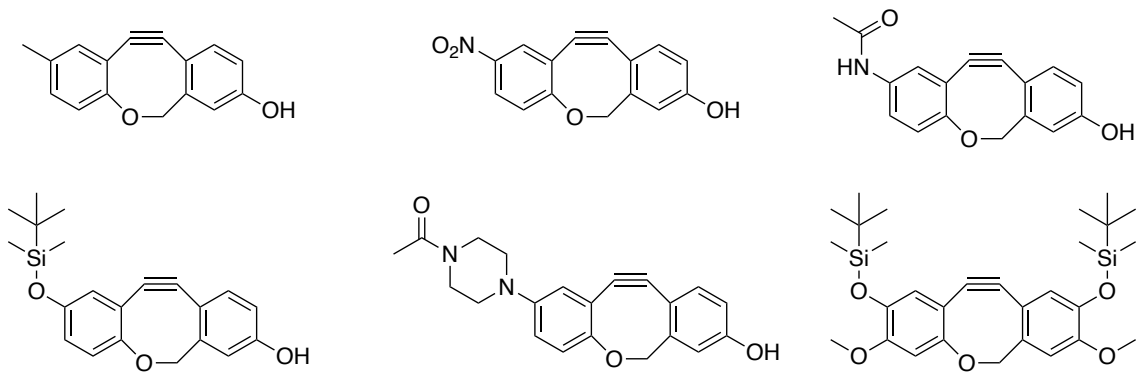

Figure 62 – Attempts at replacement of the ^{t}Bu group at position R^1.

Brief attempt was made to add a substituent at R^2 but even just a methyl group (Figure 63) was not tolerated during the Friedel crafts acylation step.

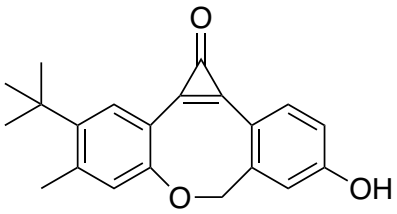

Figure 63 – Desired product of initial attempts at replacement at R^2.

Instead, focus was placed on adding a hydrophilic linker at position R^3 as we believed this would be synthetically easier. Previously addition of a lysine linker to TMDIBO had been achieved[102], and since this would allow us to compare the labelling more analogously, we aimed to introduce this as a linker in a similar fashion to TMDIBO. Our first step was to make the para nitrophenyl carbamate, which could then be reacted with a Boc-protected lysine to give us the desired product. The lysine residue was to be attached before any photochemical reaction, as it is believed the alkyne product is unstable especially in aqueous environments.[172] Leaving the photochemical step till as late as possible in the synthesis was therefore a directive for all the syntheses designed in this project. With this in mind Photo-ODIBO (**12**) was reacted with 4-nitrophenyl chloroformate to form the carbamate **14**. However, the product was not isolated perhaps as was as there were two potential phenolic leaving groups, making the compound unstable.

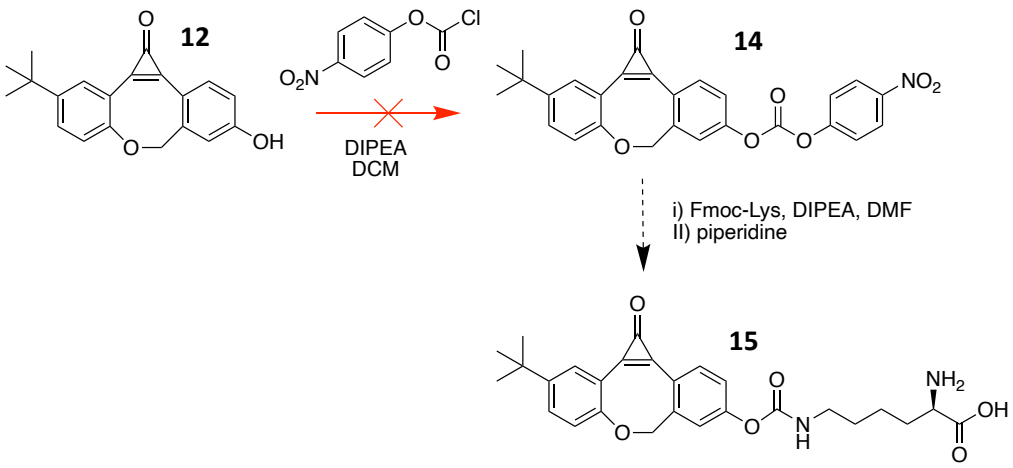

Scheme 17 – Attempted direct conjugation of lysine.

To combat this, a propyl linker was added to the phenolic handle. From this linker with a hydroxy tail, the PNP carbamate could then be formed, knowing that the PNP would be a much better leaving group than an alkoxide. To do this **12** was subjected to an S_N2 alkylation with 2-bromopropanol under reflux to give **16** (Scheme 18). **16** was then reacted with 4-nitrophenyl chloroformate to give the PNP-carbamate **17**. **17** was then subjected to the conditions used to synthesise TMDIBO-Lys, reacting with α-Fmoc-protected Lys using anhydrous DIPEA as a base. The planned route was then to deprotect the lysine to give the free amine **19**, before photochemically reacting to form **20** and then finally attaching the fluorophore. However, during the deprotection the piperidine, used to cleave the Fmoc, is believed to have reacted with the deprotected ODIBO product. This was observed via following the reaction by LCMS; Fmoc removal was observed but a side product of higher molecular weight subsequently formed and ultimately became the main product. It was suspected that the excess piperidine or Fmoc by-products have reacted with the ODIBO, but this potential side product was never to confirm this. Even when the stoichiometry of the reaction was adjusted to decrease the number of equivalents of piperidine used, degradation was still observed, but now with incomplete deprotection.

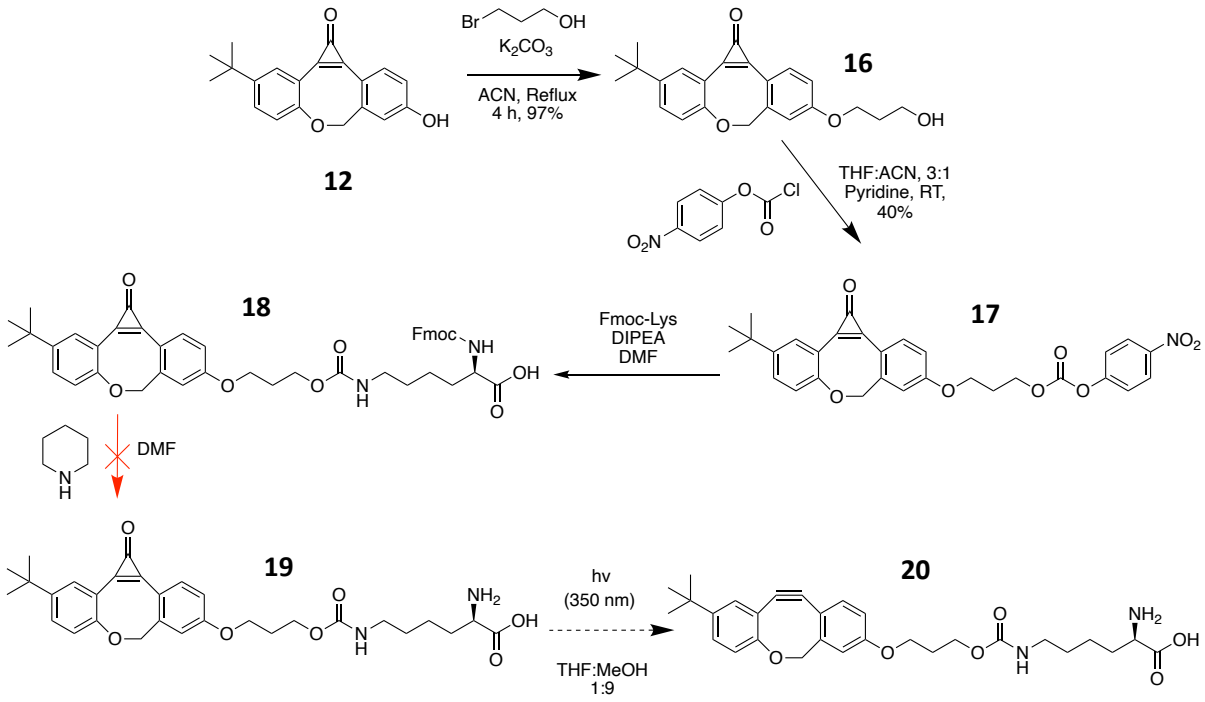

Scheme 18 - Attempted synthesis of ODIBO-Lys with ether linakge.

Instead, the order of the final few steps was switched in order to take the Photo-ODIBO-Lys-Fmoc (**18**) and photochemically react, then deprotected and finally couple with the fluorophore (Scheme 19). The photochemical reaction proceeded as it had for the original scaffold, with completion monitored by LCMS. The Fmoc protecting group was cleaved, under the previous conditions, using piperidine, which successfully led to the deprotected product (**21**). Purification was then carried out on (**21**) to remove the by-products of the deprotection (*N*-fluorenylmethyl-piperidine (Scheme 19B) and excess piperidine). After normal phase chromatography no product was isolated and reverse phase HPLC also led to insufficient material. This may have been as a consequence of the instability of the alkyne product which has been noted to be particularly unstable in aqueous systems.[172] When the crude product from the deprotection reaction (**21**) was used without purification to couple with the AlexaFluor647-NHS ester, the desired ODIBO-Lys-647 (**22**) was not isolated and only unreacted ODIBO-Lys was recovered. We believe this to be because of either residual piperidine or the by-products of the deprotection reacting with the NHS ester, with the undesired compounds potentially acting as nucleophiles for the attack and likely being in larger excess.

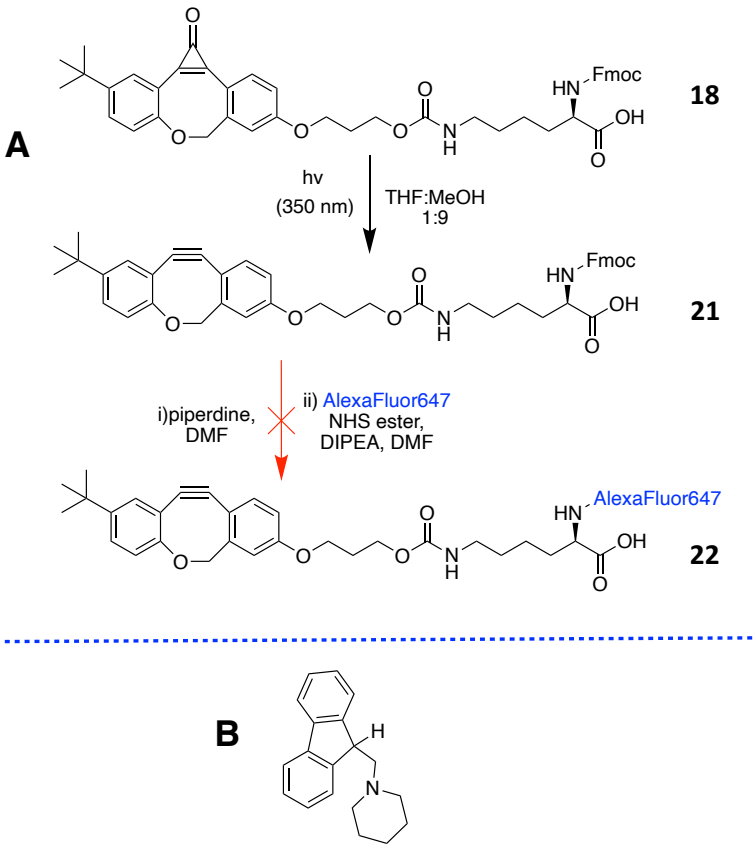

Scheme 19 – A) Alternative route to ODIBO-Lys-649 but no product was observed after final step. B) N-Fluorenylmethyl-piperidine by-product of deprotection step.

An alternative route was designed using α-protected Boc lysine to minimise the unwanted by-products following the deprotection. The synthesis was carried out as above, but now the deprotection was carried out with TFA. However, when the photo-reacted compound **24** was subjected to the TFA deprotection conditions, LCMS did not show any of the desired product (Scheme 20A) and only a complex mixture of products was observed. Upon altering the deprotection conditions to use HCl in dioxane a mass which corresponded to the deprotected product, but with HCl added was obsereved. We believe that the excess HCl was added across the reactive alkyne bond, with halogen splitting in the MS confirming chlorine had been added (Scheme 20B).

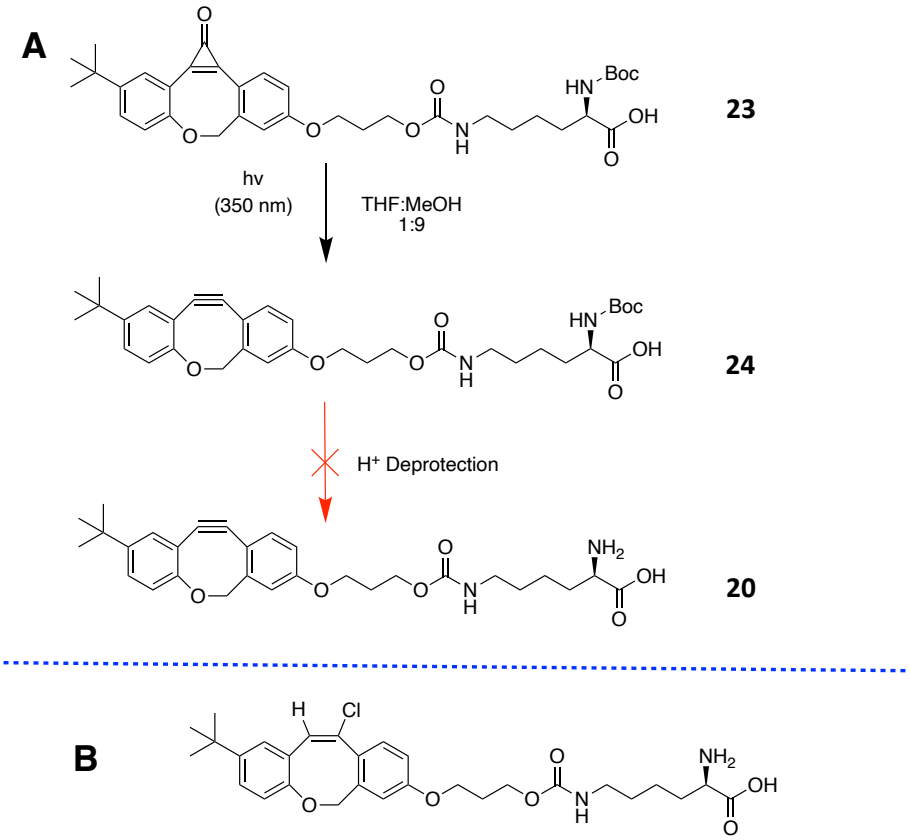

Scheme 20 – A) Using Boc-Lys to access Fluorophore tagged ODIBO-Lys. Acid deprotection failed with HCl in dioxane believed to lead to by-product B).

To combat this, the first synthetic route was attempted (*i.e.*, deprotection followed by photoreaction) but using Boc-Lys instead of Fmoc-Lys. **23** was deprotected with TFA in DCM and the product **21** was then purified by HPLC to remove any impurities before the photochemical step, as previously the alkyne had been seen to be unstable under the HPLC conditions. **20** was then photochemically reacted under the previously optimised conditions. **20** was then reacted with AlexaFluor647 NHS ester, using DIPEA as a base, in DMF, as had been used in previous fluorophore coupling reactions. Half of the crude reaction mixture was taken and HPLC purification attempted in an ammonium formate buffered aqueous system. However, no product (**22**) was isolated from the purification, only residual unreacted dye. The remaining crude reaction mixture was concentrated and left on the high vacuum pump to remove as much as possible of the DMF and DIPEA. The reaction was carried out with a slight excess (1.2 eq.) of **22** to ensure complete consumption of the NHS ester.

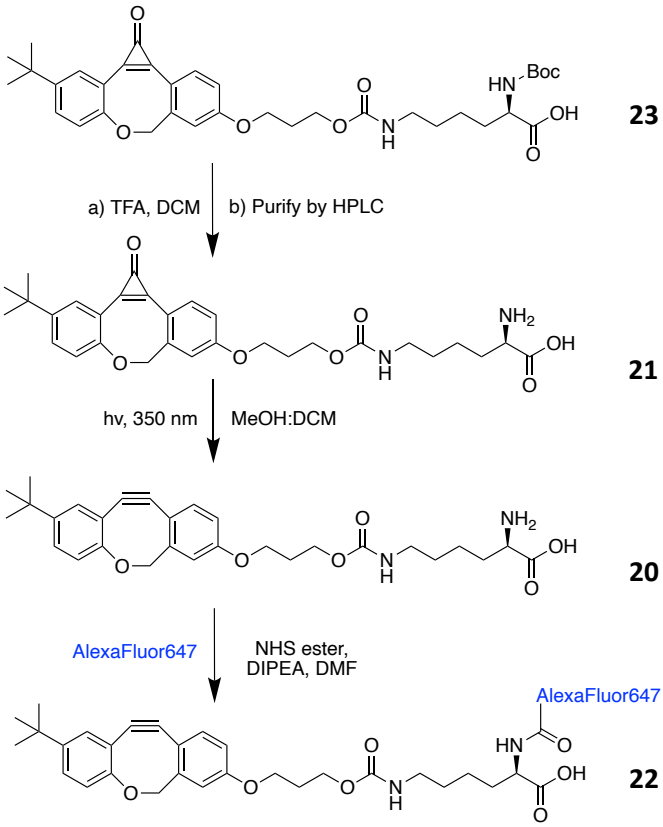

Scheme 21 – Adjusted final synthesis towards crude ODIBO-Lys-AlexaFluor647.

3.2.2. *In Vitro* Testing of ODIBO-Lys

Without further purification, the crude ODIBO-Lys-AlexaFluor647 was taken forward for *in vitro* testing. We wanted to compare the labelling of ODIBO-Lys-AlexaFluor647 with our current probe TMDIBO-Lys-AlexaFluor647. To do this, COLO205 cells were incubated either in the presence or absence of $Ac_4ManNAz$ (125 μM) for 24 h. Cells were then labelled with either ODIBO-Lys-AlexaFluor647 or TMDIBO-Lys-AlexaFluor647 and analysed via flow cytometry in accordance with the previously used protocols.

The resulting labelling is shown in Figure 64. The fluorescent intensity of the sugar-treated samples is comparable when either ODIBO-Lys-AlexaFluor647 or TMDIBO-Lys-AlexaFluor647 was used for labelling. However, in the untreated samples the fluorescence intensity is much higher with ODIBO-Lys-AlexaFluor647. This higher background signal massively reduces the contrast (SBR) from 11.5 ± 0.6 with TMDIBO-Lys-AlexaFluor647 to 2.1 ± 0.2. It is not believed this is due to unreacted dye left in the crude ODIBO. This is for several reasons: firstly, the unreacted dye is very polar and likely easily washed away, secondly little unreacted dye likely remained due to using an excess of the ODIBO precursor and thirdly the MFI of both sugar treated samples is very similar. Instead, we believe this higher

background signal to be due to the same hydrophobicity issues previously reported.[174] The more hydrophobic nature of the probe leads to more non-specific accumulation and is less easily washed away by the FACS buffer washes in the protocol. This correlates with the cLogP values shown in Figure 65, with TMDIBO being much less hydrophobic. Whilst the Lys residue reduces the cLogP to 3.767 from the original scaffold **13** (cLogP 5.784), the molecule is still very hydrophobic, largely due to the ^{t}Bu motif. This results in a polar end and a non-polar end of the molecule, which could cause potential aggregation effects, forming 3D structures to shield the non-polar end from the aqueous solution *in vitro*.

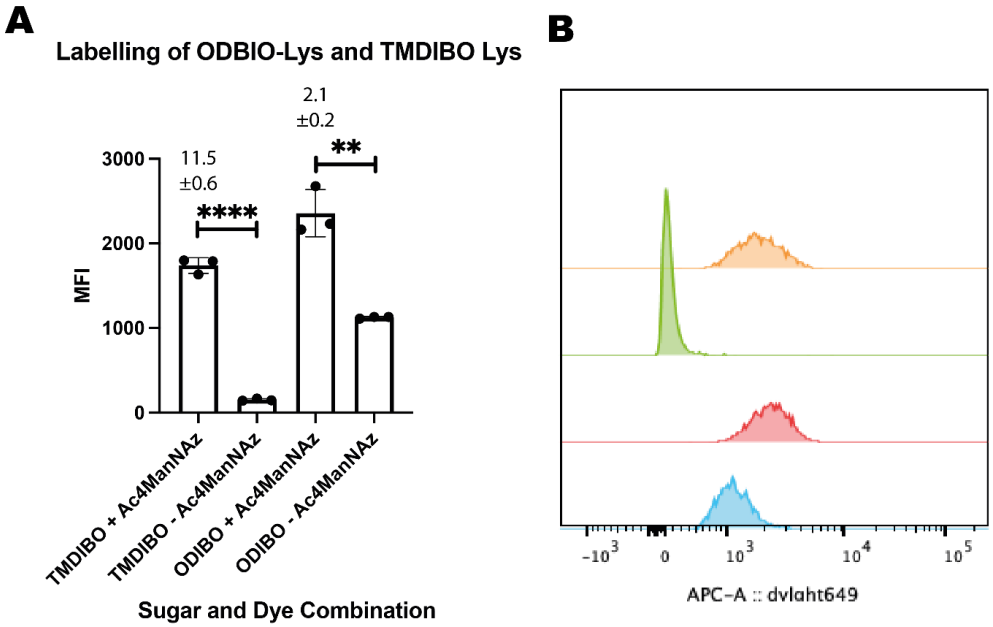

*Figure 64 – Comparison of the labelling of Ac_4ManNAz treated COLO205 cells using TMDIBO-Lys-AlexaFluor647 or ODIBO-Lys-Alexaflor647. A) COLO205 cells were incubated in the presence or absence of Ac_4ManNAz (125 µM) for 24 h. They were then incubated with the corresponding dye ((TMDIBO-Lys-AlexaFluor647 or ODIBO-Lys-Alexaflor647) (50 µM) + Sytox green cell death stain (50 nM)) for 1 h at 37 °C and analysed by flow cytometry. Median fluorescence intensity (MFI) is shown as mean ± SD. Signal-to-background ratios (SBR) relative to the control (PBS) are above each bar; n=3 technical replicates. Statistical analysis was performed using an unpaired t test with Welch correction (**** P≤0.0001,*** P≤0.001,** P≤0.01,* P≤0.05). B) Histograms giving number of events (vertical axis) versus fluorescence intensity (horizontal axis). Sugar and Dye combinations used from top to bottom, are: +Man+TMDIBO, -Man+TMDIBO, +Man+ODDIBO and -Man+ODIBO.*

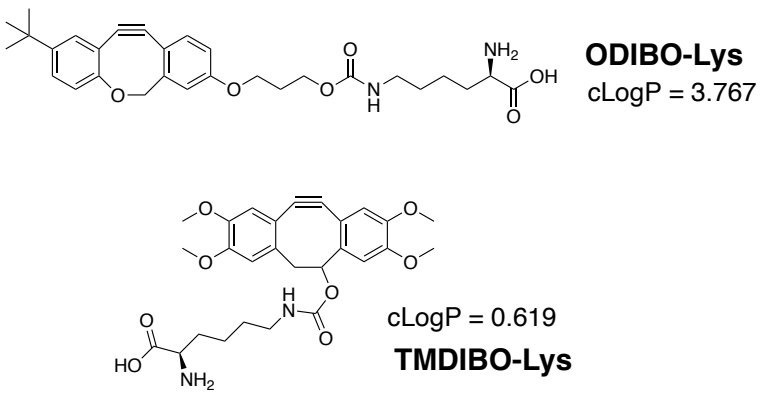

Figure 65 -comparison of cLogP values of TMDIBO-Lys and ODIBO-Lys. Values calculated on ChemDraw.

3.2.3. Kinetic Testing of ODIBO

The kinetics of the SPAAC reaction with ODIBO were tested. This has previously been explored, but we wanted to directly compare the kinetics of ODIBO with our TMDIBO probe under the same conditions in the same system.

The kinetic studies were carried out using a stopped-flow apparatus due to the anticipated fast kinetics of these SPAAC reactions, meaning NMR experiments may miss any initial rate. With SPAAC reactions being second order, pseudo first order conditions were used, with an excess of the azide probe.

Under Pseudo first order conditions with BnAz in excess the integrated first order rate law is given by:

$$ln[ODIBO] = -kt + ln[ODIBO]_0$$

However, this is in terms of concentration as opposed to absorption. As absorption (A_{ODIBO}) is proportional to concentration where c is a constant.

$$ln[ODIBO] = \ln(A_{ODIBO}) + C$$

This constant is added to both sides of the equation, but the gradient remains the same. However, as the other components of the mixture may also have non-zero absorbance at this wavelength. If we assume the absorbance due to other components is essentially constant* then the absorbance of ODIBO is given by the following equation where A_∞ is the constant and A is the measured absorbance.

$$A_{ODIBO} = A - A_\infty$$

Hence we can plot:

$$\ln(A - A_\infty)\ vs\ time$$

This then gives k_{app} which we can use to determine the second order rate constant.[176]

$$k_2 \approx k_{app}/[BnAz]_0$$

* If the absorbance of the other components of the mixture does change during the reaction this would be likely due to changes in the concertation (and hence absorption) of BnAz or the triazole product, which would change with the same rate constant as measured, and essentially add a constant to both sides of the equation but not affect the slope.

Benzyl azide was used, and methanol chosen as the solvent, to make the results comparable with many literature values for SPAAC kinetics, which tend to use this system. The presence of a distinctive UV absorbance at 310 nm in the UV spectra of ODIBO (**13**) that is not seen in the UV spectrum of

benzyl azide or the product, allowed benzyl azide to be used in excess and the decrease in absorbance at 310 nm followed. Similarly, the decrease in absorbance at 320 nm was used to follow TMDIBO consumption. Ln(A_t-A_∞) vs time was plotted for the various runs with both ODIBO (**13**) and TMDIBO (Figure 66 and Figure 67 respectively). Using the above equation, the gradient of the plot (k_{app}) can be divided by the initial concentration of benzyl azide (the reagent in excess) to give the second order rate constant k_2. The three runs were then averaged to give the calculated k_2 values for ODIBO (Table 5) TMDIBO (Table 6). The initial concentrations of the solutions used were 10 mM of benzyl azide and 0.5 mM cyclooctyne. However, it is worth noting that as during the experimental run, equal volumes of both solutions are mixed, so there is effectively a two-fold dilution of the reagents (*i.e.*, final concentrations used are: BnAz 5 mM, ODIBO 0.25 mM).

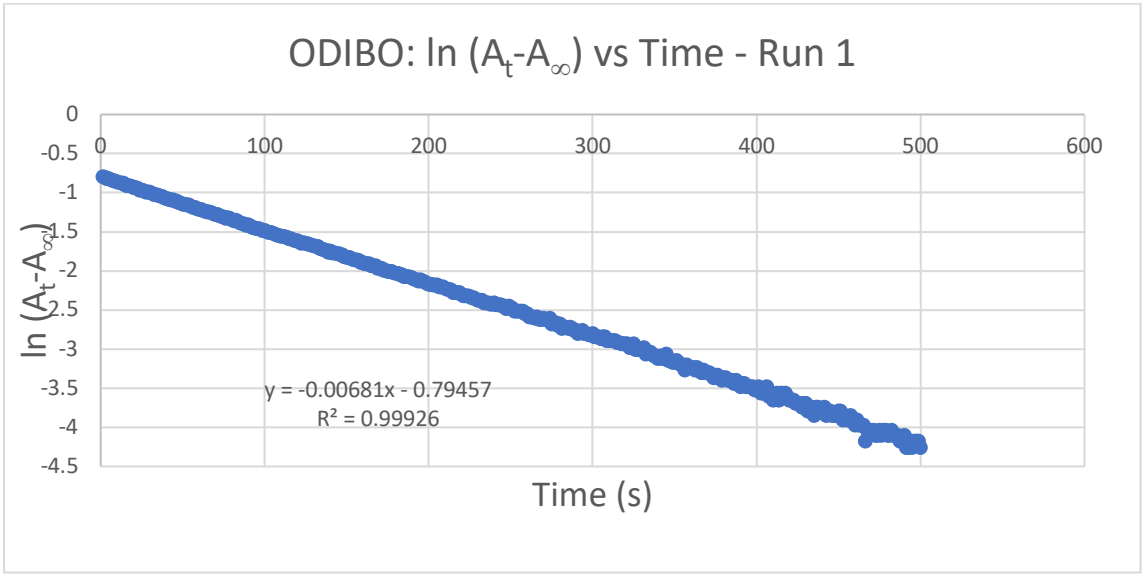

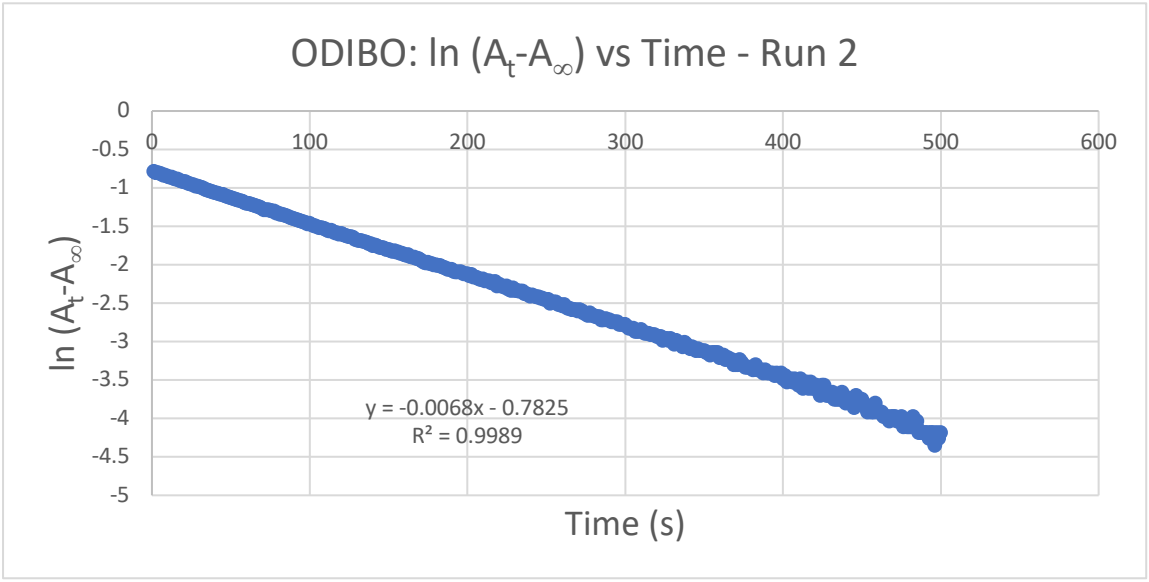

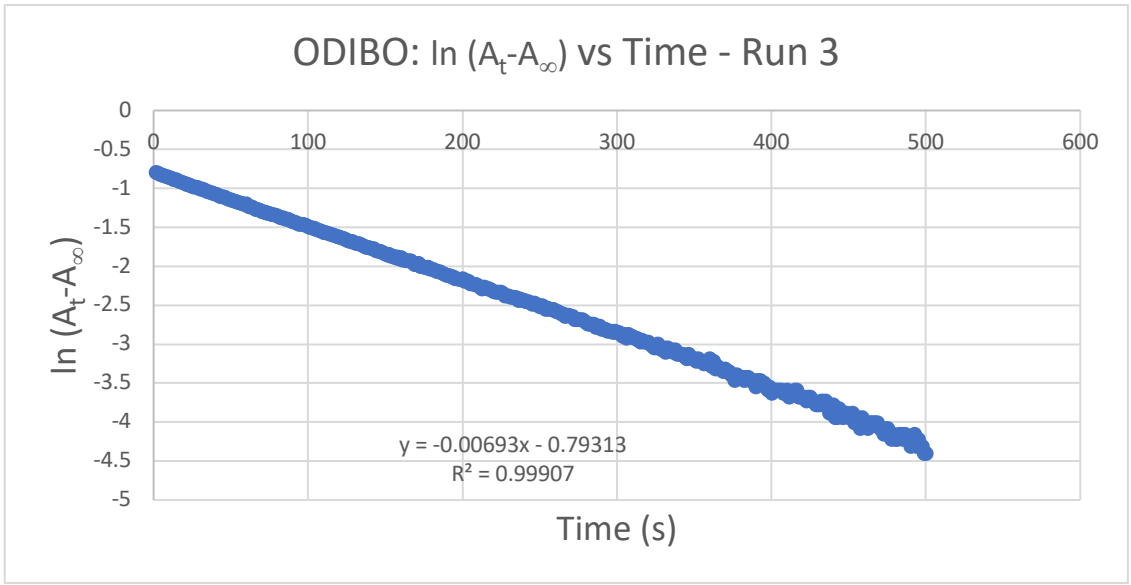

Figure 66 - Plot showing the calculated Ln (A-A∞) vs time for ODIBO. $[ODIBO]_0$ = 0.25 mM, $[BnAz]_0$ = 5 mM. Methanol was used as a solvent and the measurements were taken on a stopped-flow device at 25 °C.

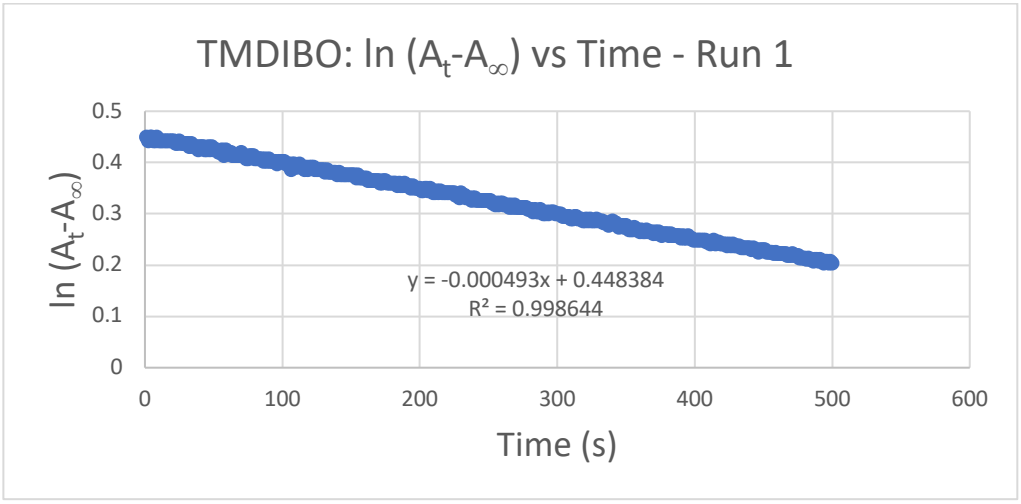

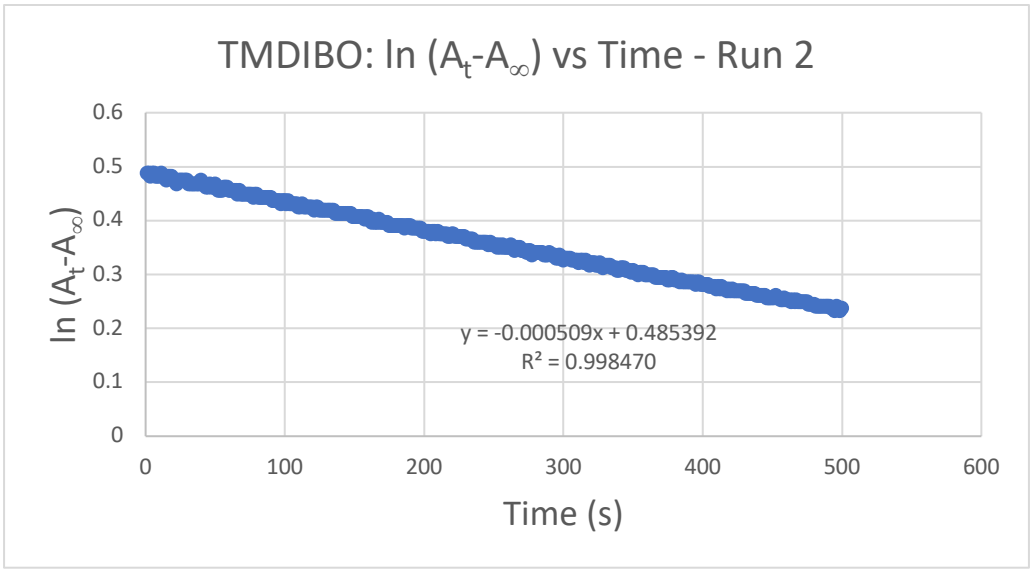

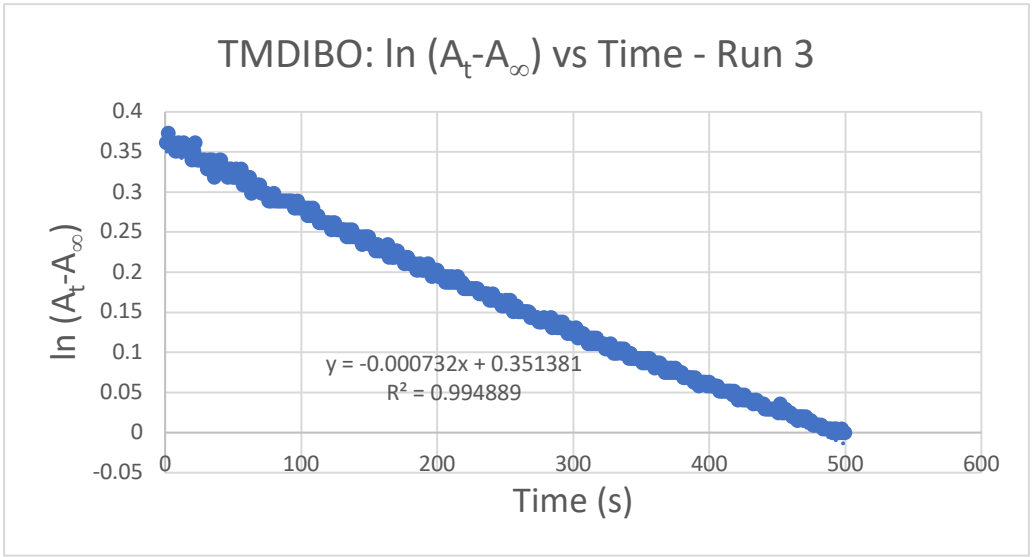

Figure 67 - Plots showing the calculated Ln (A-A∞) vs time for TMDIBO. $[TMDIBO]_0$ = 0.25 mM, $[BnAz]_0$ = 5 mM. Methanol was used as a solvent and the measurements were taken on a stopped-flow device at 25 °C.

Table 5 – Measured k_{app} and calculated k_2 for ODIBO

	ODBIO k_{app} (s^{-1})	ODBIO k_2 ($M^{-1}\,s^{-1}$)
Run 1	0.00693	1.386
Run 2	0.00681	1.362
Run 3	0.00677	1.354
Mean	0.00684	1.367
SD	8.33×10^{-5}	0.017

Table 6 - Measured k_{app} and calculated k_2 for TMDIBO

	TMDIBO k_{app} (s^{-1})	TMDIBO k_2 ($M^{-1}\,s^{-1}$)
Run 1	0.000493	0.0986
Run 2	0.000509	0.1018
Run 3	0.000732	0.1464
Mean	0.000578	0.1156
SD	1.33×10^{-4}	0.0267

The experimentally determined value for the second order rate constant of the reaction of ODIBO (**13**) with benzyl azide (in methanol) of 1.367 ± 0.017 M^{-1} s^{-1} is consistent with that previously reported in literature of 1.66 ± 0.04 M^{-1} s^{-1}.[172] Under the same conditions our TMDIBO second order rate constant of 0.1156 ± 0.0267 M^{-1} s^{-1} is consistent with our previously reported value[124] of $(9.4 \pm 0.4) \times 10^{-2}$ M^{-1} s^{-1}, with the new value perhaps being slightly higher due to the improved accuracy of measuring kinetics via stopped-flow compared to the previously used UV method.

Our kinetic results clearly show the SPAAC kinetics of ODIBO are much enhanced relative to our currently used TMDBIO, with ODIBO reacting 12 times faster. However, this is insufficient to compensate for the increased hydrophobicity, with a lysine conjugated ODBIO derivative **22** displaying a much worse SBR for the *in vitro* labelling of Ac_4ManNAz tagged glycans (relative to TMDIBO-Lys). Other attempts to reduce the hydrophobicity via replacement of the hydrophobic ^{t}Bu group were unsuccessful. This highlights the steric importance of this group in the Friedel Crafts cyclisation step, suggesting finding an alternative motif will be difficult. Due to the synthetically challenging nature of this replacement, combined with the poor *in vitro* results, and time constraints, this project was not taken any further forward, with focus being shifted to other projects.

3.3. *E,Z*-Cyclooctadiene: a novel reagent for rapid IED-DA bioorthogonal ligations

3.3.1. Trans-Cyclooctene Analogues for IED-DA Bioorthogonal Ligations

As previously mentioned, cycloalkenes with a *trans*-double bond undergo fast IED-DA reactions with tetrazines. Inspired by measurements by Sauer *et al.*[177] of the IED-DA of various dienophiles with tetrazine, the Fox group first demonstrated photochemical generation of a functionalised TCO in 2008.[177] The group subsequently published work demonstrating the rapid kinetics of the IED-DA between the functionalised TCO and dipyridyltetrazine with a K_2 of 2000 M^{-1} s^{-1} (Scheme 22).[70] This remarkable reactivity occurs as a consequence of the strain placed on the *trans*-double bond in the most stable crown conformer. This severe twist of the alkene bond results in a high energy highest occupied molecular orbital (HOMO), leading to fast reactivity in HOMO-alkene controlled cycloaddtions.[177] With a high barrier to racemisation of the double bond (35.6 kcal mol^{-1})[177] TCO has emerged as a useful bioorthogonal tool.[179]

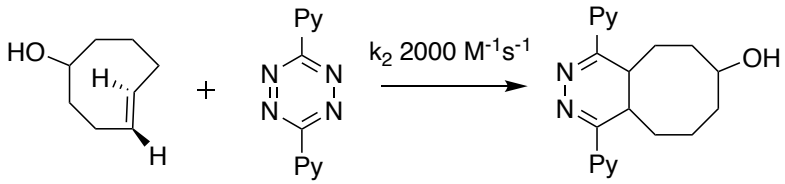

Scheme 22 - The IED-DA between TCO and dipyridyltetrazine.

Multiple attempts have been made to increase the strain via fusion of motifs to the cyclooctene ring. Fox *et al.,* were again the first to do this, hypothesising that deviation from the crown conformation would have this effect. They calculated that *cis* ring fusion results in alternative higher energy conformations of the cyclooctene, with further torsion placed on the *trans*-double bond.[180] This is highlighted in Figure 68 with non-ring fused TCO and *trans*-ring fused TCO adopting conformer 1a, whereas *cis* fusion leads to conformer 1b.

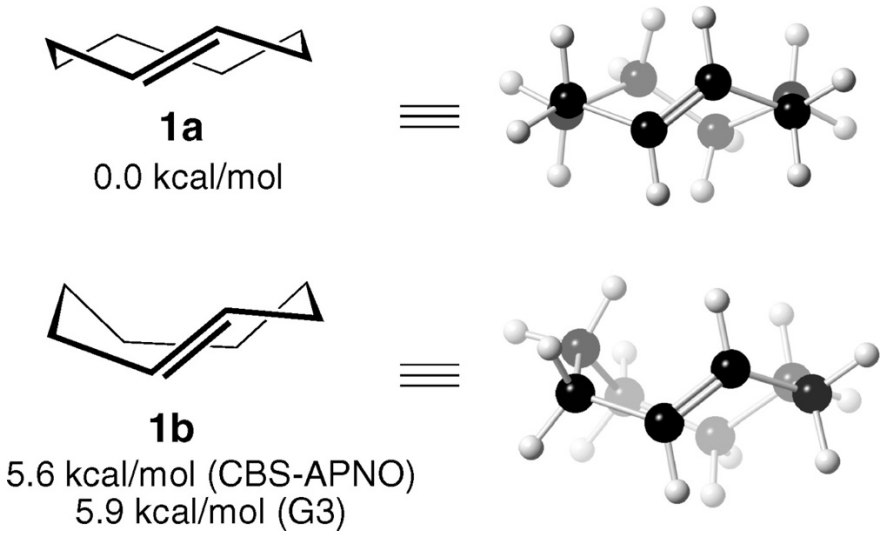

Figure 68 – TCO ring conformers. Conformer 1a is adopted by unfused TCO and higher energy trans-fused and 1B by cis fused TCO. Figure taken from Taylor et al.[180]

This computational work led them to synthesise s-TCO, with a *cis*-cyclopropane ring greatly enhancing the rate of IED-DA under the same conditions.[180] However, as is often the case, the enhanced kinetics of these TCO derivatives is accompanied by decreased stability. A non-ring fused TCO derivative showed half-life of only 3.26 hours in serum, with isomerisation to this cis-cyclooctyne the main instability.[71] TCO and s-TCO are also not stable for prolonged storage[69]. Attempts to improve stability via complexation of s-TCO with $AgNO_3$[181] and replacement of the cyclopropane ring fusion with similar dioxane fusion (d-TCO)[182] have helped increase stability. This enhanced reactivity makes TCO derivatives the fastest dienophiles for IED-DA bioorthogonal ligations to date.[69]

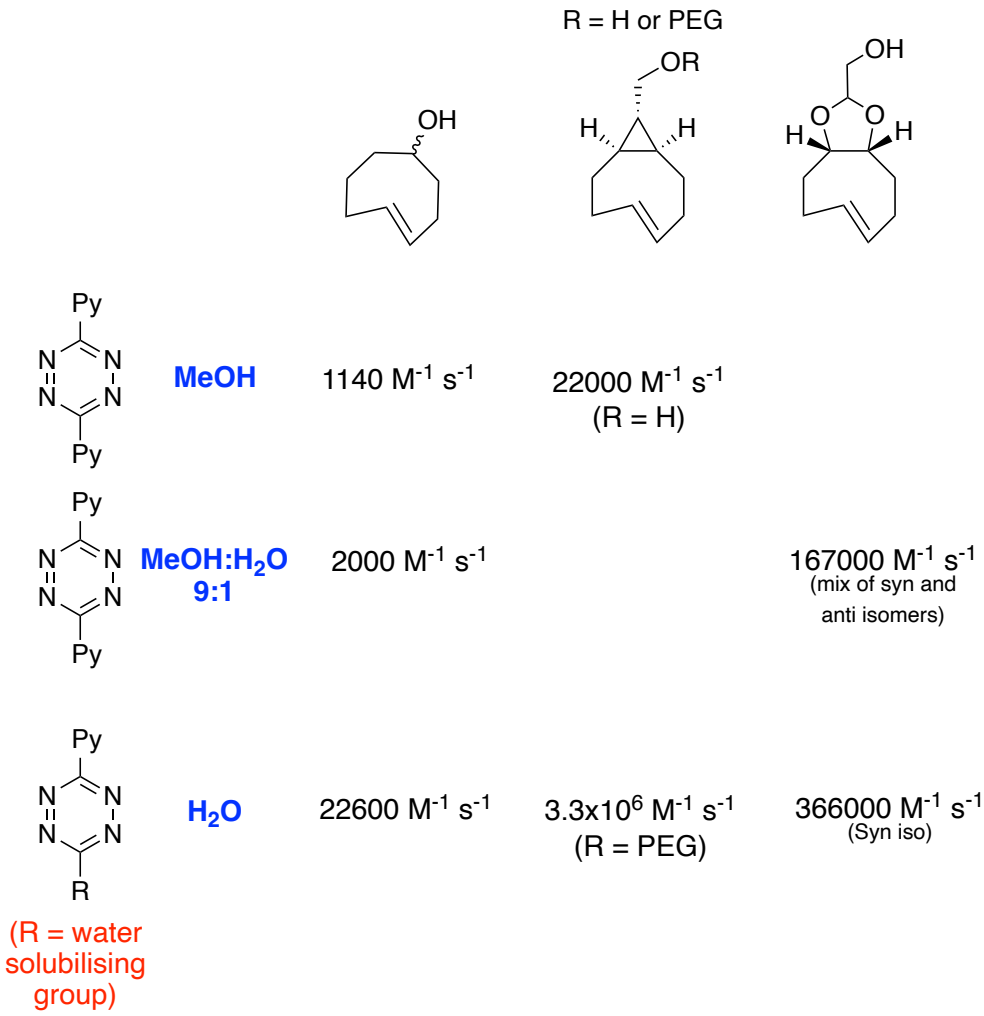

Figure 69 - A comparison of the kinetics of various dienophiles for IED-DA ligations with tetrazines. Kinetic data taken from Oliveira et al.[69]

The reaction rates of IED-DA ligations can also be fine-tuned by careful consideration of the tetrazine probe used. Just as increasing strain on the *trans*-bond can lead to increased rate via raising the HOMO energy, decreasing the LUMO energy of the tetrazine (the diene) electron-withdrawing groups (EWG) making the tetrazine more electron-poor, also decreased the activation energy required for reaction. As such when comparing the rates of IED-DA reaction it is important to use identical tetrazine probes. The development of tetrazines optimal for IED-DA *in vitro* and *in vivo* has been widely discussed elsewhere.[73, 183, 184]

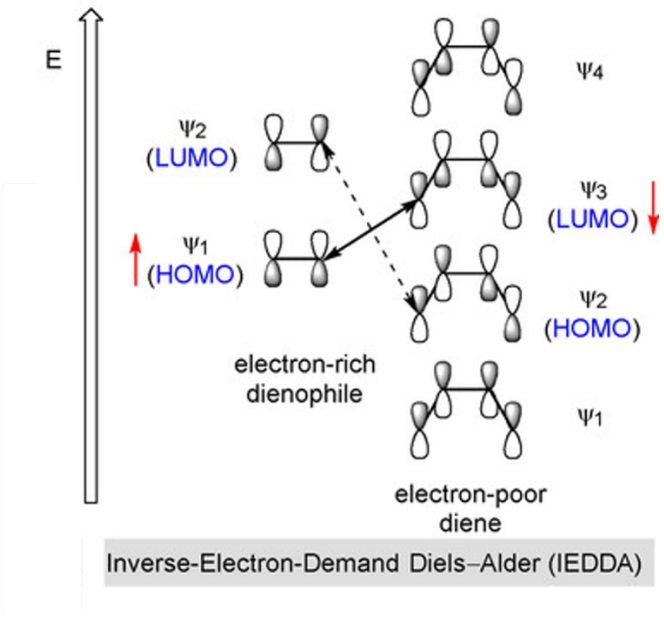

Figure 70 – Molecular orbital (MO) diagram of IED-DA. Electron poor tetrazines (and dienes in general) accelerate the reaction as does additional of electron withdrawing character to the dienophile.

As seen with SPAAC kinetics, solvent has a large effect on the rate of IED-DA with polar solvents favoured, in particular water. This is achieved via stabilisation of the activated complex, as well as hydrogen bonding between water and tetrazine decreasing the HOMO-LUMO gap.[69] Solvent polarity can also have an effect on the isomer of the product formed in some IED-DA reactions.[185] As such solvent is again an important factor when comparing IDE-DA kinetics.

Use of TCO as a chemical reporter for MOE has been limited due to the relatively large size causing a significant perturbation from the native substrate, resulting in intolerance towards the compound by native enzymes.[75] However, the rapid kinetics of TCO/Tetrazine IED-DA has led to many biological applications. This is highlighted by the first clinical use[186, 187] of click chemistry involving a tetrazine modified biopolymer and a TCO modified protodrug[188], via a click to release mechanism previously reported.[189] Genetic incorporation of TCO handles into proteins and antibodies has allowed *in vitro*[190] and *in vivo*[191] imaging via pretargeting approaches. Radiochemical imaging (PET and MRI) has exploited the fast kinetics of TCO-tetrazine ligations. The fast kinetics aids the low concentrations used in radiomedicine, as well meaning the ligation occurs before complete radioactive decay.[179] radionuclide have been conjugated to the TCO[192] or the tetrazine[193], highlighting the flexibility of this system. Further optimisation of TCO linkers for antibody-drug conjugate (ADC) drug loading could open their use in this exciting area of medicine.[69, 194, 195] Increased kinetics of IED-DA and more stable TCO like bioorthogonal handles will be needed for further application and benefit in medicine.[179]

Work by the Brindle and Leeper groups showed the use of highly strained *trans,trans*-cyclooctadiene (*E,E*-COD).[128] This diene not only showed enhanced kinetics, but also allowed for bifunctionality, as it is capable of undergoing two successive bioorthogonal ligations (IED-DA and [3+2] cycloadditions). *E,E*-COD was originally synthesised by Whitesides *et al*.[196] in 1969 via photoirradiation of cis,cis-cyclooctadiene (*Z,Z*-COD) in the presence of copper(I) chloride. This new report synthesised E,E-COD via phosphine oxide-mediated olefin inversion from (*Z,Z*)-COD, first carried out by Boeckh *et al*.[197] Despite the fast kinetics of the highly strained *E,E*-COD (20.3 kcal mol^{-1})[197] it's insolubility in water and high volatility limited use.[128]

Computational calculations carried out by Finian Leeper using (molecular mechanics 2) MM2 showed the strain energy released upon cycloaddition was unsurprisingly greater for *E,E*-COD than TCO (hence the faster kinetics). However, a cis-trans-cyclooctadiene (*E,Z*-COD) was calculated to have a larger strain energy release than *E,E*-COD and the fastest to date TCO analogue s-TCO.

3.3.2. Synthesis of *E,Z*-COD

The synthesis of *E,Z*-COD had been reported previously by students in the Leeper group, with Laia Josa Culleré designing the initial synthesis.[198] Various attempts had been made at the synthesis, which had proved challenging due to the perceived instability of the *E,Z* product once one of the double bonds had been isomerised to the trans-configuration. Although *E,Z*-COD was synthesised,[198] initial results showed much lower kinetics than anticipated, believed to be due to the initial cycloaddition being so fast that it was all over before the sample could be introduced into the UV spectrometer.

We aimed to resynthesise *E,Z*-COD and accurately measure the kinetics, using stopped-flow, which would allow for measurement of the rapid rate compared to previously used methods such as NMR. We also wanted to further probe the stability of *E,Z*-COD, particularly under physiological conditions, as this would be vital for potential future *in vitro* and *in vivo* uses. The synthetic route carried out is shown in Scheme *23*.

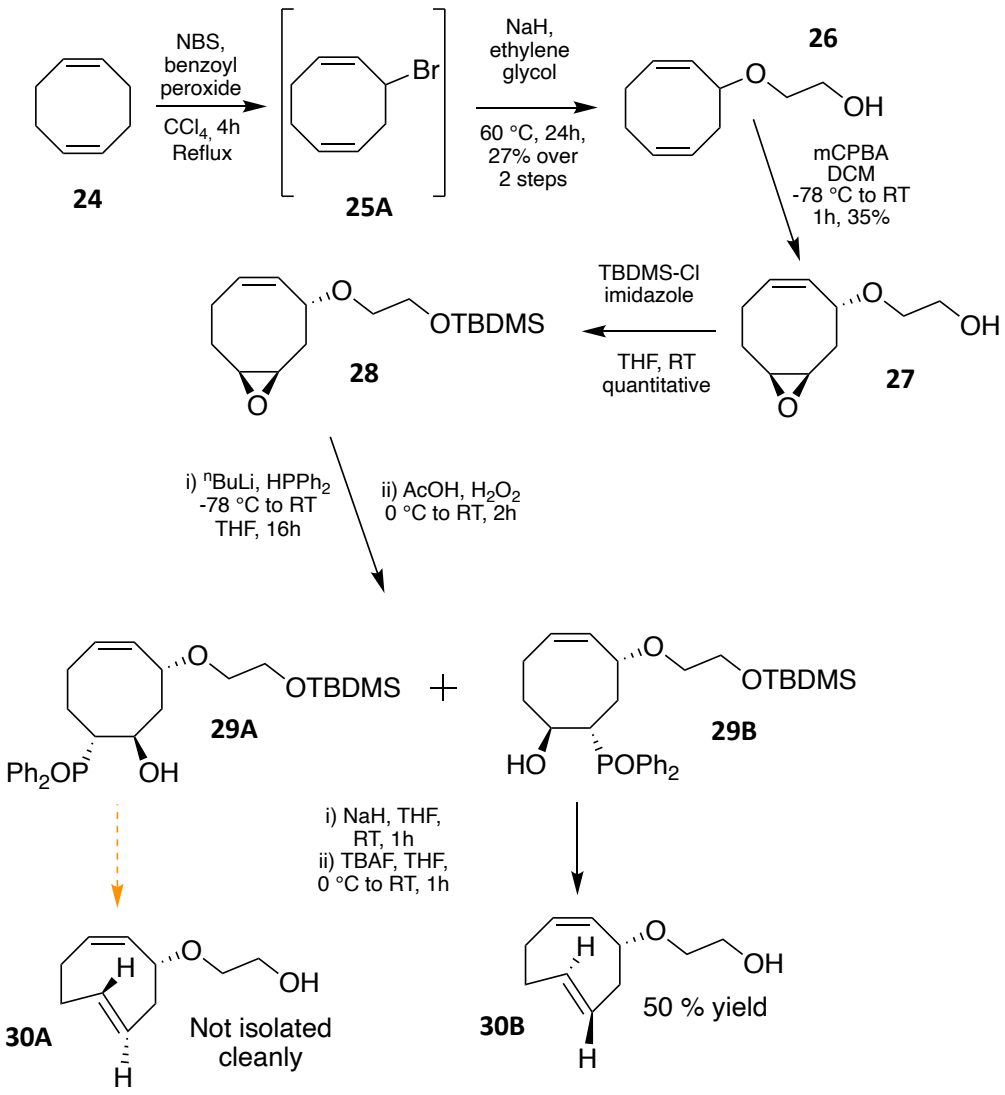

Scheme 23 - Synthesis of E,Z-COD.

The first step in the synthesis was bromination of *E,E*-cyclooctadiene using *N*-bromosuccinimide in carbon tetrachloride, which produced 1,4 and 1,5 isomeric products (25A and 25B) (Figure 71) as well as number of possible debromination by-products. In previous attempts purification had been attempted here (distillation and recrystallisation) to remove any di-brominated side products.[198, 199] The reaction has previously been shown to produce a roughly 1:1 mixture of the 1,5 and 1,4 addition isomers[198] (the numbering is in relation to the double bond position), although this is not a concern as both can react to give the required ether product **26**. It was decided that the instability of the product, particularly to silica-based chromatography, as well as the fact that the previous attempts had not fully removed any impurities, meant it was more sensible to take the crude reaction mixture through to the next stage. The crude product was added to a solution of NaH in ethylene glycol and heated at 60 °C for 24 h. Flash chromatography was then used to separate the isomeric products. Whilst this

was largely successful, the ^{1}H NMR spectra do show other species. Following epoxidation, any side products were more easily removed.

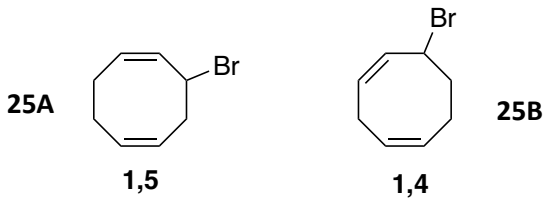

Figure 71 - The potential product and by-products of the bromination.

The epoxidation conditions were also modified from previous attempts which had used peracetic acid and sodium carbonate. Due to the decomposition of the commercially obtained peracetic acid, it was replaced with the more widely used and stable mCPBA. In the isolated product **27** the epoxidation occurs with regioselectivity for the double bond further away from the alcohol. This was confirmed in COSY NMR experiments by Laia Josa Cullére.[198] This suggests that steric hindrance from the alcohol chain is the dominating effect in determine the regioselectivity. It was suggested that the diastereoselectivity could be also explained by steric hinderance (as opposed to a potential hydrogen bonding interaction as shown in Figure 72) but this was only a hypothesis and the diastereoisomer was assumed to be as drawn in Scheme *23*. Tatiana Vilaplana[199] compared lowest energy conformation calculations and subsequent expected coupling constants of the olefinic hydrogen neighbouring the ether and the hydrogen on the ether bound carbon, for the two possible diastereoisomers. The measured coupling constants fit better with the assumed diastereoisomer (epoxidation on the opposite face to the side-chain), supporting the assumption but this has not be exhaustively confirmed. However, the low yield for this reaction could perhaps be due to the formation of the alternative products suggested, but they were either unstable or removed as part of the protocol.

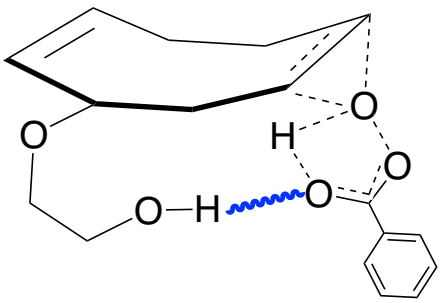

Figure 72 – A conceivable hydrogen bonding interaction for epoxidation (blue line = hydrogen bond). It is not believed this occurs and instead epoxidation occurs on the opposite face, due to steric repulsion as opposed to hydrogen bond attraction.

The next step was to protect the alcohol **27** (which is needed due to the *n*-BuLi that will be used in the phosphine oxide formation step). The TBDMS protected alcohol was obtained in quantitative yield using standard conditions. Following this the epoxide was opened via attack with lithium diphenylphosphide. The lithium diphenylphosphide was formed *in situ* using diphenylphosphine and *n*-Buli. Initial attempts at opening the epoxide under these conditions failed. As part of this protocol, first the lithium diphenylphosphide was formed at -78 °C (via addition of *n*-BuLi to diphenylphosphide in THF) and then the epoxide (**28**) was added in dropwise as a solution in THF. After allowing the reaction to warm to room temperature overnight and quenching with AcOH/H_2O_2 (to oxidise the phosphine product to the phosphine oxide), no product was identified by LCMS (and TLC), or after chromatography of the resulting crude mixture. Some unreacted starting material (**28**) was recovered.

Decomposition of the reagents was considered as a cause, and so all were replaced with fresh commercially obtained reagents. This as well as adjusting reaction times, and temperatures yielded no product. When lithium diphenylphosphide is formed a bright red colour is produced, under most of the conditions attempted this colour slowly faded over the course of the reaction. It was thought that was an indication that the reagent was formed *in situ*, but was then slowly decomposing. To combat this, the number of equivalents of *n*-BuLi and diphenylphosphine were increased (hence forming more lithium diphenylphosphide). The order of addition of reagents was also adjusted, adding the epoxide (**28**) to the diphenylphosphine and then still at -78 °C adding the *n*-BuLi dropwise. This we believed would allow the lithium diphenylphosphide to form and then be able to immediately react with the epoxide. As the *n*-BuLi was added a bright red colour would form then dissipate (indicating the above), and so *n*-BuLi was added until the red colour persisted, suggesting complete reaction of the epoxide **28**. Following quenching, work-up and flash chromatography ^{1}H NMR suggested both regioisomers had been collected as well as a large amount of a diphenylphosphine-derived impurity, likely to be diphenylphosphinic acid, a known oxidation product of diphenylphosphine.[200] These oxidised by-products are notoriously difficult to remove (as is often seen with Ph_3PO), particularly when using the polar gradient (10% MeOH in DCM) required to elute the epoxide opened products (**29A and 29B**). The regioisomers are formed due to the lithium phosphide being able to attack at either carbon of the epoxide. No significant selectivity was seen for attack at either carbon despite the protected alcohol chain being closer in proximity to one of the carbons.

The phosphine oxide regioisomers (**29A and 29B**) could not be separated by normal phase chromatography. Not only do the two isomers co-elute but they also co-elute with the diphenylphosphine-derived impurity. However, the isomers can be separated from each other and

the impurity using HPLC. Optimisation was required but a short gradient from 5-95% ACN in water removed the diphenyl phosphine oxide impurity. A long run at 95% ACN in water was then required to elute the two products, which were separated but closely eluting. Formic acid was used as an additive (0.1% formic acid) which caused partial deprotection of the silyl protected group. It is likely this occurred after elution (as multiple runs were required so the product was left in solution for hours before freeze drying to remove solvent), as if it had happened prior to elution then it is likely the HPLC would have also led to separation of the protected and deprotected products, but this was not observed. This was not an issue as both the protected and deprotected products were stable in the next step (the elimination) and full deprotection was achieved after the elimination, by addition of TBAF, as a one-pot procedure. An overlay of the ^{1}H NMR spectra of each of the regioisomers is shown below (Figure 73).

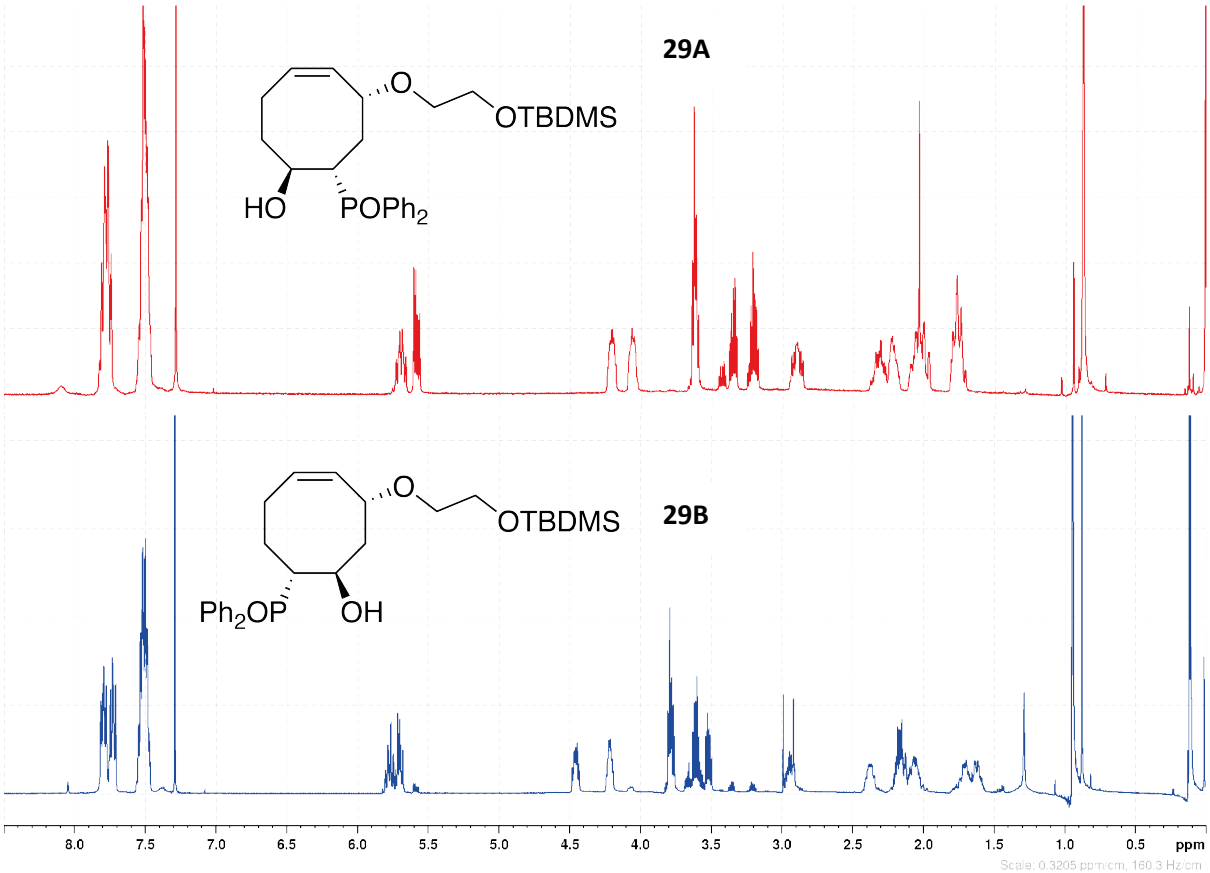

Figure 73 - Comparison of the ^{1}H NMR spectra of the two regioisomers.

The separated regioisomers were assigned by comparison of ^{1}H and 2D NMR data with those acquired by Laia Josa Cullére.[198] The elimination of the phosphine to form the trans double bond, and deprotection were carried out in one step, due to the separated regioisomers already being partially deprotected by the acidic modifier in the HPLC solvent system, and due to the small scale of the

reactions. Both isomers were subjected to identical conditions and then purified by normal phase chromatography. However, ^{1}H NMR showed that while one isomer was isolated in a reasonable degree of purity the other was not. Isomer **30B** was isolated successfully but following chromatography no clean spot on the TLC was observed for **30A**. Since they are expected to have very similar polarity and since the same column conditions were used for both, fractions around where the other isomer had been found were collected. Following concentration ^{1}H NMR showed a complex mixture of products, believed to be decomposed **30A**.

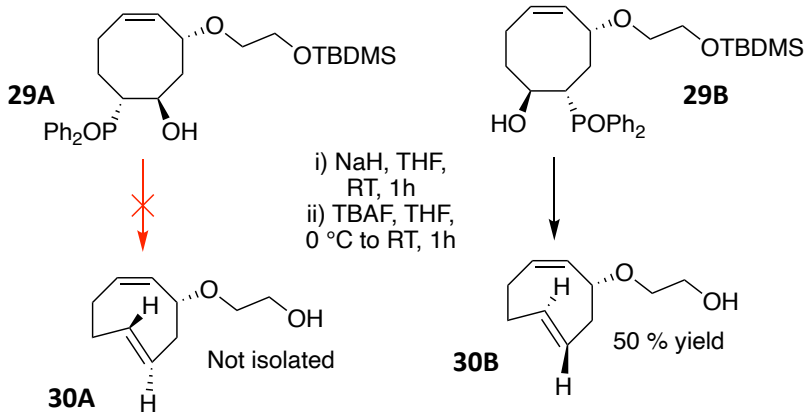

Scheme 24 - Elimination products of the two diastereoisomers.

3.3.3. Kinetic Studies of *E,Z*-COD

It is unknown if **30A** was formed but starting material consumption was observed. Despite this, **30A** was not isolated despite multiple attempts, which is surprising given that this isomer has previously been reported.[198] The kinetics of the collected isomer **30B** were then studied. Due a distinctive UV absorbance of dipyridyltetrazine at 295 nm, COD (**30B**), which has no absorbance at 295 nm, was used in excess and the decrease in UV absorbance of the tetrazine was followed (this absorbance is not present in the product either). As such COD was used at 1.19 mM and dipyridyltetrazine at 0.119 mM (before mixing) and the kinetics of the reaction as measured by stopped flow are shown in Figure 74 below. The extremely rapid rate of reaction was easily visibly seen by mixing the solutions and the immediate disappearance of the distinctive pink tetrazine colour.

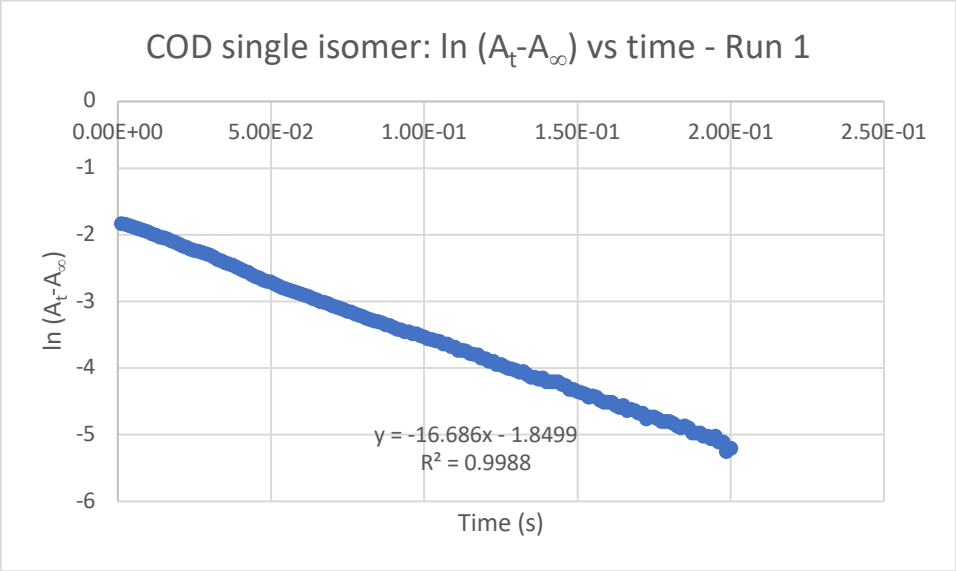
COD single isomer: ln (At-A∞) vs time - Run 1
0
0.00E+00
5.00E-02
1.00E-01
1.50E-01
2.00E-01
2.50E-01
-1
-2
-3
-4
-5
-6
ln (At-A∞)
y = -16.686x - 1.8499
R² = 0.9988
Time (s)

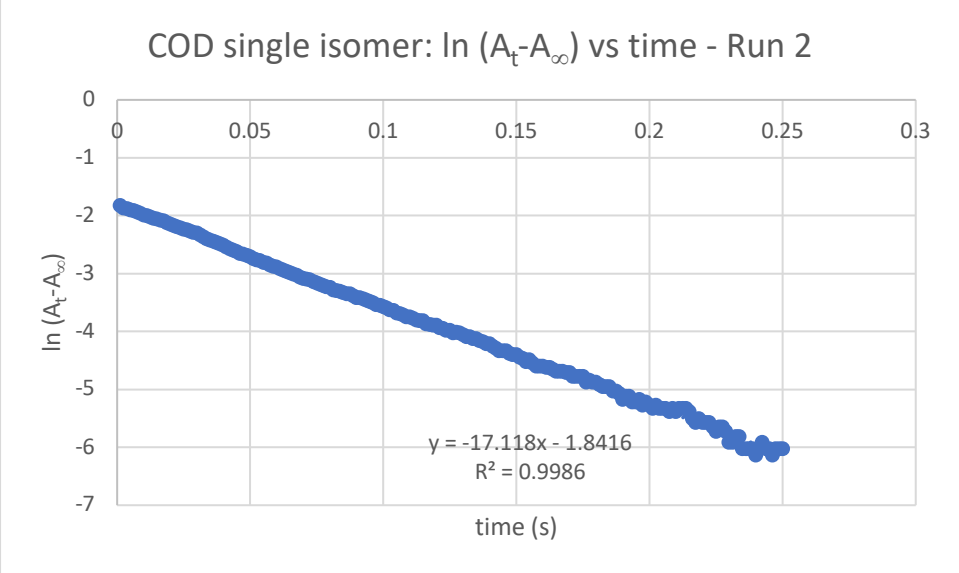
COD single isomer: ln (At-A∞) vs time - Run 2
0
0
0.05
0.1
0.15
0.2
0.25
0.3
-1
-2
-3
-4
-5
-6
-7
ln (At-A∞)
y = -17.118x - 1.8416
R² = 0.9986
time (s)

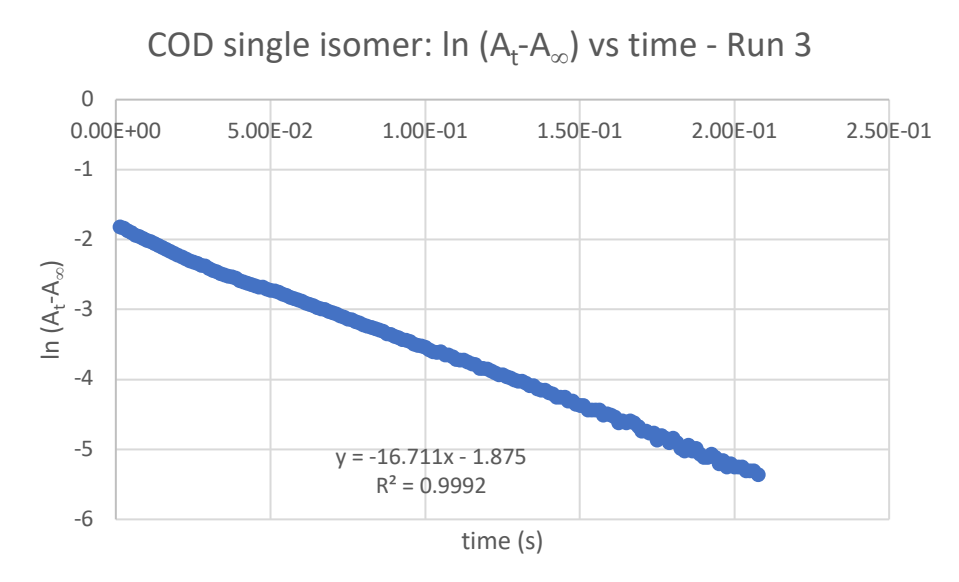
COD single isomer: ln (At-A∞) vs time - Run 3
0
0.00E+00
5.00E-02
1.00E-01
1.50E-01
2.00E-01
2.50E-01
-1
-2
-3
-4
-5
-6
ln (At-A∞)
y = -16.711x - 1.875
R² = 0.9992
time (s)

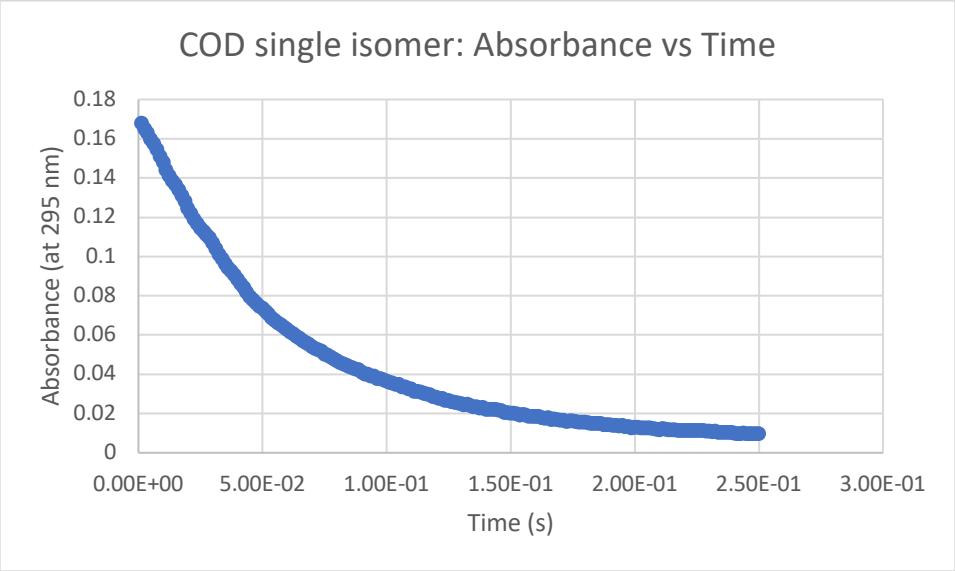

*Figure 74 - Plots of Ln A-A∞ vs time for the COD single isomer (**30B**) and a representative absorbance vs time plot (data from run 1 above).*

As previously described for the ODIBO kinetics the k_{app} and k_2 values can be easily calculated from the above plots of ln(A_t-A_∞) vs time. These calculated values are shown in Table 7 below. The calculated k_2 value of 28299.7 ± 332.8 M^{-1} s^{-1} highlights how rapid the kinetics of the COD-tetrazine reaction are. This can also be seen by the speed at which the reaction tends to completion in the absorbance plot in Figure 74, which happens within 0.25 seconds.

Table 7 - Measured k_{app} and calculated k_2 for COD (30B).

	COD (30B) k_{app}	COD (30B) k_2 (M^{-1} s^{-1})
Run 1	16.686	28043.7
Run 2	17.118	28769.7
Run 3	16.711	28085.7
Mean	15.692	28299.7
SD	0.198	332.8

As previously discussed, direct comparison of rates is difficult as conditions must be identical. In the example of the rates of strained cyclooctenes, both solvent and the tetrazine probe used are particularly important. For example, the fastest reported IED-DA rates include an s-TCO derivative at 3300000 M^{-1} s^{-1},[182] but this rate was measured in water with water solubilising groups on both the TCO and tetrazine reactants. Under conditions comparable with our method, e.g. MeOH as a solvent and dipyridyltetrazine at 25 °C, s-TCO has a rate of 22000 M^{-1} s^{-1} .[180] Other reported high rates include

sila-trans-cycloheptene (Si-TCH); no direct comparison could be found, but reaction with diphenyltetrazine in MeOH yielded a rate of 4360 M^{-1} s^{-1}.[201] s-TCO is often ranked as one of, if not the most, reactive dienophiles for IED-DA and our reagent has a larger bimolecular rate constant, and to the best of our knowledge, no TCO derivative has been reported with a higher k_2 value under the same conditions.

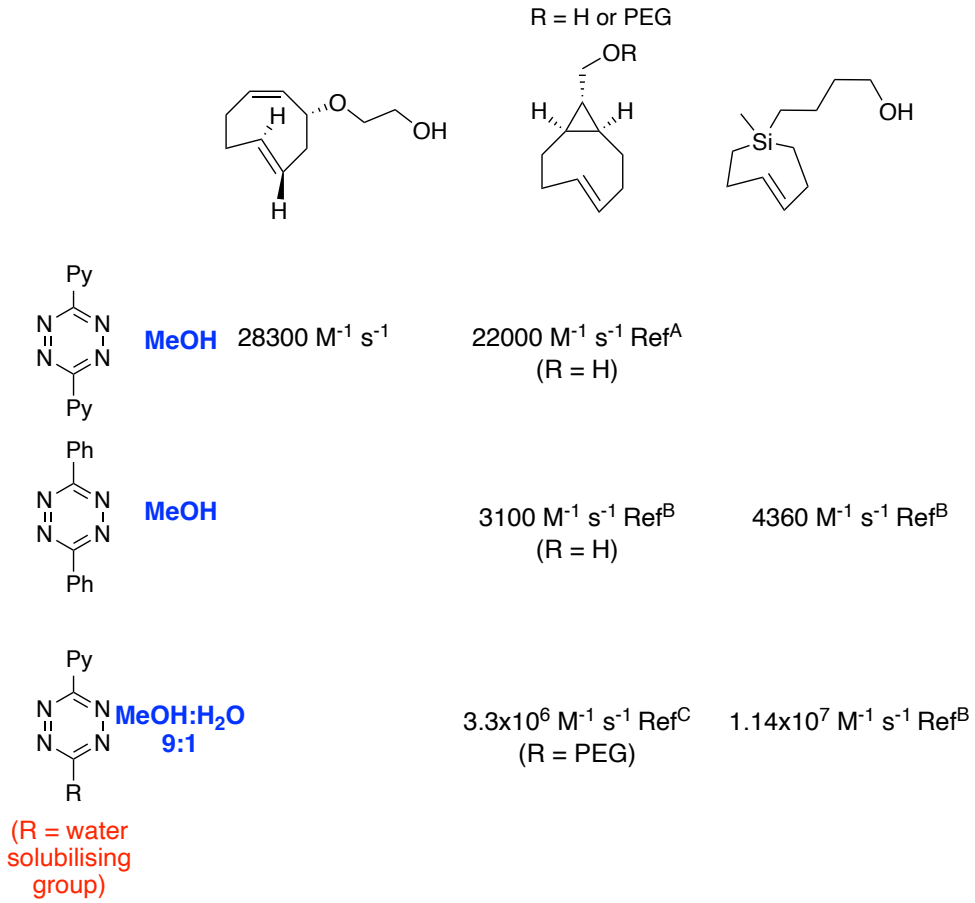

Figure 75 - comparison of IED-DA rates of E,Z-COD, s-TCO and Si-TCH. Ref A[180], Ref B[201] and Ref C[182].

We also believe that our calculated rate is a large underestimate of the actual value. This is because the ^{1}H NMR shows tetrabutylammonium salts and residual solvents. The solvents were not further removed under high vacuum due to concerns over the volatility of *E,Z*-COD. In fact, it is estimated that these impurities mean the sample is only approximately 33% *E,Z*-COD **30B**. If this is the case, then the rate constant could in fact be 3 times greater.

Due to the difficulty in the HPLC purification, scale up of the synthesis and separation of the regioisomers after phosphine addition was avoided. Instead, the mixed regioisomeric product (contaminated with diphenylphosphinic acid) was used for the elimination and deprotection steps.

The crude mixture was reacted with excess NaH and TBAF under the same conditions as previously used. Then the mix of diastereoisomers (**30A and 30B**) was collected by flash chromatography. The loss of the phosphine makes the product much less polar meaning the diphenylphosphinic acid impurity was easily removed (products eluting in 50% EtOAc in hexanes). This route avoids the need for any HPLC separation and as such is experimentally easier and more scalable.

Stopped-flow kinetic analysis was then carried out on the diastereomer mix. *E,Z*-COD was again used in excess but at 0.33 mM with dipyridyl tetrazine at 0.025 mM (concentrations before mixing). The same conditions were applied, and the resulting plots are shown in Figure 76 below.

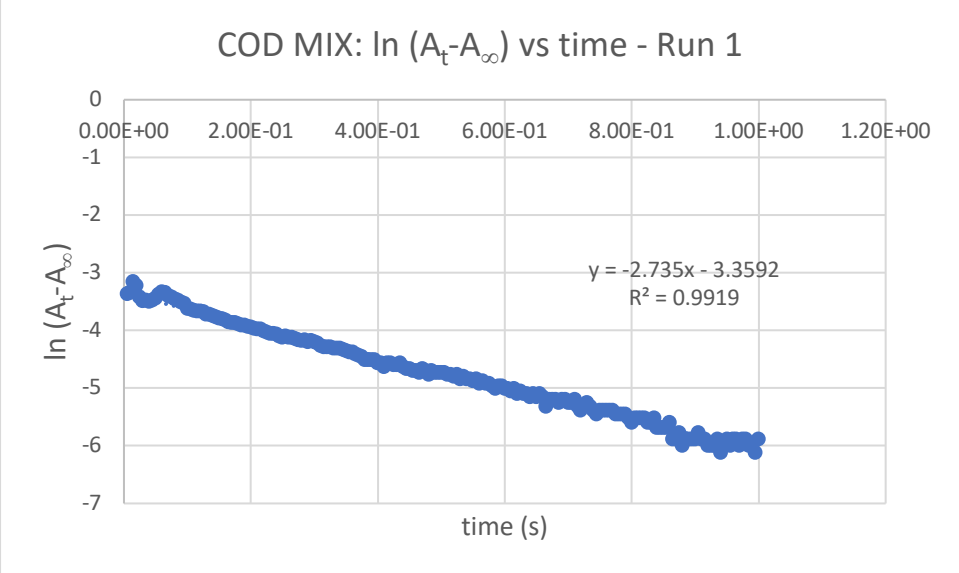

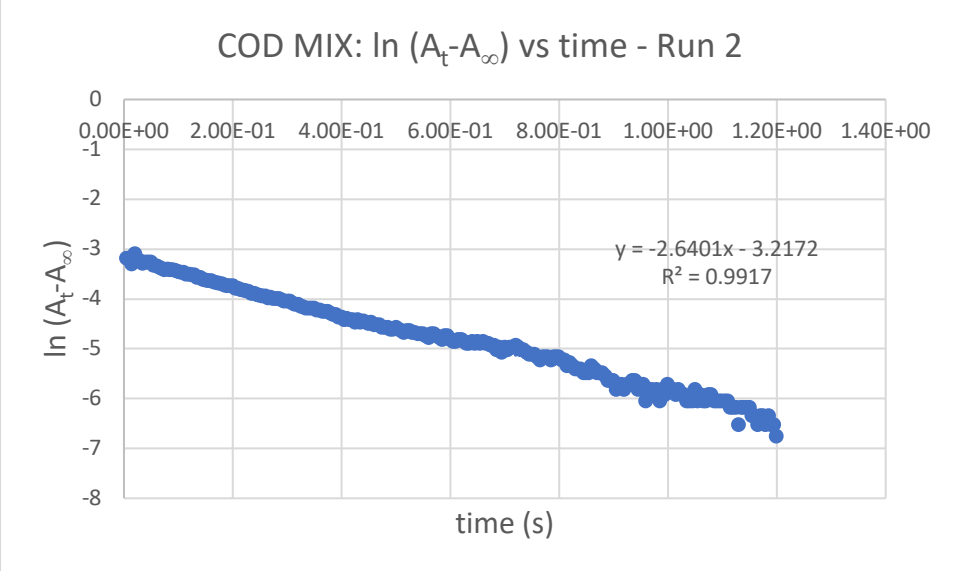

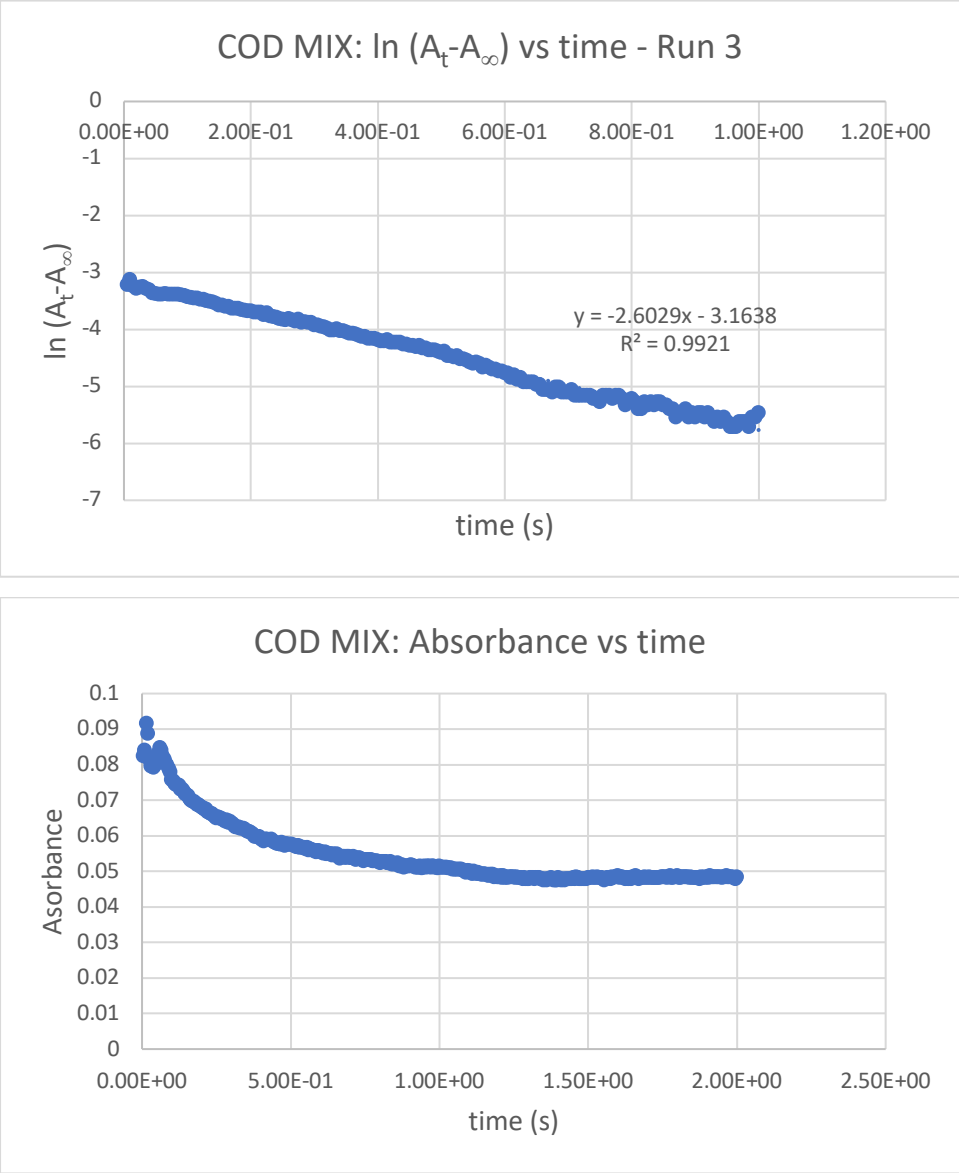

*Figure 76 - Plots of Ln A-A$_\infty$ vs time for the COD mix (**30A and 30B**) and a representative absorbance vs time plot (data from run 1 above).*

The measured k_{app} and calculated k_2 values are shown in Table 8 below. There is a near two-fold decrease in rate constant relative to the single isomer results previously described (16117.2 ± 337.1 *vs* 28299.7 ± 332.8 M^{-1} s^{-1} respectively).

Table 8 - Measured k_{app} and calculated k_2 for COD MIX (30A and 30B).

	COD MIX (30A and 30B) k_{app}	COD MIX (30A and 30B) k_2 ($M^{-1} s^{-1}$)
Run 1	2.735	16575.8
Run 2	2.640	16000.6
Run 3	2.603	15775.2
Mean	2.659	16117.2
SD	0.056	337.1

This rate decrease is perhaps not surprising given the previously collected elimination product of **30A** was a complex mixture of products and not studied via stopped flow individually. Despite the chromatography used to separate impurities from the mixture of diastereoisomers, it was clear that some impurities remained in the ^{1}H NMR. These impurities if assumed to be unreactive could account for the reduction in rate, as it would mean that the concentration of reactive *E,Z*-COD was actually much less than the 0.33 mM used for estimating the rate. It could be that diastereomer **30A** was not isolated due to this isomer being much more reactive. This isomer would then react with tetrazine much faster than *E,Z*-COD **30B** at 28299.7 $\pm$ 332.8 $M^{-1} s^{-1}$ and be unstable to the point that it is difficult to analyse or isolate, but no evidence of this has been observed.

The product of reaction between *E,Z*-COD and dipyridyl tetrazine was not isolated but HRMS was carried out on an approximately 1:1 mix of the two reagents in MeOH . As expected, the pink colour quickly dissipated and the HRMS result of 377.1989 a.u. is within expected range of the calculated value for the expected product (377.1979 a.u.) (Figure 77).

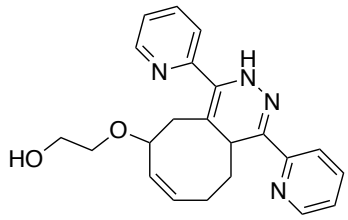

Chemical Formula: $C_{22}H_{24}N_4O_2$
Calulated Exact Mass (+H) : 377.1978
HRMS Exact Mass (+H) : 377.1989
ppm : 3.0

Figure 77 – The expected product of the IDE-DA reaction between E,Z-COD and pyridyl tetrazine, with stereochemistry ignored for simplicity. The calculated exact mass fits within expected range of the HRMS obtained value.

3.3.4. Stability of *E,Z*-COD

During the synthesis of the *E,Z*-COD analogues stability was a constant concern. Samples of both final products (diastereoisomers **30A and 30B**) dried, left in the -20 °C freezer and wrapped in foil, showed no reactivity with tetrazine after two months, indicating decomposition. To combat this all kinetic runs were conducted out on the same day as the elimination was carried out. Further evidence of the instability was seen in trying to collect ^{1}H NMR of either the mixture or separated (**30A and 30B**) diastereoisomers. Using $CDCl_3$ ^{1}H NMR could be collected but leaving that same sample to run overnight to gain a large scan number ^{13}C NMR, the ^{1}H NMR collected as part of that experiment showed clear decomposition compared to the earlier scan. Leaving the sample for a further day to attempt to obtain 2D data, resulted in a ^{1}H NMR spectrum which no longer contained the initial material. This is likely due to the slight acidity of $CDCl_3$ and could be due to isomerisation of the *trans* double bond.

As is often the case with bioorthogonal reagents, stability and enhanced kinetics need to be balanced. The fastest reacting probes such as Si-TCH also show poor stability, particularly to biological thiols and nucleophiles in general.[201] In order to have any real applications *in vitro* and particularly *in vivo* as a bioorthogonal reagent *E,Z*-COD would need to show reasonable stability, alongside its enhanced kinetics. As such we wanted to model the stability of *E,Z*-COD in a mimic of a biological system. A model previously carried out within the group to study the stability of *E,E*-COD and related products was used.[128] This involved making NMR samples of glutathione (sample adjusted to approximately pH 7) and *E,Z*-COD (mix of diastereoisomers) in a 1:1 mixture of CD_3CN and D_2O at 10 mM. Control samples of the single compounds were also made at the same concentration and all the samples were followed by ^{1}H NMR at various time points, with the samples heated to 37 °C between scans (Figure 78).

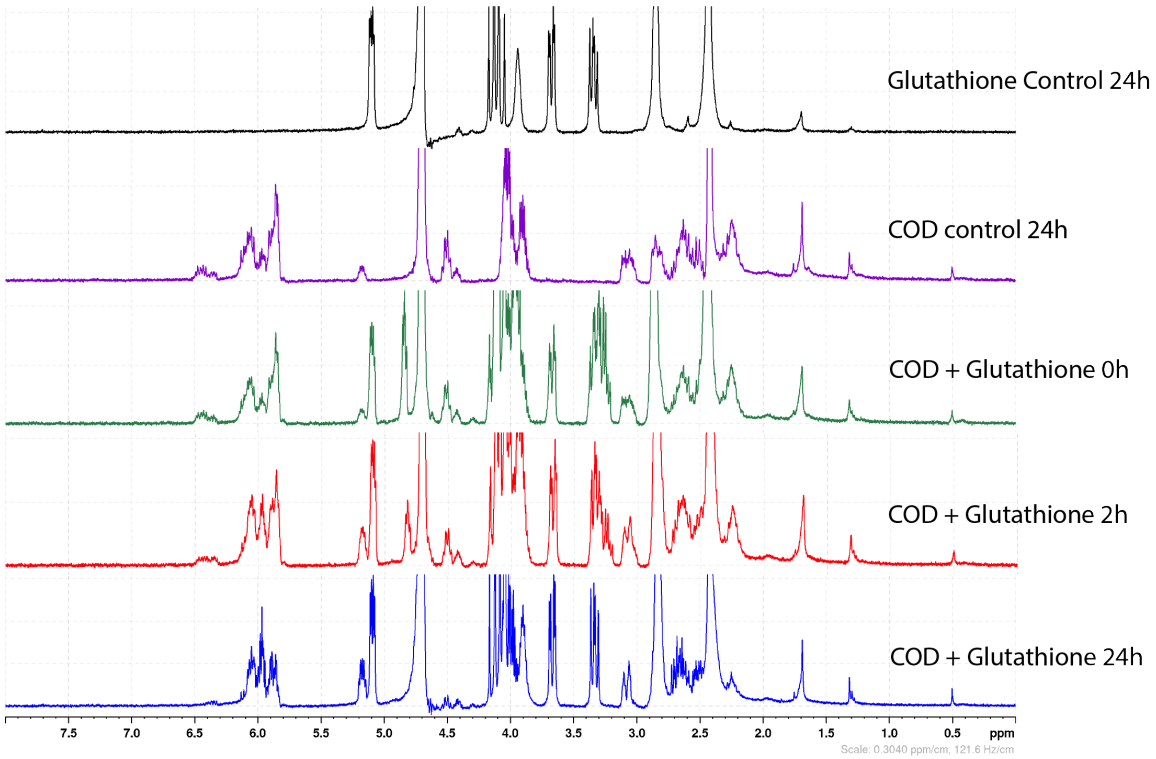

Figure 78 – ^{1}H NMR spectra of (from top to bottom) 10 mM glutathione (reduced) only at 24 hours, E,Z-COD only at 24 hours, and then a 1:1 mixture of E,Z-COD and glutathione at 0h, 2h and 24h. All samples were dissolved in a 1:1 mixture of CD_3CN and D_2O (spectra ran with reference to D_2O). Samples heated to 37 °C between scans and glutathione solution was adjusted to pH 7 before addition to control and mixed samples.

The *E,Z*-COD and glutathione mixed sample showed some changes in the spectrum obtained over the time course. This included changes to the multiplet at ≈ 6 ppm, formation of a new multiplet at ≈ 4.2 ppm and conversion of a complex multiplet to a doublet of doublets in the peak at ≈ 3.3 ppm. Some of these changes are because of glutathione oxidation as shown in Figure 79, with oxidation forming a disulfide bridged dimer, which matches a commercially obtained sample of the oxidised form. There does appear to be some change in the relevant COD peaks in the mixed sample, particularly at ≈ 6 ppm, ≈ 4.4 ppm and 2-3 ppm. With the complexity of the spectra these changes are difficult to understand but isomerisation of the trans double bond is likely based on previous work on TCO. These changes appear to be slow, with the 2 hour time point seemingly identical to the starting mixture, which due to the rapid kinetics of *E,Z*-COD would likely be within the time course of any *in vitro* or *in vivo* use, as opposed to longer time points such as 24 hours. The mix of COD diastereomers alone (COD control) does not show any obvious changes over the 24 hours despite being heated to 37 °C (Figure 80). This is somewhat surprising given the previously noted instability of the compound. The fact that it does not degrade in an aqueous based solvent system (unlike in $CDCl_3$), offers hope for potential biological applications.

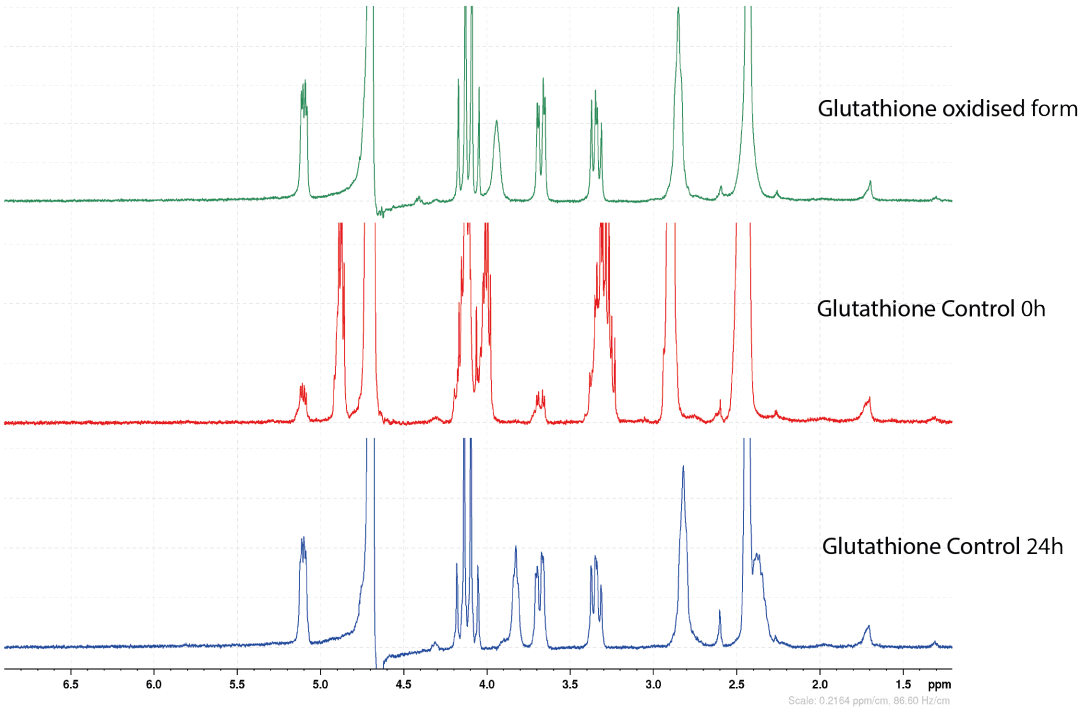

Figure 79 - ^{1}H NMR spectra of (from top to bottom) commercially obtained oxidised glutathione, 10 mM glutathione (reduced) only at 0 hours, and then 24 hours. All samples were dissolved in a 1:1 mixture of CD_3CN and D_2O (spectra ran with reference to D_2O). Samples heated to 37 °C between scans and glutathione solution was adjusted to pH 7.

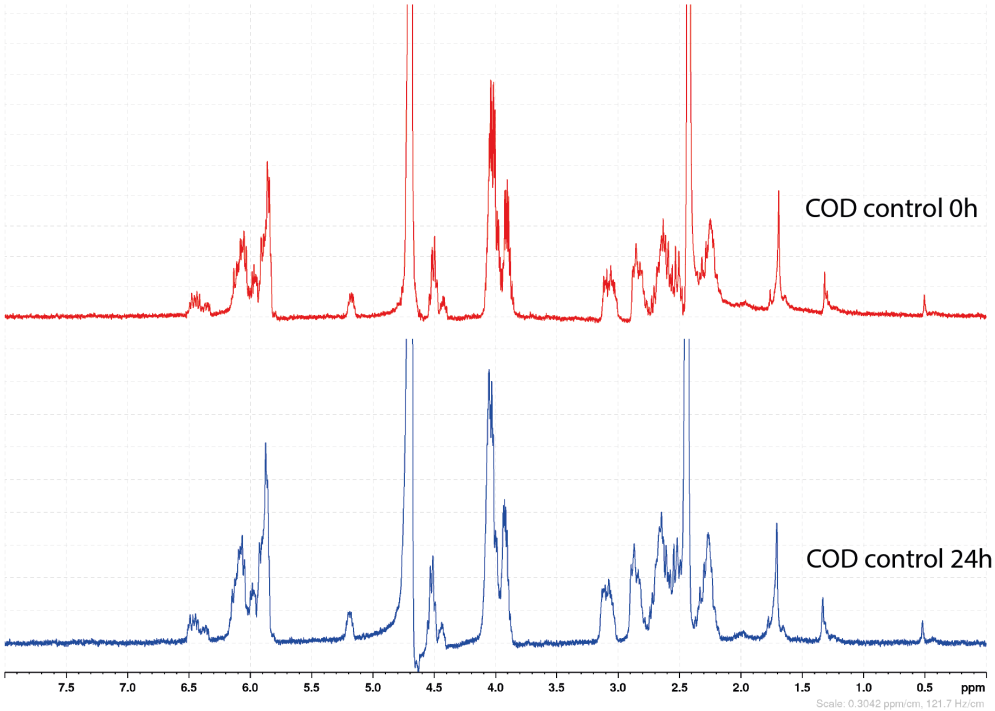

Figure 80 – ^{1}H NMR spectra of (from top to bottom) of a 10 mM mixture of E,Z-COD diastereoisomers at 0h then 24h. All samples were dissolved in a 1:1 mixture of CD_3CN and D_2O (spectra ran with reference to D_2O). Samples heated to 37 °C between scans.

In an attempt to show a biological application of *E,Z*-COD we turned to our MOE experience. Based on the previously employed double-click strategy using TMDIBO-TCO[102] we wanted to prepare a similar probe but replacing the TCO "second click" with the much enhanced kinetics of *E,Z*-COD. To do this *E,Z*-COD (**30A and 30B**) was reacted with 4-nitrophenyl chloroformate to form *E,Z*-COD-PNP (**31**). The reaction was carried out on very small scale and with the instability of *E,Z*-COD likely further increased due to the reactive PNP group only ^{1}H NMR were collected. However, this supported formation of *E,Z*-COD-PNP and so ligation with TMDIBO-Lys under the same conditions previously used to make TMDIBO-TCO were used. LCMS and TLC indicated starting material consumption, but the isolated product appeared to be a complex mixture as oppose to clean TMDIBO-Lys-*E,Z*-COD. The material recovered did appear to contain peaks via ^{1}H NMR for both TMDIBO and *E,Z*-COD. The complex mixture was incubated with Ac_4ManNAz treated COLO205 cells, but no contrast was observed after Tz-PEG_{11}-AlexaFluor647 treatment, suggesting the product had not been isolated.

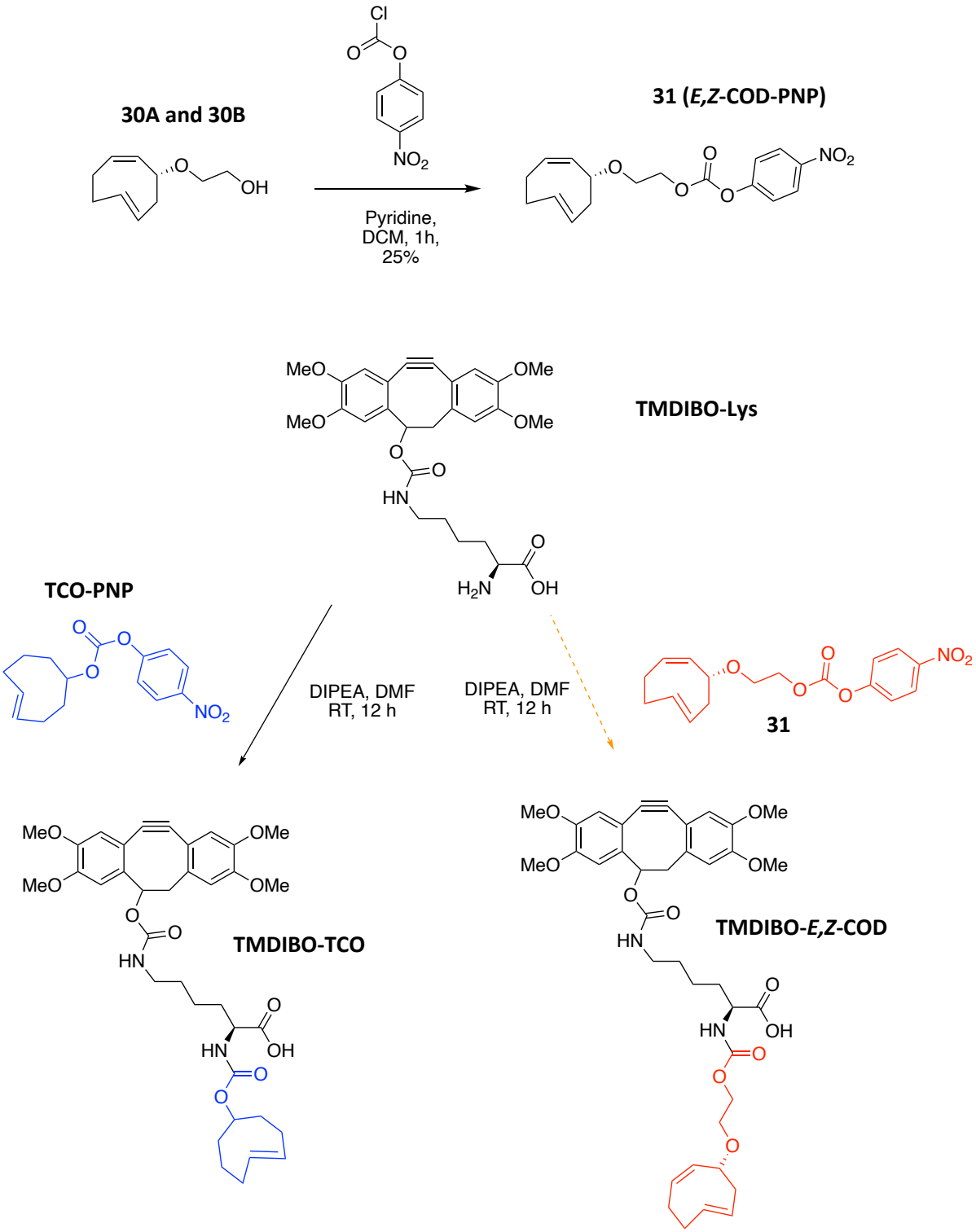

Figure 81 – Synthesis of E,Z-COD-PNP and attempted synthesis of TMDIBO-E,Z-COD (red) using the same methodology which was successful in the synthesis of TMDBIO-TCO (blue).

3.4. Summary and Future Work

3.4.1. Summary

ODIBO was proven to have enhanced kinetics for SPAAC compared to our standard probe of TMDIBO. However, the hydrophobicity of ODIBO remained a problem. Attempts at reducing the hydrophobicity were synthetically challenging. The particularly hydrophobic ^{t}Bu motif was not successfully replaced despite multiple groups being attached prior to the Friedel Crafts cyclisation step, including groups with various electron donating and withdrawing effects and sterically repulsive groups.

Alternative routes to reduce the hydrophobicity via conjugation of a hydrophilic lysine residue were eventually successful. Despite significantly reducing the cLogP, the probe showed much reduced contrast *in vitro* relative to a comparable TMDIBO-Lys analogue. Ac_4ManNAz treated COLO205 cells showed SBR of 11.5 $\pm$ 0.6 with TMDIBO-Lys-AlexaFluor647 and only 2.1 $\pm$ 0.2 with ODIBO-Lys-AlexaFluor647 at the same concentration. Sugar treated cells showed similar MFI with both probes, but the ODIBO-Lys non sugar treated control showed much higher MFI. This higher background signal is believed to be due to the increased nonspecific binding (and reduced ability to be washed away with aqueous solutions), caused by the increased hydrophobicity of the probe.

A novel strained cyclooctene probe *E,Z*-COD was synthesised as a mixture of diastereoisomers and one of the isomers was collected individually (**30B**). Collection of the other isomer (**30A**) was not achieved. Kinetic measurements conducted using stopped flow showed rapid IED-DA rates with dipyridyl tetrazine. The isolated diastereoisomer **30B** has a k_2 value of 28299.7 $\pm$ 332.8 M^{-1} s^{-1} , which is the fastest reported IED-DA kinetics with dipyridyl tetrazine in methanol. It remains to be seen why diastereoisomer **30A** could not be isolated, with degradation or the possibility that it is much more reactive to the point of instability/too fast to measure via our system, possible causes.

Attempts to make a TMDIBO-Lys-*E,Z*-COD analogue for double click labelling in a comparable method to TMDIBO-Lys-TCO were unsuccessful, despite synthesis of *E,Z*-COD-PNP. An alternative biological application is sought to prove the use of *E,Z*-COD as a bioorthogonal reagent.

3.4.2. Future Work

As attempts to reduce the hydrophobicity of ODIBO *via* a linker were not sufficient, it is believed that replacement of the hydrophobic ^{t}Bu motif is needed (Figure 82). However, this had proved synthetically challenging and so further understanding of the Friedel Crafts cyclisation step is needed. If an alternative group could be used here, allowing for much reduced hydrophobicity, then perhaps the enhanced SPAAC kinetics can be fully harnessed in a biological setting.

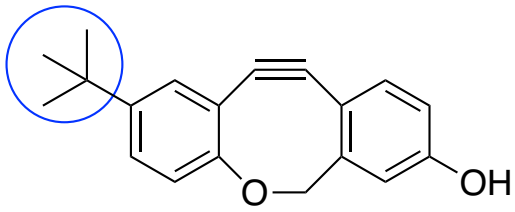

Figure 82 - Required replacement of the ^{t}Bu group.

The rapid IED-DA kinetics of E,Z-COD make it an exciting bioorthogonal chemistry tool. A biological application of E,Z-COD would prove its suitability as a replacement for alternative strained cyclooctenes such as TCO and s-TCO.

Further understanding of the relative kinetics and stability of the different diastereomeric products (**30A and 30B**) is needed. It would be of great interest if it were deduced as to why isomer **30A** was not isolated in these experiments, and if a suitable method for the isolation of **30A** was found, which would allow kinetic measurement of the isolated isomer. Isolation of the isomers via a stereoselective synthesis would be optimal. Perhaps a photochemical and/or flow-based synthesis could be envisaged to do this, in a similar fashion to other TCO analogues. This may be difficult due to a lack of control over the isomerisation (in terms of position and the formation of *E,E*-COD).This may not only allow access to the not-isolated isomer **30A** but also make the synthesis in general more robust and scalable. Application of *E,Z*-COD in a biological setting, could make use of the enhanced kinetics for increased imaging contrast.

4. Chemically Tagged Fucose Analogues for MOE

4.1. Introduction to Fucose MOE

4.1.1. Fucosylation in Cancer

The overexpression of fucose in cancer was first shown by Hakomori *et al.* in 1979,[202] who demonstrated the increase in fucose levels of glycolipids in hepatoma cells relative to normal hepatocytes. Fucosylation is the transfer of an L-fucose residue to a glycan, with the process regulated by fucosyltransferases, guanosine diphosphate (GDP)-fucose synthesis enzymes, and GDP-fucose transporters.[203] As with other monosaccharide pathways, the generation of the activated monosaccharide (the donor) is vital, with this then added to the protein/polysaccharide via transferases. Two pathways exist for the biosynthesis of GDP-fucose, the salvage pathway which starts from L-fucose and the *de novo* pathway which utilises D-mannose and D-glucose as substrates (Figure 83). The *de novo* pathway dominates, with the FX protein the rate-limiting enzyme in the pathway, and this enzyme often found overexpressed in cancer.[203, 204]

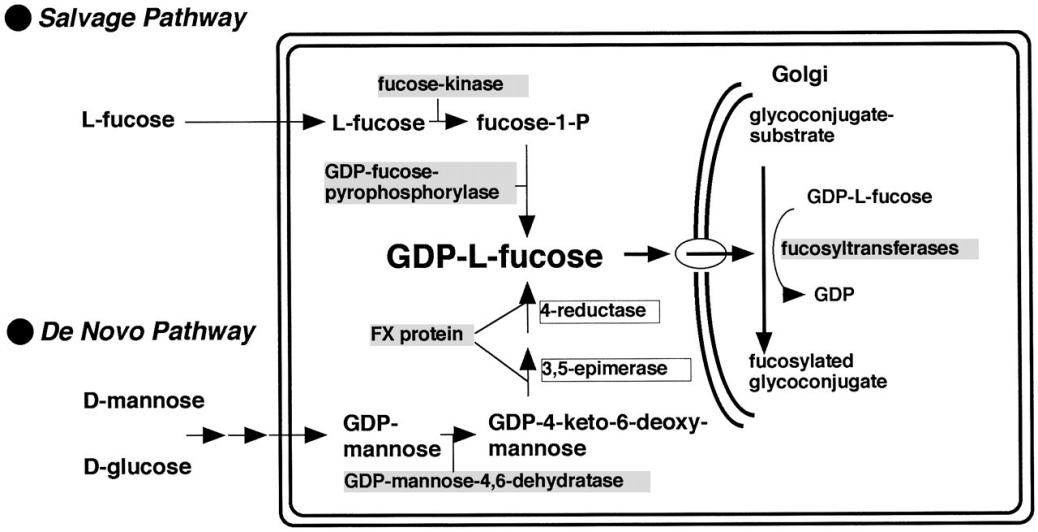

Figure 83 - The fucosylation biosynthetic pathway. Figure taken from Noda et al.[204]

Due to the complex nature of the pathway and the functional role of fucosylation, variable levels of the key biosynthetic enzymes are seen under different conditions, in particular in cancer.[203] This is particularly seen with the fucosyltransferase (FUT) family of enzymes (Figure 84) which add fucose to *N* or *O*-glycans, α1,2-(FUT1 and 2), α1,3/4-(FUT 3, 4, 5, 6, 7, 9, 10, 11), α1,6-(FUT8) or directly attach

the fucose to serine/threonine residue of epidermal growth factor (EGF) like repeats (POFUT1 and 2).[205, 206] For example, FUT4 has been found to be upregulated[206] and downregulated[207] in different tumour models. FUT3-7 are known to be important in the synthesis of Lewis antigens, which are important cancer biomarkers.[208] FUT8 is the only transferase capable of core fucosylation (in which α-1,6 linked fucose is added to the innermost *N*-acetylglucosamine) and has been found to be overexpressed in several malignant tumours.[205] Due to the vital role of fucose in cancer, further understanding is of vital importance for the development of fucose based diagnostics and therapies.[209]

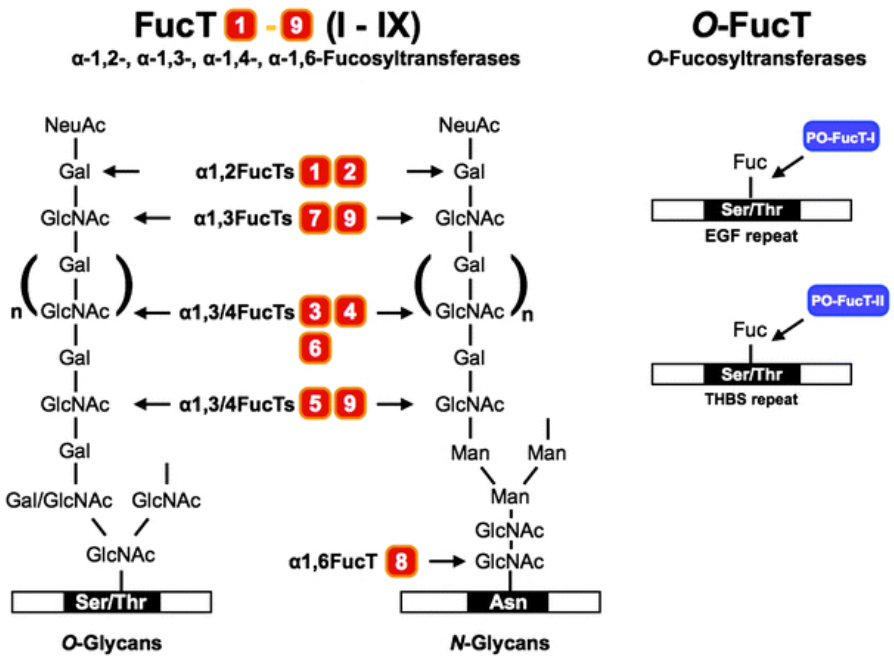

Figure 84 – The fucosyltransferases are essential in the transfer of fucose from GDP-fucose to the highlighted residues. Figure taken from Tu et al.[210]

4.1.2. Fucose Metabolic Engineering

Despite the biological importance of fucosylation and the growing field of MOE, there have been much fewer examples of fucose tagged analogues compared to mannosamine (as well as GlcN and GalN). This could be due to the salvage pathway not being as active as the *de novo* pathway as previously mentioned. As well as this multiple chemically tagged sugars (some developed for MOE) have shown cell toxicity and acted as inhibitors for fucosylation.[211-213]

The widely used azide chemical reporter was applied to the design and synthesis of fucose analogues by the Bertozzi group.[214] They reported the importance of the position of substitution with only the monosaccharide with the azide handle in the 6-positon showing labelling of Jurkat cells via Staudinger

ligation (and only at concentrations >100 μM). Cell lysates from sugar-treated Jurkat cells also only showed labelling with 6-azido fucose (6-Az-Fuc), visualising using western blot. Notably at the concentrations required for labelling with 6-Az-Fuc, significant cell death was observed.[214, 215]

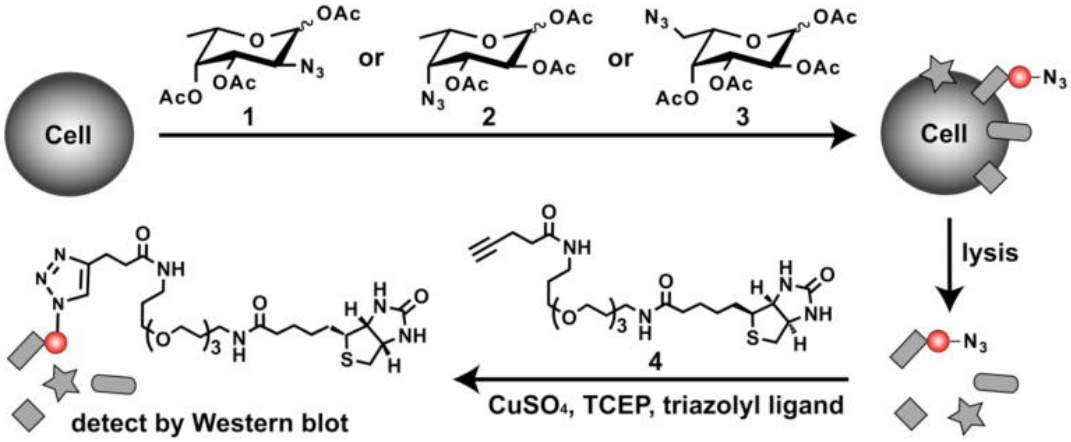

Figure 85 – Azido fucose analogues synthesised and detected by flow cytometry and from western blot analysis (as shown) by Rabuka et al. Of the analogues only compound 3 (6-azido fucose) showed any incorporation. Figure taken from Rabuka et al.[214]

Alternative chemical reporters to the azide have also been employed. Alkynyl groups have been used as first described by Sawa *et al.*[216] who synthesised 6-alkynyl fucose (6-Alk-Fuc). This probe was successfully incorporated into Jurkat cells which were subjected to CuAAC with an azide-biotin probe, and then reacted with a fluorescent streptavidin to allow visualisation by flow cytometry. They also demonstrated the 6-alkynyl handle was much less cytotoxic and had less of an effect on cell growth compared to 6-Az-Fuc.[216] However, a similar alkynyl mannosamine analogue showed much greater fluorescent intensity post reaction with the azide probe system relative to the 6-alkynyl fucose, demonstrating the much better tolerance towards unnatural substrates of the sialic acid pathway (SBR of 3 for alkynyl fucose and 15 for alkynyl mannosamine).[215]

In 2016 Kizuka *et al.*[217] synthesised a range of alkynyl fucose analogues with varying chain lengths from the 6-position. 7-Alkynyl fucose (7-Alk-Fuc) showed the greatest incorporation and also showed low cytotoxicity relative to the 6-azido fucose probe previously developed. In an enzyme activity assay, they also demonstrated the efficiency of utilisation of the GDP activated form of the various analogues by FUT8. They found 7-Alk-Fuc to act as the most efficient donor but also noted that the other substrates were transferred, but with decreasing efficiency with increasing chain length.[217] This is perhaps unsurprising as increasing chain length perturbs more from the natural substrate.

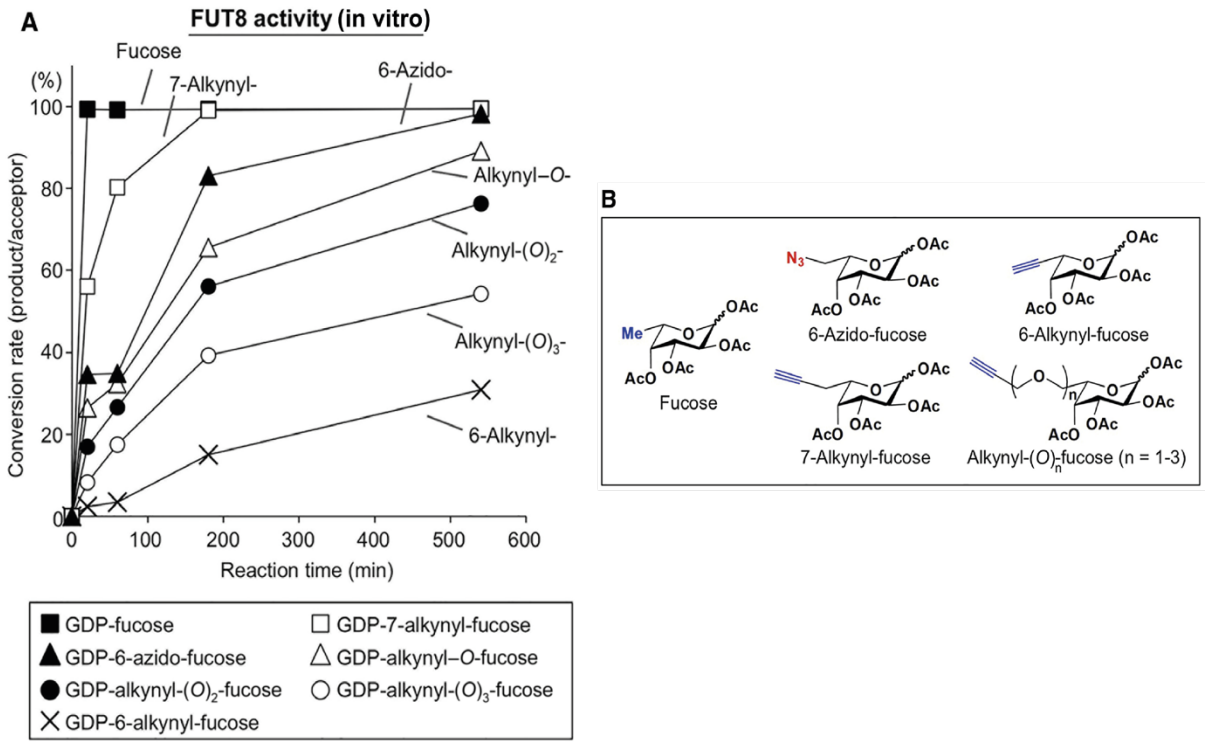

Figure 86 - A) FUT8 activity assay using various fucose analogues. A fluorescent N-glycan was used as the acceptor and N-glycan products bearing the corresponding fucose analogues were detected with distinct retention times by HPLC. B) Fucose analogues used in the study. Figure adapted from Kizuka et al.[217]

Modelling of the FUT8-GDP-fucose was carried out by Kizuka *et al.*, by superposition of *Caenorhabditis elegans* POFUT1 in complex with GDP-Fuc onto human FUT8.[217] This modelling suggested a long chain could sterically clash with a flexible loop of the protein. However, as discussed FUT8 is only one of the many transferases (although an important one in cancer) and transferases are just one step in the biosynthetic pathway which must be tolerant to the substrate at all steps. This was highlighted by Ma *et al*[218] who showed the level of GDP-6-Alk-Fuc produced in cells was higher than that of GDP-7-Alk-Fuc, which suggests other elements in the biosynthesis are more tolerant to the 6-Alk tag than the 7-Alk (in comparison to FUT8). They also showed that most fucosyltransferases were somewhat efficient when GDP-7-Alk-Fuc was used as a substrate, with little tolerance towards GDP-6-Alk-Fuc or GDP-6-Az-Fuc. Computational modelling of FUT8 showed little flexibility around the 6-postion of fucose (although this does not explain the intolerance towards GDP-6-Alk-Fuc). However, the POFUT enzymes were found to be much more promiscuous, with tolerance towards all three tagged analogues, and computational modelling showing space around the 6-position for modification.[218] POFUT1 and 2 are known to be upregulated in a number of cancers[219-223], and important in NOTCH signalling[224], but are used for the fucosylation of intracellular proteins and so are not useful in MOE. Despite the lack of flexibility in FUT8, other FUT enzymes could be more tolerant towards chemically modified substrates.

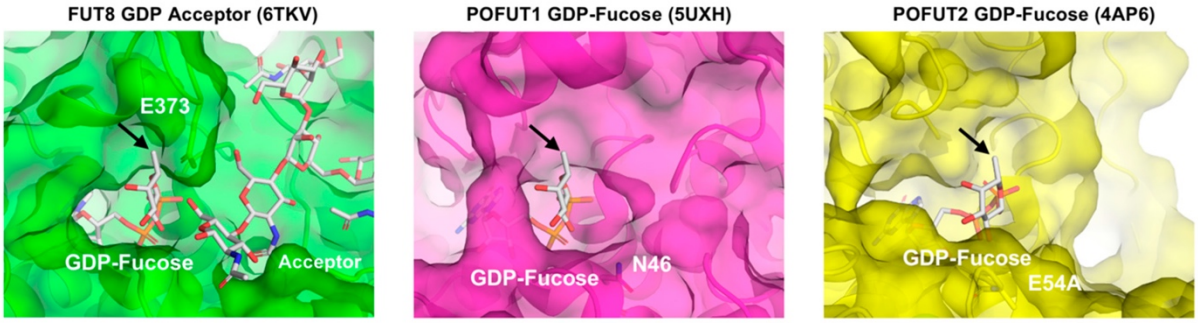

Figure 87 - Structural comparison among FUT8-GDP-acceptor complex (PDB code: 6TKV, green), POFUT-GDP-Fuc complex (PDB code: 5UXH, magenta) and POFUT2-GDP-Fuc complex (PDB code: 4AP6, yellow). The arrow highlights the methyl group (C-6) of fucose. Figure taken from Ma et al[218]

With incorporation efficiency clearly a challenge we considered whether the enhanced kinetics of methyl cyclopropenes could compensate for any reduced incorporation. In particular, if we could strike a balance between incorporation and kinetics in order to generate contrast *in vitro* as was demonstrated by the reduced incorporation but enhanced kinetics of ManNCyoc leading to greater labelling than the better incorporated but slower amide linked derivatives.[91] To do this we aimed to synthesise a range of cyclopropene tagged monosaccharides with variable linkage to the monosaccharide.

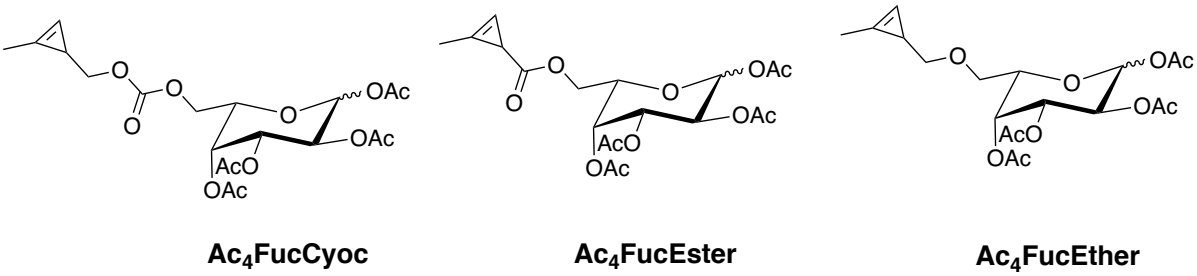

Figure 88 – Potential cyclopropene tagged fucose analogues.

4.2. Synthesis of Cyclopropene Tagged Fucose Analogues

4.2.1. Synthesis of Ac_4FucCyoc

To test the synthetic plans in the fucose project, synthetic steps were first conducted using 1,2:3,4-di-O-isopropylidene-α-D-galactopyranose. No stereochemical inversion is induced, so the resulting products will remain in the D-configuration. Whilst other monosaccharides are naturally found in the D-configuration, fucose is found as L-fucose in nature. Thus, the analogues synthesised using 1,2:3,4-di-O-isopropylidene-α-D-galactopyranose would be the incorrect enantiomer to be fucose mimics.

However, it is vastly cheaper to purchase the naturally occurring D-form, than L-galactose. As such, the chemistry was first tested and optimised on 1,2:3,4-di-O-isopropylidene-α-D-galactopyranose and then carried out on 1,2:3,4-di-O-isopropylidene-α-L-galactopyranose (which was synthesised from commercially available L-galactose - Scheme 25). For simplicity all compounds are drawn in the L-configuration as this is the active configuration used for *in vitro* work.

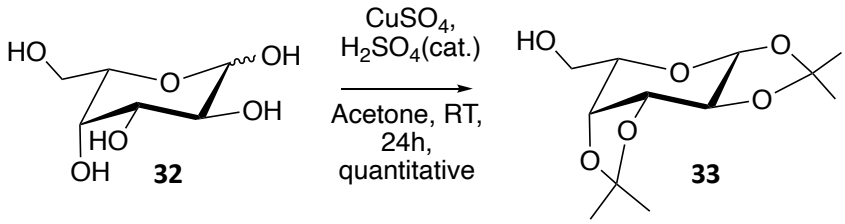

Scheme 25 - Acetonide protection of L-galactose. For D-galactose the acetonide protected material is commercially available.

Based on the successful synthesis of 7-alkynyl fucose[217] a similar scheme was designed. First the methyl cyclopropene carbonate would be attached to the sugar. The same conditions as previously used to form the carbamates with the amino sugars were employed to couple Cyoc-PNP (**1**) to the free -OH at C-6 of the starting material to form the carbonate **34**. Then the protecting groups would be removed, which had blocked the other hydroxyl positions, using either standard acidic conditions or a Lewis acid promoter system to give **35**.[225] Finally the free hydroxyl groups would be acetylated under standard conditions to give Ac_4FucCyoc (**36**). However, deprotection was not achieved. Perhaps unsurprisingly, given the previously mentioned instability of methyl cyclopropenes to acid, the acid (TFA) removal of the isopropylidene groups was unsuccessful. An alternative method using a triethylsilane/boron trifluoride etherate combination was also unsuccessful, perhaps due to the large excess of reagents required (almost 10 equiv.).

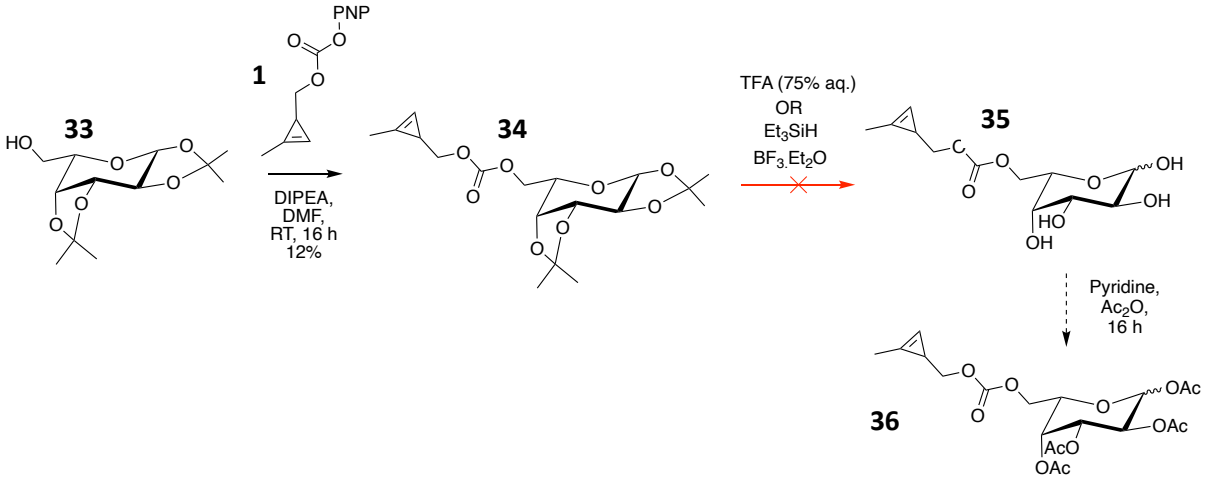

Scheme 26 - Initial attempts at synthesis of Ac_4FucCyoc.

Therefore, an alternative synthesis was designed. This would involve replacing the acetonide protecting groups with acetyl groups first and then attaching the methyl cyclopropene motif. However, to do this, we would need to protect the free hydroxyl which would later act as the handle to attach bioorthogonal chemical reporters (Scheme 27). As such, first the acetonide-protected material (either commercial for D- or synthesised for L-) was reacted with benzyl bromide using sodium hydride. This gave **37** in a lower than expected 55% yield. With the 6-hydroxyl now orthogonally protected, the acetonide protecting groups could be cleaved with TFA and then the free hydroxyl groups fully acetylated using standard conditions, giving **38** in 52% yield. The benzyl protecting group was then removed under hydrogenation conditions with Pd/C in a 1:1 mixture of EtOAc:MeOH. The cleavage was complete within one hour and the filtrate after catalyst removal **39** did not require further purification. Finally, the methyl cyclopropene was attached via a carbonate linkage by reacting the free hydroxyl of **39** with 1 under the conditions previously used.

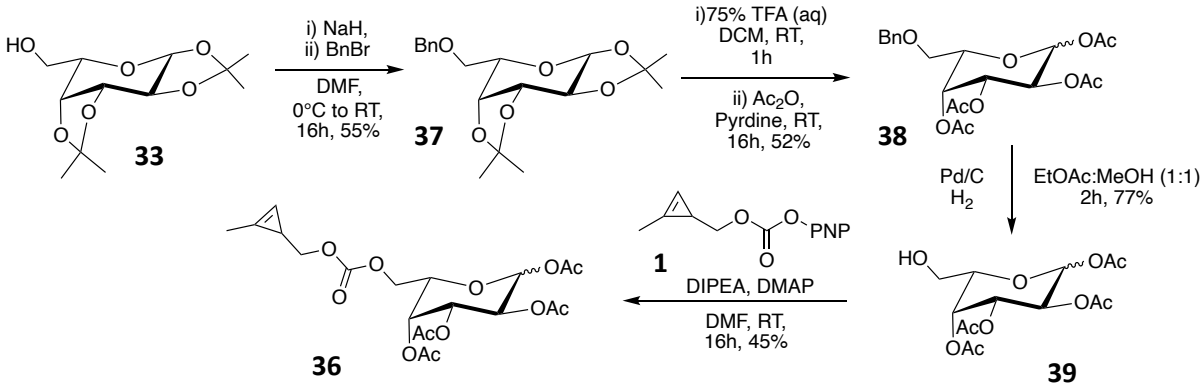

Scheme 27 - Synthesis of Ac_4FucCyoc.

4.2.2. Synthesis of Methylcyclopropene Tagged Fucose Analogues with Varying Linkages

We then aimed to use a similar methodology to attach methylcyclopropenes with differing linkages to the fucose analogue. We envisioned two substrates with shorter linkers (Figure 89), which we hoped would result in greater incorporation, due to less variance from the natural substrate. This would have to be balanced against the kinetics of IED-DA reactions between cyclopropenes and tetrazines, with electron withdrawing groups such as esters, slowing the rate with electron poor tetrazines.[69, 108, 113] This balance of incorporation efficiency versus kinetics is well known for IED-DA based MOE.[108]

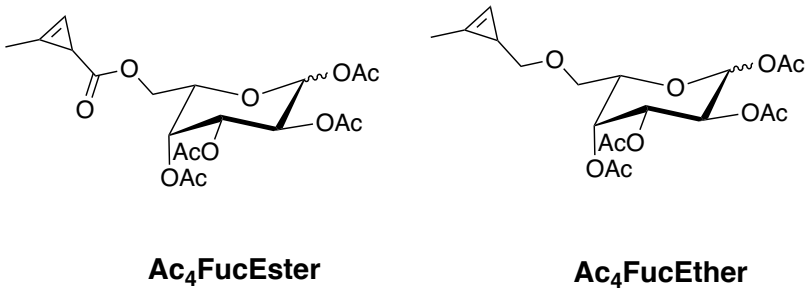

Ac_4FucEster **Ac_4FucEther**

Figure 89 - Alternative methylcyclopropene fucose analogues – Ac_4FucEster and Ac_4FucEther.

Initial attempts at synthesising the Ac_4FucEster sugar focused on making the acid chloride of the methyl cyclopropene (**40**) *in situ* and reacting this with **39** (Scheme 28). This method has previously been used to make amide-linked methylcyclopropene-tagged monosaccharides,[148] but we were unable to isolate the ester product. Instead, the reactive pentafluoro ester of the methyl cyclopropene acid **41** was synthesised, and this was coupled **39** under the same conditions as was used to synthesise the Ac_4FucCyoc analogue. To synthesise the ether analogue, multiple conditions were attempted to convert the methyl cyclopropene alcohol to various good leaving groups, including the alkyl bromide (**42**) and the tosylate (**43**). In other methyl cyclopropene based syntheses the alcohol was never collected after silyl deprotection and only used as an intermediate. As such, attempts aimed to remove the silyl protecting group and then convert the alcohol straight to the reactive handle (as is done similarly in the synthesis of Cyoc-PNP **1**). TLC indicated deprotection of the silyl protected cyclopropene alcohol and subsequent consumption of that species, but no clear LCMS peak or TLC spot for the activated leaving group products **42** and **43** could be seen. Due to the anticipated reactivity and volatility of the alkylating agents **42** and **43** and, after some attempts to isolate them, it was decided to try and make them and immediately react them *in situ* with **39**. No Ac4FucEther product was observed or collected.

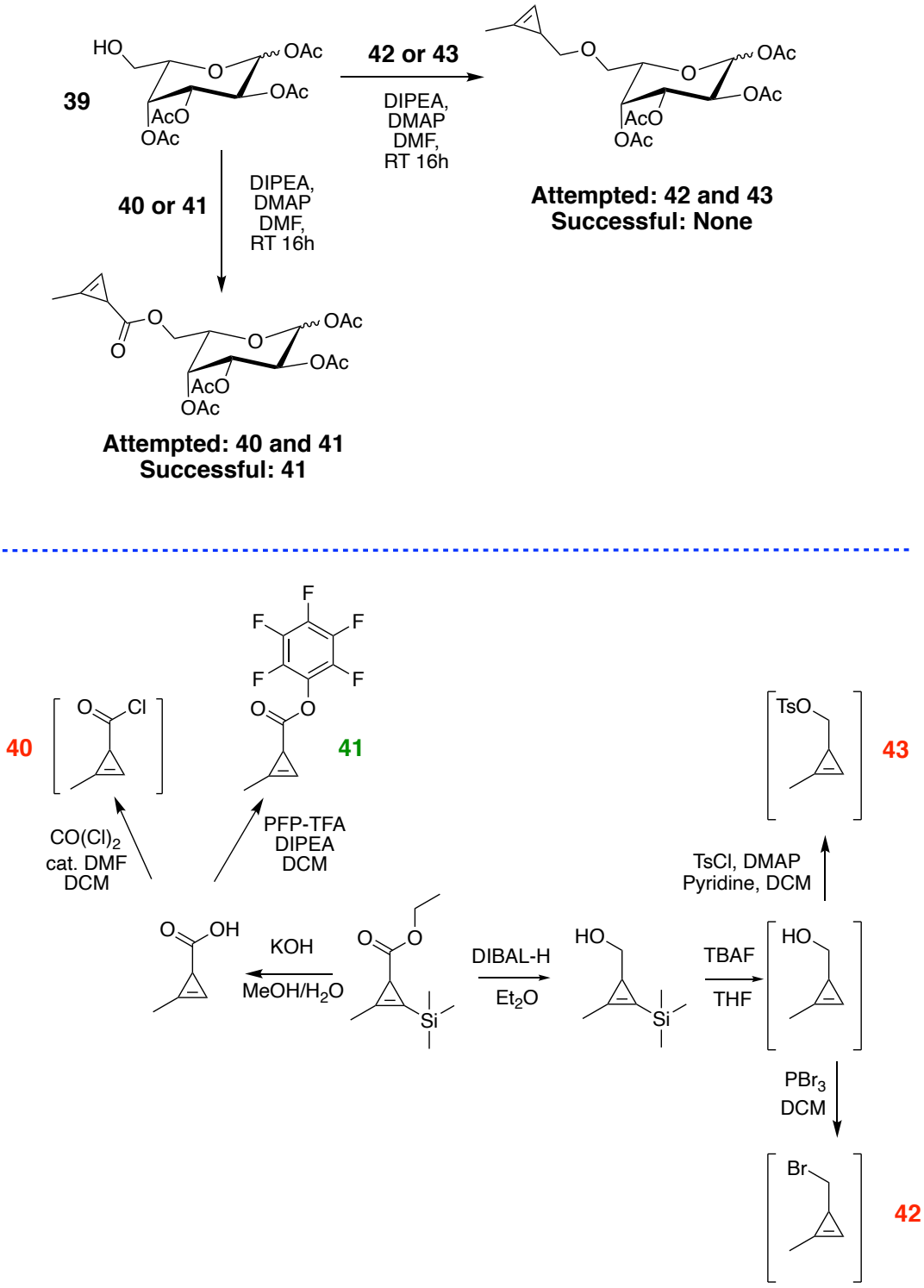

Scheme 28 - Attempted synthesis of fucose ester and ether linked methylcyclopropene analogues. Ac_4FucEster was successfully synthesised using B. Ac_4FucEther was not collected. Species in brackets were not isolated due to potentially being unstable and/or volatile and so it remains uncertain if they were synthesised as intermediates.

An alternative approach was employed, by placing a strong leaving group (a tosylate) on our sugar and then react this with the methyl cyclopropene alcohol (Scheme 29). However, the tosylate of a mimic substrate **44** (directly reacting tosyl chloride with 1,2:3,4-di-O-isopropylidene-α-D-galactopyranose)

showed no reaction with the methyl cyclopropene alcohol. Elevated temperatures are likely required, which are incompatible with the methyl cyclopropene motif.

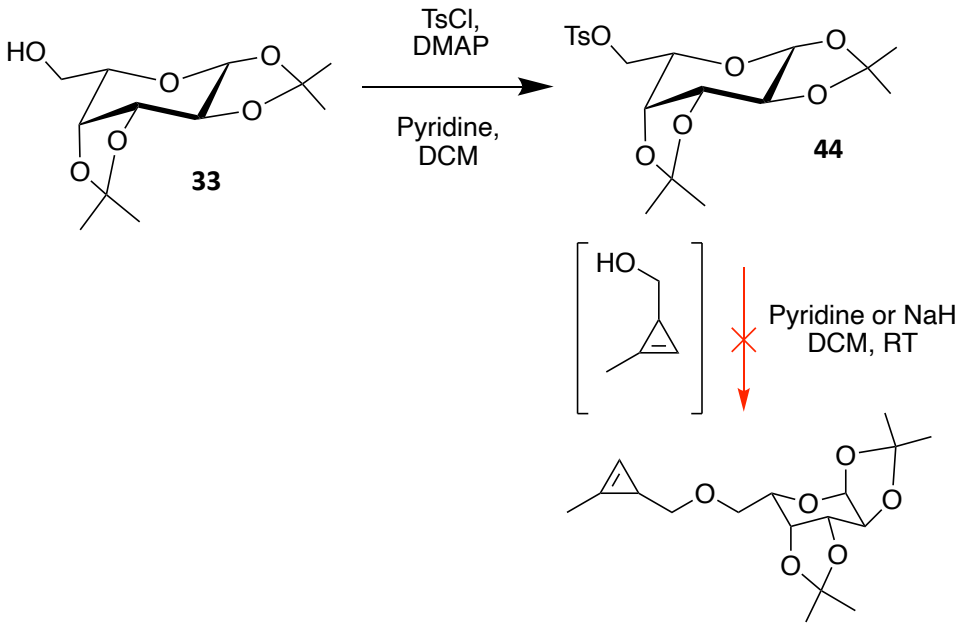

Scheme 29 - Alternative attempted synthesis of Ac_4FucEther

4.2.3. *In vitro* testing of fucose analogues

To test the MOE potential of the synthesised fucose mimics (FucCyoc and FucEster), *in vitro* studies were conducted in a fashion similar to our previous work. Initially, the same conditions as we had employed for our acetylation studies, 125 μM sugar, 24-hour incubation and labelling using 5 μM of our Tetrazine-PEG_{11}-AlexaFluor647 probe were used. Due to the success of our previous work on acetylation, a small sample of Ac_4FucCyoc was reacted under the previous selective deacetylation conditions to give Ac_3FucCyoc, which would also be tested to see if hydrophobicity was limiting incorporation.

As can be seen in Figure 90 both Ac_3FucCyoc and Ac_4FucEster showed no statistically significant contrast relative to the non-sugar treated samples (which were treated with Tz alone) in COLO205 cells at 125 μM. Ac_4FucCyoc showed very modest but statistically significant contrast, giving and SBR of 1.2±0.0. Whilst this is far too low to be of any biological relevance, particularly given the large decrease in contrast always seen when applied *in vivo*, it offers the potential that cyclopropene tagged fucose analogues can be used for MOE. Notably a sample treated with 125 μM Ac_4FucCyoc and an excess (1 mM) Ac_4Fucose showed an MFI in line with the control treated samples. Whilst this is only

one sample and replicates are needed, it does suggest that Ac_4FucCyoc is being incorporated as part of the fucose scavenger pathway as anticipated.

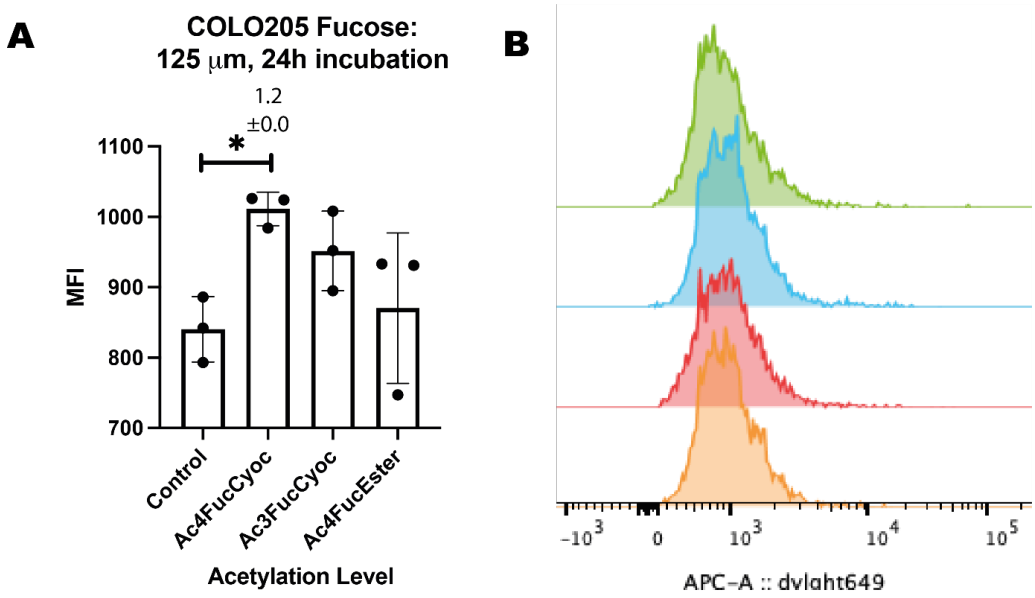

*Figure 90 – Treatment of COLO205 cells with fucose analogues. A) COLO205 cells were incubated in the presence or absence (control) of the indicated fucose sugar at 125 μM) for 24 h. They were then incubated with dyes (Tz-AlexaFluor647 (5 μM); + Sytox green cell death stain, (50 nM)) for 1 h at 37 °C and analysed by flow cytometry. Median fluorescence intensity (MFI) is shown as mean ± SD. Signal-to-background ratios (SBR) relative to the control (untreated) are shown above each bar when the SBR is significantly more than 1; n=3 technical replicates. Statistical analysis was performed using an unpaired t test with Welch correction (**** P≤0.0001,*** P≤0.001,** P≤0.01,* P≤0.05). B) Histogram giving number of events (vertical axis) versus fluorescence intensity (horizontal axis) In each panel the sugars used, from top to bottom, are: control, Ac_4FucCyoc, Ac_3FucCyoc and Ac_4FucEster. An independent replicate conducted on a different day produced comparable results*

We hypothesised that as we had previously seen with other tagged monosaccharides, perhaps other cell lines would potentially show increased fucosylation of surface glycans and hence would incorporate more tagged fucose. The two cell lines that previously showed increased levels of sialyation, MDA-MB-231 and PANC-1 (Figure 91), were treated with Ac_4FucCyoc again at 125 μM. However, no contrast was seen in either cell line treated with Ac_4FucCyoc (other sugars were not tested due to previous lack of contrast and experimental constraints). Given the increased sialyation observed in these cell lines (relative to COLO205) we are surprised to not also see an increase in fucosylation, given both are well associated with tumour aggression.[37, 209]

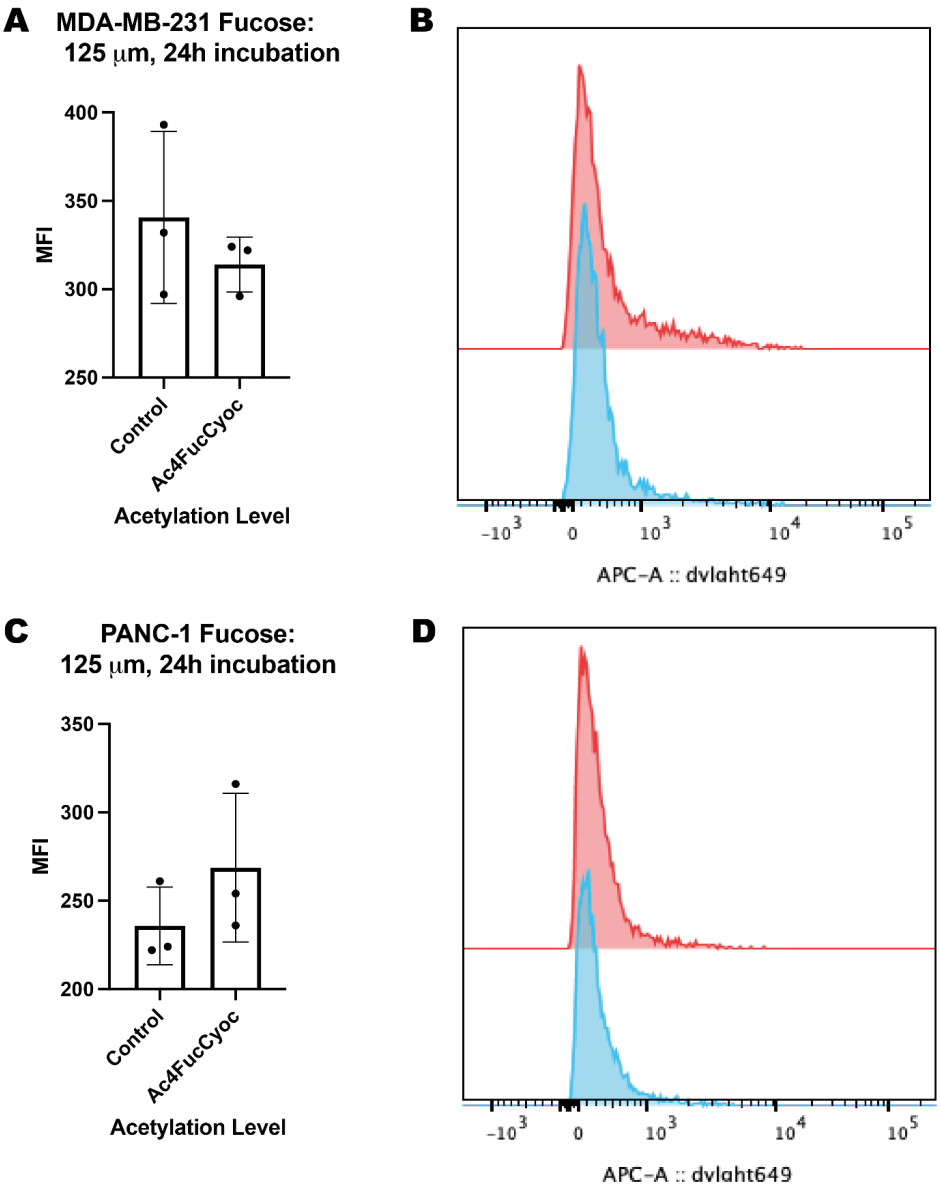

Figure 91 – Treatment of MDA-MB-231 and PANC-1 cells with fucose analogues. A) MDA-MB-231 and C) PANC-1 cells were incubated in the presence or absence (control) of the indicated fucose sugar at 125 μM) for 24 h. They were then incubated with dyes (Tz-AlexaFluor647 (5 μM); + Sytox green cell death stain, (50 nM)) for 1 h at 37 °C and analysed by flow cytometry. Median fluorescence intensity (MFI) is shown as mean ± SD. B) and D) Histograms giving number of events (vertical axis) versus fluorescence intensity (horizontal axis). In each panel the sugars used, from top to bottom, are: control and then Ac_4FucCyoc.

In an attempt to increase the minimal contrast previously seen in COLO205 cells with our fucose analogue, the experimental conditions were altered. The final concentration of the sugar in the cell medium was increased to 200 μM and incubation time increased to 48 hours. This mimics the conditions used in previous fucose MOE analogue reports[217] and is shorter incubation than that used in the report of 6-azido fucose (72 hours but at 125 μM).[214] Using these new conditions, COLO205 cells which had shown minimal contrast, and PANC-1 cells which had shown none, were treated.

The resulting flow cytometry data and analysis is shown in Figure 92. COLO205 cells showed enhanced contrast at the increased concentration and incubation times, with an SBR of 1.9±0.1. This statistically significant contrast further supports the use of Ac_4FucCyoc as a novel probe for imaging tumour fucosylation. Ac_4FucEster also showed some modest contrast under the new conditions, with an SBR of 1.3±0.0. With PANC-1 cells, the sugar treated samples again showed no contrast, but there was large variability in the MFI measured for Ac_4FucCyoc (it is unclear why) and this may have rendered a small increase in SBR statistically insignificant. It is not known why COLO205 cells are the only cell line to currently show contrast with Ac_4FucCyoc and Ac_4FucEster, but it maybe that this cell line makes more use of one (or more) of the FUT isozymes that can accept these modifications to their substrate.

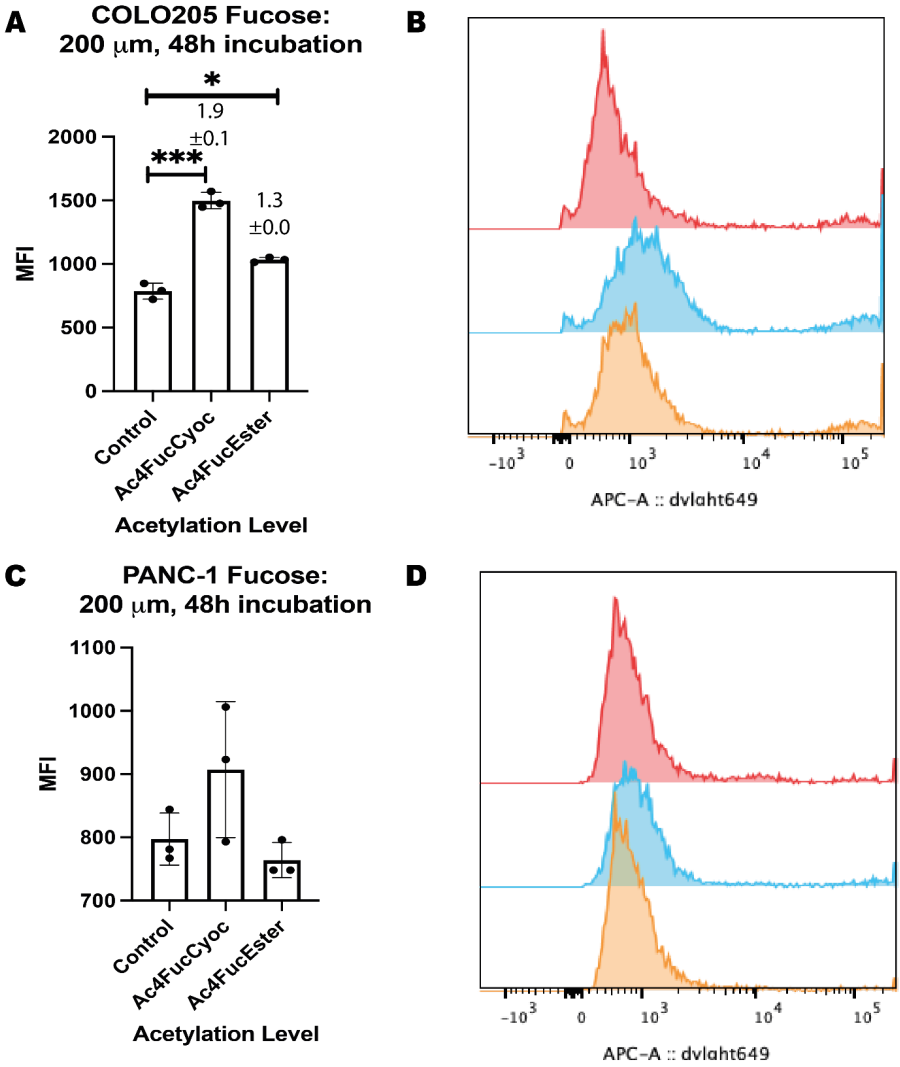

*Figure 92 - Treatment of COLO205 cells with fucose analogues using alternative conditions. A) COLO205 C)PANC-1 cells were incubated in the presence or absence (control) of the indicated fucose sugar at 200 μM for 48 h. They were then incubated with dyes (Tz-PEG_{11}-AlexaFluor647 (5 μM) + Sytox green cell death stain, (50 nM)) for 1 h at 37 °C and analysed by flow cytometry. Median fluorescence intensity (MFI) is shown as mean ± SD. Signal-to-background ratios (SBR) relative to the control (no-sugar) are shown above each bar when the SBR is significantly more than 1; n=3 technical replicates. Statistical analysis was performed using an unpaired t test with Welch correction (**** P≤0.0001,*** P≤0.001,** P≤0.01,* P≤0.05). B) and D) Histograms giving number of events (vertical axis) versus fluorescence intensity (horizontal axis). In each panel the sugars used, from top to bottom, are: control, Ac_4FucCyoc, and Ac_4FucEster.*

Previous work within the group in developing isonitrile tagged monosaccharides had found that direct conjugation of isonitrile tagged glycans with a fluorescent tetrazine showed no contrast. However, when the same labelled cells were first reacted with tetrazine conjugated to a biotin motif (at much higher concentration – 100 μM), then washed and subsequently tagged with a fluorescent neutravidin, SBRs of up to 5.8 were observed.[92] The indirect labelling approach is widely used in MOE development, and is known to generally enhance contrast *in vitro*.[100] The disadvantage of this approach is that it is not applicable *in vivo*, but we believed it would allow us to better understand what analogues were incorporated well and thus further develop the process. In the isonitrile example the dipyridyl tetrazine used was conjugated to biotin or the fluorophore via a PEG_3-linker.[92] To make our results more comparable to our standard conditions, (Tz-PEG_{11}-Biotin **46**) was synthesised which contained the PEG_{11}-linker that was used for our other studies.

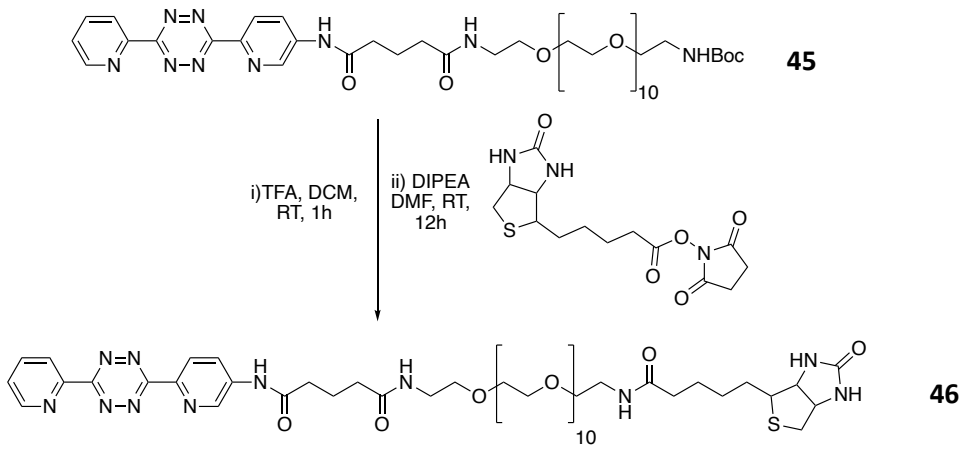

Scheme 30 - Synthesis of Tetrazine-PEG_{11}-biotin

As well as the cyclopropene analogues previously discussed, metabolic labelling with a TCO bearing fucose was also studied. Georgia Edmonds a Part III student in the Leeper group had successfully synthesised Ac_4FucTCO (figure Y) as part of her project. This analogue would act as an extreme example to test the hypothesis that reduced incorporation could be compensated by enhanced kinetics. The large perturbation from L-fucose when the TCO motif is conjugated was expected to result in very low if any incorporation. Ac_4FucTCO was synthesised via reaction of **39** with TCO-PNP under the standard conditions.

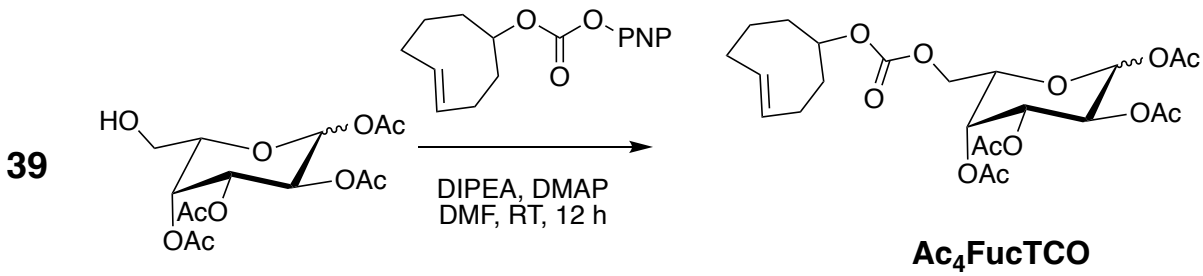

Scheme 31 - Synthesis of Ac_4FucTCO carried out by Georgia Edmonds.

COLO205 cells were again used, with 200 μm final sugar concentration and 48-hour incubation post-sugar treatment. Following 1 hour incubation at 37 °C with 100 μm Tz-biotin **46** and subsequent 30-minute incubation with NeutrAvidin Protein-DyLight650 the results of the treated samples (or various controls) are shown in Figure 93. There was an enhancement in SBR values (calculated against the -sugar, +Tz-biotin, +NeutrAvidin control samples) with Ac_4FucCyoc and Ac_4FucEster relative to the single step labelling approach previously used with values of 2.6 ± 0.1 and 1.7 ± 0.1 respectively. This confirms our hypothesis that this approach can be used to increase contrast, believed to be due to a decrease in non-specific binding of the fluorophore conjugated compound. This has further supported these cyclopropene analogues as fucose MOE agents. Remarkably, the SBR generated from Ac_4FucTCO was 34.7 ± 0.5, with no obvious effect on viability detected when gating cell populations by Sytox green signal. This large SBR is surprising given the previously discussed substrate specificity limitations of the fucose salvage pathway. They make Ac_4FucTCO a very exciting tool for fucose MOE. The large number of different FUT and fucosylation enzymes in general, and the potential for each to be expressed in various levels in different cell lines makes understanding this incorporation difficult. It could be that one particular FUT is more tolerant than for example FUT8, and this enzyme is upregulated in COLO cells. Further investigation of the incorporation of these analogues in multiple cell lines is needed to probe this.

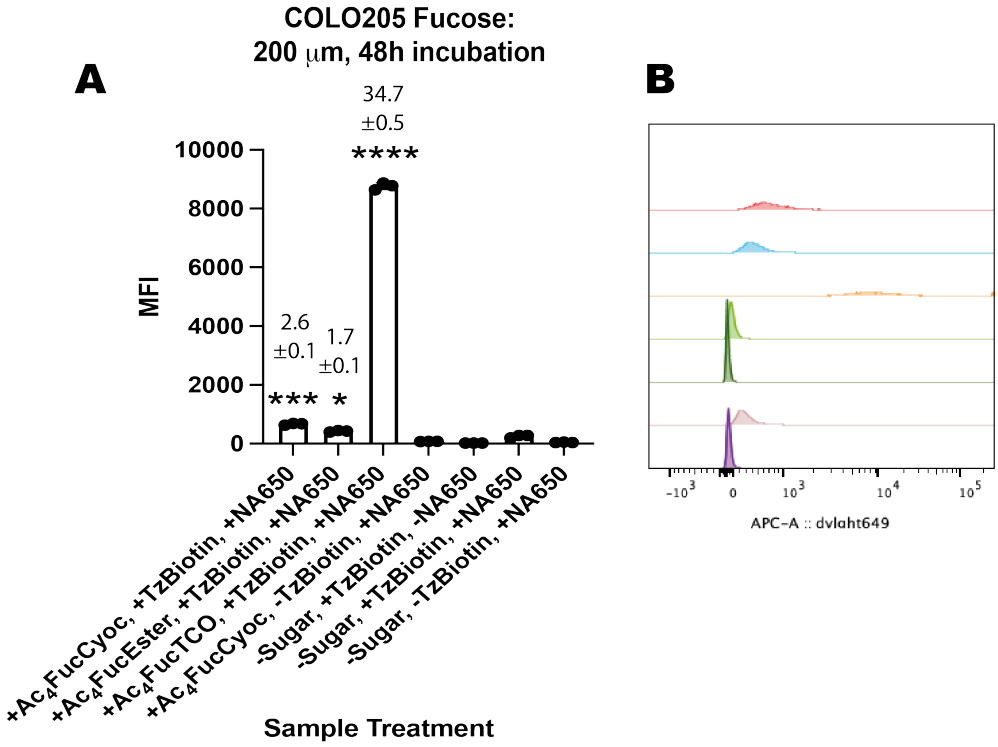

*Figure 93 - Treatment of COLO205 cells with fucose analogues using alternative dye combination. COLO205 cells were incubated in the presence or absence (control) of the indicated fucose sugar at 200 μM for 48 h. They were then incubated with either Tz biotin (100 μM + Sytox green cell death stain, (50 nM)) or FACS buffer containing sytox alone (50 nM) for 1 h at 37 °C. Cells were then incubated with NeutrAvidin Protein-DyLight650 (50 μg ml^{-1}) or FACS buffer alone as indicated above, and analysed by flow cytometry. Median fluorescence intensity (MFI) is shown as mean ± SD. Signal-to-background ratios (SBR) relative to the control (-sugar, +Tz biotin, +NeutrAvidin) are shown above each bar when the SBR is significantly more than 1; n=3 technical replicates. Statistical analysis was performed using an unpaired t test with Welch correction (**** P≤0.0001,*** P≤0.001,** P≤0.01,* P≤0.05). B) Shows histograms giving number of events (vertical axis) versus fluorescence intensity (horizontal axis). The histogram plots from top to bottom correspond with the conditions shown in A) from left to right.*

4.3. Summary and Future Work

4.3.1. Summary

In summary, three novel chemically tagged fucose analogues have been synthesised. These compounds are tagged either with cyclopropene or TCO chemical reporter groups, which can subsequently undergo IED-DA reactions with tetrazine. Despite the enhanced kinetics of cyclopropene chemical reporters, little or no contrast in COLO205, PANC-1 or MDA-MB-231 cells was observed when cells were treated with 125 μM sugar under our previous labelling conditions.

Increasing the incubation time to 48 hours and the sugar concentration to 200 μM led to SBR ratios of 1.9 ± 0.1 and 1.3 ± 0.0 for Ac_4FucCyoc and Ac_4FucEster respectively in COLO205 cells. However, previous work[92] had shown that replacing the direct labelling approach with a Tz-biotin/ NeutraAvidin

approach could reduce non-specific accumulation, and hence reduce background signal and increase SBR. Applying this labelling system to our previously optimised conditions led to an increase in SBR to 2.6 ± 0.1 and 1.7 ± 0.1 for Ac_4FucCyoc and Ac_4FucEster respectively.

A novel FucTCO synthesised by Georgia Edmonds was also tested via the Tz-biotin/NeutraAvidin labelling protocol and generated an SBR of 34.7 ± 0.5. The enhanced kinetics of the TCO are believed to be compensating for the lack on substrate promiscuity in the fucose salvage pathway.

4.3.2. Future Work

Further understanding on the incorporation of these dienophile-tagged fucose analogues is needed, in particular for how the large TCO motif is tolerated, despite the computational modelling in other examples suggesting FUT8 in particular is not tolerant towards large motifs.[218] It may be that other FUT enzymes are more substrate promiscuous, and if upregulated, they allow these large motifs to be tolerated. If this is the case, these enzymes need to be further studied and computational modelling of their crystal structures could allow for development of more Fucose MOE agents.

In vivo experiments with Ac_4FucTCO are being planned, which to the best of our knowledge would be the first example of fucose MOE *in vivo*. We believe that the well characterised over expression of fucose in nearly all cancers makes this a promising target.

Further pushing the boundaries of what substrates can be tolerated by the fucose salvage pathway could allow enhanced kinetics even beyond that of TCO. As we have previously described *E,Z*-COD shows greater IED-DA kinetics than TCO and so a FucCOD analogue could be imagined to display even greater contrast, if it were equally well tolerated, and stable in the cellular environment.

5. Experimental

5.1. General Experimental

All commercially obtained chemicals were used without further purification. NMR spectra were recorded on a 400 MHz Avance III HD Smart Probe Spectrometer. ^{1}H NMR spectra were obtained at 400 MHz and ^{13}C NMR at 100 MHz. Chemical shift values are given in ppm and coupling constants in Hz. Multiplicity is indicated as follows s (singlet); d (doublet); t (triplet); q (quartet); m (multiplet), dd (doublet of doublets); etc. Solvent was removed on a Büchi rotary evaporator.

TLC was conducted on Merck Kieselgel 60 F254. TLC plates were visualised with ceric ammonium molybdate and permanganate stains.

Flash chromatography was carried out using a CombiFlash Rf+ system with RediSep Rf columns (0.040-0.063 mm).

HRMS were recorded on a Waters Acquity UPLC system running in positive mode with an electrospray source.

Semi-prep HPLC was performed on an Agilent 1100 using a diode array detector (G1315B) set to monitor 210, 254, 280, 510 and/or 650 nm wavelengths. ChemStation Software was used to set-up methods and sequences for the runs. The instrument was used with a reverse phase Zorbax SB-C18 (250 mm x 10 mm, 5 µm; Agilent) semiprep column. Specific elution gradients are described alongside the relevant compounds.

5.2. Acetylation

ManNAz, GalNAz and GlcNAz fully acetylated and fully deacetylated were synthesised as previously described.[116]

ManNCyoc, GalNCyoc and GlcNCyoc fully acetylated and fully deacetylated were synthesised as previously described.[113]

5.2.1. General Procedure for Mono/di-acetylated Sugars

The unacetylated tagged sugars (ManNAz, GalNAz, GlcNAz, ManNCyoc, GalNCyoc and GlcNCyoc) (1 eq.) were dissolved in pyridine (0.1 M). Acetic anhydride (1 or 2 eq.) dissolved in pyridine (1 mL) was added dropwise. The reaction mixture was stirred at room temperature overnight, then concentrated *in vacuo*. The resulting residue was purified using flash chromatography eluting with 5-10% MeOH in DCM.

Mono and di-acetylated derivatives were obtained as a mixture of different degrees of acetylation. Section 2 contains spectra showing how the major degree of acetylation was assigned using ^{1}H NMR. The major level of acetylation for cyclopropene tagged sugars was determined by integration of the ^{1}H peaks for the acetyl groups (~2.1 ppm) relative to the alkene proton of the cyclopropene (~6.7 ppm) – note that the peak at ca. 2.17 ppm is the methyl group on the cyclopropene. For the azido sugars, the major level was assigned by comparison of the integral of the main anomeric signal with the acetyl peaks. The level of acetylation was also confirmed using HRMS.

Azido Tagged sugars

HRMS: (ESI+) AcManNAz: 327.0814, AcGalNAz: 327.0850, AcGlcNAz: 327.0904
($C_{10}H_{16}N_4O_7.Na^+$, requires 327.0911).
Ac_2ManNAz: 369.1017, Ac_2GalNAz: 369.1044, Ac_2GlcNAz: 369.1026
($C_{12}H_{18}N_4O_8.Na^+$, requires 369.1017).

Cyclopropene Tagged sugars

HRMS: (ESI+) AcManNCyoc: 354.1162, AcGalNCyoc: 354.1164, AcGlcNCyoc: 354.1165.
($C_{14}H_{21}NO_8.Na^+$, requires 354.1159).
Ac_2ManNCyoc: 396.1266, Ac_2GalNCyoc: 396.1270, Ac_2GlcNCyoc: 396.1267
($C_{12}H_{18}N_4O_8.Na^+$, requires 396.1265).

5.2.2. General Procedure for Triacetylated Sugars

The fully acetylated tagged sugars (Ac_4ManNAz, Ac_4GalNAz, Ac_4GlcNAz, Ac_4ManNCyoc, Ac_4GalNCyoc and Ac_4GlcNCyoc) were dissolved in THF (0.1 M) and 7M ammonia in MeOH (10 eq.) added. The reaction mixture was stirred at room temperature for 2 h and then concentrated *in vacuo*. The resulting brown residue was purified by flash chromatography eluting with 50% EtOAc in hexanes.

Azido Tagged Sugars

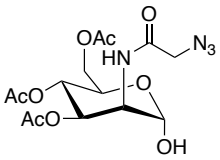

Ac_3ManNAz: (42% yield) δ_H (400 MHz, CD_3OD) 5.33 (dd, *J* = 10.0, 4.5 Hz, 1H), 5.18 (d, *J* = 10.0 Hz, 1H), 5.07-5.11 (m, 1H), 4.54 (dd, *J* = 4.5, 1.5 Hz, 1H), 4.24-4.32 (m, 2H), 4.08-4.14 (m, 2H), 3.97 (d, *J* = 4.0 Hz, 1H), 2.08 (s, 3H), 2.07 (s, 3H), 1.98 (s, 3H).

δ_C (100 MHz, CD_3OD) 171.1, 170.3, 170.3, 169.2, 93.0, 69.6, 67.7, 66.4, 62.9, 60.1, 51.1, 22.3, 19.2, 19.3.

HRMS: (ESI+) Ac_3ManNAz: 411.1120 ($C_{12}H_{18}N_4O_8$.Na+, requires 411.1122).

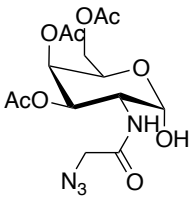

Ac_3GalNAz: (50% yield) δ_H (400 MHz, CD_3OD) 5.42-5.44 (m, 1H), 5.26 (dd, *J* = 11.3, 3.3 Hz), 5.22 (d, *J* = 3.3 Hz), 4.41-4.51 (m, 2H), 4.10-4.21 (m, 2H), 2.17 (s, 3H), 2.04 (s, 3H), 1.97 (s, 3H).

δ_C (100 MHz, CD_3OD) 170.8, 170.8, 170.6, 169.0, 91.5, 70.5, 68.4, 67.7, 65.8, 61.8, 51.3, 19.3, 19.2, 19.2.

HRMS: (ESI+) Ac_3GalNAz: 411.1125 ($C_{12}H_{18}N_4O_8$.Na+, requires 411.1122).

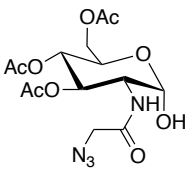

Ac_3GlcNAz: (43% yield) δ_H (400 MHz, CD_3OD) 5.33 (t, *J* = 10.2, 1H), 5.15 (d, *J* = 3.3 Hz, 1H), 5.04 (t, *J* = 10.2, 1H), 4.20-4.30 (m, 3H), 4.08-4.13 (m, 1H), 3.87 (s, 2H), 2.07 (s, 3H), 2.03 (s, 3H), 2.00 (s, 3H).

δ_C (100 MHz, CD_3OD) 171.1, 170.9, 170.0, 168.9, 91.0, 71.1, 69.0, 66.9, 65.8, 62.2, 52.3, 51.3, 19.3, 19.2, 19.2.

HRMS: (ESI+) $Ac_3GlcNAz$: 411.1140 ($C_{12}H_{18}N_4O_8$.Na+, requires 411.1122).

Cyclopropene Tagged sugars

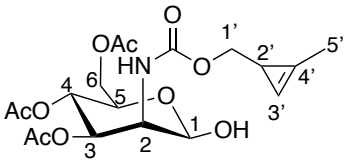

$Ac_3ManNCyoc$: The following assignments were confirmed using COSY, HSQC and HMBC spectra. Note, because the (2-methylcycloprop-2-en-1-yl)methanol used to synthesise this compound was racemic, there are two diastereoisomers differing in the stereochemistry of the chiral centre of the cyclopropene ring. The existence of two isomers was not evident for any of the mannosamine peaks but was seen for some of the (2-methylcycloprop-2-en-1-yl)methyl peaks. Where this is the case, the different isomers have been distinguished with prime (') and double-prime (").

$Ac_3ManNCyoc$: (27% yield) δ_H (400 MHz, CD_3OD) 6.67 (br s, 1H, 3'-H), 5.31 (dd, *J* = 10.2, 4.4 Hz, 1H, 3-H), 5.21 (t, *J* = 10.2 Hz, 1H, 4-H), 5.08 (br s, 1H, 1-H), 4.29 (dd, *J* = 11.8, 6.0 Hz, 1H, 6-H_A), 4.19-4.23 (m, 2H, 2 & 5-H), 4.10 (dd, *J* = 11.8, 2.5 Hz, 1H, 6-H_B), 4.01 (dd, *J* = 11.4, 4.7 Hz, 0.5H, 1'-H_A), 3.96 (dd, *J* = 11.0, 5 Hz, 0.5H, 1''-H_A) , 3.89 (dd, *J* = 11.3 & 5.2 Hz, 0.5H, 1''-H_B) , 3.83 (dd, *J* = 11.0 & 5.6 Hz, 0.5H, 1'-H_B), 2.16 (s, 3H, 5'-H), 2.08, 2.07 and 1.98 (each 3H, s, OAc), 1.67 (br t, *J* = 5.0 Hz, 1H, 2'-H).

δ_C (100 MHz, CD_3OD) 172.6, 171.9 & 171.8 (Me*C*OO), 159.4 (NHCOO), 122.1 (C-4'), 103.1 & 103.0 (C-3' & 3''), 95.1 (C-1), 73.9 (C-1') & 73.6 (C-1''), 71.5 (C-3), 69.3 (C-5), 68.1 (C-4), 64.5 (C-6), 54.2 (C-2), 20.9 & 20.8 (*Me*COO), 18.4 (C-2'), 11.70 & 11.67 (C-5' & 5'').

HRMS: (ESI+) $Ac_3ManNCyoc$: 438.1377 ($C_{18}H_{25}NO_{10}$.Na^+, requires 438.1376).

The deacetylation reaction is anomerically selective for the α-anomer as reported by Fiandor et al.[123] For $Ac_3GalNCyoc$ and $Ac_3GlcNCyoc$ this can be seen by the presence of a doublet in the ^{1}H NMR spectra with a coupling constant approximately 3 Hz (the β-anomer would have a much larger constant of around 8 Hz as the two protons are antiperiplanar to each other). In the ^{1}H NMR spectrum of $Ac_3ManNCyoc$ the anomeric proton cannot be resolved, but we assume it is also the α-anomer.

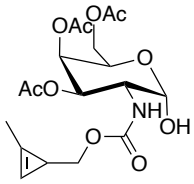

Ac_3GalNCyoc: (32% yield) δ_H (400 MHz, CD_3OD) 6.66 (s, 1H), 5.42 (d, *J* = 3.2 Hz, 1H), 5.21 (d, *J* = 3.2 Hz, 1H), 4.47 (t, *J* = 6.4 Hz, 1H), 3.76-4.22 (m, 6H), 2.18 (s, 3H), 2.16 (s, 3H), 2.03 (s, 3H), 1.97 (s, 3H).
δ_C (100 MHz, CD_3OD) 170.8, 170.8, 170.7, 157.8, 120.8, 101.4, 92.1, 72.2, 68.6, 67.8, 65.7, 61.7, 49.9, 19.3, 19.2, 19.2, 16.9, 10.2.
HRMS: (ESI+) Ac_3GalNCyoc: 438.1377 ($C_{18}H_{25}NO_{10}.Na^+$, requires 438.1376).

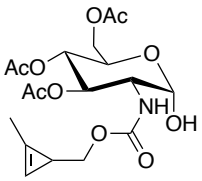

Ac_3GlcNCyoc: (22% yield) δ_H (400 MHz, CD_3OD) 6.66 (s, 1H), 5.29 (t, *J* = 10.1 Hz, 1H), 5.19 (s, 1H), 5.01 (t, *J* = 9.6 Hz, 1H), 4.22-4.29 (m, 2H), 4.06-4.15 (m, 1H) 3.82-4.03 (m, 3H), 2.14 (s, 3H), 2.07 (s, 3H), 2.03 (s, 3H), 2.00 (s, 3H), 1.63 (t, *J* = 5.3 Hz, 1H).
δ_C (100 MHz, CD_3OD) 171.1, 170.8, 170.0, 157.5, 120.6, 101.4, 91.6, 71.2 69.2, 66.9, 65.5, 62.2, 54.1, 19.4, 19.3, 19.3, 16.8, 10.8.
HRMS: (ESI+) Ac_3GlcNCyoc: 438.1375 ($C_{18}H_{25}NO_{10}.Na^+$, requires 438.1376).

5.2.3. Anomeric Protection

GlcNAz 1-NMeOMe (**2**)

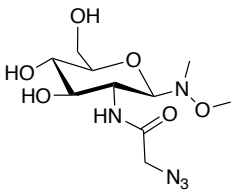

GlcNAz (100 mg, 0.38 mmol) was dissolved in water (2 mL) and cooled to 0 °C. *N,O*-dimethylhydroxylamine (41 mg, 0.42 mmol) and sodium acetate (35 mg, 0.42 mmol) dissolved in water (0.5 ml) were added dropwise. The reaction mixture was allowed to warm to room temperature, stirred overnight and then concentrated *in vacuo*. Purification by flash chromatography (eluting with 10% MeOH in DCM) to **2** (32 mg, 28%) as a white solid.

δ_H (400 MHz, CD_3OD) 4.23 (d, *J* = 9.9 Hz, 1H), 3.86-3.93 (m, 4H), 3.72 (dd, *J* = 12.1, 5.4 Hz, 1H), 3.49 (s, 3H), 3.36 (s, 1H), 3.32-3.33 (m, 1H), 3.24-3.28 (m, 1H), 2.73 (s, 3H).

δ_C (100 MHz, CD_3OD) 168.9, 91.7, 78.3, 75.7, 70.4, 61.9, 59.1, 52.7, 51.9, 36.8.

The spectroscopic data are in accordance with previous literature.[119]

Ac_3GlcNAz 1-NMeOMe (**3**)

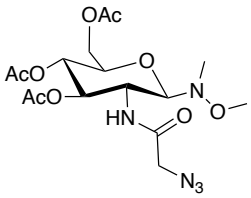

2 (32 mg, 0.11mmol) was dissolved in pyridine (1.5 mL), acetic anhydride (1 mL) added and the reaction mixture was stirred at room temperature for 2 hours. The crude reaction mixture was concentrated *in vacuo* and purified by flash chromatography (eluting with 50% EtOAc in hexanes) to give **3** (23 mg, 49%) as a clear oil.

δ_H (400 MHz, CD_3OD) 5.26 (t, *J* = 9.9 Hz, 1H), 4.98 (t, *J* = 9.7 Hz, 1H), 4.43 (d, *J* = 9.7 Hz, 1H), 4.30 (dd, *J* = 12.3, 4.9 Hz, 1H), 4.09-4.21 (m, 2H), 3.85 (d, *J* = 2 Hz, 2H), 3.73-3.77 (m, 1H), 3.45 (s, 3H), 2.71 (s, 3H), 2.07 (s, 3H), 2.03 (s, 3H), 2.00 (s, 3H).

δ_C (100 MHz, CD_3OD) 171.0, 170.6, 169.9, 168.7, 91.7, 73.9, 73.2, 68.8, 62.1, 59.2, 51.7, 50.8, 36.8, 19.3, 19.2, 19.2.

The spectroscopic data are in accordance with previous literature.[119]

Ac_3GlcNAz (**4**)

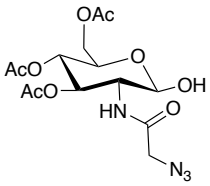

3 (23 mg, 0.05 mmol) was dissolved in THF:H_2O (9:1, 1.5 mL), *N*-chlorosuccinimide (21 mg, 0.1 mmol) was added and the reaction mixture heated to 60 °C for 3 h. The reaction mixture was concentrated in vacuo and purified by flash chromatography (eluting with 5% MeOH in DCM) to give Ac_3GalNAz (3 mg, 15%) as a clear oil.

δ_H (400 MHz, CD_3OD) 5.33 (t, *J* = 9.9 Hz, 1H), 5.15 (d, *J* = 3.5 Hz, 1H), 5.02 (t, *J* = 9.6 Hz, 1H), 4.19-4.29 (m, 3H), 4.07-4.12 (m, 1H), 3.87 (d, J = 1.1 Hz, 2H), 2.07 (s, 3H), 2.03 (s, 3H), 2.00 (s, 3H).

5.3. ODIBO

3-(*tert*-Butyldimethylsilyloxy)benzaldehyde (**8**)

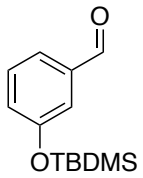

3-Hydroxybenzaldehyde (2.00 g, 16.4 mmol) was dissolved in anhydrous DCM (50 mL) and imidazole (1.34 g, 19.7 mmol) and tert-butyldimethylsilyl chloride (2.97 g, 19.7 mmol) were added. The reaction mixture was stirred at room temperature for 3 h and then concentrated *in vacuo*. Purification via flash chromatography (10% EtOAc in hexanes) gave **8** (3.75 g, 97%) as a colourless oil.

δ_H (400 MHz, $CDCl_3$) 9.98 (s, 1H), 7.50 (dt, *J* = 7.6, 1.2 Hz, 1H), 7.42 (t, *J* = 7.8 Hz, 1H), 7.35-7.45 (m, 1H), 7.11-7.14 (m, 1H), 1.02 (s, 9H), 0.25 (s, 6H).

δ_C (100 MHz, $CDCl_3$) 192.1, 156.4, 137.9, 130.1, 126.5, 123.6, 119.9, 25.6, 18.2, -4.4.

The spectroscopic data are consistent with those previously reported in the literature.[175]

(3-((*tert*-Butyldimethylsilyl)oxy)phenyl)methanol (**9**)

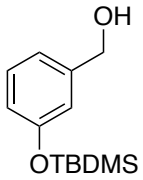

8 (3.75 g, 15.8 mmol) was dissolved in anhydrous methanol (40 mL) and cooled to 0 °C. $NaBH_4$ (658 mg, 17.4 mmol) was added portionwise and the reaction mixture allowed to warm to room temperature and stirred for 30 minutes. The crude mixture was quenched with saturated ammonium chloride (40 mL). EtOAc (80 mL) was added, and the organic layer collected. The aqueous layer was further extracted with EtOAc (2 × 60 mL) and the combined organics dried over $MgSO_4$, concentrated *in vacuo,* and purified by flash chromatography (20% EtOAc in hexanes). This afforded **9** (3.27 g, 94%) as a colourless oil.

δ_H (400 MHz, $CDCl_3$) 7.23 (t, J = 7.8 Hz, 1H), 7.68 (d, *J* = 7.6 Hz, 1H), 7.68 (s, 1H), 6.79 (dd, *J* = 8.1, 2.2 Hz, 1H), 4.66 (s, 2H), 1.01 (s, 9H), 0.23 (s, 1H).

δ_C (100 MHz, $CDCl_3$) 155.9, 142.5, 129.5, 119.8, 119.3, 118.6, 65.2, 25.7, 18.2, -4.4.

The spectroscopic data are consistent with those previously reported in the literature.[175]

tert-Butyl(3-((4-(*tert*-butyl)phenoxy)methyl)phenoxy)dimethylsilane (**10**)

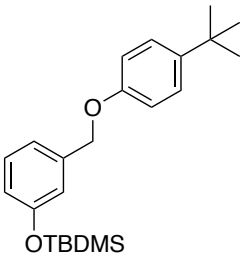

A solution of alcohol **9** (3.27 g, 14.7 mmol), 4-tert-butylphenol (2.21 g, 14.7 mmol) and triphenylphosphine (3.86 g, 14.7 mmol) in anhydrous THF (50 mL) was cooled to 0 °C. DIAD (2.88 mL, 14.7 mmol) was added dropwise. The reaction mixture was stirred for 5 min, allowed to warm to room temperature and stirred for an additional 30 min, and then concentrated *in vacuo*. Purification by flash chromatography (10% EtOAc in hexanes) gave aryl ether **10** (4.2 g, 77% yield) as a colourless oil.

δ_H (400 MHz, $CDCl_3$) 7.33 (d, *J* = 8.7 Hz, 2H), 7.25 (t, *J* = 7.8 Hz, 1H), 7.04 (d, *J* = 7.8 Hz, 1H), 6.91-6.95 (m, 3H), 6.81 (d, *J* = 8.7 Hz, 1H), 5.03 (s, 2H), 1.32 (s, 9H), 1.00 (s, 9H), 0.20 (s, 6H).

δ_C (100 MHz, $CDCl_3$) 156.5, 155.9, 143.6, 138.9, 129.5 126.2, 120.2, 119.5, 119.1, 114.3, 69. 7, 34.1, 31.5, 25.7, 18.2, 4.4.

Spectroscopic data are consistent with those previously reported in literature.[175]

3-(*tert*-Butyl)-9-((*tert*-butyldimethylsilyl)oxy)dibenzo[*b,f*]cyclopropa[*d*]oxocin-1(7*H*)-one (**11**)

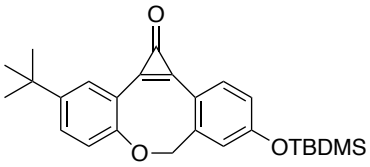

To a solution of $AlCl_3$ (358 mg, 2.69 mmol) in dry DCM (65 mL) under a nitrogen atmosphere, tetrachlorocyclopropene (0.33 mL, 2.69 mmol) in dry DCM (1 mL) was added dropwise. The reaction mixture was stirred at room temperature for 15 min before being cooled to -78 °C. Aryl ether **10** (1.00 g, 2.69 mmol) in dry DCM (2 mL) was added over 20 min and the reaction mixture was stirred at -78 °C for 3 hours, then allowed to warm to room temperature and stirred for 30 minutes. Aqueous HCl (5 %, 30 mL) was added, and the organics extracted with DCM (50 mL). The organic layer was washed with brine, dried over $MgSO_4$, and concentrated *in vacuo*. The crude product was purified by flash chromatography (2% MeOH in DCM) to give **11** (605 mg, 53%) as a yellow amorphous solid.

δ_H (400 MHz, $CDCl_3$) 7.98 (d , *J* = 2.5 Hz, 1H), 7.94 (d , *J* = 8.9 Hz, 1H), 7.54 (dd, *J* = 7.5, 2.5 Hz, 1H), 7.24 (d , *J* = 8.5 Hz, 1H), 6.99-7.01 (m, 2H), 5.28 (d , *J* = 12.2 Hz, 1H), 4.80 (d , *J* = 12.2 Hz, 1H), 1.37 (s, 9H), 1.03 (s, 9H), 0.29 (s, 6H).

δ_C (100 MHz, $CDCl_3$) 160.6, 159.8, 153.1, 148.1, 143.6, 142.0, 140.9, 135.5, 132.3, 131.2, 122.3, 122.0, 120.7, 118.0, 116.7, 78.6, 34.6, 31.3, 25.6, 18.3, -4.3.

Spectroscopic data are consistent with those previously reported in literature.[175]

Photo-ODIBO (12)

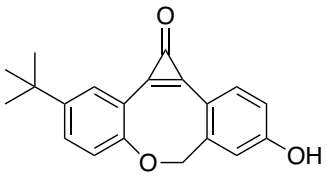

To a solution of **11** (400 mg, 0.95 mmol) in anhydrous THF (8 mL) was added TBAF (0.97 mL of a 1M solution in THF). The reaction mixture was stirred at room temperature for 30 min then quenched with saturated ammonium chloride (30 mL) and DCM (70 mL). The aqueous layer was extracted with DCM (2 × 40 mL) and the combined organic layers were dried over $MgSO_4$ and concentrated *in vacuo.* Purification by flash chromatography (5% MeOH in DCM) gave photo-ODIBO **12** (225 mg, 77%) as an off-white powder.

δ_H (400 MHz, DMSO) 10.78 (br, s, 1H), 7.75-7.59 (m, 2H), 7.62 (dd, *J* = 8.5, 2.6 Hz, 1H), 7.27 (d, *J* = 8.5 Hz, 1H), 7.09 (d, *J* = 2.4 Hz, 1H), 6.99 (dd, *J* = 8.4, 2.4 Hz, 1H), 5.30 (d, *J* = 12.2 Hz, 1H), 4.82 (d, *J* = 12.2 Hz, 1H), 1.33 (s, 9H).

δ_C (100 MHz, DMSO) 162.2, 160.4, 152.9, 148.0, 143.6, 141.7, 140.7, 135.5, 131.0, 130.7, 122.0, 117.4, 117.2, 116.8, 114.5, 78.7, 34.5, 31.9.

Spectroscopic data are consistent with those previously reported in literature.[172, 175]

3-(*tert*-Butyl)-9-(3-hydroxypropoxy)dibenzo[*b*,*f*]cyclopropa[*d*]oxocin-1(7*H*)-one (16)

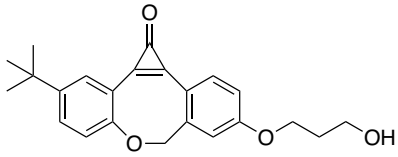

Photo-ODIBO **12** (90 mg, 0.29 mmol) was dissolved in anhydrous acetonitrile (10 mL) and potassium carbonate (80 mg, 0.58 mmol) and 3-bromopropanol (40 μL, 0.35 mmol) were added, the reaction mixture was heated under reflux for 4 h, then allowed to cool to room temperature and concentrated *in vacuo*. Purification by flash chromatography (5% MeOH in DCM) gave **16** (103 mg, 97%) as an off-white solid.

δ_H (400 MHz, $CDCl_3$) 7.95 (m, 1H), 7.88 (d, *J* = 8.1 Hz, 1H), 7.51 (d, *J* = 8.5 Hz, 1H), 7.20 (d, *J* = 8.1 Hz, 1H), 6.97-7.01 (m, 2H), 5.25 (d, *J* = 12.2 Hz, 1H), 4.74 (d, *J* = 12.2 Hz, 1H), 4.21 (t, *J* = 5.8 Hz, 1H), 3.89 (t, *J* = 5.8 Hz, 1H), (quint, *J* = 5.8 Hz, 1H), 1.36 (s, 1H).

δ_C (100 MHz, $CDCl_3$) 162.2, 160.4, 152.9, 148.0, 143.6, 141.7, 140.7, 135.5, 131.0, 130.7, 130.0, 117.4, 117.2, 168.2, 114.5, 78.7, 65.6, 59.2, 34.6, 59.2, 34.6, 31.9, 31.3.

HRMS: (ESI+) 365.1755 ($C_{23}H_{24}O_4.H^+$, requires 365.1753).

Photo-ODIBO-PNP (**17**)

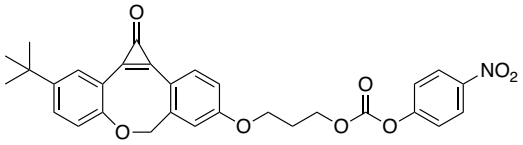

Alcohol **16** (55 mg, 0.18 mmol) was dissolved in anhydrous THF:acetonitrile 3:1 (3 mL) and anhydrous pyridine (51 μL, 0.6 mmol) and 4-nitrophenyl chloroformate (49 mg, 0.25 mmol) were added. The reaction mixture was stirred at room temperature for 2 hours. The reaction mixture was diluted with EtOAc (30 mL) and washed with water (20 mL), then brine (20 mL). The organic layer was dried over $MgSO_4$, concentrated *in vacuo*, and purified by flash chromatography (20% EtOAc in DCM). This afforded photo-ODIBO-PNP **17** (37 mg, 40%) as an off-white solid.

δ_H (400 MHz, $CDCl_3$) 8.29 (dt, *J* = 9.2, 2.2 Hz, 2H), 7.96-7.99 (m, 2H), 7.54 (dd, *J* = 8.5, 2.6 Hz, 1H), 7.40 (dt, *J* = 9.2, 2.2 Hz, 2H), 7.23 (d, *J* = 2.6 Hz, 1H), 7.05-7.08 (m, 2H), 5.28 (d, *J* = 12.2 Hz, 1H), 4.82 (d, *J* = 12.2 Hz, 1H), 4.54 (t, *J* = 6.1 Hz, 2H), 4.26 (t, *J* = 6.1 Hz, 2H), 2.33 (quint, *J* = 6.1 Hz, 2H), 1.38 (s, 9H).

δ_C (100 MHz, $CDCl_3$) 171.1, 161.7, 160.4, 155.4, 152.4, 148.1, 140.7, 135.5, 131.1, 130.7, 125.3, 121.7, 111.7, 114.4, 65.8, 64.3, 60.4, 53.4, 34.6, 31.3, 28.4, 21.0, 14.2.

HRMS: (ESI+) 637.3124 ($C_{35}H_{44}N_2O_9.H^+$, requires 637.3125).

Photo-ODIBO-Lys-Boc (**23**)

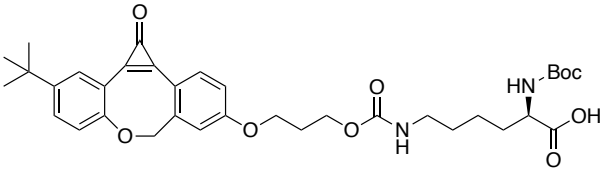

To a stirred solution of photo-ODIBO-PNP **17** (13 mg, 24.5 μM) in anhydrous DMF (1 ml) was added N^{α}-Boc-L-Lys-OH (8 mg, 29.4 μM). DIPEA (18 μL, 100 μM) was added and the reaction stirred at room temperature overnight. The reaction mixture was concentrated *in vacuo* and purified by flash chromatography (10% MeOH in DCM) to give photo-ODIBO-Lys-Boc **23** (8 mg, 51%) as a clear oil.

δ_H (400 MHz, MeOD) 8.03 (s, 1H), 7.96 (d, *J* = 8.4 Hz, 1H), 7.67 (d, *J* = 8.5 Hz, 1H), 7.28 (d, *J* = 8.5 Hz, 1H), 7.22 (s, 1H), 7.16 (d, *J* = 8.4 Hz, 1H), 5.37 (d, *J* = 12.2 Hz, 1H), 4.48 (d, *J* = 12.2 Hz, 1H), 4.22 – 4.26 (m, 4H), 4.00-4.08 (m, 1H), 3.11 (t, *J* = 6.4 Hz), 2.17 (t, *J* = 6.4 Hz), 1.75-1.85 (m, 1H), 1.60-1.70 (m, 1H), 1.47-1.56 (m, 2H), 1.44 (s, 9H), 1.40 (s, 10H) 1.26-1.34 (m, 1H)

δ_C (100 MHz, MeOD) 177.6, 167.2, 158.9, 157.6, 156.3, 149.2, 146.7, 129.4, 126.2, 125.1, 122.9, 120.9, 117.7, 117.5, 117.2, 114.1, 113.7, 109.8, 77.6, 65.5, 64.5, 61.0, 60.1, 54.4, 42.3, 40.2, 33.8, 32.6, 30.4, 28.8, 27.4.

HRMS: (ESI+) 637.3124 ($C_{35}H_{44}N_2O_9.H^+$, requires 637.3125).

Photo-ODIBO-Lys (**19**)

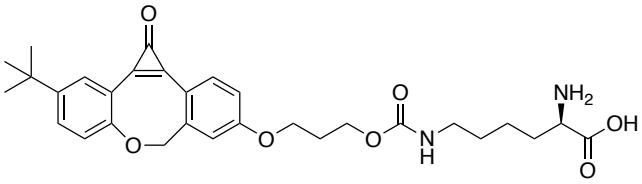

To a stirred solution of photo-ODIBO-Lys-Boc **23** (15 mg, 23.6 μM) in DCM (2 mL) was added trifluoracetic acid (0.5 mL). The reaction mixture was stirred at room temperature for 1 hour before being concentrated *in vacuo*. The crude reaction mixture was purified by HPLC (5-95% ACN in H2O (+0.1% FA)) and freeze dried to afford photo-ODIBO-Lys **19** (7 mg, 55%) as an off white solid.

δ_H (400 MHz, DMSO) 7.87 (d, *J* = 8.4 Hz, 1H), 7.79 (d, *J* = 2.5 Hz, 1H), 7.65 (dd, *J* = 8.6, 2.5 Hz, 1H), 7.35 (d, *J* = 2.4 Hz, 1H), 7.30 (d, *J* = 8.6 Hz, 1H), 7.19 (dd, *J* = 8.4, 2.4 Hz, 1H), 7.11-7.44 (m, 1H), 5.40 (d, *J* = 12.3 Hz, 1H), 4.88 (d, *J* = 12.3 Hz, 1H), 4.20 (t, *J* = 6.1 Hz, 2H), 4.11 (t, *J* = 6.1 Hz, 2H), 3.10 (t, *J* = 6.1 Hz, 1H), (q, *J* = 6.3 Hz, 2H), 1.99-2.08 (m, 2H), 1.64-1.74 (m, 1H), 1.48-1.57 (m, 1H), 1.34 (s, 9H), 1.22-1.26 (m, 2H), 0.84-0.89 (m, 1H).

δ_C (100 MHz, DMSO) 170.1, 162.2, 160.4, 156.6, 151.5, 147.8, 144.4, 142.0, 141.6, 135.3, 131.4, 130.1, 122.7, 117.8, 117.6, 117.2, 115.3, 78.4, 65.5, 60.8, 54.6, 34.7, 31.5, 31.2, 29.6, 29.4, 28.9, 22.9.

HRMS: (ESI+) 537.2607 ($C_{30}H_{36}N_2O_7.H^+$, requires 537.2601).

ODIBO-Lys (**20**)

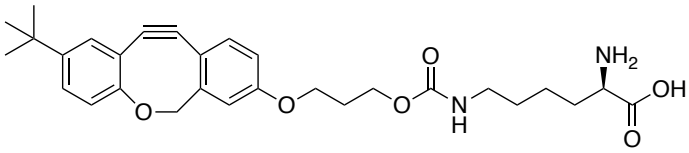

Photo-ODIBO-Lys (5 mg, 9.3 μmol) was dissolved in THF (0.5 mL) and diluted with MeOH (9.5 mL). The solution was then irritated at 350 nm in a Rayonet RMR-600 Photochemical Reactor. At ten-minute intervals the irradiation was stopped, and the solution violently shaken, for a total irradiation time of 30 minutes. The reaction mixture was concentrated *in vacuo* and used without any further purification to give ODIBO-Lys (5 mg, quantitative).

HRMS: (ESI+): (ESI+) 509.2647 ($C_{29}H_{36}N_2O_6.H^+$, requires 509.2652).

Due to the instability of the substrate and the small scale of reaction, NMR data was not attempted, and the fluorescent dye coupling carried out without purification as described in chapter 3.2.1 of the results and discussion.

5.4. *E,Z*-COD

(1*Z*,5*Z*)-3-bromocycloocta-1,5-diene (**25A**) and (1*Z*,4*Z*)-6-bromocycloocta-1,4-diene (**25B**)

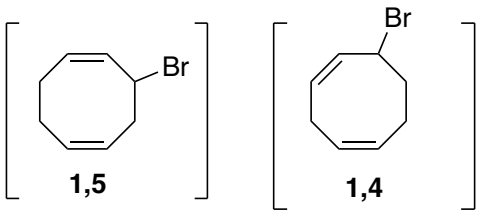

N-bromosuccinimide (4.08 g, 22.8 mmol) and benzoyl peroxide (160 mg, 0.66 mmol) were dissolved in anhydrous CCl_4 (16 mL). (*Z,Z*)-Cyclooctadiene (4.0 mL, 32.6 mmol) was added and the reaction mixture heated to reflux for 3 h, before being allowed to cool to room temperature and stirred overnight. The crude reaction mixture was filtered to remove the precipitate, washed with DCM (50 mL), and the filtrate washed with saturated sodium hydrogen carbonate (40 mL), dried over $MgSO_4$, and concentrated *in vacuo*. Due to the instability of **25A** and **25B** the crude product was carried through to the next step without further purification.

2-(((2*Z*,6*Z*)-Cycloocta-2,6-dien-1-yl)oxy)ethan-1-ol (**26**)

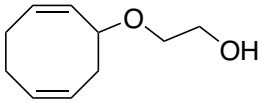

NaH, 90% (1.00 g, 48.9 mmol) was added portionwise over one hour to ethylene glycol (12 mL) cooled to 0 °C. The mixture was stirred at room temperature for 1 h, and then the crude product of the first step bromides **25A** and **25B** was added dropwise. The reaction mixture was heated at 60 °C overnight, then quenched by the addition of water (30 mL), and extracted with EtOAc (3 × 50 mL). The combined organic layers were dried over $MgSO_4$, concentrated *in vacuo*, and purified by flash chromatography (50% EtOAc in hexanes) to give alcohol **26** (1.24 g, 27% over two steps).

δ_H (400 MHz, $CDCl_3$) 5.52-5.67 (m, 4H), 4.70-4.75 (m, 1H), 3.63-3.69 (m, 1H), 3.57-3.62 (m, 1H), 2.85-2.87 (m, 1H), 2.67-2.74 (m, 1H), 2.11-2.46 (m, 6H).

δ_C (100 MHz, $CDCl_3$) 131.8, 128.9, 128.9, 126.4, 77.4, 69.9, 62.9, 35.0, 28.4, 27.8.

HRMS: (ESI+) 191.1044 ($C_{10}H_{16}O_2.Na^+$, requires 191.1048).

2-(((1*R*,3*R*,8*S*,*Z*)-9-Oxabicyclo[6.1.0]non-4-en-3-yl)oxy)ethan-1-ol (**27**)

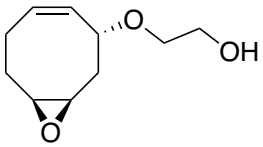

Alcohol **26** (700 mg, 3.25 mmol) was dissolved in anhydrous DCM (10 mL) and cooled to -78 °C. mCPBA (756 mg, 3.25 mmol) dissolved in anhydrous DCM (5 mL) was added dropwise. The reaction mixture was stirred at -78 °C for 30 min, then allowed to warm to room temperature and stirred for 1 h, diluted with DCM (40 mL), washed with saturated sodium hydrogen carbonate (30 mL), brine (30 mL) and concentrated in vacuo. Purification by flash chromatography (100% EtOAc) gave epoxide **27** (208 mg, 35%) as a colourless oil.

δ_H (400 MHz, $CDCl_3$) 5.62-5.68 (m, 1H), 5.48 (ddd, *J* = 12.0, 6.0, 2.5 Hz, 1H), 4.46 (quint, *J* = 4.9 Hz, 1H), 3.72-3.76 (m, 2H), 3.60-3.64 (m, 1H), 3.51-3.55 (m, 1H), 3.08-3.11 (m, 1H), 3.02-3.06 (m, 1H), 2.42-2.49 (m, 2H), 2.22-2.32 (m, 1H), 2.14-2.22 (m, 2H), 1.73-1.82 (m, 1H).

δ_C (100 MHz, $CDCl_3$) 132.8, 128.6, 73.7, 70.0, 62.0, 57.5, 54.1, 35.1, 28.7, 24.5.

HRMS: (ESI+) 185.1143 ($C_{10}H_{16}O_2.H^+$, requires 185.1172).

(2-(((1*R*,3*R*,8*S*,*Z*)-9-Oxabicyclo[6.1.0]non-4-en-3-yl)oxy)ethoxy)(*tert*-butyl)dimethylsilane (**28**)

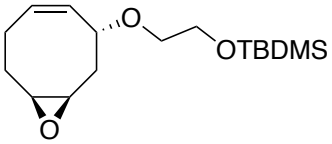

Imidazole (210 mg, 3.09 mmol) and TBDMS-Cl (374 mg, 2.48 mmol) were added to a stirred solution of **27** (228 mg, 1.24 mmol) in anhydrous THF (5 ml) at room temperature. After 2 hours the reaction was quenched with water (20 mL) and the organic layer extracted with EtOAc (3 × 30 mL). The combined organics were washed with brine, dried over $MgSO_4$, and concentrated *in vacuo*. The crude product was purified by flash chromatography (15% EtOAc in hexanes) to give protected epoxide **28** (369 mg, 99%) as a colourless oil.

δ_H (400 MHz, $CDCl_3$) 5.57-5.63 (m, 1H), 5.47 (ddd, *J* = 12.0, 6.0, 2.4 Hz, 1H), 4.44 (quint, *J* = 4.9 Hz, 1H), 3.74 (t, J = 5.4 Hz, 2H), 3.52-3.57 (m, 1H), 3.44-3.49 (m, 1H), 3.05-3.09 (m, 1H), 2.98-3.03 (m, 1H), 2.38-2.44 (m, 2H), 2.11-2.27 (m, 3H), 1.71-1.80 (m, 1H), 0.90 (s, 9H), 0.07 (s, 6H).
δ_C (100 MHz, $CDCl_3$) 133.3, 128.1, 73.7, 70.3, 62.8, 57.4, 54.3, 35.0, 28.7, 25.9, 24.5, 18.4, -5.2.
HRMS: (ESI+) 299.2034 ($C_{16}H_{30}O_3Si.H^+$, requires 299.2042).

(1*R*,3*R*,8*R*,*Z*)-3-(2-((*tert*-Butyldimethylsilyl)oxy)ethoxy)-8-((diphenylphosphaneyl)oxy)cyclooct-4-en-1-ol (**29A**) and ((1*S*,3*R*,8*S*,*Z*)-3-(2-((*tert*-butyldimethylsilyl)oxy)ethoxy)-8-hydroxycyclooct-4-en-1-yl)diphenylphosphine oxide (**29B**)

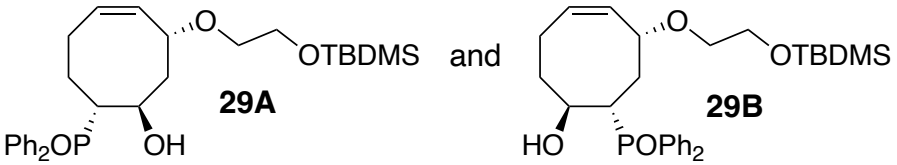

A stirred solution of diphenylphosphine (0.56 ml, 3.2 mmol) in anhydrous THF (4 mL) was cooled to -78 °C. Epoxide **28** (200 mg, 0.67 mmol) was added in THF (0.5 ml). *n*-BuLi (1.6 M in Hexanes, 2.00 ml, 3.2 mmol) was then added to the mixture dropwise. The reaction was stirred at -78 °C for 1 hour before being allowed to warm to room temperature and stirred overnight. The reaction mixture was cooled to 0 °C and diluted with THF (4 mL). Acetic acid (70 μL) and hydrogen peroxide (100 μL) were added and the quenched reaction allowed to stir at room temperature for 2 hours. Water (20 mL) was added, and the organic layer extracted with EtOAc (3 × 30 mL). The combined organics were washed with brine, dried over $MgSO_4$, and concentrated *in vacuo*. The crude product was purified by flash chromatography (5% MeOH in DCM) giving a mixture of the regioisomers containing a large amount of diphenylphosphine-derived impurity.

For experiments using the mixture of diastereoisomeric products (**29A** and **29B**) the impure product was carried through to the next step without any further purification. For kinetic comparison of (**29A** and **29B**) some of the crude product was further purified by HPLC (5-95% ACN in H_2O + 0.1% formic acid) to give regioisomers **29A** and **29B**, however the products were partially deprotected due to the acidic eluting solvent.

(1*R*,3*R*,8*R*,*Z*)-3-(2-((*tert*-butyldimethylsilyl)oxy)ethoxy)-8-((diphenylphosphaneyl)oxy)cyclooct-4-en-1-ol (**29A**)

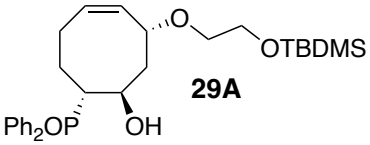

δ_H (400 MHz, $CDCl_3$) 7.74-7.80 (m, 4H), 7.45-7.55 (m, 6H), 5.66-5.75 (m, 1H) 5.58-5.60 (dd, *J* = 11.2, 5.9 Hz, 1H), 4.17-4.21 (m, 1H), 4.02-4.09 (m, 1H), 3.59-3.64 (m, 2H), 3.32-3.38 (m, 1H), 3.17-3.23 (m, 1H), 2.83-2.92 (m, 1H), 2.28-2.38 (m, 1H), 2.17-2.24 (m, 1H), 1.94-2.10 (m, 2H), 1.70-1.82 (m, 2H), 0.87 (s, 9H), 0.00 (s, 3H), -0.02 (s, 3H) - Due to the partial silyl deprotection (discussed in section 3.3.2) the *tert*-butyl and methyl groups integrate out to 7H and 2H respectively.

δ_C (100 MHz, $CDCl_3$) 133.6, 131.8 (d, *J* = 2.2 Hz), 131.6 (d, *J* = 2.2 Hz), 131.5 (d, *J* = 9.1 Hz), 130.7 (d, *J* = 9.0 Hz), 129.1, 128.7 (d, *J* = 3.4 Hz), 128.6 (d, *J* = 3.7 Hz), 78.3 (d, *J* = 19.3 Hz), 72.7 (d, *J* = 5.6 Hz), 69.6, 61.8, 42.2 (d, *J* = 71.0 Hz), 37.2 (d, *J* = 6.2 Hz), 33.5, 29.7, 23.6.

((1*S*,3*R*,8*S*,*Z*)-3-(2-((*tert*-butyldimethylsilyl)oxy)ethoxy)-8-hydroxycyclooct-4-en-1-yl)diphenylphosphine oxide (**29B**)

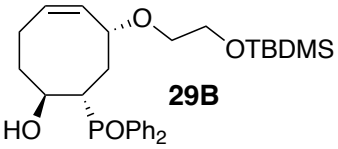

δ_H (400 MHz, $CDCl_3$) 7.77-7.81 (m, 2H), 7.70-7.75 (m, 2H), 7.47-7.55 (m, 6H), 5.73-5.81 (m, 1H), 5.68-5.71 (m, 1H), 4.44-4.48 (m, 1H), 4.19-4.24 (m, 1H), 3.76-3.80 (m, 2H), 3.57-3.65 (m, 1H), 3.50-3.53 (m, 1H), 2.90-2.96 (m, 1H), 2.34-2.40 (m, 1H), 2.10-2.20 (m, 2H), 2.00-2.09 (m, 1H), 1.57-1.74 (m, 2H), 0.94 (s, 9H), 0.11 (s, 3H), 0.10 (s, 3H). – - Due to the partial silyl deprotection (discussed in section 3.3.2) the *tert*-butyl and methyl groups integrate out to 7H and 2H respectively.

δ_C (100 MHz, $CDCl_3$) 144.8, 134.1, 131.6, 131.5 (d, *J* = 8.9 Hz), 130.5 (d, *J* = 9.2 Hz), 129.4, 128.7 (d, *J* = 7.7 Hz), 128.6 (d, *J* = 7.5 Hz), 73.2, 71.1 (d, *J* = 6.0 Hz), 70.1, 63.0, 45.0 (d, *J* = 70.4 Hz), 42.9, (d, *J* = 7.0 Hz), 27.0 (d, *J* = 16.6 Hz), 26.4, 26.0, 18.5, -5.1.

HRMS: (ESI+) 501.2586 ($C_{28}H_{41}O_4PSi.H^+$, requires 501.2590).

2-(((*R*,2*Z*,6*E*)-Cycloocta-2,6-dien-1-yl)oxy)ethan-1-ol (30A) and 2-(((*R*,2*Z*,6*E*)-Cycloocta-2,6-dien-1-yl)oxy)ethan-1-ol (30B)

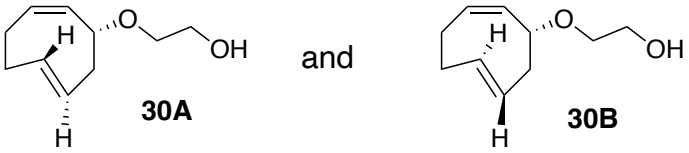

Regioisomer **29A** or **29B** (14 mg, 0.03 mmol) was dissolved in anhydrous THF (1 mL) and NaH 90% (1 mg, 0.09 mmol) was added. The reaction was stirred at room temperature for 1 hour before being cooled to 0 °C, diluted with THF (3 mL) and TBAF (1 M in THF, 0.1 mL, 0.1 mmol). The reaction was stirred at room temperature for 1 hour, concentrated *in vacuo* and purified by flash chromatography (50 % EtOAc in hexanes) to give the *E,Z*-COD product.

2-(((*R*,2*Z*,6*E*)-Cycloocta-2,6-dien-1-yl)oxy)ethan-1-ol (30B)

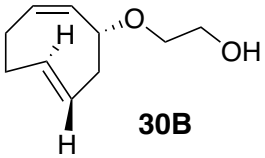

(50% yield) δ_H (400 MHz, $CDCl_3$) 6.01-6.10 (m, 1H), 5.66-5.72 (m, 1H), 5.44-5.51 (m, 2H), 4.03 (m, 1H), 3.74-3.76 (m, 2H), 3.61-3.66 (m, 1H), 3.51-3.56 (m, 1H), 2.67-2.73 (m, 1H), 2.18-2.26 (m, 4H), 1.94-2.00 (m, 2H).

HRMS: 169.1221 ($C_{10}H_{16}O_2.H^+$, requires 169.1229).

2-(((*R*,2*Z*,6*E*)-Cycloocta-2,6-dien-1-yl)oxy)ethan-1-ol (30A)

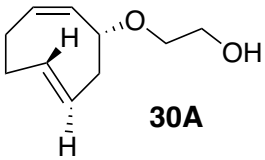

30A was not successfully collected. The products are unstable and degrade even in dark at -20 °C.

2-(((*R*,2*Z*,6*E*)-cycloocta-2,6-dien-1-yl)oxy)ethyl (4-nitrophenyl) carbonate (31)

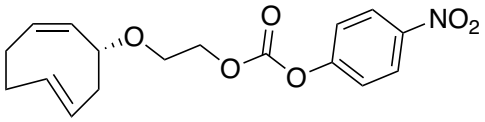

E,Z-COD (31 mg, 0.19 mmol) as a 1:1 mixture of diastereoisomers (**30A** and **30B**) was dissolved in anhydrous DCM (2 mL). Anhydrous pyridine (86 μL, 1.00 mmol) was added followed by 4-nitrophenylchloroformate (45 mg, 0.23 mmol). The reaction was stirred at room temperature for 1 hour, until complete by LCMS. The reaction mixture was diluted with DCM (10 mL) and the organic layer washed with brine (2 x 5 mL). The organic layer was dried over $MgSO_4$, concentrated *in vacuo,* and purified by flash chromatography (20 % EtOAc in hexanes) to give **31** (16 mg, 25%) as a yellow oil.

δ_H (400 MHz, $CDCl_3$) 8.30 (d, *J* = 8.8 Hz, 2H), 7.40 (d, *J* = 8.8 Hz, 2H), 5.64-5.67 (m, 1H) 5.40-5.65 (m, 2H), 4.41-4.48 (m, 2H), 4.02-4.08 (m, 1H), 3.65-3.86 (m, 2H), 2.62-2.73 (m, 1H), 2.45-2.53 (m, 1H), 2.19-2.30 (m, 3H), 1.94-2.00 (m, 1H), 1.85 (t, *J* = 7.9 Hz, 1H).

^{13}C NMR was not collected due to small scale and expected instability of the product, particularly in $CDCl_3$.

5.5. Fucose

1,2:3,4-Di-*O*-isopropylidene-α-L-galactopyranose (**33**)

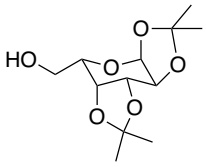

L-Galactose (250 mg, 1.4 mmol) and anhydrous copper(II) sulfate (555 mg, 3.5 mmol) were suspended in anhydrous acetone (7.5 mL) and stirred vigorously. Concentrated H_2SO_4 (0.2 mL) was added dropwise, and the reaction stirred overnight. The reaction was filtered to remove the precipitate and the filtrate neutralised with $CaCO_3$. The resulting crude product was concentrated *in vacuo* and purified by flash chromatography (50% EtOAc in hexanes) to give **33** (375 mg, quantitative).

δ_H (400 MHz, $CDCl_3$) 5.57 (d, *J* = 5.0 Hz, 1H), 4.61 (d, *J* = 7.9 Hz, 1H), 4.33 (d, *J* = 5.0 Hz, 1H), 4.27 (d, *J* = 7.9 Hz, 1H), 3.82-3.90 (m, 2H), 3.71-3.76 (m, 1H), 1.53 (s, 3H), 1.46 (s, 3H), 1.34 (s, 6H).
δ_C (100 MHz, $CDCl_3$) 109.4, 108.6, 96.3, 71.6, 70.8, 70.6, 68.1, 62.2, 26.0, 25.9, 24.9, 24.3.
Spectroscopic data are consistent with those previously reported in literature.[226]

1,2:3,4-Di-*O*-isopropylidene-6-*O*-benzyl-L-galactopyranoside (**37**)

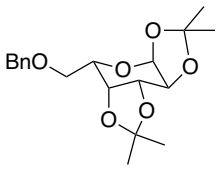

Alcohol **33** (100 mg, 0.38 mmol) was dissolved in anhydrous DMF (8 mL) and cooled to 0 °C. NaH (90%, 20 mg, 0.80 mmol) was added and the reaction allowed to warm to room temperature and stirred for 30 min. The reaction was re-cooled to 0 °C, benzyl bromide (80 μL, 0.57 mmol) added dropwise, allowed to warm to room temperature and stirred overnight. The reaction was cooled to 0 °C, and quenched with water, and diluted with EtOAc (25 mL). The organic layer was washed with 1M HCl (10 mL), saturated aqueous sodium thiosulphate (10 mL) and brine (10 mL). The organics were dried over $MgSO_4$, concentrated *in vacuo,* and purified by flash chromatography (20% EtOAc in hexanes) to give **37** (75 mg, 55%) as a clear oil.

δ_H (400 MHz, $CDCl_3$) 7.28-7.38 (m, 5H), 5.57 (d, *J* = 5.2 Hz, 1H), 4.56-4.66 (m, 3H), 4.29-4.34 (m, 2H), 4.03 (t, *J* = 6.1 Hz, 1H), 3.71-3.75 (m, 1H), 3,64-3.68 (m, 1H), 1.57 (s, 3H), 1.47 (s, 3H), 1.36 (s, 6H).
δ_C (100 MHz, $CDCl_3$) 138.4, 128.3, 127.8, 127.6, 109.2, 108.6, 96.4, 73.3, 71.2, 70.7, 70.6, 68.9, 66.9, 26.1, 26.0, 25.0, 24.5.

1,2,3,4-Tetra-*O*-acetyl- 6-*O*-benzyl-α-L-galactopyranoside (38)

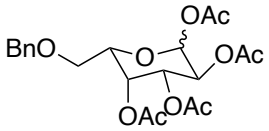

37 (244 mg, 0.7 mmol) was dissolved in DCM (2 mL), cooled to 0 °C and 75% aq. TFA (5 mL) was added. The reaction mixture was stirred at room temperature for 1 h, then concentrated *in vacuo* and redissolved in pyridine (3 mL). Acetic anhydride (3 mL) and DMAP (5 mg, 0.04 mmol) were added. The reaction mixture was stirred at room temperature for 2 hours, then concentrated *in vacuo*, resuspended in EtOAc (30 mL), washed with 1M HCl (15 mL), saturated sodium hydrogen carbonate (15 mL) and brine (15 mL), and concentrated *in vacuo*. Purification by flash chromatography (50% EtOAc in hexanes) gave 38 (159 mg, 52%) as a mixture of anomers (α:β, 0.4:0.6 measured via comparison of the anomeric proton integrations).

δ_H (400 MHz, $CDCl_3$) 7.30-7.38 (m, 10H) 6.38 (d, *J* = 2.8 Hz, 1H, α), 5.72 (d, *J* = 8.3 Hz, 1H, β), 5.59 (m, 1H, α) 5.53 (d, *J* = 3.2 Hz, 1H, β), 5.30-5.37 (m, 2H, α) 5.10 (dd, *J* = 10.5 and 3.2, 1H, β), 5.10 (dd, *J* = 12.1 and 4.5, 1H, β), 4.41-4.58 (m, 4H, α and β), 4.31 (t, *J* = 6.4 Hz, 1H, α), 4.01 (t, *J* = 6.3 Hz, 1H, β), 3.43-3.70 (m, 4H, α and β), 2.01-2.17 (m, 24H, α and β)

δ_C (100 MHz, $CDCl_3$) 170.0, 170.0, 169.9, 169.9, 169.4, 169.0, 168.9, 137.4, 137.4, 128.0, 127.9, 128.9, 92.3, 89.3, 73.6, 73.5, 72.8, 71.0, 70.1, 68.1, 67.9, 67.7, 67.3, 67.2, 66.8, 66.7, 21.0, 20.9, 20.8, 20.6, 20.6, 20.5, 14.2, 14.1.

Spectroscopic data are consistent with those previously reported in literature.[227]

1,2,3,6-tetra-O-acetyl-L-galactopyranose (39)

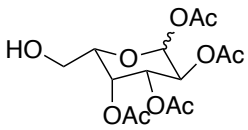

38 (159 mg, 0.36 mmol) was dissolved in a 1:1 mixture of EtOAc:MeOH (5 ml) and Pd/C (20 mg) added. The reaction was degassed and placed under a nitrogen atmosphere, and this process repeated twice. The reaction was then further degassed, and the atmosphere replaced with hydrogen. The reaction mixture was vigorously stirred for 1 h, before being filtered through Celite, washing with EtOAc. The filtrate was concentrated *in vacuo* to give alcohol **39** (80 mg, 77%) as a mixture of anomers (α:β, 0.4:0.6) without the need for further purification.

δ_H (400 MHz, $CDCl_3$) 6.31-6.37 (m, 1H, α), 5.71 (d, *J* = 8.3 Hz, 1H, β), 5.59 (s, 1H, α), 5.43 (d, *J* = 2.8 Hz, 1H, β), 5.31-5.38 (m, 2H, α and β), 5.11 (dd, *J* = 10.6 and 3.5 Hz, 1H, β), 4.18 (t, *J* = 6.4 Hz, 1H, α), 3.90

(t, *J* = 6.2 Hz, 1H, β), 3.65-3.81 (m, 2H, α and β), 3.45-3.56 (m, 2H, α and β) 2.01-2.17 (m, 24H, α and β).

δ_C (100 MHz, $CDCl_3$) 170.9, 170.8, 170.4, 170.1, 169.9, 169.5, 169.2, 169.1, 92.3, 89.7, 74.5, 71.6, 70.9, 68.3, 68.2, 67.5, 67.5, 66.7, 60.7, 60.4, 21.0, 20.9, 20.8, 20.6, 20.6, 20.5, 20.5, 14.2, 14.1

Spectroscopic data are consistent with those previously reported in literature.[228]

Ac_4FucCyoc

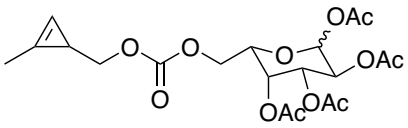

Alcohol **39** (50 mg, 0.14 mmol) was dissolved in anhydrous DMF (2 mL) and DMAP (20 mg, 0.08 mmol) and anhydrous DIPEA (0.10 mL, 0.57 mmol) were added, and the mixture stirred at room temperature for 10 min. (2-Methylcycloprop-2-enyl)methyl (4-nitrophenyl) carbonate dissolved in anhydrous DMF (0.5 mL) was added dropwise and the reaction stirred at room temperature overnight. The reaction mixture was concentrated *in vacuo*, redissolved in EtOAc (20 mL) and washed with 1M HCl (10 mL), saturated sodium hydrogen carbonate (10 mL) and brine (10 mL). The organic layer was dried over $MgSO_4$, concentrated *in vacuo,* and purified by flash chromatography (40 %EtOAc in hexanes) to give Ac_4FucCyoc (29 mg, 45%) as a clear oil. Mixture of anomers (α:β, 0.4:0.6)

δ_H (400 MHz, $CDCl_3$) 6.57 (s, 1H) 6.40 (s, 1H, α), 5.73 (d, *J* = 8.3 Hz, 1H, β), 5.53 (s, 1H, α), 5.46 (d, *J* = 2.7 Hz 1H, β), 5.34-5.37 (m, 2H, α and β), 5.10 (dd, *J* = 10.3 and 3.2, 1H, β), 4.40 (t, *J* = 6.1 Hz, 1H, α), 4.19-4.23 (m, 2H), 4.17 (t, *J* = 5.7 Hz, 1H, β), 3.94-4.10 (m, 4H), 2.00-2.18 (m, 15H), 1.69 (t, *J* = 4.9 Hz, 1H, α).

δ_C (400 MHz, $CDCl_3$) 170.1, 170.0, 169.9, 169.9, 169.4, 168.9, 168.7, 154.9, 154.8, 120.3, 101.8, 101.8, 92.1, 89.7, 71.7, 70.8, 68.9, 67.8, 67.6, 67.3, 66.9, 66.4, 64.6, 64.2, 20.9, 20.8, 20.6, 20.5, 16.7, 16.6, 11.6.

HRMS: (ESI+) 481.1324 ($C_{20}H_{26}O_{12}.Na^+$, requires 481.1322).

Ac_4FucEster

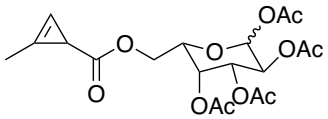

Alcohol **39** (25 mg, 0.07 mmol) was dissolved in anhydrous DMF (1 mL), DMAP (10 mg, 0.04 mmol) and anhydrous DIPEA (0.05 mL, 0.29 mmol) were added, and the reaction stirred at room temperature for 10 min. **41** (synthesised according to a literature protocol,[75] 21 mg, 0.08 mmol) dissolved in anhydrous DMF (1 mL) was added dropwise and the reaction stirred at room temperature overnight. The reaction mixture was concentrated *in vacuo* and purified by flash chromatography (40 % EtOAc in hexanes) to give Ac_4FucEster (12 mg, 43%) as a clear oil.

δ_H (400 MHz, $CDCl_3$) 6.40 (s, 1H, α), 6.32 (s, 1H), 5.72 (d, *J* = 8.2 Hz, 1H, β), 5.49-5.52 (m, 1H, α), 5.42-5.46 (m, 1H, β), 5.32-5.36 (m, 2H, α and β), 5.10 (d, *J* = 10.6 Hz,1H, β), 4.37 (t, *J* = 6.5 Hz, 1H, α), 4.15-4.25 (m, 2H), 4.07 (t, *J* = 5.9 Hz, 1H, β), 2.00-2.18 (m, 15H), 1.62 (s, 1H).

δ_C (400 MHz, $CDCl_3$) 171.2, 170.2, 170.2, 170.1, 170.1, 170.1, 170.0, 170.0, 169.9, 169.4, 169.0, 169.0, 94.4, 94.3, 92.2, 87.6, 7.18, 71.7, 70.9, 68.8, 68.7, 67.9, 67.5, 67.3, 67.3, 66.7, 66.5, 66.5, 31.6, 22.7, 21.0, 20.9, 20.8, 20.6, 19.8, 19.8, 14.2, 14.1, 10.4, 10.3.

HRMS: (ESI+) 451.1212 ($C_{19}H_{24}O_{11}.Na^+$, requires 451.1216).

5.6. Synthesis of Probes

Tetrazine-PEG$_{11}$-AlexaFluor647/AlexaFluor488[128] and TMDIBO-Lys-AlexaFluor647[102] were synthesised as previously described.

Tetrazine-PEG$_{11}$-biotin (**46**)

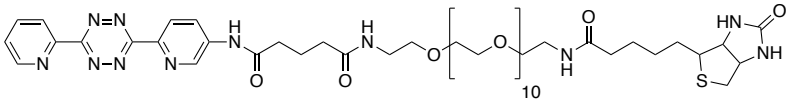

Tetrazine-PEG$_{11}$-NHBoc **45** (11 mg, 11 μM) was dissolved in DCM (1.5 mL) TFA (0.4 mL) added, and the reaction stirred at room temperature for 1 hour. The reaction mixture was concentrated *in vacuo* and resuspended in anhydrous DMF (0.5 mL). Anhydrous DIPEA (10 μL, 30 μM) was added followed by biotin-NHS ester (4.5 mg, 30 μM) and the reaction stirred at room temperature overnight. The reaction mixture was concentrated in vacuo and purified by HPLC (5-95% ACN in H_2O (+0.1% FA)) and freeze dried to afford Tz-PEG$_{11}$-biotin as a pink oil (5 mg, 42 %).

δ_H (400 MHz, $CDCl_3$) 9.92 (s, br, 1H), 9.05 (d, *J* = 2.3 Hz, 1H), 9.00 (d, *J* = 4.6 Hz, 1H), 8.72-8.76 (m, 2H), 8.66 (dd, *J* = 8.7, 2.3 Hz, 1H), 8.02 (td, *J* = 8.0, 1.6 Hz, 1H), 7.59-7.61 (m, 1H), 6.90 (t, *J* = 5.2 Hz, 1H), 6.68 (t, *J* = 5.2 Hz, 1H), 5.81 (s, br, 1H), 5.22 (s, br, 1H), 4.53-4.57 (m, 1H), 4.35-4.38 (m, 1H), 3.56-3.69 (m, 48H), 3.43-3.50 (m, 4H), 3.16-3.20 (m, 1H), 2.94 (dd, *J* = 12.7, 4.9 Hz, 1H), 2.78 (d, *J* = 12.7, 1H), 2.60 (t, *J* = 8.0, 1.6 Hz, 2H), 2.39 (t, *J* = 8.0, 1.6 Hz, 2H), 2.24 (td, *J* = 7.3, 2.4 Hz, 2H), 2.11 (quint, *J* = 6.9, 2H) 1.67-1.73 (m, 2H), 1.44-1.51 (m, 2H)

HRMS: (ESI+) 1118.5553 ($C_{51}H_{81}N_{11}O_{15}S.-H^+$, requires 1118.5556).

5.7. Biological Procedures

General experimental for biological conditions

The culture conditions for the various cell lines were as follows. All cells were incubated at 37 °C under 5% CO_2. The culture media used for COLO205 and Jurkat cells was RPMI 1640 21875-034, Dulbecco's Modified Eagle's Medium (DMEM), 41966-029 was used for MDA-MB-231, PANC-1 and HEK293 cells. All media was supplemented with 10% foetal bovine serum. A Vi-CELL™ Cell Viability Analyzer as used to access cell viability and determine cell seeding density. Cells were passaged before reaching confluency. A BD FACSymphony™ A5 Cell Analyzer was used for all flow cytometry experiments. 10,000 events were collected for each sample, and data analysis was performed using FlowJo flow cytometry analysis software (Tree Star, Ashland, OR). PBS (phosphate buffered saline; water, NaCl, KCl, Na_2HPO_4, KH_2PO_4; Fisher Scientific, Loughborough, UK).

General procedure for single sugar cell surface glycan labelling and detection by flow cytometry

In Costar® clear TC-treated 6-well plates, cells were seeded at a density of 2.5 x 10^5 cells per well, in 2 ml of media. After 24 h the cells were pulsed with the sugar (stock solution 110 mM in DMSO) to make a final sugar concentration of 125 µM or left unpulsed. After 24 h the contents of each well was transferred to a centrifuge tube and the wells were washed with PBS. Each well was then incubated with 0.5 mL Trypsin EDTA (0.25%) for 3 minutes, quenched by addition of fresh media and transferred to the corresponding centrifuge tube. Each tube was centrifuged (1000 g, 4 °C, 3 min) and the supernatant removed. The pellet was resuspended in 1 mL ice cold FACS buffer (1% FBS in PBS) and transferred to 1.5 mL Eppendorf tubes. Cells were centrifuged and resuspended in 100 µL labelling buffer (5 µM Tz-PEG_{11}-Alexa647 or 50 µM TMDIBO-Lys-Alexa647 + 50 nM Sytox green cell death stain). The Eppendorf tubes were incubated in a hot block with orbital shaking (450 rpm, 37 °C, 1 h). The cells were washed three times with 700 µL ice-cold FACS buffer, filtered through a 50 µm cut-off membrane into flow cytometry tubes, and kept on ice. Each sample was analysed by flow cytometry. The viable cell population (population of interest) was determined by gating cells to exclude those with high levels of SYTOX Green (cell death marker). The far-red median fluorescence intensity (MFI, Alexa Fluor 647 fluorophore) of the viable cell population was then assessed. Data points were collected in triplicate.

General procedure for single sugar cell surface glycan labelling with detection by flow cytometry using Tz-PEG$_{11}$-biotin and neutravidin (for fucose analogues)

The protocol was carried out as above other than the cells were pulsed with the sugar (stock solution 110 mM in DMSO) to make a final sugar concentration of 125 or 200 µM or left unpulsed. Cells were then incubated for a further 24 or 48 hours as described. They were then treated as above until the cells were resuspended in 100 µL labelling buffer (100 µM Tz-PEG$_{11}$-biotin + 50 nM Sytox green cell death stain). The Eppendorf tubes were incubated in a hot block with orbital shaking (450 rpm, 37 °C, 1 h). The cells were washed three times with 700 µL ice-cold FACS buffer and resuspended in 100 µL neutravidin labelling buffer (50 µg/mL NeutrAvidin-Dylight660 in FACS buffer, Invitrogen) or 100 µl FACS buffer as a control. Cells were again then treated as above.

General procedure for dual sugar cell surface glycan labelling and detection by flow cytometry

The protocol was carried out as above other than the cells were seeded at a density of 5 x 10^5 cells per well, in 2 ml of media. They were treated as above until being resuspended in 100 µL labelling buffer (5 µM Tz-PEG$_{11}$-AlexaFluor488 and 50 µM TMDIBO-Lys-AlexaFluor647). The Eppendorf tubes were incubated in a hot block with orbital shaking (450 rpm, 37 °C, 1 h). The cells were again treated as above other than, as no Sytox stain was used (due to crossover with the 488 probe), the cells were instead gated FSC vs SSC to select single cells.

General procedure for cell viability and growth analysis in sugar treated cells

In Costar® clear TC-treated 6-well plates, cells were seeded at a density of 5 x 10^5 cells per well, in 2 ml of media. After 24 h the cells were pulsed with the appropriate sugar(s) at the stated concentration or pulsed with the same volume of DMSO. After 24 h the contents of each well was transferred to a centrifuge tube and the wells were washed with PBS. Each well was then incubated with 0.5 mL Trypsin EDTA (0.25%) for 3 minutes, quenched by addition of fresh media and transferred to the corresponding centrifuge tube. Each tube was centrifuged (1000 g, 4 °C, 3 min) and the supernatant removed. and resuspended in 2 mL fresh medium. Cell suspensions were then analysed by a Vi-CELL™ XR Cell Viability Analyzer, Cell viability and number were determined.

General procedure for Fluorescent Microscopy

Cells were seeded into an Ibidi µ-Slide 8-well plate at 1×10^5 cells ml^{-1} and allowed to adhere to the plate surface for 24 h. After adhesion, cells were pulsed with either sugar (125 µM) (+), or unpulsed (-) and left for 24 h. Cells were then washed 3 times in ice cold FACS buffer and incubated (60 min, 37 °C) in situ in 150 µL of FACS buffer containing 5 µM Tz-PEG_{11}-AlexaFluor647 or 50 µM TMDIBO-Lys-AlexaFluor647. After being washed, as above, cells were fixed in PBS containing 4% formalin (15 min, 37 °C), washed again as above, then stained with 150 µL of 300 nM DAPI (15 min, 37 °C), then washed as above, 300 µL PBS added and analysed by microscopy. Slides were scanned on a high content imaging Operetta CLS (Perkin Elmer) in confocal mode using a sCMOS camera and a 40x water immersion objective. Images were taken in three channels, DAPI, AlexaFluor647 and brightfield and in 3D with z stacks at intervals of 0.5 µm. LED power and exposure times remained the same between experimental and control conditions within each experiment. Images were processed and exported from Harmony software (Perkin Elmer) then Fiji (ImageJ) software was used to create the plot profile of Alexa Fluor 647 intensity distribution across the cells.

6. References

1. M. E. Taylor and K. Drickamer, *Introduction to Glycobiology*, Oxford University Press, Oxford, 3rd edn., 2011.
2. K. W. Moremen, M. Tiemeyer and A. V. Nairn, *Nat. Rev. Mol. Cell Biol.*, 2012, **13**, 448-462.
3. R. D. Cummings, *Mol. Biosyst.*, 2009, **5**, 1087-1104.
4. M. M. Fuster and J. D. Esko, *Nat. Rev. Cancer.*, 2005, **5**, 526-542.
5. H. H. Freeze and A. D. Elbein, *Essentials of Glycobiology. 2nd edition*, 2009.
6. W. K. Chou, S. Hinderlich, W. Reutter and M. E. Tanner, *J. Am. Chem. Soc.,* 2003, **125**, 2455-2461.
7. C. M. West and G. W. Hart, *Essentials of Glycobiology [Internet]. 3rd edition*, 2017.
8. H. J. An, J. W. Froehlich and C. B. Lebrilla, *Curr. Opin. Chem. Biol.*, 2009, **13**, 421-426.
9. A. Varki, *Cold Spring Harb. Perspect. Biol.*, 2011, **3**, 1-14.
10. G. W. Hart and R. J. Copeland, *Cell*, 2010, **143**, 672-676.
11. D. H. Dube and C. R. Bertozzi, *Nat. Rev. Drug Discovery*, 2005, **4**, 477-488.
12. L. L. Lairson, B. Henrissat, G. J. Davies and S. G. Withers, *Annu. Rev. Biochem.*, 2008, **77**, 521-555.
13. C. Reily, T. J. Stewart, M. B. Renfrow and J. Novak, *Nat. Rev. Nephrology*, 2019, **15**, 346-366.
14. D. Thomas, A. K. Rathinavel and P. Radhakrishnan, *Biochim. Biophys. Acta - Rev. Cancer,* 2021, **1875**, 188464.
15. S. S. Pinho and C. A. Reis, *Nat. Rev. Cancer.*, 2015, **15**, 540-555.
16. A. Magalhães, H. O. Duarte and C. A. Reis, *Cancer Cell,* 2017, **31**, 733-735.
17. S. S. Pinho, J. Figueiredo, J. Cabral, S. Carvalho, J. Dourado, A. Magalhães, F. Gärtner, A. M. Mendonça, T. Isaji, J. Gu, F. Carneiro, R. Seruca, N. Taniguchi and C. A. Reis, *Biochim. Biophys. Acta. Gen. Subj.*, 2013, 1830, 2690-2700.
18. G. Berx, K. F. Becker, H. Höfler and F. Van Roy, *Hum. Mutat.*, 1998, **12**, 226-237.
19. C. Slawson and G. W. Hart, *Nature Rev. Cancer.*, 2011, **11**, 678-684.
20. Z. Ma and K. Vosseller, *Amino Acids*, 2013, **45**, 719-733.
21. Z. Ma and K. Vosseller, *J. Biol. Chem.*, 2014, **289**, 34457-34465.
22. O. Warburg, *Science (New York, N.Y.)*, 1956, **123**, 309-314.
23. M. G. Vander Heiden, L. C. Cantley and C. B. Thompson, *Science (New York, N.Y.)*, 2009, **324**, 1029-1033.
24. Y. Fardini, V. Dehennaut, T. Lefebvre and T. Issad, *Front. Endocrinol. (Lausanne)*, 2013, **4**, 99-99.
25. I. Brockhausen, H. Schachter and P. Stanley, *Essentials of Glycobiology. 2nd edition*, 2009.
26. M. R. Kudelka, T. Ju, J. Heimburg-Molinaro and R. D. Cummings, *Adv. Cancer Res.*, 2015, **126**, 53-135.
27. D. W. Kufe, *Nat. Rev. Cancer*, 2009, **9**, 874-885.
28. C. Anish, B. Schumann, Claney L. Pereira and Peter H. Seeberger, *Chem. Biol.*, 2014, **21**, 38-50.
29. A. Takada, K. Ohmori, T. Yoneda, K. Tsuyuoka, A. Hasegawa, M. Kiso and R. Kannagi, *Cancer Res.*, 1993, **53**, 354-361.
30. M. Ugorski and A. Laskowska, *Acta Biochim. Pol.*, 2002, **49**, 303-311.
31. S. R. Stowell, T. Ju and R. D. Cummings, *Annu. Rev. Pathol.: Mech. Dis.*, 2015, **10**, 473-510.
32. R. Amon, E. M. Reuven, S. Leviatan Ben-Arye and V. Padler-Karavani, *Carbohydr. Res.*, 2014, **389**, 115-122.
33. C. Büll, M. A. Stoel, M. H. Den Brok and G. J. Adema, *Cancer Res.*, 2014, **74**, 3199-3204.
34. C. Büll, T. J. Boltje, N. Balneger, S. M. Weischer, M. Wassink, J. J. van Gemst, V. R. Bloemendal, L. Boon, J. van der Vlag, T. Heise, M. H. den Brok and G. J. Adema, *Cancer Res.*, 2018, **78**, 3574.
35. A. F. Swindall and S. L. Bellis, *J. Biol. Chem.*, 2011, **286**, 22982-22990.

36. M. J. Schultz, A. F. Swindall, J. W. Wright, E. S. Sztul, C. N. Landen and S. L. Bellis, *J. Ovarian Res.*, 2013, **6**, 25.
37. E. Rodrigues and M. S. Macauley, *Cancers (Basel)*, 2018, **10**, 207.
38. C. Dobie and D. Skropeta, *Br. J. Cancer*, 2021, **124**, 76-90.
39. A. Varki, *FASEB J.l*, 1991, **5**, 226-235.
40. I. Maru, Y. Ohta, K. Murata and Y. Tsukada, *J. Biol. Chem.*, 1996, **271**, 16294-16299.
41. C. L. Jacobs, S. Goon, K. J. Yarema, S. Hinderlich, H. C. Hang, D. H. Chai and C. R. Bertozzi, *Biochemistry*, 2001, **40**, 12864-12874.
42. H. C. Hang, C. Yu, D. L. Kato and C. R. Bertozzi, *Proc. Natl. Acad. Sci.*, 2003, **100**, 14846-14851.
43. E. M. Sletten and C. R. Bertozzi, *Angew. Chem. Int. Ed.,* 2009, **48**, 6974-6998.
44. R. E. Bird, S. A. Lemmel, X. Yu and Q. A. Zhou, *Bioconjug. Chem.*, 2021, **32**, 2457-2479.
45. D. M. Patterson, L. A. Nazarova and J. A. Prescher, *ACS Chem. Biol.*, 2014, **9**, 592-605.
46. J. C. Jewett and C. R. Bertozzi, *Chem. Soc. Rev.*, 2010, **39**, 1272-1279.
47. B. A. Griffin, S. R. Adams and R. Y. Tsien, *Science*, 1998, **281**, 269-272.
48. C. R. Bertozzi, *Acc. Chem. Res.*, 2011, **44**, 651-653.
49. J. A. Prescher and C. R. Bertozzi, *Nat. Chem. Biol.*, 2005, **1**, 13-21.
50. M. Grammel and H. C. Hang, *Nat. Chem. Biol.*, 2013, **9**, 475-484.
51. R. J. Griffin, *Prog. Med. Chem.*, 1994, **31**, 121-232.
52. T. Saegusa, Y. Ito and T. Shimizu, *J. Org. Chem.*, 1970, **35**, 2979-2981.
53. E. Saxon and C. R. Bertozzi, *Science (New York, N.Y.)*, 2000, **287**, 2007-2010.
54. E. Saxon, J. I. Armstrong and C. R. Bertozzi, *Org. Lett.*, 2000, **2**, 2141-2143.
55. S. S. van Berkel, M. B. van Eldijk and J. C. M. van Hest, *Angew. Chem. Int. Ed.*, 2011, **50**, 8806-8827.
56. F. L. Lin, H. M. Hoyt, H. van Halbeek, R. G. Bergman and C. R. Bertozzi, *J. Am. Chem. Soc.*, 2005, **127**, 2686-2695.
57. R. Huisgen and H. Nakaten, *Justus Liebigs Ann. Chem.*, 1951, **573**, 181-195.
58. V. V. Rostovtsev, L. G. Green, V. V. Fokin and K. B. Sharpless, *Angew. Chem. Int. Ed.*, 2002, **41**, 2596-2599.
59. C. W. Tornøe, C. Christensen and M. Meldal, *J. Org. Chem*, 2002, **67**, 3057-3064.
60. L. Li and Z. Zhang, *Molecules*, 2016, **21**, 1393.
61. N. J. Agard, J. M. Baskin, J. A. Prescher, A. Lo and C. R. Bertozzi, *ACS Chem. Biol.*, 2006, **1**, 644-648.
62. H. C. Kolb and K. B. Sharpless, *Drug Discovery Today*, 2003, **8**, 1128-1137.
63. M. Boyce and C. R. Bertozzi, *Nat. Methods*, 2011, **8**, 638-642.
64. D. C. Kennedy, C. S. McKay, M. C. B. Legault, D. C. Danielson, J. A. Blake, A. F. Pegoraro, A. Stolow, Z. Mester and J. P. Pezacki, *J. Am. Chem. Soc.*, 2011, **133**, 17993-18001.
65. L. Zhang, X. Chen, P. Xue, H. H. Sun, I. D. Williams, K. B. Sharpless, V. V. Fokin and G. Jia, *J. Am. Chem. Soc.,* 2005, **127**, 15998-15999.
66. J. R. Johansson, T. Beke-Somfai, A. Said Stålsmeden and N. Kann, *Chem. Rev.*, 2016, **116**, 14726-14768.
67. N. J. Agard, J. A. Prescher and C. R. Bertozzi, *J. Am. Chem. Soc.*, 2004, **126**, 15046-15047.
68. J. Dommerholt, F. P. J. T. Rutjes and F. L. van Delft, *Top. Curr. Chem.,* 2016, **374**, 16-16.
69. B. L. Oliveira, Z. Guo and G. J. L. Bernardes, *Chem. Soc. Rev.*, 2017, **46**, 4895-4950.
70. M. L. Blackman, M. Royzen and J. M. Fox, *J. Am. Chem. Soc.*, 2008, **130**, 13518-13519.
71. R. Rossin, S. M. van den Bosch, W. ten Hoeve, M. Carvelli, R. M. Versteegen, J. Lub and M. S. Robillard, *Bioconjug. Chem.*, 2013, **24**, 1210-1217.
72. Y. Fang, J. C. Judkins, S. J. Boyd, C. W. am Ende, K. Rohlfing, Z. Huang, Y. Xie, D. S. Johnson and J. M. Fox, *Tetrahedron*, 2019, **75**, 4307-4317.
73. N. K. Devaraj, R. Weissleder and S. A. Hilderbrand, *Bioconjug. Chem.*, 2008, **19**, 2297-2299.
74. S. Eising, F. Lelivelt and K. M. Bonger, *Angew. Chem. Int. Ed.*, 2016, **55**, 12243-12247.

75. D. M. Patterson, L. A. Nazarova, B. Xie, D. N. Kamber and J. A. Prescher, *J. Am. Chem. Soc.*, 2012, **134**, 18638-18643.
76. S. T. Laughlin and C. R. Bertozzi, *Proc. Natl. Acad. Sci.*, 2009, **106**, 12-17.
77. K. T. Pilobello and L. K. Mahal, *Microchip-Based Assay Systems*, Springer, 2007, pp. 193-203.
78. A. M. Duijvestijn, E. Horst, S. Pals, B. Rouse, A. Steere, L. Picker, C. Meijer and E. Butcher, *Am. J. Pathol.*, 1988, **130**, 147.
79. H. Ohba and R. Bakalova, *Cancer Chemother. Pharmacol.*, 2003, **51**, 451-458.
80. E. Saxon and C. R. Bertozzi, *Annu. Rev. Cell Dev. Biol.*, 2001, **17**, 1-23.
81. B. Schumann, S. A. Malaker, S. P. Wisnovsky, M. F. Debets, A. J. Agbay, D. Fernandez, L. J. S. Wagner, L. Lin, Z. Li, J. Choi, D. M. Fox, J. Peh, M. A. Gray, K. Pedram, J. J. Kohler, M. Mrksich and C. R. Bertozzi, *Mol. Cell*, 2020, **78**, 824-834.e815.
82. S. Goon and C. R. Bertozzi, *J. Carbohydr. Chem.*, 2002, **21**, 943-977.
83. S. J. Luchansky, H. C. Hang, E. Saxon, J. R. Grunwell, C. Yu, D. H. Dube and C. R. Bertozzi, *Methods Enzymol.*, 2003, **362**, 249-272.
84. T. J. Sminia, H. Zuilhof and T. Wennekes, *Carbohydr. Res.*, 2016, **435**, 121-141.
85. J. G. Bekesi and R. J. Winzler, *J. Biol. Chem.*, 1969, **244**, 5663-5668.
86. D. O. Keppler, J. F. Rudigier, E. Bischoff and K. F. Deckker, *Eur. J. Biochem.*, 1970, **17**, 246-253.
87. L. K. Mahal, K. J. Yarema and C. R. Bertozzi, *Science (New York, N.Y.)*, 1997, **276**, 1125-1128.
88. D. J. Vocadlo, H. C. Hang, E. J. Kim, J. A. Hanover and C. R. Bertozzi, *Proc. Natl. Acad. Sci. U. S. A.*, 2003, **100**, 9116-9121.
89. M. Boyce, I. S. Carrico, A. S. Ganguli, S.-H. Yu, M. J. Hangauer, S. C. Hubbard, J. J. Kohler and C. R. Bertozzi, *Proc. Natl. Acad. Sci.*, 2011, **108**, 3141.
90. X. Zhang, R. Li, Y. Chen, S. Zhang, W. Wang and F. Li, *Chem. Sci.*, 2016, **7**, 6182-6189.
91. J. Hassenrück and V. Wittmann, *Beilstein J. Org. Chem.*, 2019, **15**, 584-601.
92. S. Stairs, A. A. Neves, H. Stöckmann, Y. A. Wainman, H. Ireland-Zecchini, K. M. Brindle and F. J. Leeper, *Chembiochem.*, 2013, **14**, 1063-1067.
93. S. J. Moons, G. J. Adema, M. T. G. M. Derks, T. J. Boltje and C. Büll, *Glycobiology*, 2019, **29**, 433-445.
94. E. Tan, R. T. Almaraz, H. S. Khanna, J. Du and K. J. Yarema, *Curr. Protoc. Chem. Biol.*, 2010, **2**, 171-194.
95. M. I. Zol-Hanlon and B. Schumann, *Comm. Chem.*, 2020, **3**, 102.
96. P.-A. Gilormini, A. R. Batt, M. R. Pratt and C. Biot, *Chem. Sci.*, 2018, **9**, 7585-7595.
97. J. A. Prescher, D. H. Dube and C. R. Bertozzi, *Nature*, 2004, **430**, 873-877.
98. S. T. Laughlin, J. M. Baskin, S. L. Amacher and C. R. Bertozzi, *Science (New York, N.Y.)*, 2008, **320**, 664-667.
99. Y. Guérardel, L.-Y. Chang, E. Maes, C.-J. Huang and K.-H. Khoo, *Glycobiology*, 2005, **16**, 244-257.
100. A. A. Neves, H. Stöckmann, R. R. Harmston, H. J. Pryor, I. S. Alam, H. Ireland-Zecchini, D. Y. Lewis, S. K. Lyons, F. J. Leeper and K. M. Brindle, *FASEB J.*, 2011, **25**, 2528-2537.
101. A. A. Neves, Y. A. Wainman, A. Wright, M. I. Kettunen, T. B. Rodrigues, S. McGuire, D.-E. Hu, F. Bulat, S. G. Crich, H. Stöckmann, F. J. Leeper and K. M. Brindle, *Angew. Chem. Int. Ed.*, 2016, **55**, 1286-1290.
102. A. A. Neves, H. Stöckmann, Y. A. Wainman, J. C. H. Kuo, S. Fawcett, F. J. Leeper and K. M. Brindle, *Bioconjug. Chem.*, 2013, **24**, 934-941.
103. J. E. G. A. Dold, J. Pfotzer, A.-K. Späte and V. Wittmann, *Chembiochem*, 2017, **18**, 1242-1250.
104. R. Zhang, J. Zheng and T. Zhang, *RSC Advances*, 2020, **10**, 15990-15996.
105. P. Agarwal, B. J. Beahm, P. Shieh and C. R. Bertozzi, *Angew. Chem. Int. Ed.*, 2015, **54**, 11504-11510.
106. A. K. Späte, J. E. Dold, E. Batroff, V. F. Schart, D. E. Wieland, O. R. Baudendistel and V. Wittmann, *Chembiochem*, 2016, **17**, 1374-1383.

107. A.-K. Späte, V. F. Schart, S. Schöllkopf, A. Niederwieser and V. Wittmann, *Chem. Eur. J.* 2014, **20**, 16502-16508.
108. L. M. Haiber, M. Kufleitner and V. Wittmann, *Frontiers in chemistry*, 2021, **9**, 654932-654932.
109. J. Yang, J. Šečkute, C. M. Cole and N. K. Devaraj, *Angew. Chem. Int. Ed.*, 2012, **51**, 7476-7479.
110. D.-C. Xiong, J. Zhu, M.-J. Han, H.-X. Luo, C. Wang, Y. Yu, Y. Ye, G. Tai and X.-S. Ye, *Org. Biomol. Chem.*, 2015, **13**, 3911-3917.
111. A. K. Späte, V. F. Schart, J. Häfner, A. Niederwieser, T. U. Mayer and V. Wittmann, *Beilstein J. Org. Chem.*, 2014, **10**, 2235-2242.
112. A.-K. Späte, H. Bußkamp, A. Niederwieser, V. F. Schart, A. Marx and V. Wittmann, *Bioconjug. Chem.*, 2014, **25**, 147-154.
113. D. M. Patterson, K. A. Jones and J. A. Prescher, *Mol. BioSyst*, 2014, **10**, 1693-1697.
114. *https://www.molinspiration.com, (Accessed* 11.11.2020).
115. S. Fouad, *Optimisation of Cyclopropene-Tagged Mannosamine for Metabolic Labelling of Glycans in Cancer*, University of Cambridge, 2018, MChem Thesis.
116. S. T. Laughlin and C. R. Bertozzi, *Nat. Protoc.*, 2007, **2**, 2930-2944.
117. R. LoBrutto, A. Jones, Y. V. Kazakevich and H. M. McNair, *J. Chromatogr. A*, 2001, **913**, 173-187.
118. M. H. Hyun, S. C. Han, B. H. Lipshutz, Y. J. Shin and C. J. Welch, *J. Chromatogr. A*, 2002, **959**, 75-83.
119. S. Dasgupta and M. Nitz, *J. Org. Chem.*, 2011, **76**, 1918-1921.
120. R. Khan, P. A. Konowicz, L. Gardossi, M. Matulová and S. De Gennaro, *Aust. J. Chem.*, 1996, **49**, 293-298.
121. M. Mikamo, *Carbohydr. Res.*, 1989, **191**, 150-153.
122. E. Kaya, F. Sonmez, M. Kucukislamoglu and M. Nebioglu, *Chem. Pap.*, 2012, **66**, 312-315.
123. J. Fiandor, M. T. Garciá-López, F. G. De Las Heras and P. P. Méndez-Castrillón, *Synthesis*, 1985, **1985**, 1121-1123.
124. H. Stöckmann, A. A. Neves, S. Stairs, H. Ireland-Zecchini, K. M. Brindle and F. J. Leeper, *Chem. Sci.*, 2011, **2**, 932-936.
125. H. Stockmann, *The Development of New Agents for Molecular Imaging in Cancer*, University of Cambridge Cambridge, 2011, PhD Thesis.
126. Y. A. Wainman, *Developing Novel Chemical Probes for Molecular Imaging of Glycans in Cancer*, University of Cambridge 2014, PhD Thesis.
127. R. Rossin, P. R. Verkerk, S. M. van den Bosch, R. C. Vulders, I. Verel, J. Lub and M. S. Robillard, *Angew. Chem. Int. Ed.*, 2010, **49**, 3375-3378.
128. H. Stöckmann, A. A. Neves, H. A. Day, S. Stairs, K. M. Brindle and F. J. Leeper, *Chem. Commun.*, 2011, **47**, 7203-7205.
129. T. U. Semple, L. A. Quinn, L. K. Woods and G. E. Moore, *Cancer Res.*, 1978, **38**, 1345-1355.
130. P. Rawla, T. Sunkara and A. Barsouk, *Gastroenterology Review*, 2019, **14**, 89-103.
131. A.-K. Späte, H. Bußkamp, A. Niederwieser, V. F. Schart, A. Marx and V. Wittmann, *Bioconjug. Chem..*, 2013, **25**, 147-154.
132. J. E. G. A. Dold and V. Wittmann, *Chembiochem*, 2020, **22**, 1243-1251.
133. W. Qin, K. Qin, X. Fan, L. Peng, W. Hong, Y. Zhu, P. Lv, Y. Du, R. Huang, M. Han, B. Cheng, Y. Liu, W. Zhou, C. Wang and X. Chen, *Angew. Chem. Int. Ed.*, 2018, **57**, 1817-1820.
134. K. Qin, H. Zhang, Z. Zhao and X. Chen, *J. Am. Chem. Soc.*, 2020, **142**, 9382-9388.
135. T. Heise, C. Büll, D. M. Beurskens, E. Rossing, M. I. de Jonge, G. J. Adema, T. J. Boltje and J. D. Langereis, *Bioconjug. Chem.*, 2017, **28**, 1811-1815.
136. S. Wu and H.-J. Butt, *Phys. Chem. Chem. Phys.*, 2017, **19**, 23585-23596.
137. E. A. Te Velde, T. Veerman, V. Subramaniam and T. Ruers, *Eur J Surg Oncol.,* 2010, **36**, 6-15.
138. Z. Vincent, K. Urakami, K. Maruyama, K. Yamaguchi and M. Kusuhara, *Genes Cancer*, 2014, **5**, 250-260.
139. R. Fisher, L. Pusztai and C. Swanton, *Br. J. Cancer*, 2013, **108**, 479-485.

140. F. Dall'olio and M. Chiricolo, *Glycoconjugate Journal*, 2001, **18**, 841-850.
141. O. M. T. Pearce and H. Läubli, *Glycobiology*, 2015, **26**, 111-128.
142. R. Cailleau, R. Young, M. Olivé and W. J. Reeves, Jr., *J. Natl. Cancer Inst.*, 1974, **53**, 661-674.
143. M. Lieber, J. Mazzetta, W. Nelson-Rees, M. Kaplan and G. Todaro, *Int. J. Cancer*, 1975, **15**, 741-747.
144. M. M. Trivedi and J. K. Mills, *Biomed. Signal Process. Control*, 2020, **57**, 101726.
145. T. Kojima, H. Yamaguchi, T. Ito, D. Kyuno, T. Kono, T. Konno and N. Sawada, *World J Gastroenterol., 2014*, , **20**, 10813–10824.
146. Y. Hu and J. M. Schomaker, *Chembiochem*, 2021, **22**, 3254-3262.
147. Y. A. Wainman, A. A. Neves, S. Stairs, H. Stöckmann, H. Ireland-Zecchini, K. M. Brindle and F. J. Leeper, *Org. Biomol. Chem.*, 2013, **11**, 7297-7300.
148. C. M. Cole, J. Yang, J. Šečkutė and N. K. Devaraj, *Chembiochem*, 2013, **14**, 205-208.
149. A. Niederwieser, A.-K. Späte, L. D. Nguyen, C. Jüngst, W. Reutter and V. Wittmann, *Angew. Chem. Int. Ed.*, 2013, **52**, 4265-4268.
150. Y. Liang, J. L. Mackey, S. A. Lopez, F. Liu and K. N. Houk, *J. Am. Chem. Soc.*, 2012, **134**, 17904-17907.
151. A. C. Croce and G. Bottiroli, *Eur. J. Histochem.*, 2014, **58**, 2461-2461.
152. https://www.bio-rad-antibodies.com/flow-cytometry-autofluorescence.html, (accessed 23.02.2022).
153. U. Schneider, H.-U. Schwenk and G. Bornkamm, *Int. J. Cancer*, 1977, **19**, 621-626.
154. F. L. Graham, W. C. Russell, J. Smiley and R. Nairn, *J. Gen. Virol.*, 1977, **36**, 59-72.
155. M. R. Karver, R. Weissleder and S. A. Hilderbrand, *Angew. Chem.*, 2012, **124**, 944-946.
156. X. Dai, H. Cheng, Z. Bai and J. Li, *Journal of Cancer*, 2017, **8**, 3131-3141.
157. https://www.phe-culturecollections.org.uk/products/celllines/generalcell, (accessed 14/01/22).
158. https://drugdevelopment.labcorp.com/industry-solutions/oncology/preclinical/complete-cell-line-list.html , (accessed 18/01/2022, 2022).
159. R. M. Pinto, R. I. Olariu, J. Lameiras, F. T. Martins, A. A. Dias, G. J. Langley, P. Rodrigues, C. D. Maycock, J. P. Santos, M. F. Duarte, M. T. Fernandez and M. L. Costa, *J. Mol. Struct.*, 2010, **980**, 163-171.
160. S. J. Luchansky, K. J. Yarema, S. Takahashi and C. R. Bertozzi, *J. Biol. Chem.*, 2003, **278**, 8035-8042.
161. J. B. Thoden, T. M. Wohlers, J. L. Fridovich-Keil and H. M. Holden, *J. Biol. Chem.*, 2001, **276**, 15131-15136.
162. F. Bulat, *targeted imaging agents for detecting tumour cell death following therapy*, University of Cambridge, 2019, PhD Thesis.
163. N. E. Mbua, J. Guo, M. A. Wolfert, R. Steet and G.-J. Boons, *Chembiochem*, 2011, **12**, 1912-1921.
164. J. M. Baskin, J. A. Prescher, S. T. Laughlin, N. J. Agard, P. V. Chang, I. A. Miller, A. Lo, J. A. Codelli and C. R. Bertozzi, *Proc. Natl. Acad. Sci. U. S. A.*, 2007, **104**, 16793-16793.
165. X. Ning, J. Guo, M. A. Wolfert and G. J. Boons, *Angew. Chem. Int. Ed.*, 2008, **47**, 2253-2255.
166. M. F. Debets, S. S. van Berkel, J. Dommerholt, A. J. Dirks, F. P. J. T. Rutjes and F. L. van Delft, *Acc. Chem. Res.*, 2011, **44**, 805-815.
167. J. Dommerholt, S. Schmidt, R. Temming, L. J. Hendriks, F. P. Rutjes, J. C. Van Hest, D. J. Lefeber, P. Friedl and F. L. Van Delft, *Angew. Chem. Int. Ed.*, 2010, **49**, 9422-9425.
168. T. Bakkum, T. van Leeuwen, A. J. C. Sarris, D. M. van Elsland, D. Poulcharidis, H. S. Overkleeft and S. I. van Kasteren, *ACS Chem. Biol.*, 2018, **13**, 1173-1179.
169. M. F. Debets, S. S. van Berkel, S. Schoffelen, F. P. J. T. Rutjes, J. C. M. van Hest and F. L. van Delft, *Chem. Commun.*, 2010, **46**, 97-99.
170. J. C. Jewett, E. M. Sletten and C. R. Bertozzi, *J. Am. Chem. Soc.*, 2010, **132**, 3688-3690.

171. G. de Almeida, E. M. Sletten, H. Nakamura, K. K. Palaniappan and C. R. Bertozzi, *Angew. Chem. Int. Ed.*, 2012, **51**, 2443-2447.
172. C. D. McNitt and V. V. Popik, *Org. Biomol. Chem.*, 2012, **10**, 8200-8200.
173. R. N. Butler, W. J. Cunningham, A. G. Coyne and L. A. Burke, *J. Am. Chem. Soc.*, 2004, **126**, 11923-11929.
174. M. Wang, C. D. McNitt, H. Wang, X. Ma, S. M. Scarry, Z. Wu, V. V. Popik and Z. Li, *7810 | Chem. Commun*, 2018, **54**, 7810-7813.
175. K. Durie, J. Yatvin, C. D. McNitt, R. A. Reese, C. Jung, V. V. Popik and J. Locklin, *Langmuir*, 2016, **32**, 6600-6605.
176. M. Ahmad and J. Hamer, *J. Chem. Educ.*, 1964, **41**, 249.
177. F. Thalhammer, U. Wallfahrer and J. Sauer, *Tetrahedron Lett.*, 1990, **31**, 6851-6854.
178. M. Royzen, G. P. A. Yap and J. M. Fox, *J. Am. Chem. Soc.*, 2008, **130**, 3760-3761.
179. R. Selvaraj and J. M. Fox, *Curr. Opin. Chem. Biol.*, 2013, **17**, 753-760.
180. M. T. Taylor, M. L. Blackman, O. Dmitrenko and J. M. Fox, *Journal of the American Chemical Society*, 2011, **133**, 9646-9649.
181. H. E. Murrey, J. C. Judkins, C. W. am Ende, T. E. Ballard, Y. Fang, K. Riccardi, L. Di, E. R. Guilmette, J. W. Schwartz, J. M. Fox and D. S. Johnson, *J. Am. Chem. Soc.*, 2015, **137**, 11461-11475.
182. A. Darko, S. Wallace, O. Dmitrenko, M. M. Machovina, R. A. Mehl, J. W. Chin and J. M. Fox, *Chem. Sci.*, 2014, **5**, 3770-3776.
183. S. Mayer and K. Lang, *Synthesis*, 2017, **49**, 830-848.
184. J. Šečkutė and N. K. Devaraj, *Curr. Opin. Chem. Biol.*, 2013, **17**, 761-767.
185. K. Müller and J. Sauer, *Tetrahedron Lett.*, 1984, **25**, 2541-2544.
186. https://cen.acs.org/pharmaceuticals/Click-chemistry-sees-first-use/98/web/2020/10, (accessed 21.01.21).
187. Phase 1 Study of SQ3370 in Patients With Advanced Solid Tumors, https://ClinicalTrials.gov/show/NCT04106492, (accessed 21.01.21).
188. K. Wu, N. A. Yee, S. Srinivasan, A. Mahmoodi, M. Zakharian, J. M. Mejia Oneto and M. Royzen, *Chem. Sci.*, 2021, **12**, 1259-1271.
189. R. M. Versteegen, R. Rossin, W. ten Hoeve, H. M. Janssen and M. S. Robillard, *Angew. Chem. Int. Ed.*, 2013, **52**, 14112-14116.
190. T. Plass, S. Milles, C. Koehler, J. Szymański, R. Mueller, M. Wießler, C. Schultz and E. A. Lemke, *Angew. Chem. Int. Ed.*, 2012, **51**, 4166-4170.
191. A. Rondon, N. Ty, J.-B. Bequignat, M. Quintana, A. Briat, T. Witkowski, B. Bouchon, C. Boucheix, E. Miot-Noirault, J.-P. Pouget, J.-M. Chezal, I. Navarro-Teulon, E. Moreau and F. Degoul, *Sci. Rep.*, 2017, **7**, 14918.
192. Z. Li, H. Cai, M. Hassink, M. L. Blackman, R. C. Brown, P. S. Conti and J. M. Fox, *Chem. Commun.*, 2010, **46**, 8043-8045.
193. B. M. Zeglis, K. K. Sevak, T. Reiner, P. Mohindra, S. D. Carlin, P. Zanzonico, R. Weissleder and J. S. Lewis, *J. Nucl. Med.*, 2013, **54**, 1389-1396.
194. Y. Takayama, K. Kusamori and M. Nishikawa, *Molecules*, 2019, **24**, 172.
195. R. Rossin, S. M. J. van Duijnhoven, W. ten Hoeve, H. M. Janssen, L. H. J. Kleijn, F. J. M. Hoeben, R. M. Versteegen and M. S. Robillard, *Bioconjug. Chem.*, 2016, **27**, 1697-1706.
196. G. M. Whitesides, G. L. Goe and A. C. Cope, *J. Am. Chem. Soc.*, 1969, **91**, 2608-2616.
197. D. Boeckh, R. Huisgen and H. Noeth, *J. Am. Chem. Soc.*, 1987, **109**, 1248-1249.
198. L. Josa Culleré, *Preparation of (E,E) 1,5-Cycloctadiene Analogues as Potential New Agents for Molecular Imaging in Cancer*, University of Cambridge, 2013, MChem Thesis.
199. T. G. Vilaplana, *(E,Z)-1,5-cyclooctadienes as Potential New Agents For Dynamic Cancer Imaging*, University of Cambridge, 2014, Part III project report.
200. D. Wittenberg and H. Gilman, *J. Org. Chem.*, 1958, **23**, 1063-1065.

201. Y. Fang, H. Zhang, Z. Huang, S. L. Scinto, J. C. Yang, Christopher W. am Ende, O. Dmitrenko, D. S. Johnson and J. M. Fox, *Chem. Sci.*, 2018, **9**, 1953-1963.
202. H. Baumann, E. Nudelman, K. Watanabe and S.-i. Hakomori, *Cancer Res.*, 1979, **39**, 2637-2643.
203. E. Miyoshi, K. Moriwaki, N. Terao, C.-C. Tan, M. Terao, T. Nakagawa, H. Matsumoto, S. Shinzaki and Y. Kamada, *Biomolecules*, 2012, **2**, 34-45.
204. K. Noda, E. Miyoshi, J. Gu, C.-X. Gao, S. Nakahara, T. Kitada, K. Honke, K. Suzuki, H. Yoshihara, K. Yoshikawa, K. Kawano, M. Tonetti, A. Kasahara, M. Hori, N. Hayashi and N. Taniguchi, *Cancer Res.*, 2003, **63**, 6282-6289.
205. C.-Y. Chen, Y.-H. Jan, Y.-H. Juan, C.-J. Yang, M.-S. Huang, C.-J. Yu, P.-C. Yang, M. Hsiao, T.-L. Hsu and C.-H. Wong, *Proc. Natl. Acad. Sci. U. S. A.*, 2013, **110**, 630-635.
206. X. Yan, Y. Lin, S. Liu, F. aziz and Q. Yan, *Biomed. Pharmacother.*, 2015, **70**, 299-304.
207. A. Blanas, L. A. M. Cornelissen, M. Kotsias, J. C. van der Horst, H. J. van de Vrugt, H. Kalay, D. I. R. Spencer, R. P. Kozak and S. J. van Vliet, *Glycobiology*, 2018, **29**, 137-150.
208. E. Mas, E. Pasqualini, N. Caillol, A. El Battari, C. Crotte, D. Lombardo and M.-O. Sadoulet, *Glycobiology*, 1998, **8**, 605-613.
209. M. Shan, D. Yang, H. Dou and L. Zhang, in *Prog. Mol. Biol. Transl. Sci.*, ed. L. Zhang, Academic Press, 2019, vol. 162, pp. 93-119.
210. Z. Tu, Y.-N. Lin and C.-H. Lin, *Chem. Soc. Rev.*, 2013, **42**, 4459-4475.
211. W. F. Zandberg, J. Kumarasamy, B. M. Pinto and D. J. Vocadlo, *J. Biol. Chem.*, 2012, **287**, 40021-40030.
212. N. M. Okeley, S. C. Alley, M. E. Anderson, T. E. Boursalian, P. J. Burke, K. M. Emmerton, S. C. Jeffrey, K. Klussman, C.-L. Law, D. Sussman, B. E. Toki, L. Westendorf, W. Zeng, X. Zhang, D. R. Benjamin and P. D. Senter, *Proc. Natl. Acad. Sci.*, 2013, **110**, 5404.
213. J. G. Allen, M. Mujacic, M. J. Frohn, A. J. Pickrell, P. Kodama, D. Bagal, T. San Miguel, E. A. Sickmier, S. Osgood, A. Swietlow, V. Li, J. B. Jordan, K.-W. Kim, A.-M. C. Rousseau, Y.-J. Kim, S. Caille, M. Achmatowicz, O. Thiel, C. H. Fotsch, P. Reddy and J. D. McCarter, *ACS Chem. Biol.*, 2016, **11**, 2734-2743.
214. D. Rabuka, S. C. Hubbard, S. T. Laughlin, S. P. Argade and C. R. Bertozzi, *J. Am. Chem. Soc*, 2006, **128**, 12078-12079.
215. T. L. Hsu, S. R. Hanson, K. Kishikawa, S. K. Wang, M. Sawa and C. H. Wong, *Proc. Natl. Acad. Sci..*, 2007, **104**, 2614-2619.
216. M. Sawa, T.-L. Hsu, T. Itoh, M. Sugiyama, S. R. Hanson, P. K. Vogt and C.-H. Wong, *Proc. Natl. Acad. Sci.*, 2006, **103**, 12371.
217. Y. Kizuka, S. Funayama, H. Shogomori, M. Nakano, K. Nakajima, R. Oka, S. Kitazume, Y. Yamaguchi, M. Sano, H. Korekane, T. L. Hsu, H. Y. Lee, C. H. Wong and N. Taniguchi, *Cell. Chem. Bio.*, 2016, **23**, 782-792.
218. C. Ma, H. Takeuchi, H. Hao, C. Yonekawa, K. Nakajima, M. Nagae, T. Okajima, R. S. Haltiwanger and Y. Kizuka, *Int. J. Mol. Sci.*, 2020, **21**, 1-18.
219. S. Dong, Z. Wang, B. Huang, J. Zhang, Y. Ge, Q. Fan and Z. Wang, *Biochem. Biophys. Res. Commun.*, 2017, **483**, 171-177.
220. S. Wahby, J. Jarczyk, A. Fierek, J. Heinkele, C.-A. Weis, M. Eckstein, T. Martini, S. Porubsky, M. Hafner and P. Erben, *Transl. Oncol.*, 2021, **14**, 100900.
221. Y. Du, D. Li, N. Li, C. Su, C. Yang, C. Lin, M. Chen, R. Wu, X. Li and G. Hu, *Cell Death Dis.*, 2018, **9**, 995-995.
222. S. Yokota, K. Ogawara, R. Kimura, F. Shimizu, T. Baba, Y. Minakawa, M. Higo, A. Kasamatsu, Y. Endo-Sakamoto, M. Shiiba, H. Tanzawa and K. Uzawa, *Int. J. Oncol.*, 2013, **43**, 1864-1870.
223. Q. Leng, J.-H. Tsou, M. Zhan and F. Jiang, *J. Cancer Res. Clin. Oncol.*, 2018, **144**, 2109-2115.
224. M. Stahl, K. Uemura, C. Ge, S. Shi, Y. Tashima and P. Stanley, *J. Biol. Chem.*, 2008, **283**, 13638-13651.
225. G. J. Ewing and M. J. Robins, *Org. Lett.*, 1999, **1**, 635-636.
226. D. J. Keith and S. D. Townsend, *J. Am. Chem. Soc.*, 2019, **141**, 12939-12945.

227. D. S. Larsen and R. J. Stoodley, *J. Chem. Soc., Perkin Trans.* 1., **5**, 1990, 1339-1352.
228. M. Lopez, J. Trajkovic, L. F. Bornaghi, A. Innocenti, D. Vullo, C. T. Supuran and S.-A. Poulsen, *J. Med. Chem.*, 2011, **54**, 1481-1489.

7. Appendices

7.1. Appendix 1: Variable Acetylation Experiments Flow Cytometry Histograms

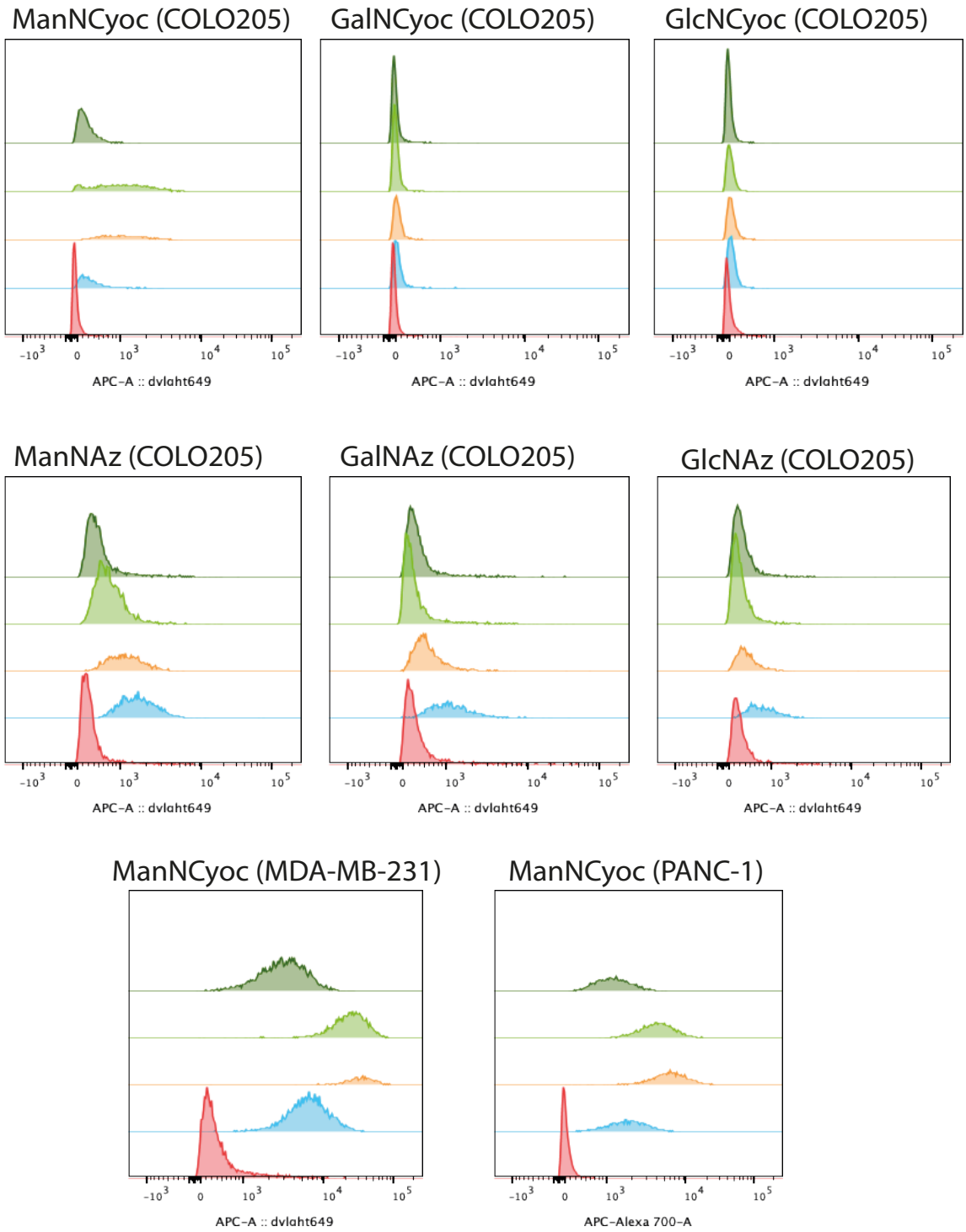

Figure 94 -. Flow cytometry results with the different sugars and cell lines. Histograms giving number of events (vertical axis) versus fluorescence intensity (horizontal axis). In each panel the sugars used, from top to bottom, are mono-, di-, tri- and tetra-acetylated and then the no-sugar control.

7.2. Appendix 2: NMR Spectra

1.

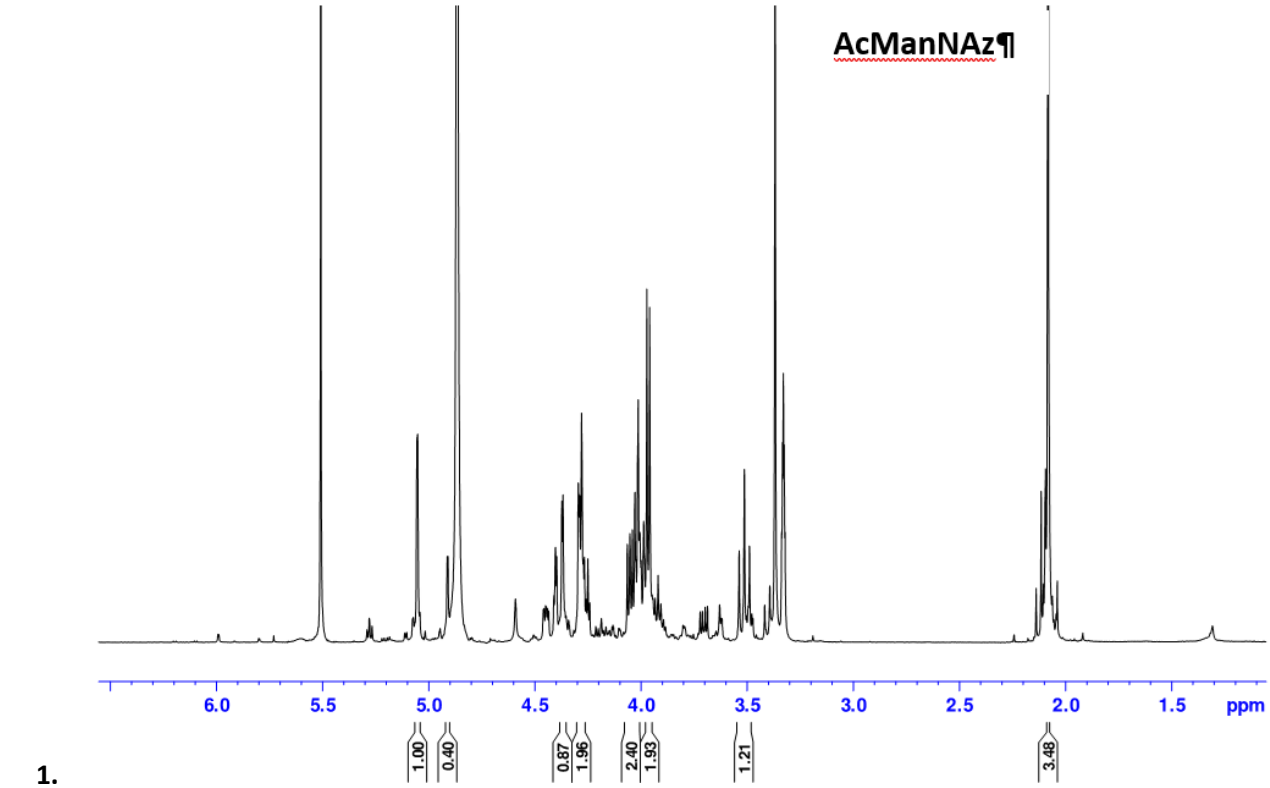

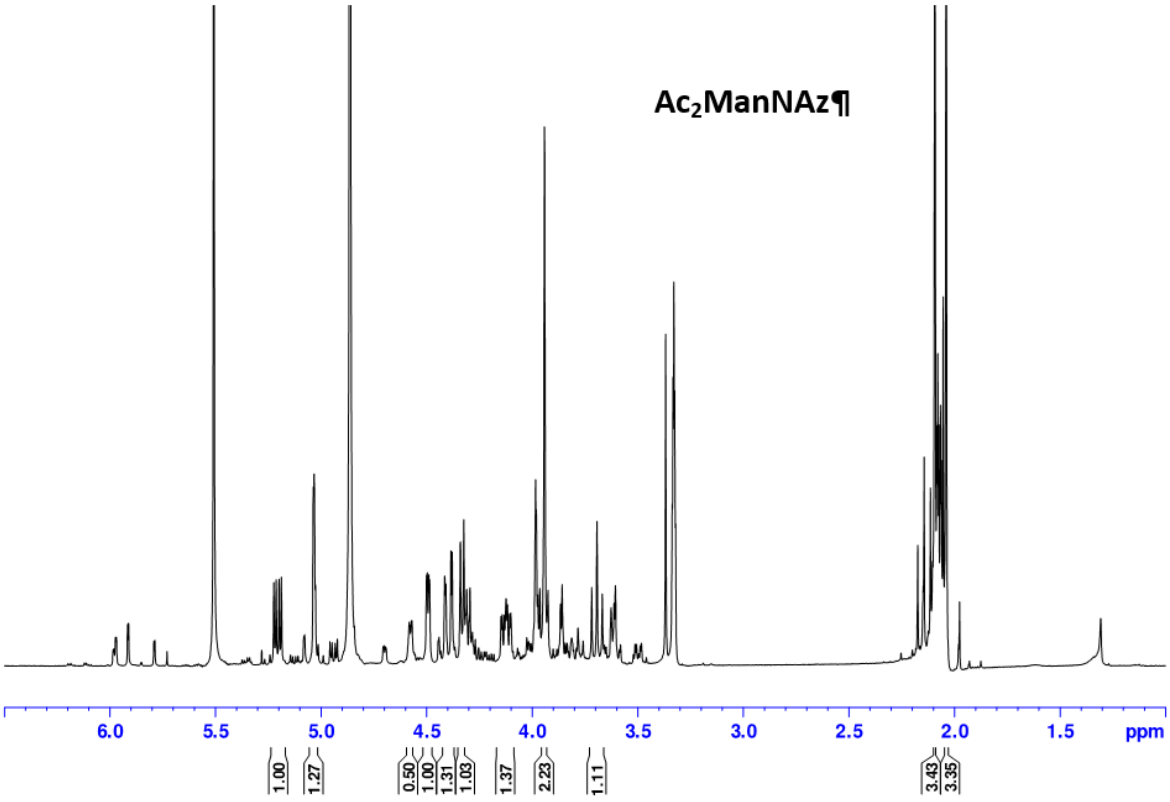

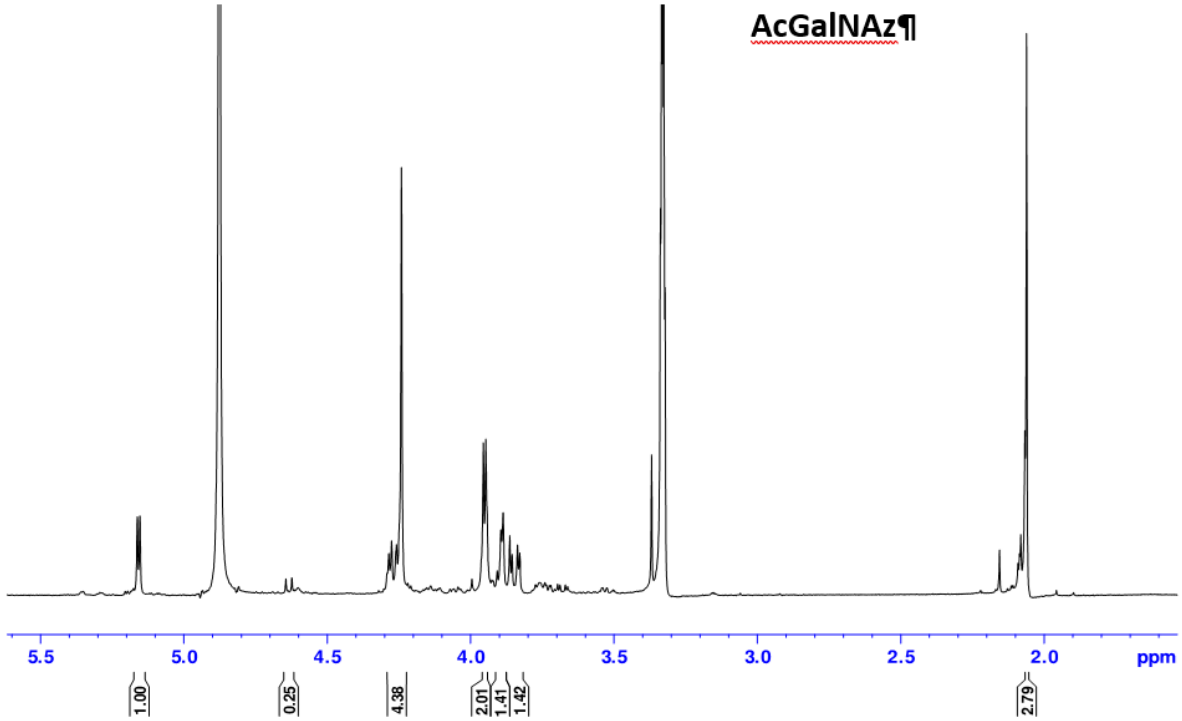
AcGalNAz¶
5.5
5.0
4.5
4.0
3.5
3.0
2.5
2.0
ppm
1.00
0.25
4.38
2.01
1.41
1.42
2.79

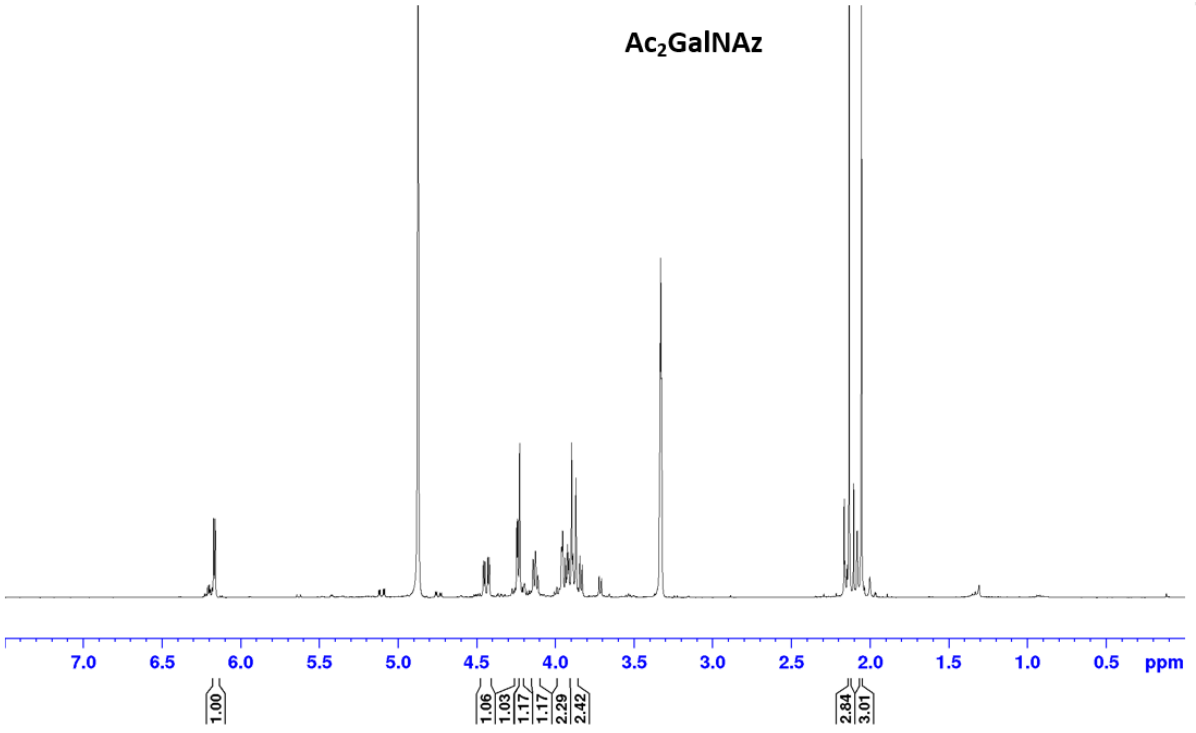
Ac2GalNAz
7.0
6.5
6.0
5.5
5.0
4.5
4.0
3.5
3.0
2.5
2.0
1.5
1.0
0.5
ppm
1.00
1.06
1.03
1.17
1.17
2.29
2.42
2.84
3.01

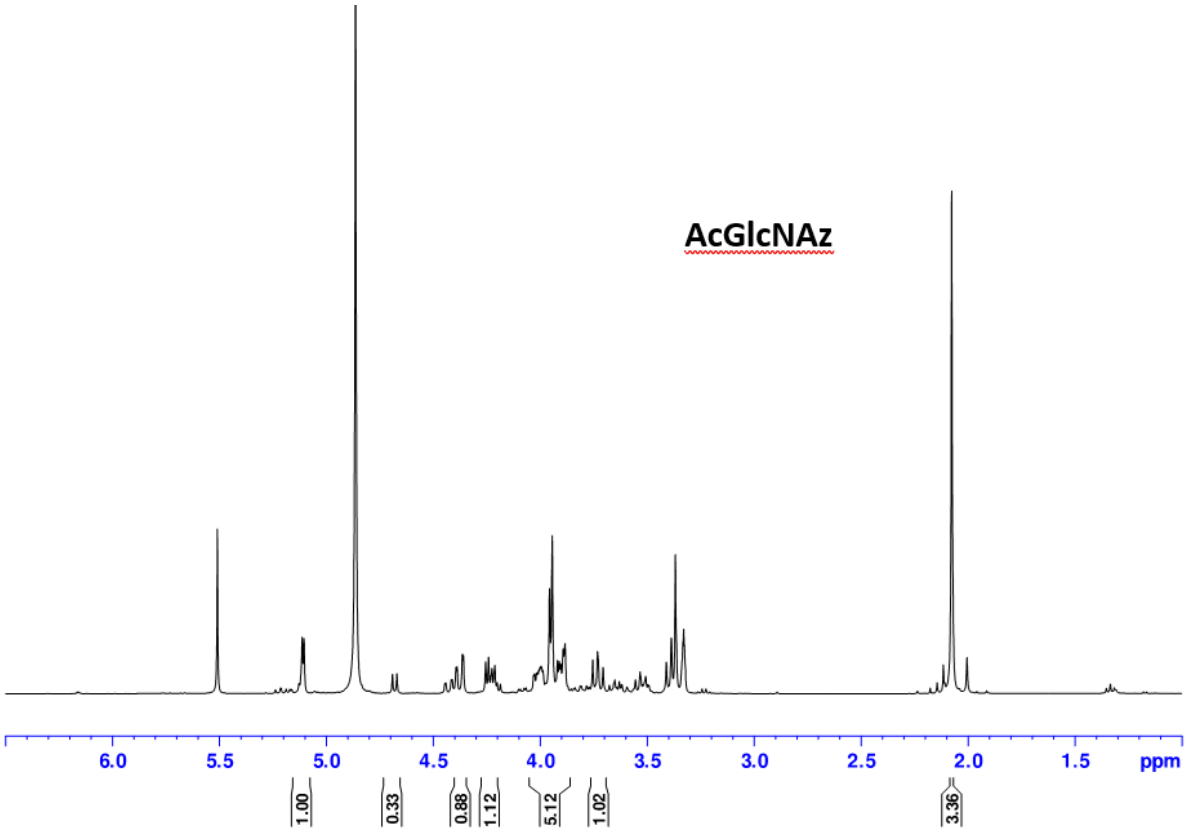
AcGlcNAz
6.0
5.5
5.0
4.5
4.0
3.5
3.0
2.5
2.0
1.5
ppm
1.00
0.33
0.88
1.12
5.12
1.02
3.36

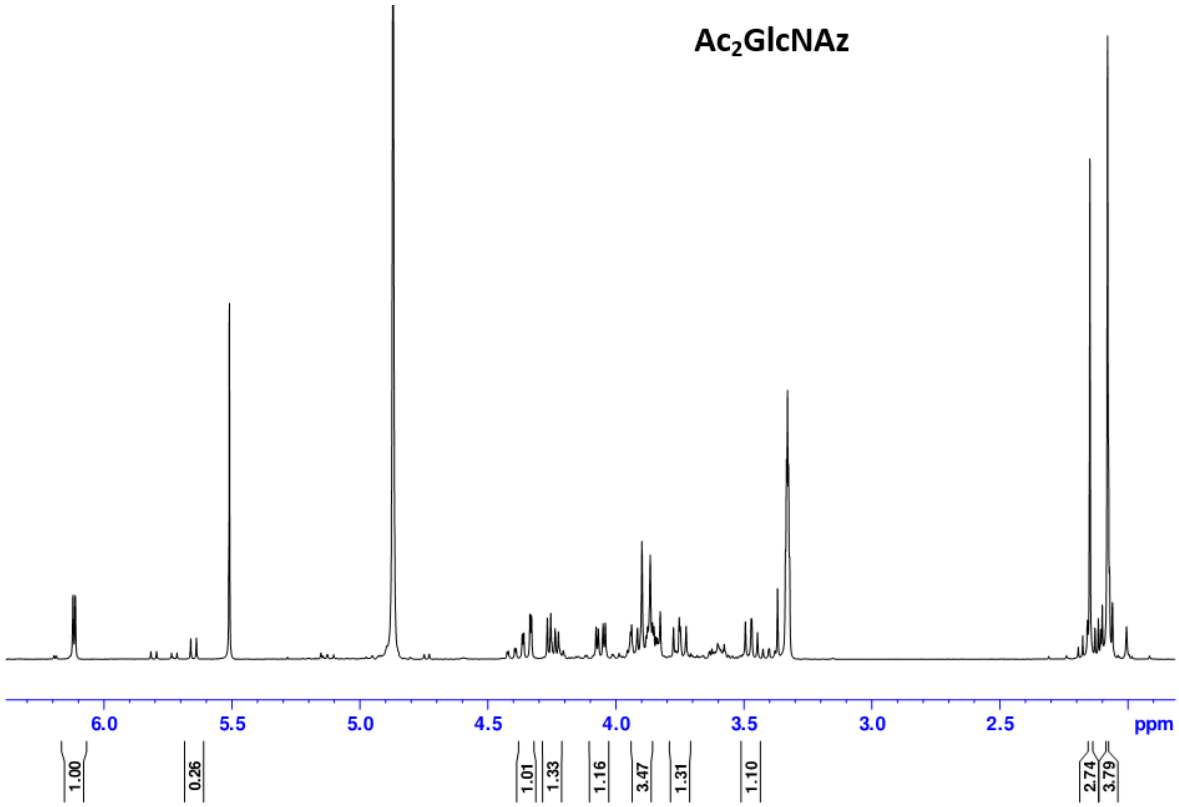
Ac2GlcNAz
6.0
5.5
5.0
4.5
4.0
3.5
3.0
2.5
ppm
1.00
0.26
1.01
1.33
1.16
3.47
1.31
1.10
2.74
3.79

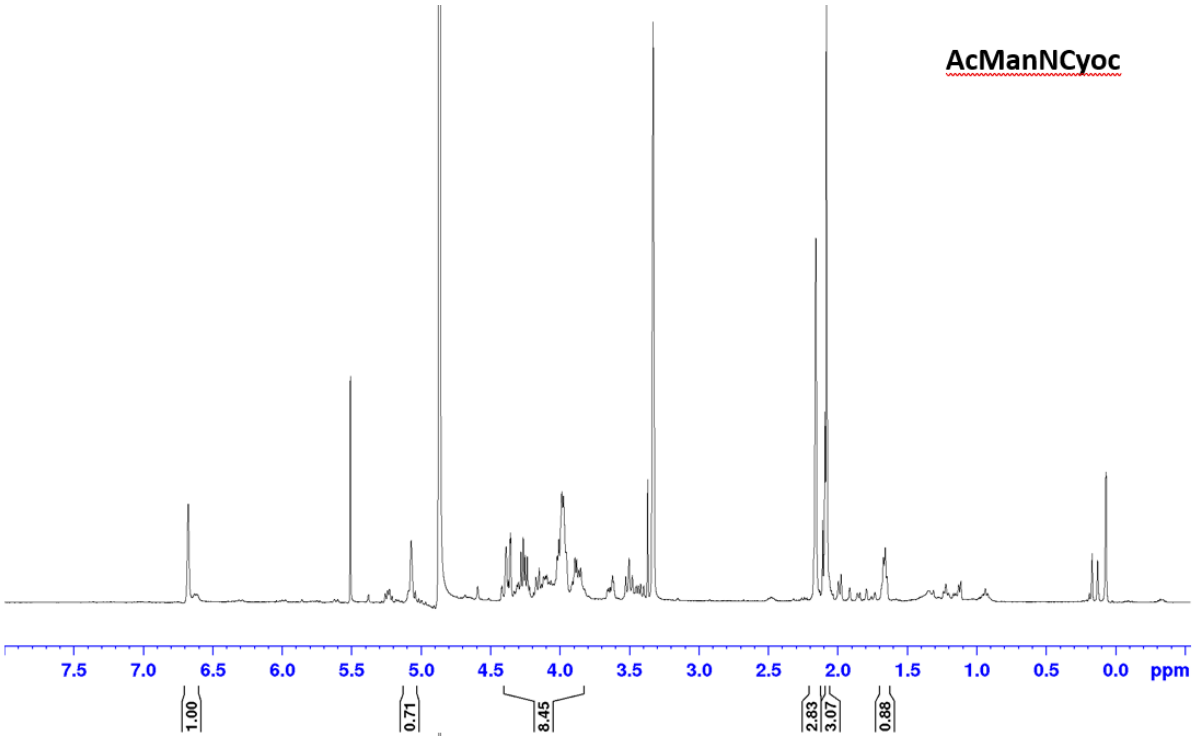
AcManNCyoc
7.5 7.0 6.5 6.0 5.5 5.0 4.5 4.0 3.5 3.0 2.5 2.0 1.5 1.0 0.5 0.0 ppm
1.00
0.71
8.45
2.83
3.07
0.88

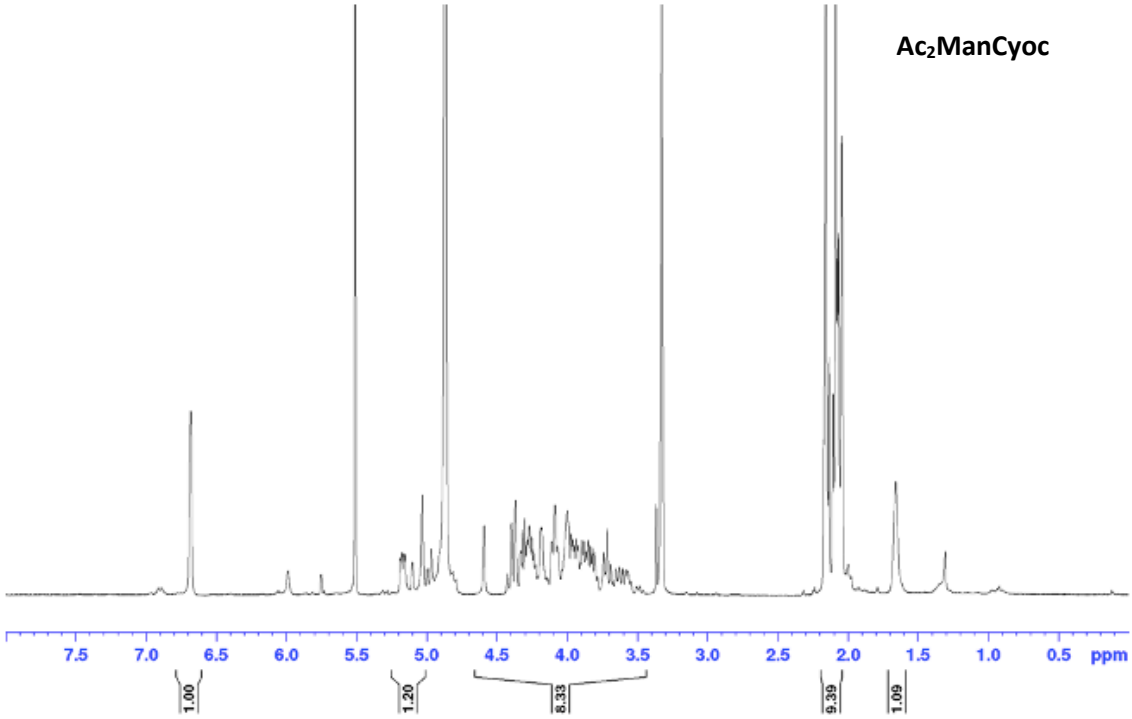
Ac2ManCyoc
7.5 7.0 6.5 6.0 5.5 5.0 4.5 4.0 3.5 3.0 2.5 2.0 1.5 1.0 0.5 ppm
1.00
1.20
8.33
9.39
1.09

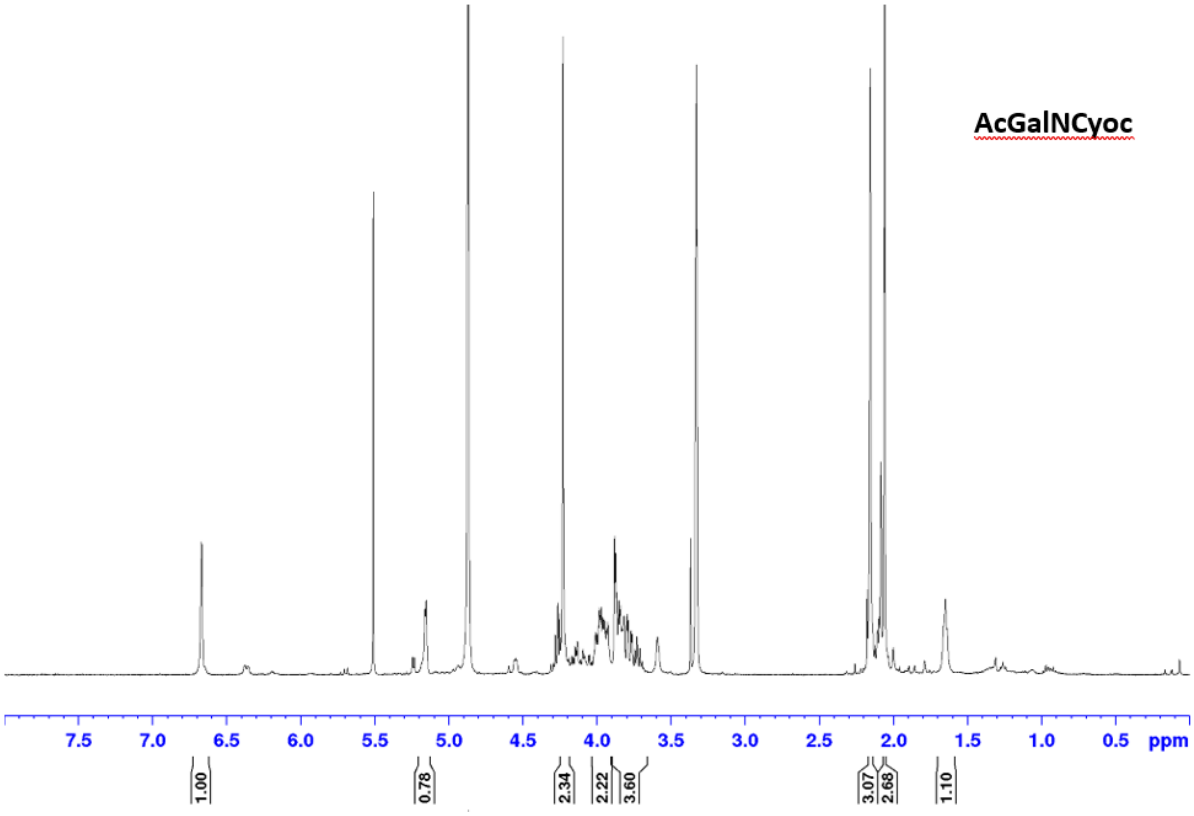
AcGalNCyoc
7.5 7.0 6.5 6.0 5.5 5.0 4.5 4.0 3.5 3.0 2.5 2.0 1.5 1.0 0.5 ppm
1.00
0.78
2.34
2.22
3.60
3.07
2.68
1.10

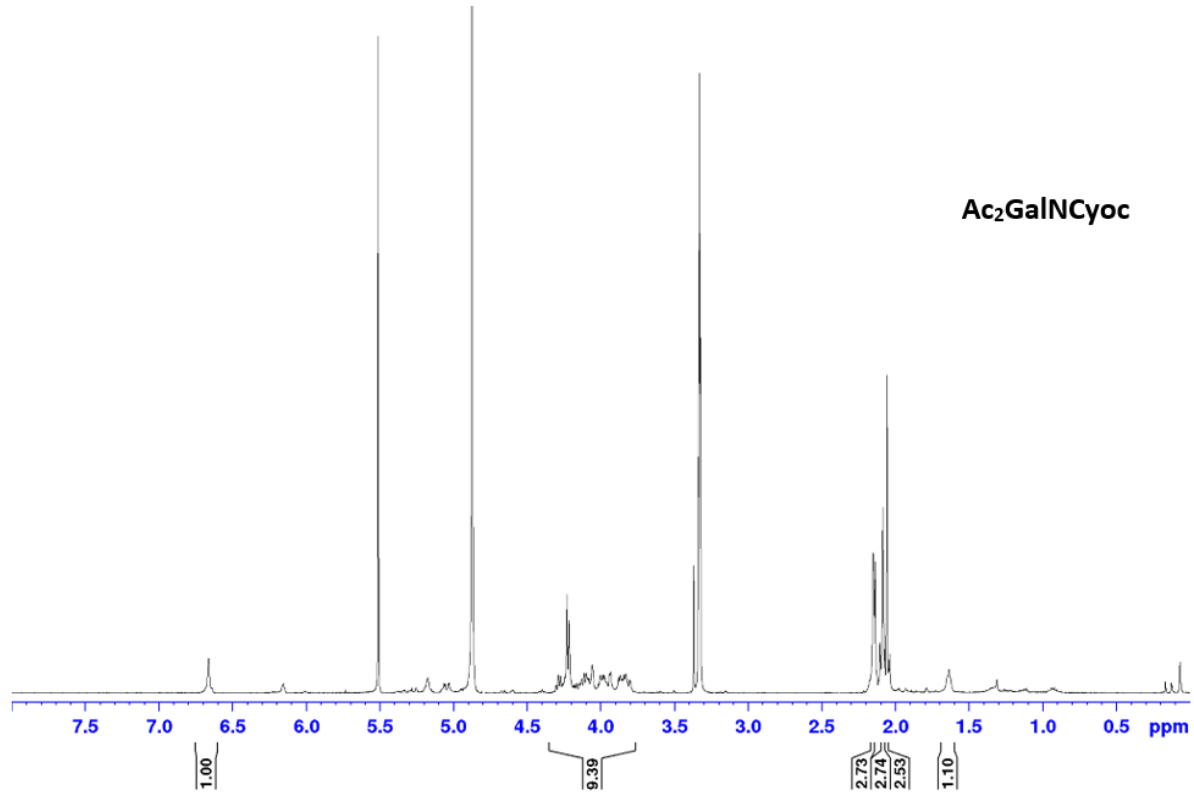
Ac2GalNCyoc
7.5 7.0 6.5 6.0 5.5 5.0 4.5 4.0 3.5 3.0 2.5 2.0 1.5 1.0 0.5 ppm
1.00
9.39
2.73
2.74
2.53
1.10

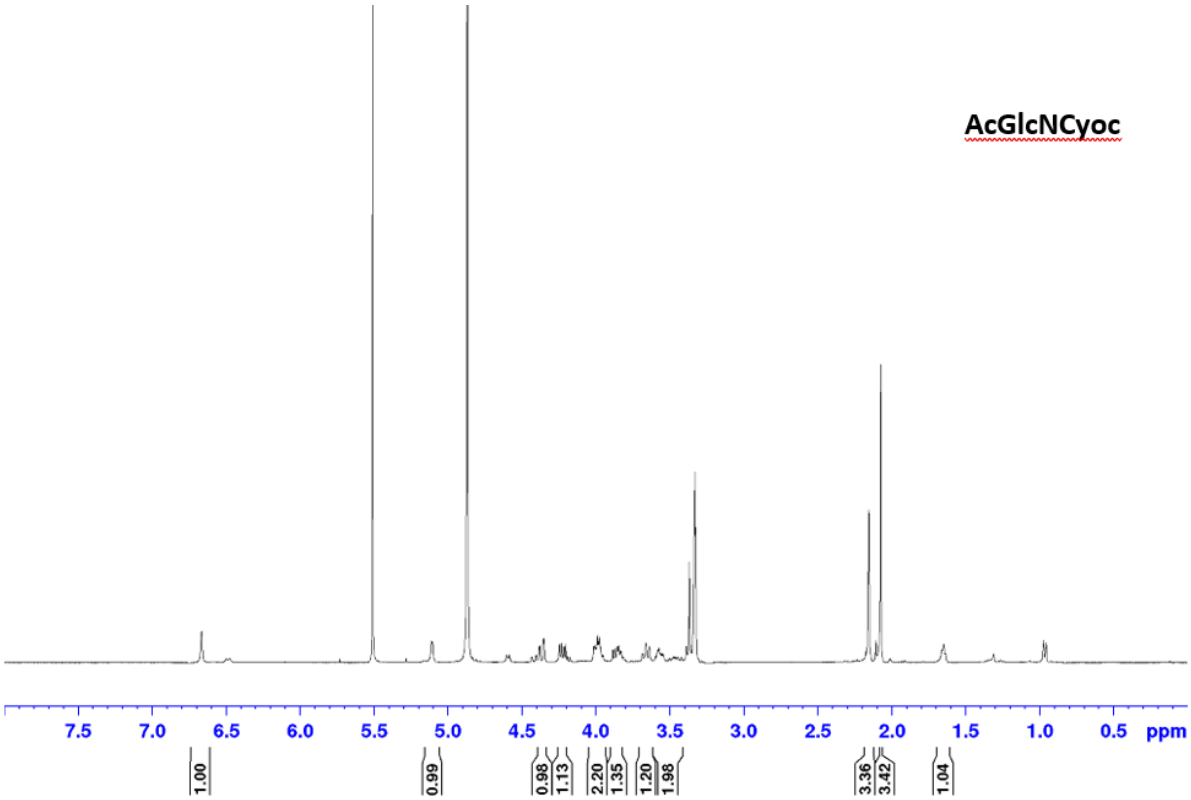
AcGlcNCyoc
7.5 7.0 6.5 6.0 5.5 5.0 4.5 4.0 3.5 3.0 2.5 2.0 1.5 1.0 0.5 ppm
1.00
0.99
0.98
1.13
2.20
1.35
1.20
1.98
3.36
3.42
1.04

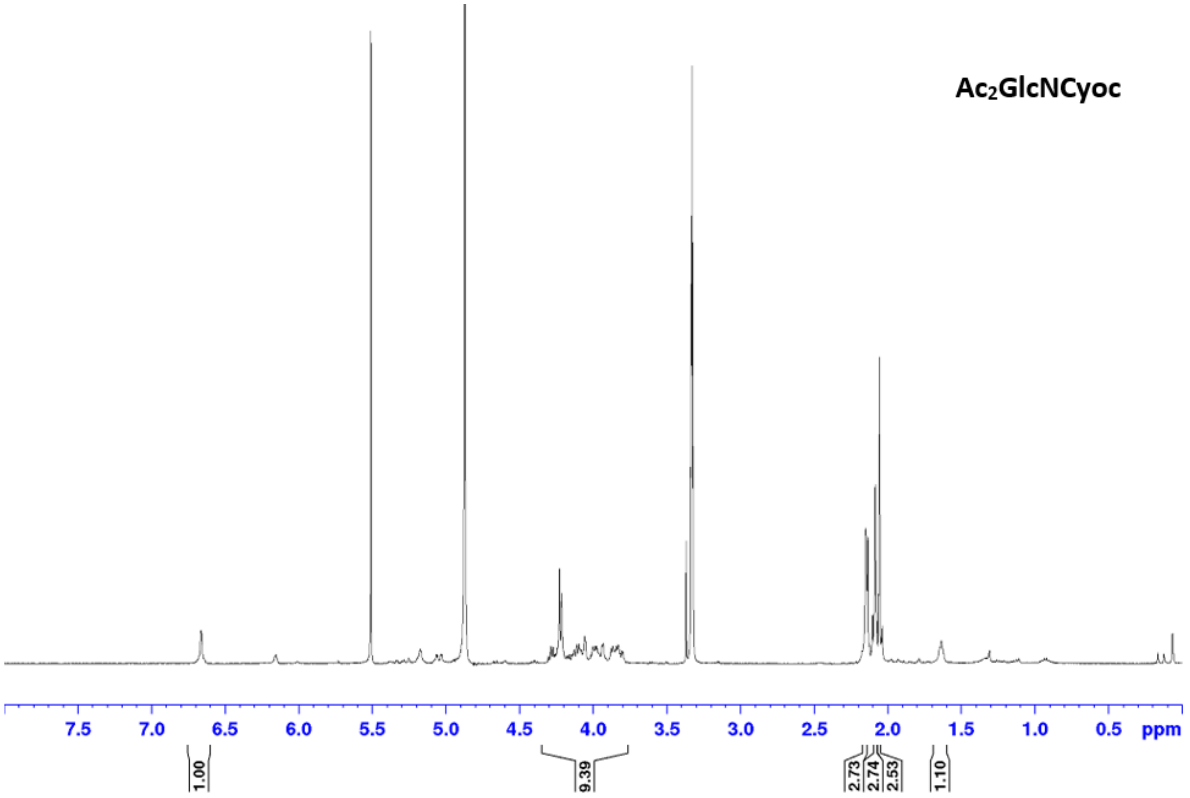
Ac2GlcNCyoc
7.5 7.0 6.5 6.0 5.5 5.0 4.5 4.0 3.5 3.0 2.5 2.0 1.5 1.0 0.5 ppm
1.00
9.39
2.73
2.74
2.53
1.10

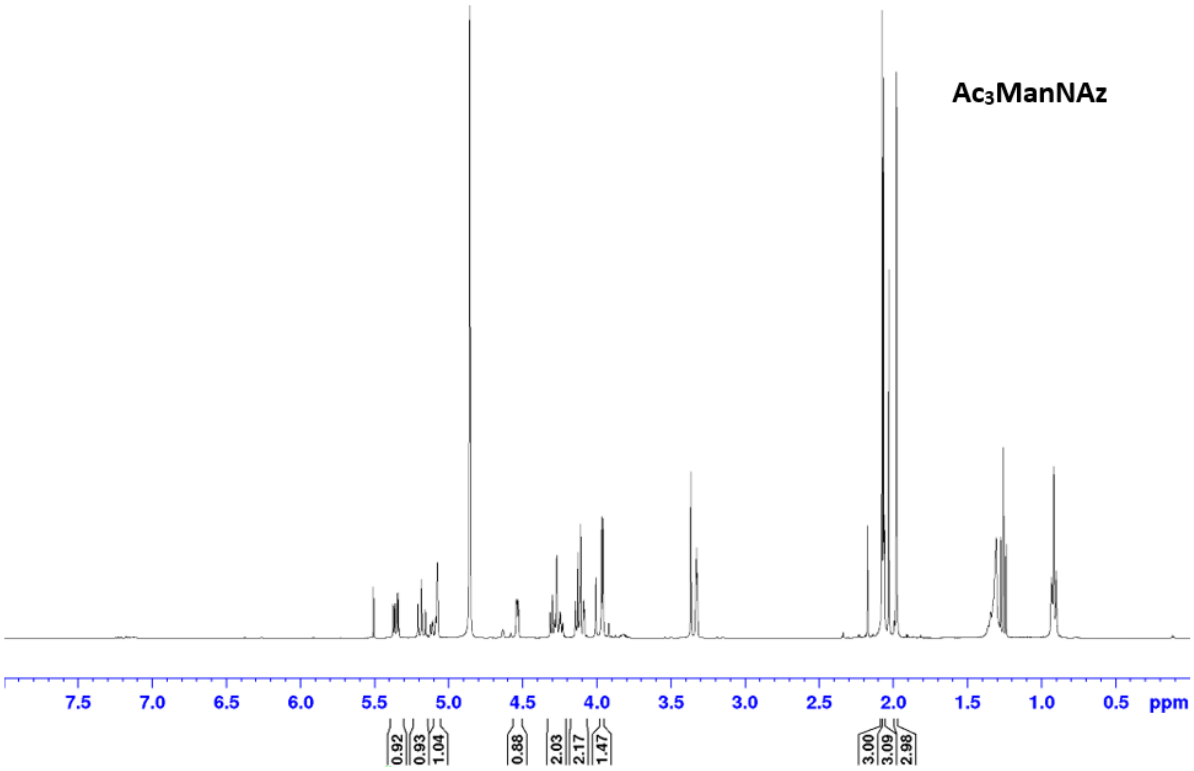
Ac3ManNAz
7.5
7.0
6.5
6.0
5.5
5.0
4.5
4.0
3.5
3.0
2.5
2.0
1.5
1.0
0.5
ppm
0.92
0.93
1.04
0.88
2.03
2.17
1.47
3.00
3.09
2.98

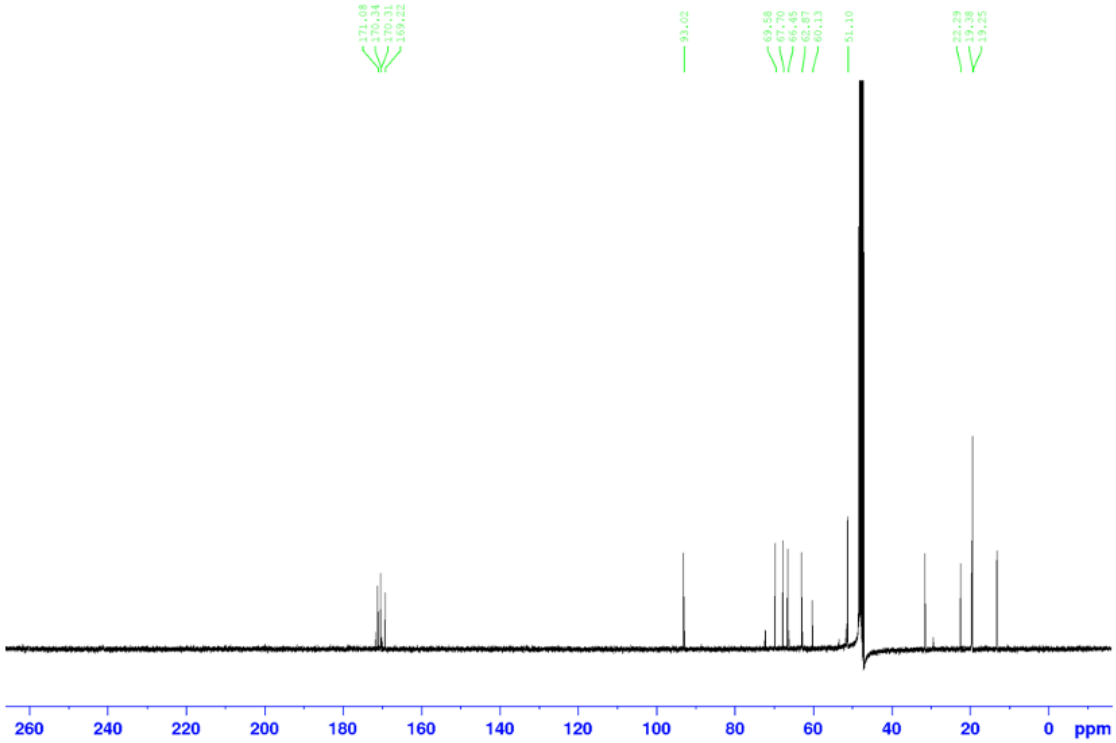
171.08
170.34
170.31
169.22
93.02
69.58
67.70
66.45
65.57
60.13
51.10
22.29
19.38
19.25
260
240
220
200
180
160
140
120
100
80
60
40
20
0
ppm

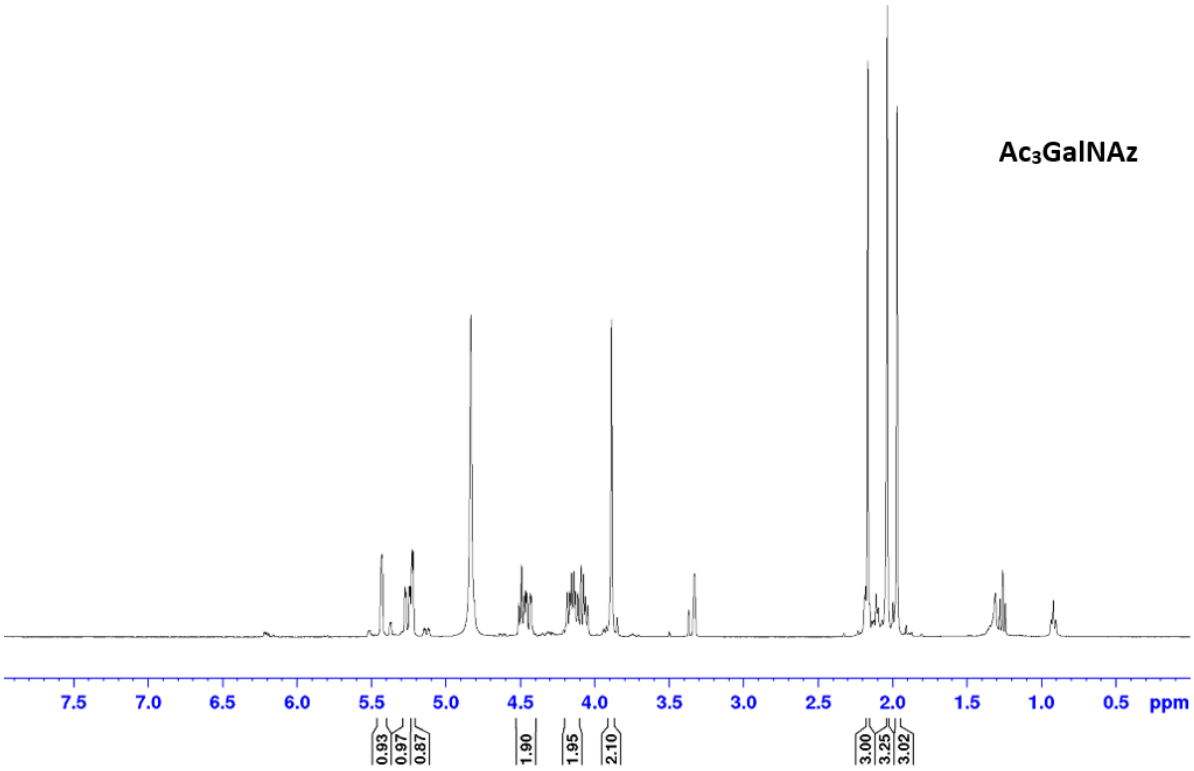
Ac3GalNAz
7.5
7.0
6.5
6.0
5.5
5.0
4.5
4.0
3.5
3.0
2.5
2.0
1.5
1.0
0.5
ppm
0.93
0.97
0.87
1.90
1.95
2.10
3.00
3.25
3.02

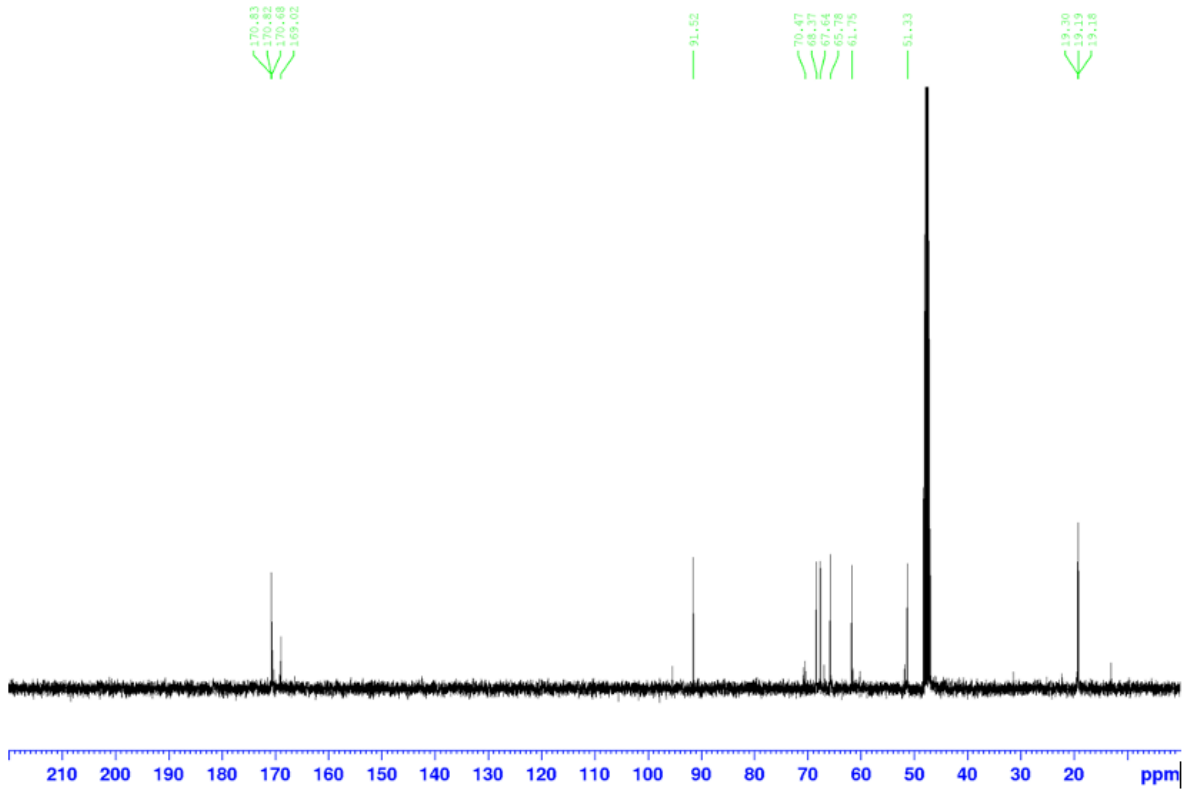
170.83
170.82
170.68
169.02
91.52
70.47
68.37
67.64
65.78
61.75
51.33
19.30
19.19
19.18
210
200
190
180
170
160
150
140
130
120
110
100
90
80
70
60
50
40
30
20
ppm

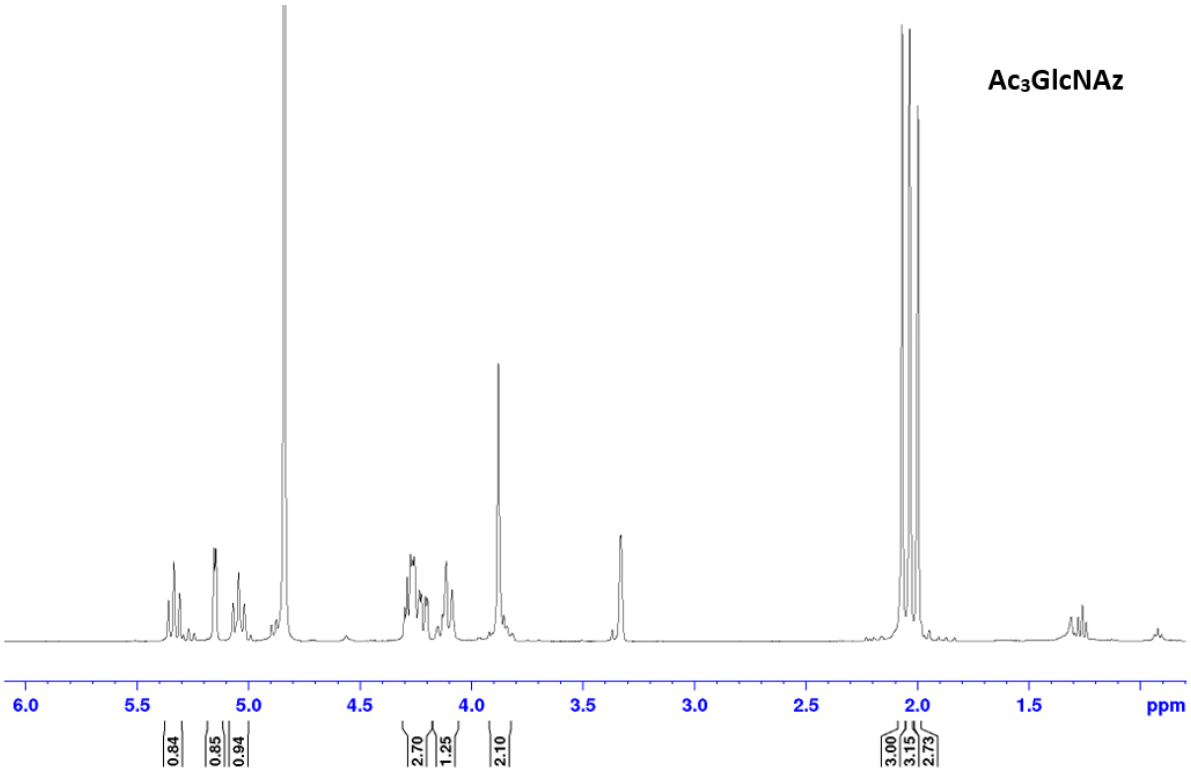
Ac3GlcNAz
6.0
5.5
5.0
4.5
4.0
3.5
3.0
2.5
2.0
1.5
ppm
0.84
0.85
0.94
2.70
1.25
2.10
3.00
3.15
2.73

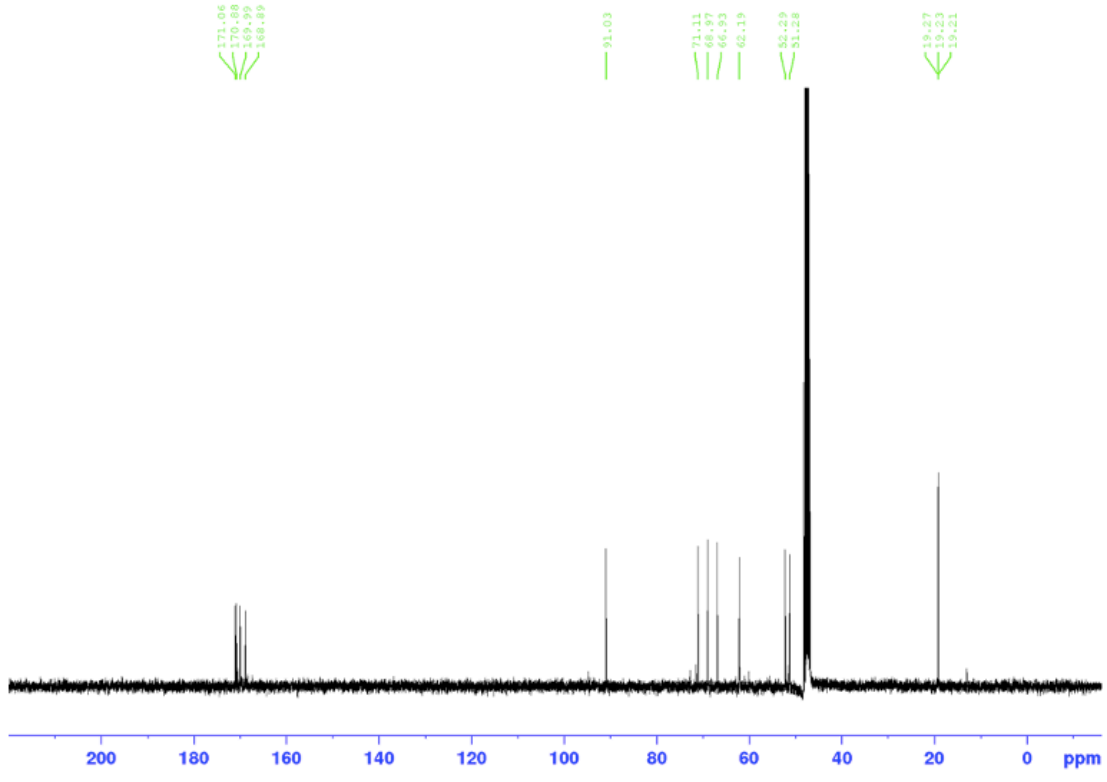
171.06
170.88
169.99
168.89
91.03
71.11
68.97
66.93
62.19
52.29
51.28
19.27
19.23
19.21
200
180
160
140
120
100
80
60
40
20
0
ppm

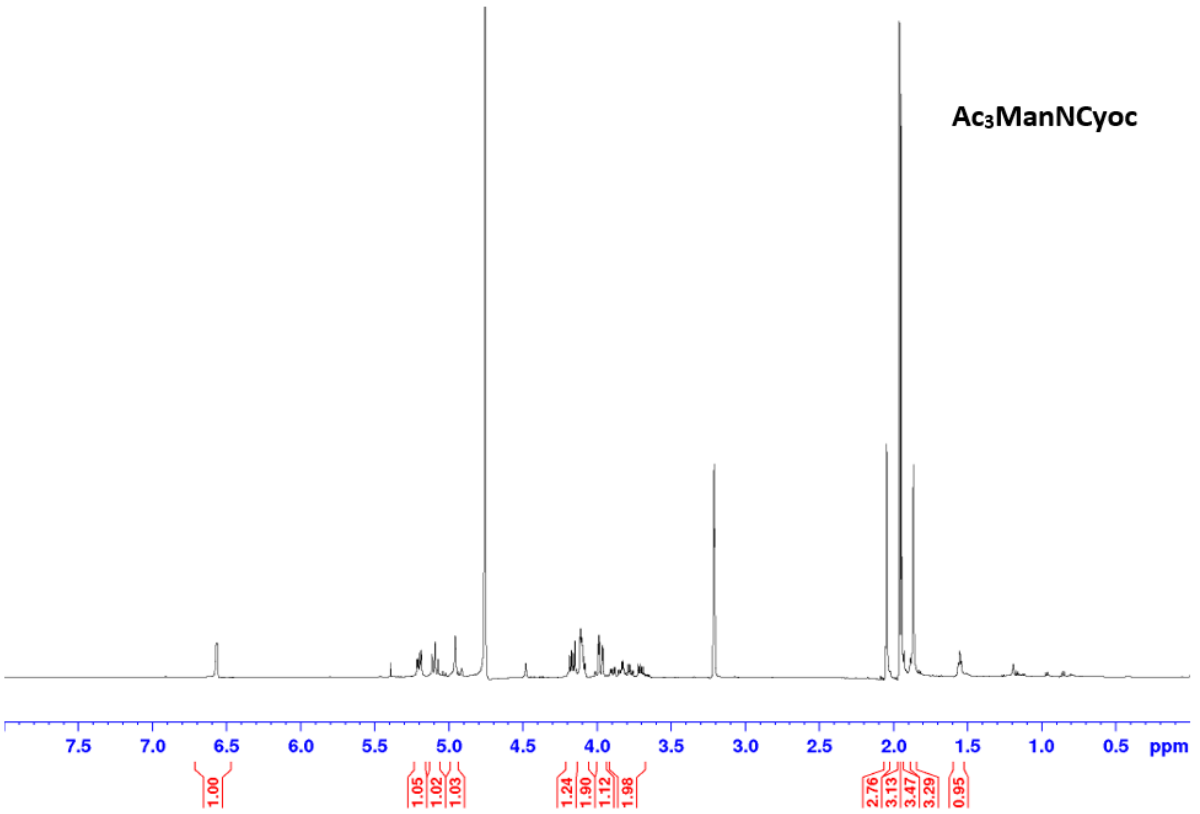
Ac3ManNCyoc
7.5 7.0 6.5 6.0 5.5 5.0 4.5 4.0 3.5 3.0 2.5 2.0 1.5 1.0 0.5 ppm
1.00 1.05 1.02 1.03 1.24 1.90 1.12 1.98 2.76 3.13 3.47 3.29 0.95

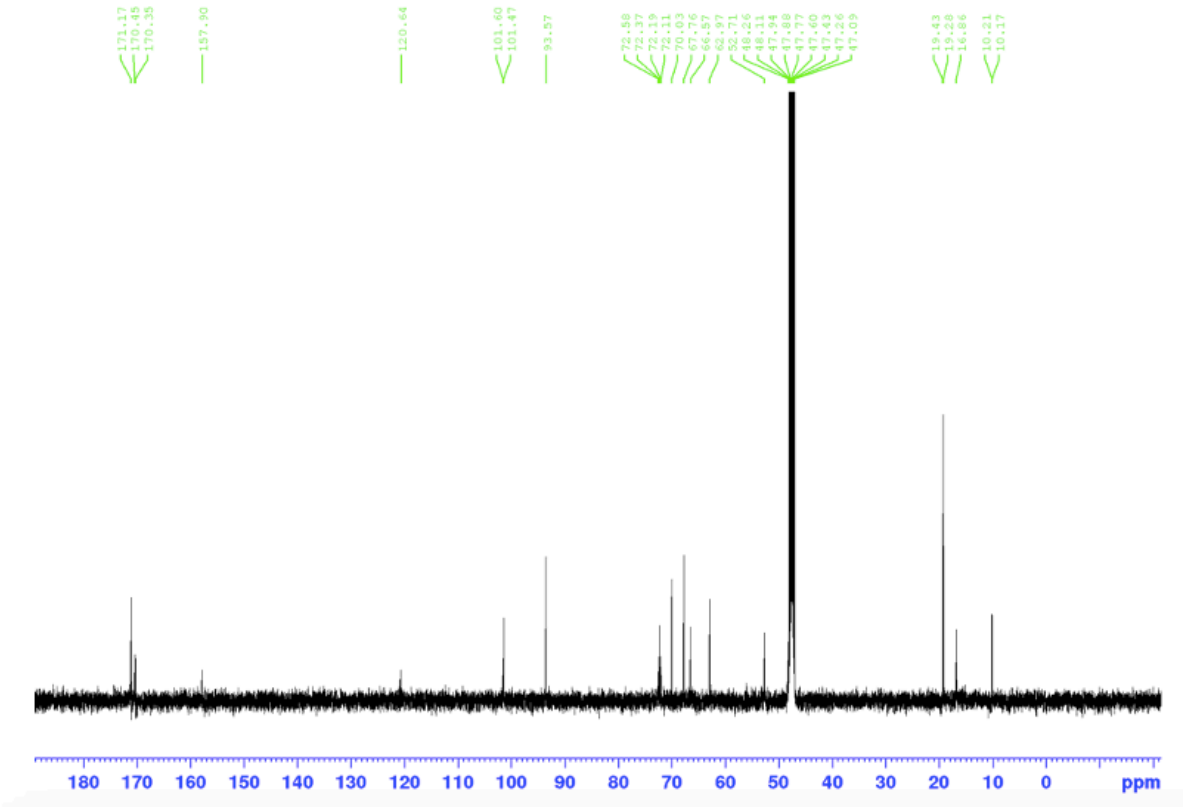
171.17 170.45 170.35 157.90 120.64 101.60 101.47 93.57 72.58 72.37 72.19 72.11 70.03 67.76 66.57 62.97 52.71 48.26 48.11 47.94 47.88 47.77 47.60 47.43 47.26 47.09 19.43 19.28 16.86 10.21 10.17
180 170 160 150 140 130 120 110 100 90 80 70 60 50 40 30 20 10 0 ppm

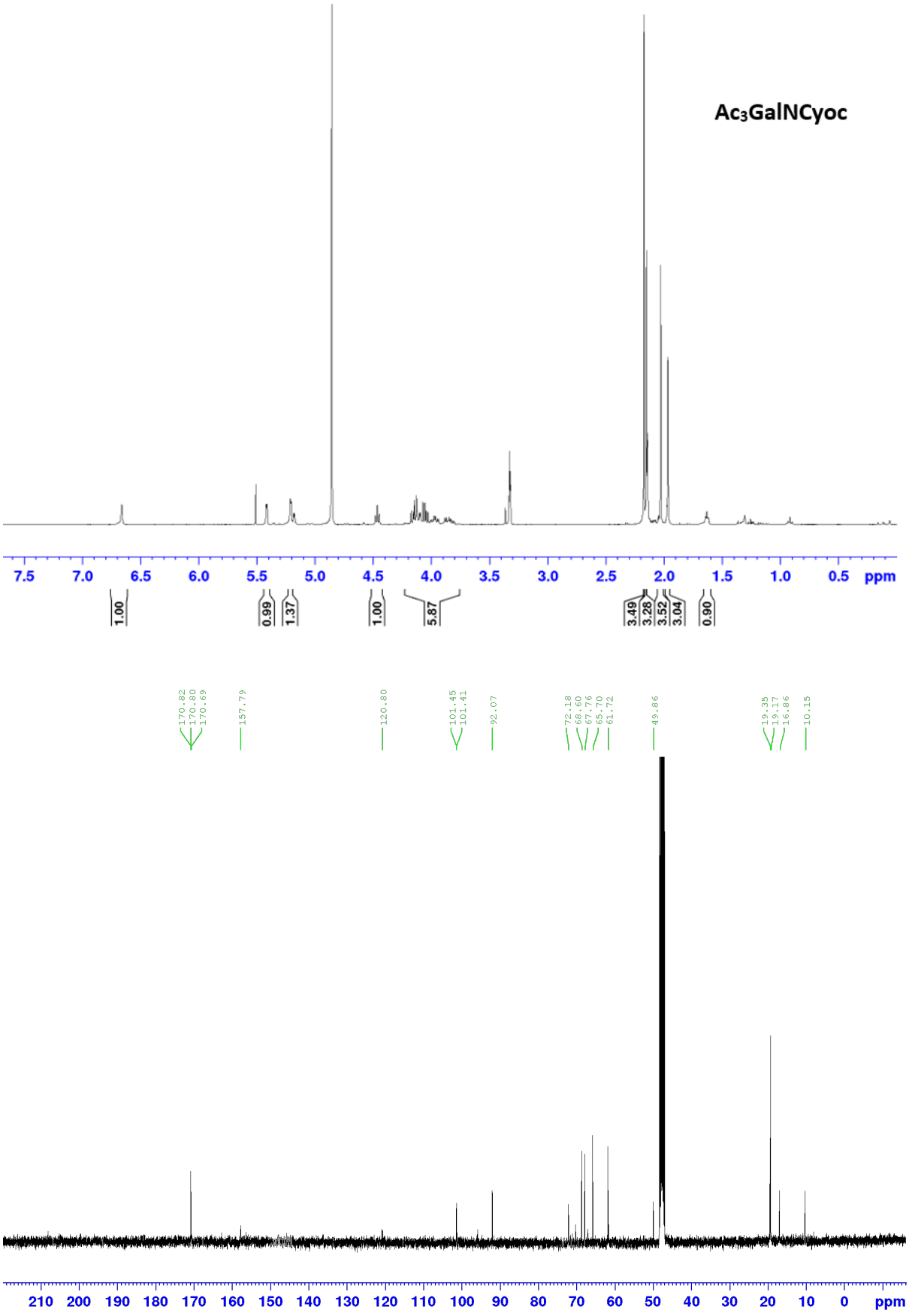
Ac3GalNCyoc
7.5 7.0 6.5 6.0 5.5 5.0 4.5 4.0 3.5 3.0 2.5 2.0 1.5 1.0 0.5 ppm
1.00 0.99 1.37 1.00 5.87 3.49 3.28 3.52 3.04 0.90
170.82 170.80 170.69 157.79 120.80 101.45 101.41 92.07 72.18 68.60 67.76 65.70 61.72 49.86 19.35 19.17 16.86 10.15
210 200 190 180 170 160 150 140 130 120 110 100 90 80 70 60 50 40 30 20 10 0 ppm

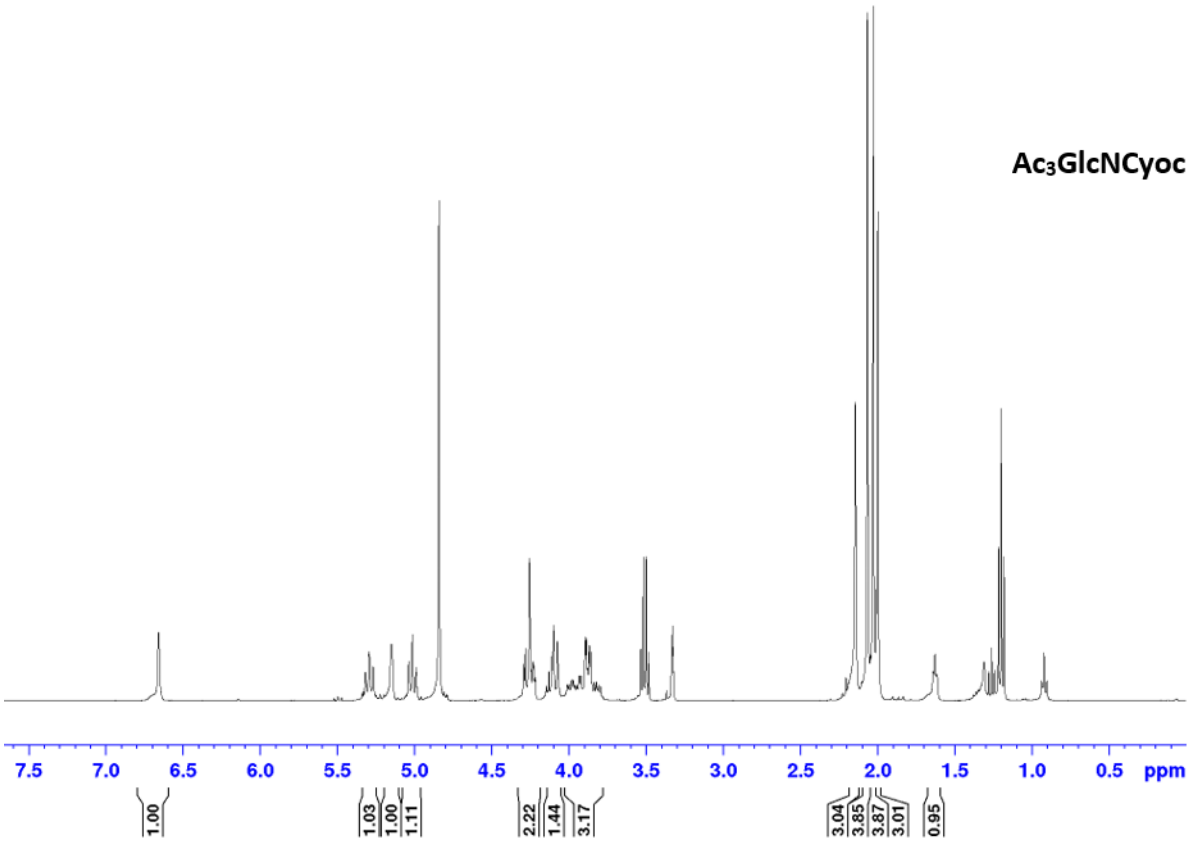
Ac3GlcNCyoc
7.5
7.0
6.5
6.0
5.5
5.0
4.5
4.0
3.5
3.0
2.5
2.0
1.5
1.0
0.5
ppm
1.00
1.03
1.00
1.11
2.22
1.44
3.17
3.04
3.85
3.87
3.01
0.95

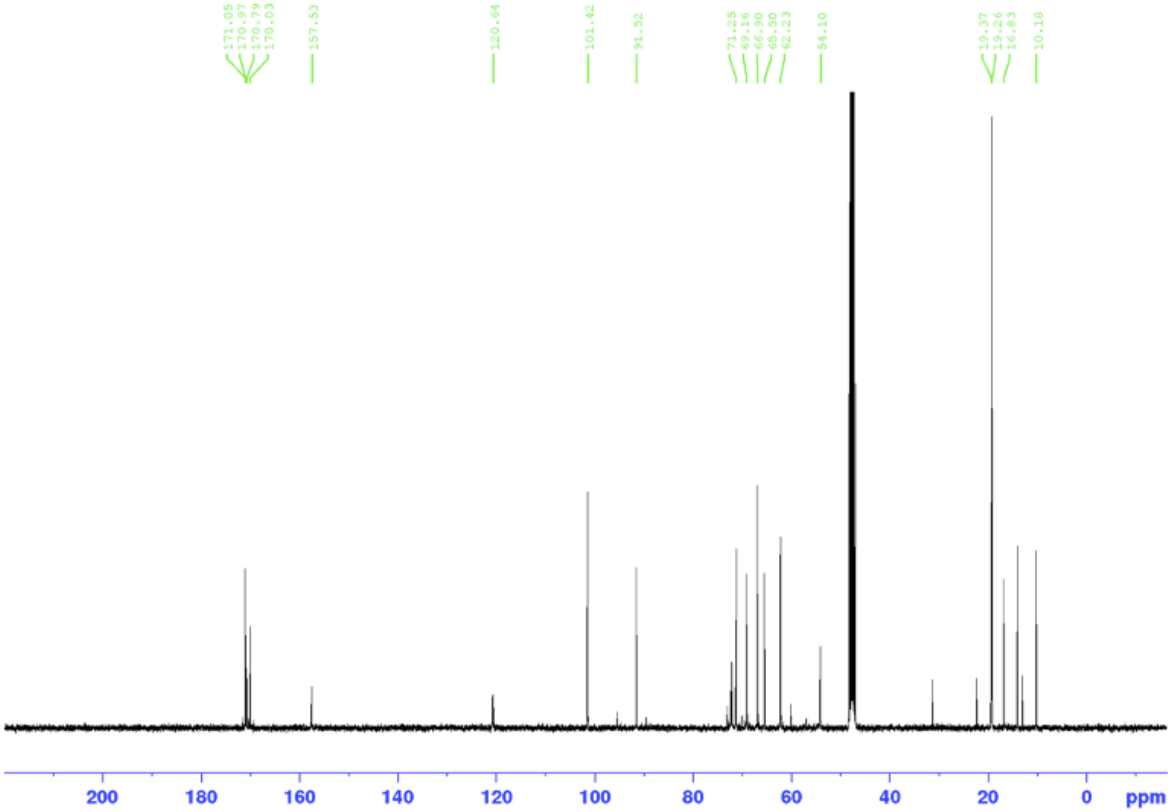
171.05
170.97
170.79
170.03
157.53
120.64
101.42
91.52
71.25
69.16
66.90
65.90
62.23
54.10
19.37
19.26
16.83
10.18
200
180
160
140
120
100
80
60
40
20
0
ppm

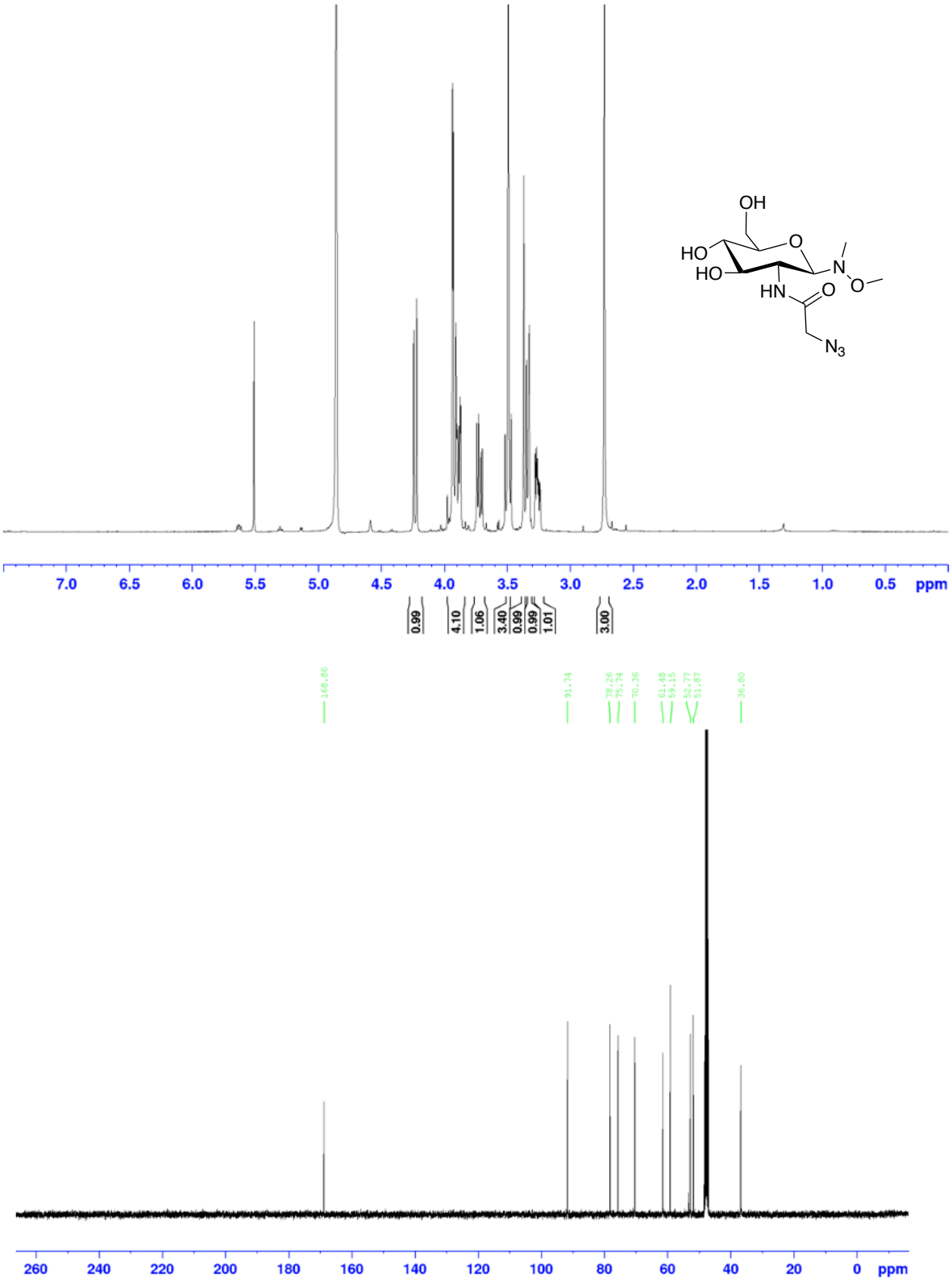
OH
HO
HO
O
N
O
HN
O
N3
7.0
6.5
6.0
5.5
5.0
4.5
4.0
3.5
3.0
2.5
2.0
1.5
1.0
0.5
ppm
0.99
4.10
1.06
3.40
0.99
0.99
1.01
3.00
168.86
91.74
78.26
75.74
70.36
61.48
59.15
52.77
51.87
36.80
260
240
220
200
180
160
140
120
100
80
60
40
20
0
ppm

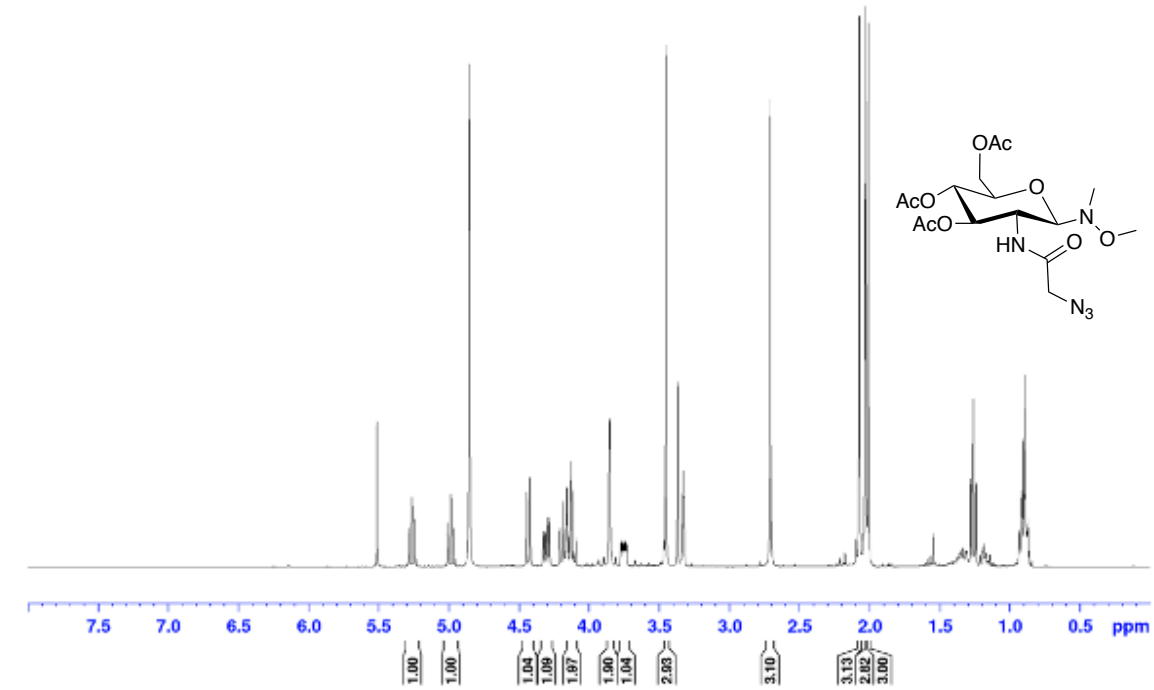
OAc
AcO
AcO
O
N
O
HN
O
N3
7.5 7.0 6.5 6.0 5.5 5.0 4.5 4.0 3.5 3.0 2.5 2.0 1.5 1.0 0.5 ppm
1.00 1.00 1.04 1.08 1.07 1.90 1.04 2.03 3.10 3.13 2.02 3.00

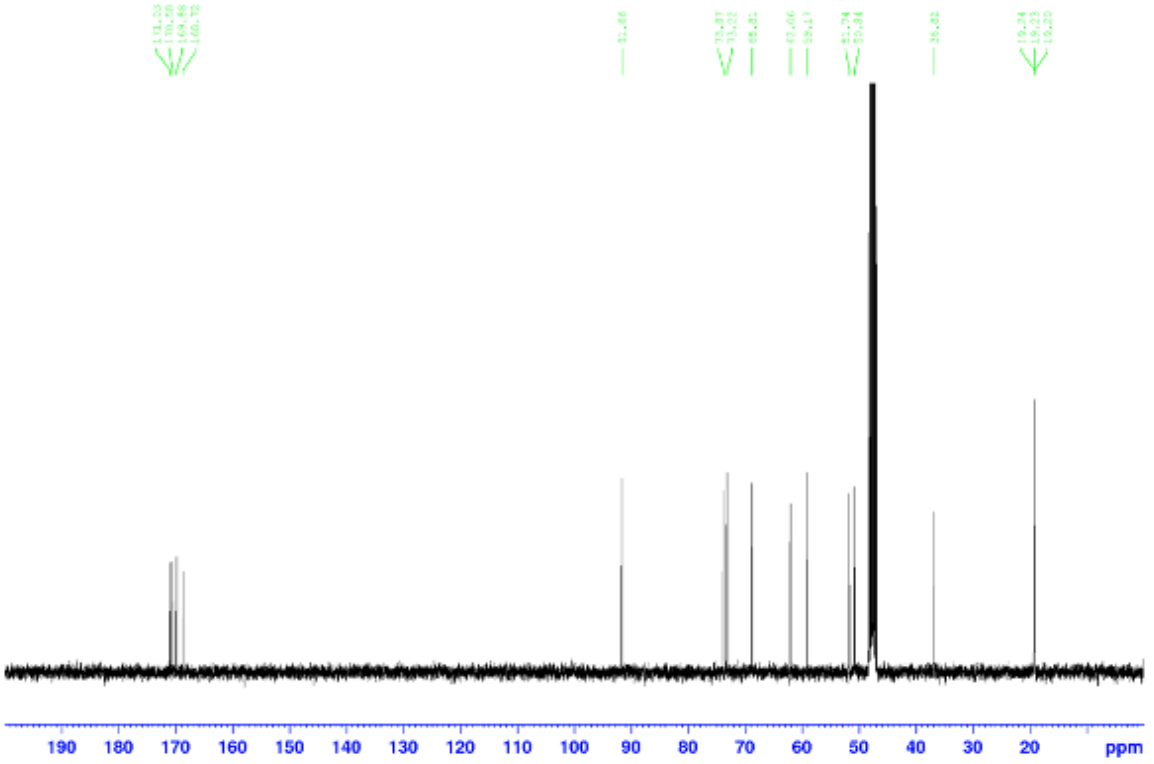
190 180 170 160 150 140 130 120 110 100 90 80 70 60 50 40 30 20 ppm

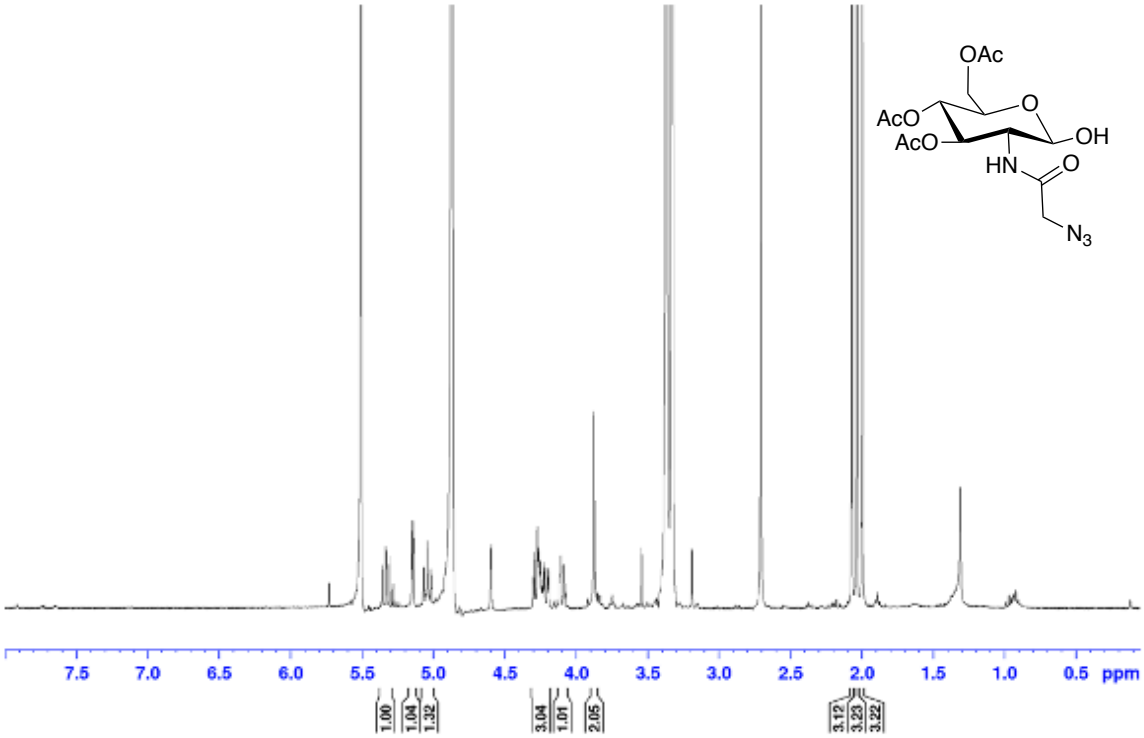
OAc
AcO
AcO
O
OH
HN
O
N3
7.5
7.0
6.5
6.0
5.5
5.0
4.5
4.0
3.5
3.0
2.5
2.0
1.5
1.0
0.5
ppm
1.00
1.04
1.32
3.04
1.01
2.05
3.12
3.23
3.22

ODIBO NMR

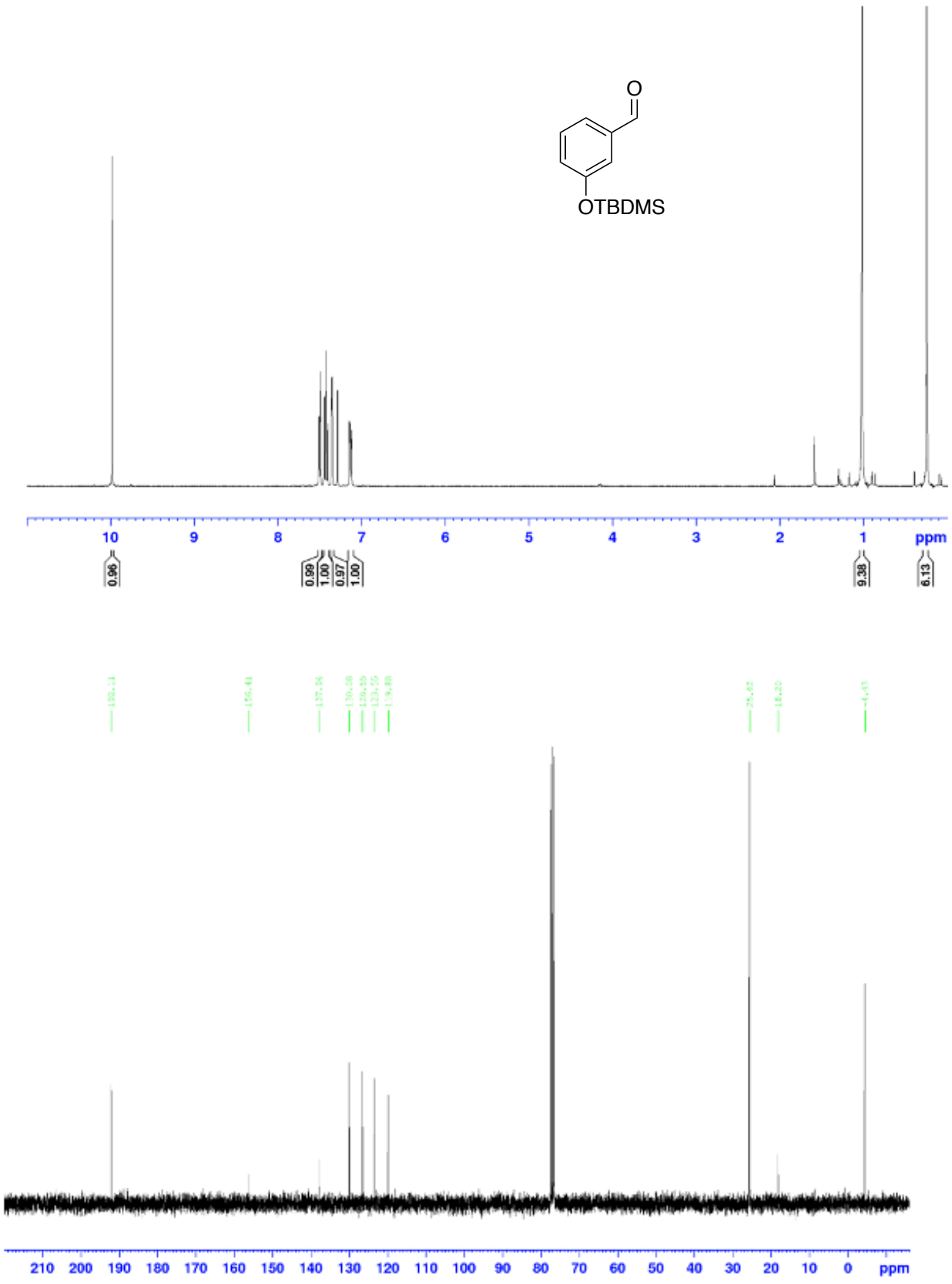
O
OTBDMS
10
9
8
7
6
5
4
3
2
1
ppm
0.96
0.99
1.00
0.97
1.00
9.38
6.13
210
200
190
180
170
160
150
140
130
120
110
100
90
80
70
60
50
40
30
20
10
0
ppm

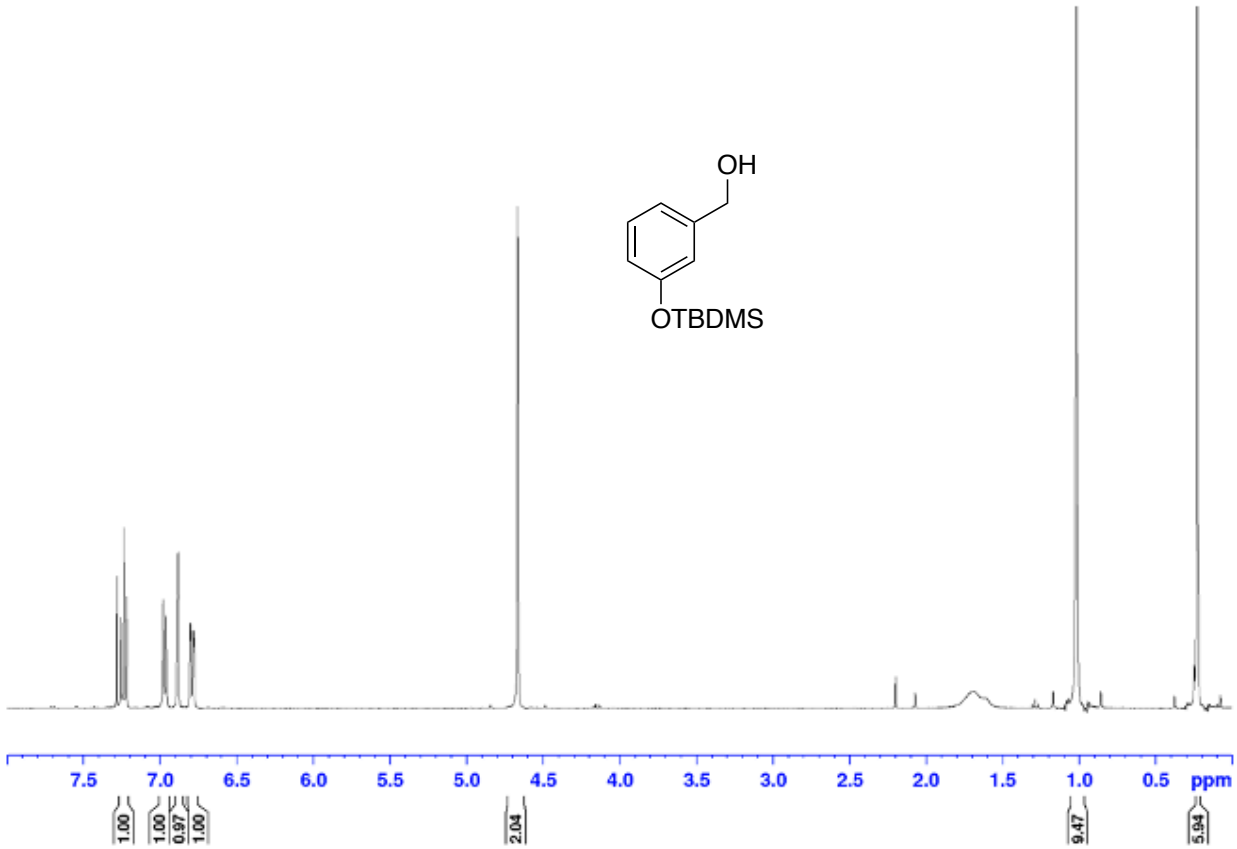
OH
OTBDMS
7.5
7.0
6.5
6.0
5.5
5.0
4.5
4.0
3.5
3.0
2.5
2.0
1.5
1.0
0.5
ppm
1.00
1.00
0.97
1.00
2.04
9.47
5.94

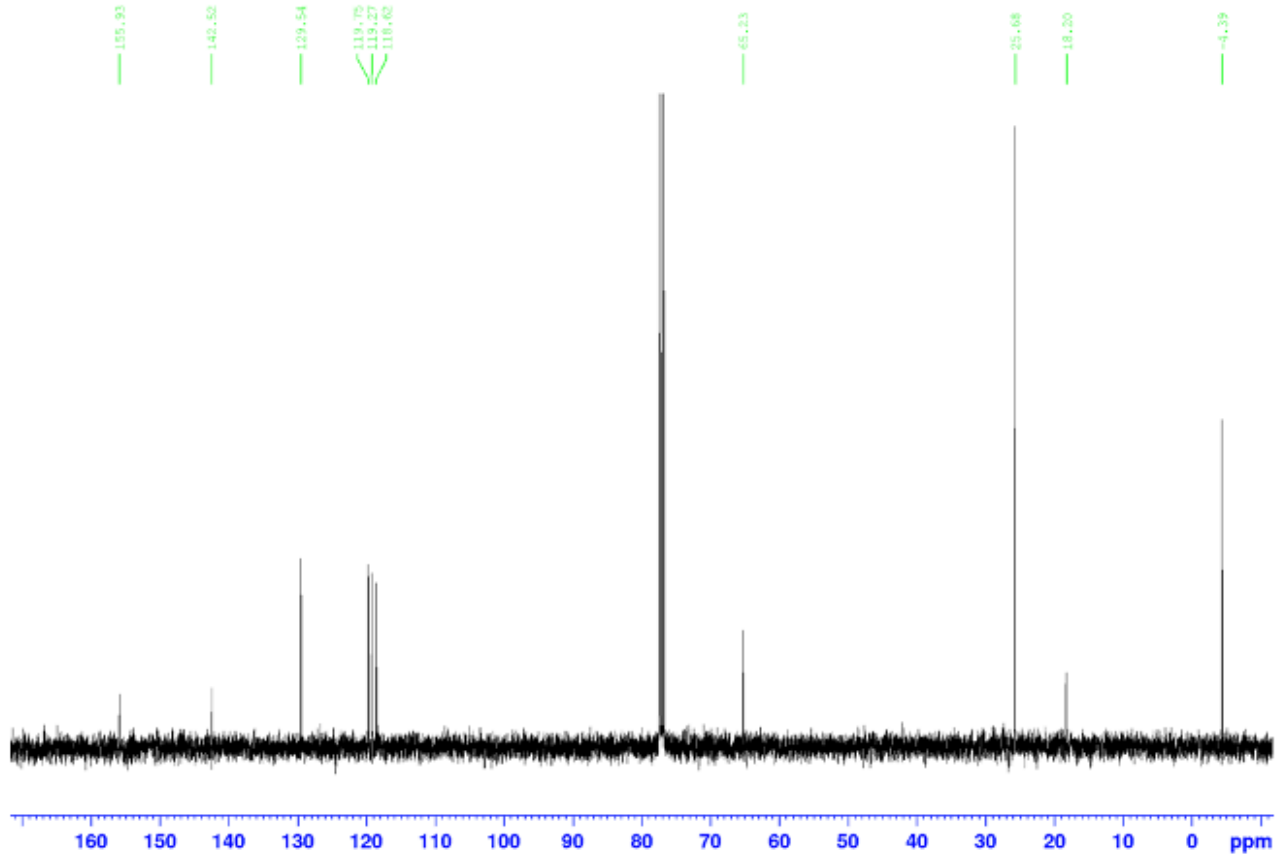
155.93
142.52
129.54
119.79
119.27
118.62
65.23
25.68
18.20
-4.39
160
150
140
130
120
110
100
90
80
70
60
50
40
30
20
10
0
ppm

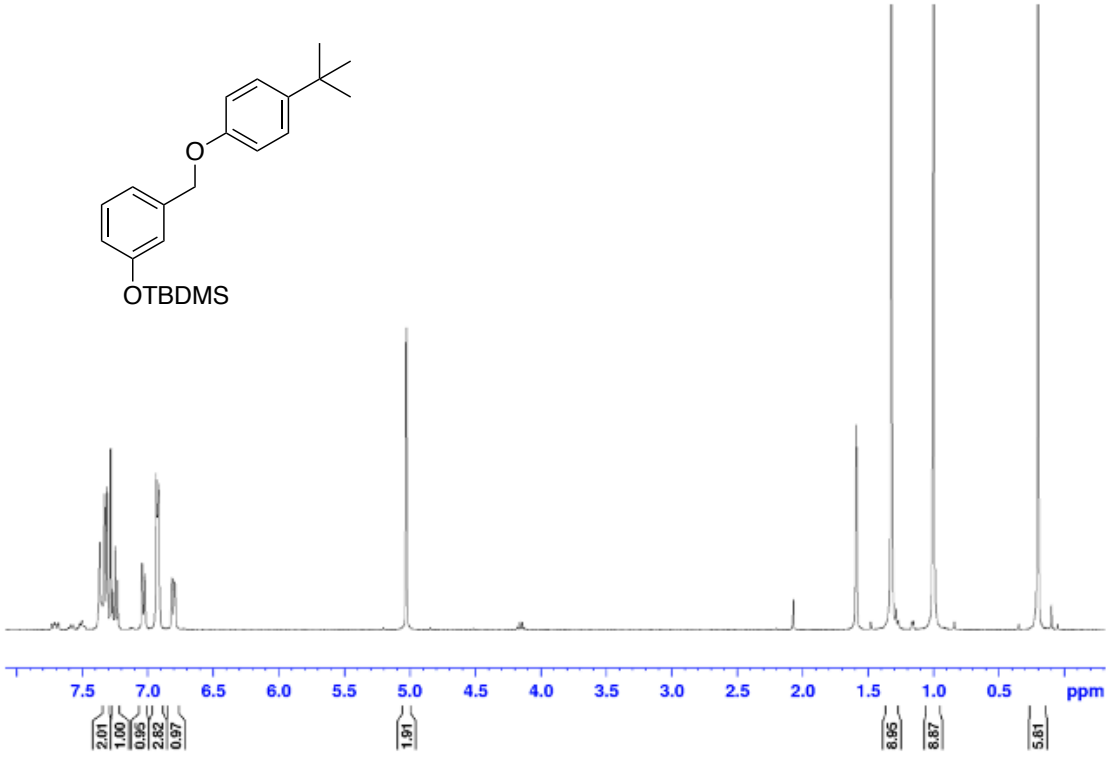
O
OTBDMS
7.5
7.0
6.5
6.0
5.5
5.0
4.5
4.0
3.5
3.0
2.5
2.0
1.5
1.0
0.5
ppm
2.01
1.00
0.95
2.82
0.97
1.91
6.95
6.87
5.81

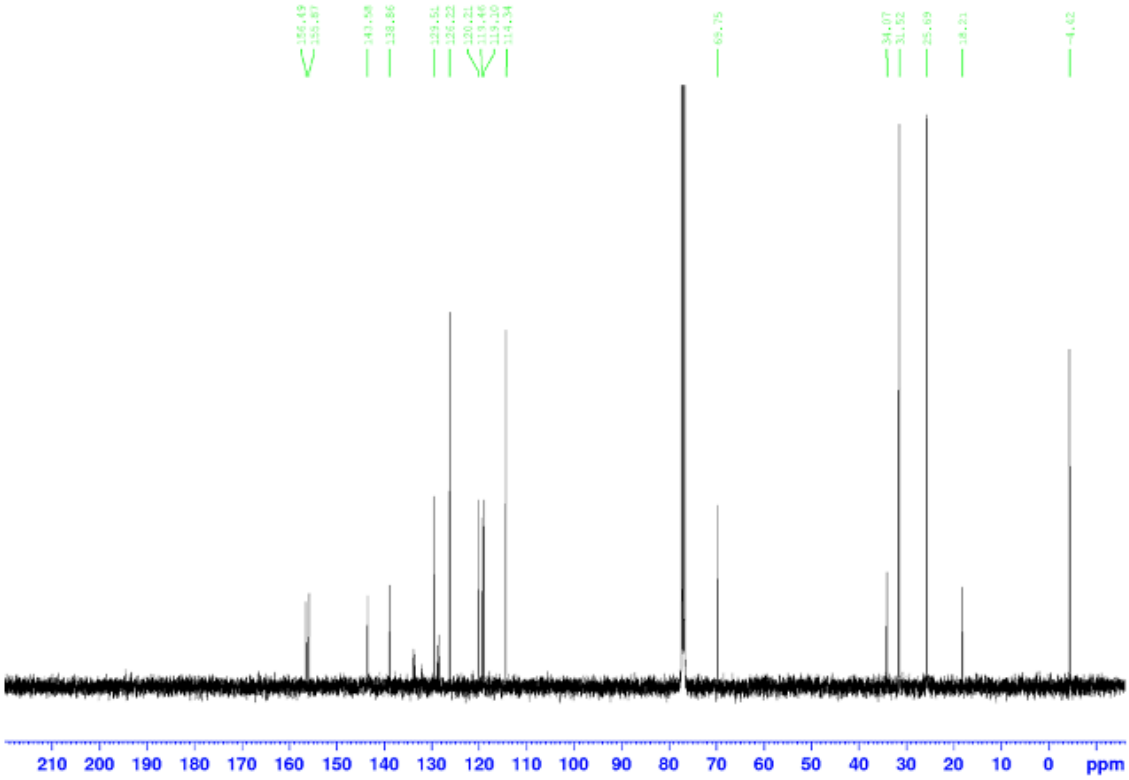
210
200
190
180
170
160
150
140
130
120
110
100
90
80
70
60
50
40
30
20
10
0
ppm

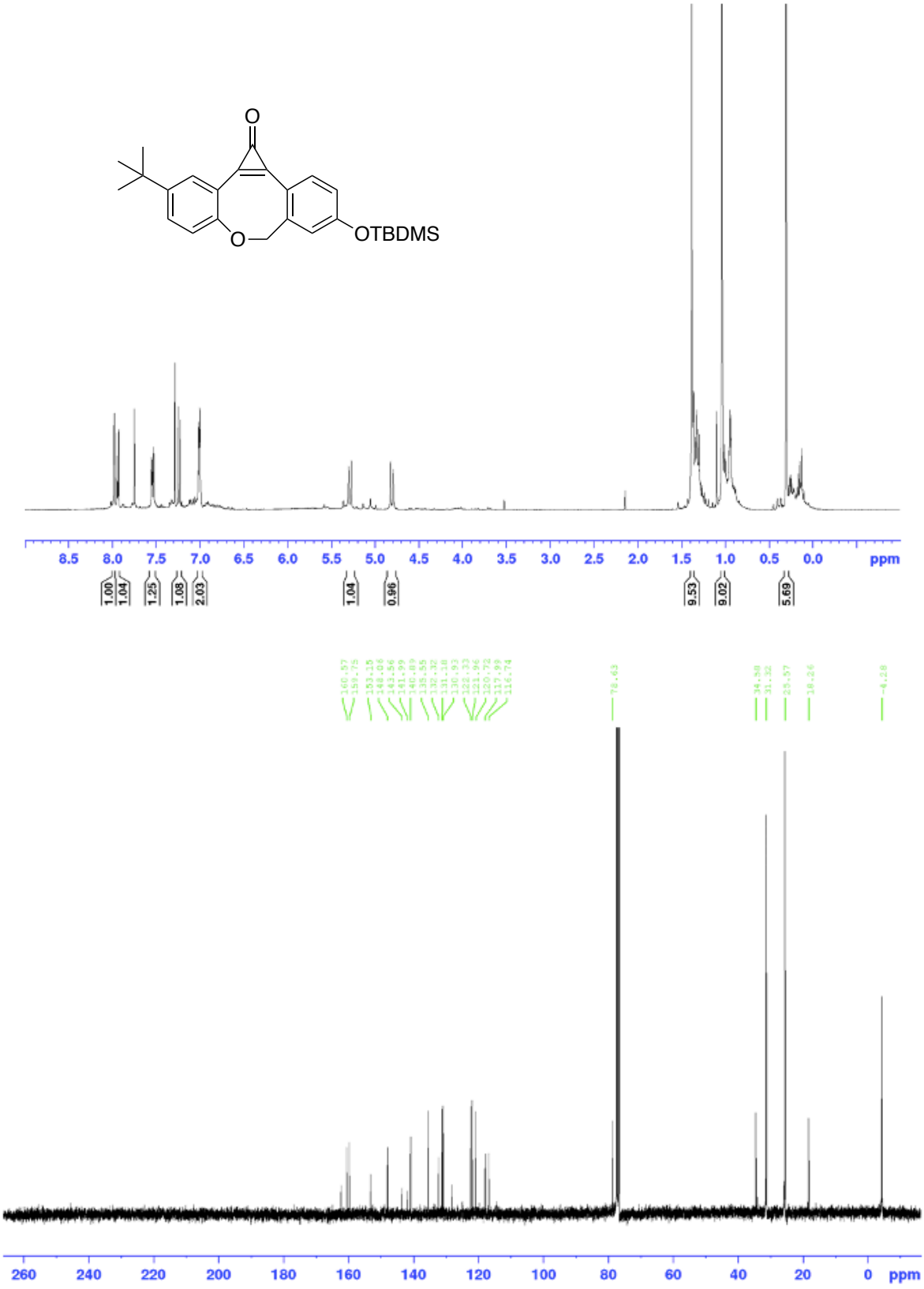
O
O
OTBDMS
8.5 8.0 7.5 7.0 6.5 6.0 5.5 5.0 4.5 4.0 3.5 3.0 2.5 2.0 1.5 1.0 0.5 0.0 ppm
1.00 1.04 1.25 1.08 2.03 1.04 0.96 9.53 9.02 5.69
160.57 159.75 153.15 148.06 143.56 141.99 140.09 135.55 132.32 131.18 130.93 122.33 121.96 120.72 117.98 116.74 78.43 34.30 31.32 25.57 18.26 -4.28
260 240 220 200 180 160 140 120 100 80 60 40 20 0 ppm

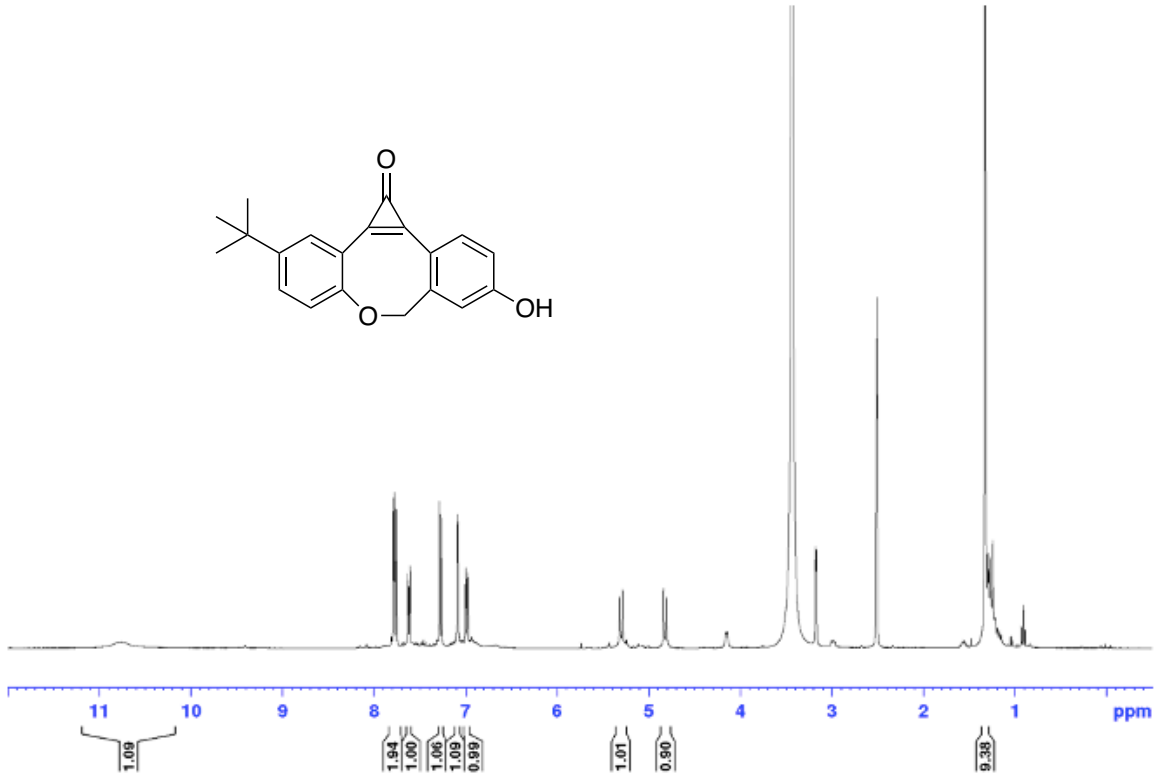
O
O
OH
11
10
9
8
7
6
5
4
3
2
1
ppm
1.09
1.94
1.00
1.06
1.09
0.99
1.01
0.90
9.38

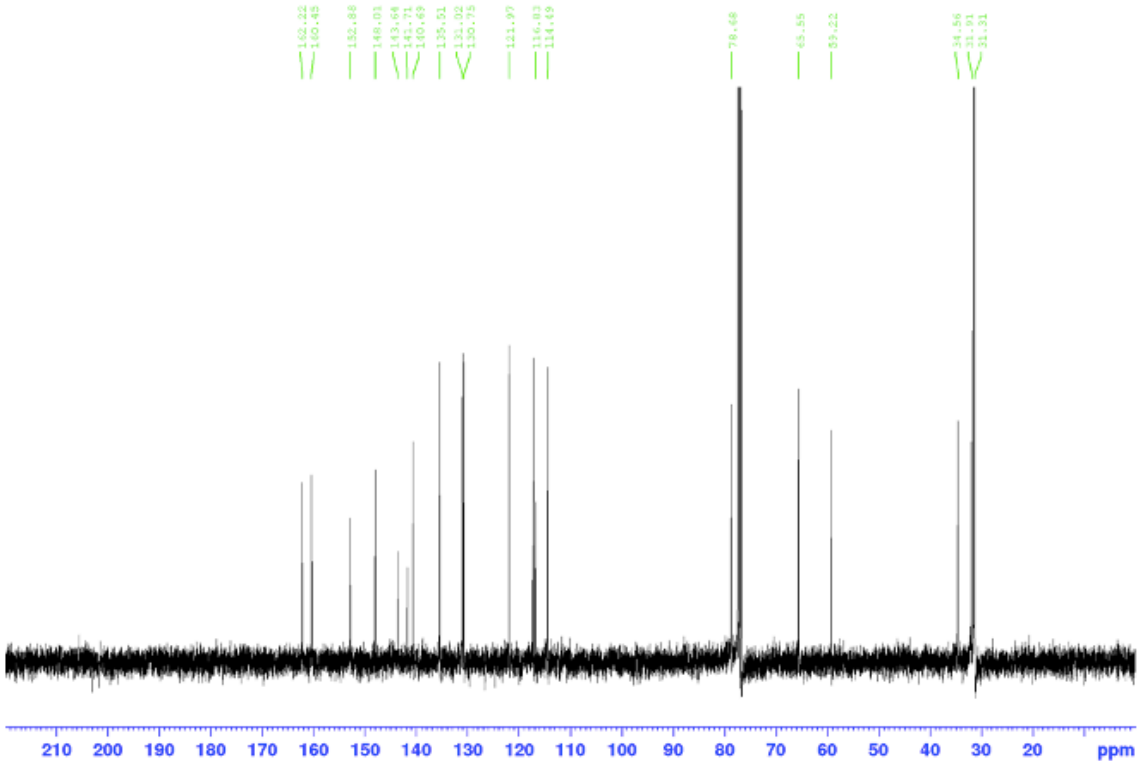
160.22
160.48
152.88
148.01
143.64
143.71
140.49
135.51
131.02
130.73
121.97
116.83
114.49
78.48
65.55
59.22
34.56
31.91
31.31
210
200
190
180
170
160
150
140
130
120
110
100
90
80
70
60
50
40
30
20
ppm

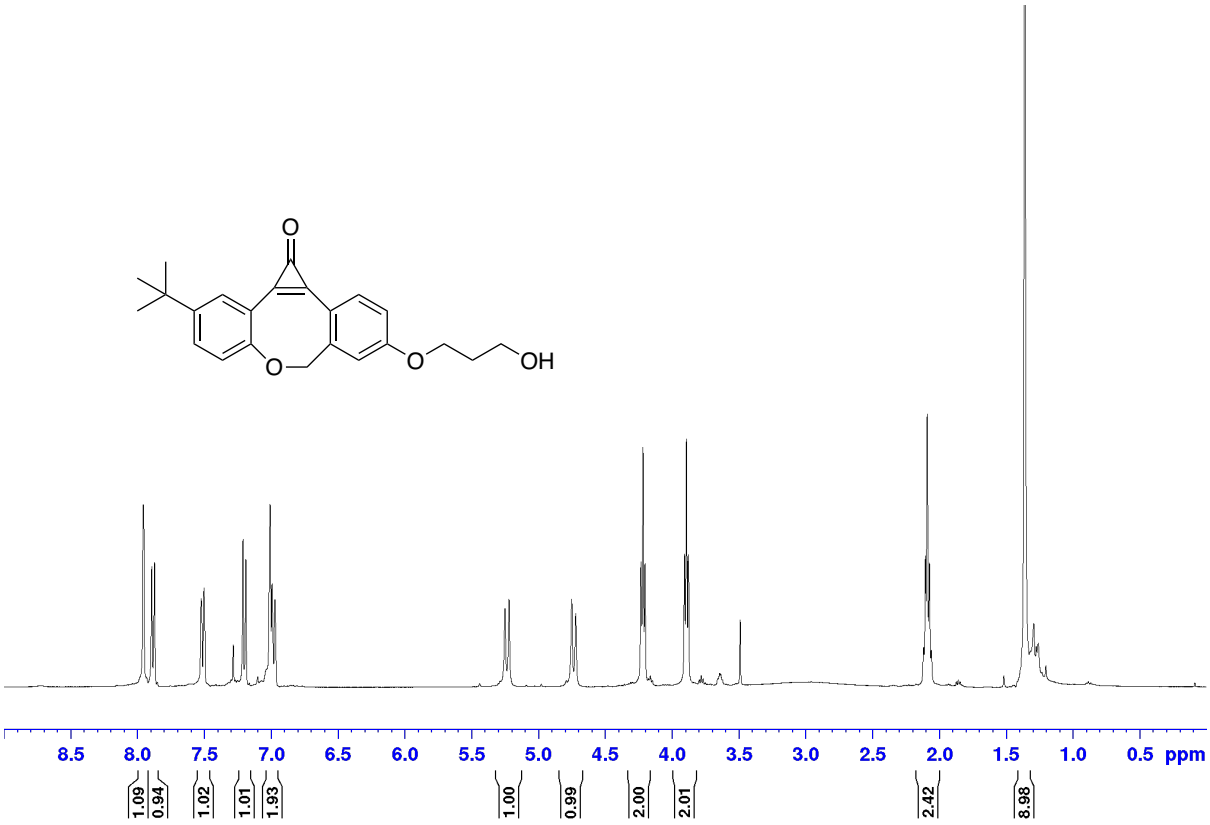
O
O
O
OH
8.5 8.0 7.5 7.0 6.5 6.0 5.5 5.0 4.5 4.0 3.5 3.0 2.5 2.0 1.5 1.0 0.5 ppm
1.09 0.94 1.02 1.01 1.93 1.00 0.99 2.00 2.01 2.42 8.98

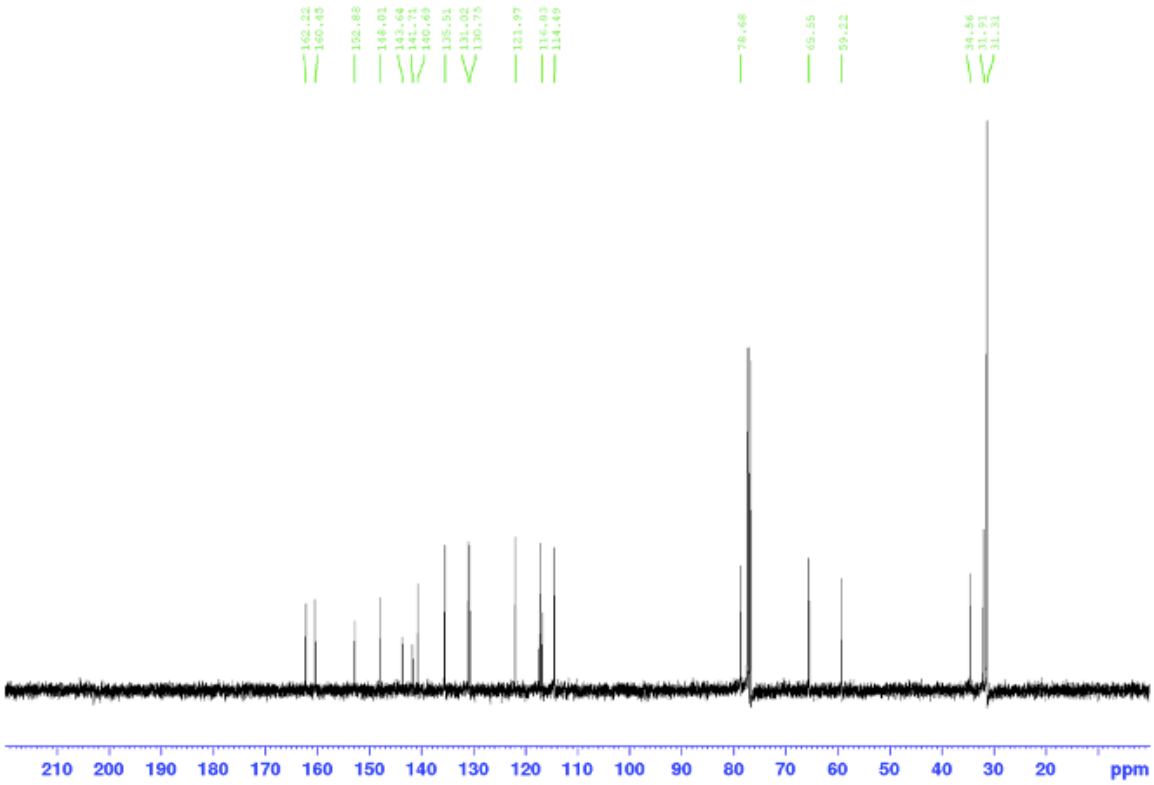
162.22
160.45
152.88
148.01
143.64
141.71
140.69
135.51
131.02
130.75
121.97
116.83
114.49
78.68
65.55
59.22
34.56
31.91
31.31
210 200 190 180 170 160 150 140 130 120 110 100 90 80 70 60 50 40 30 20 ppm

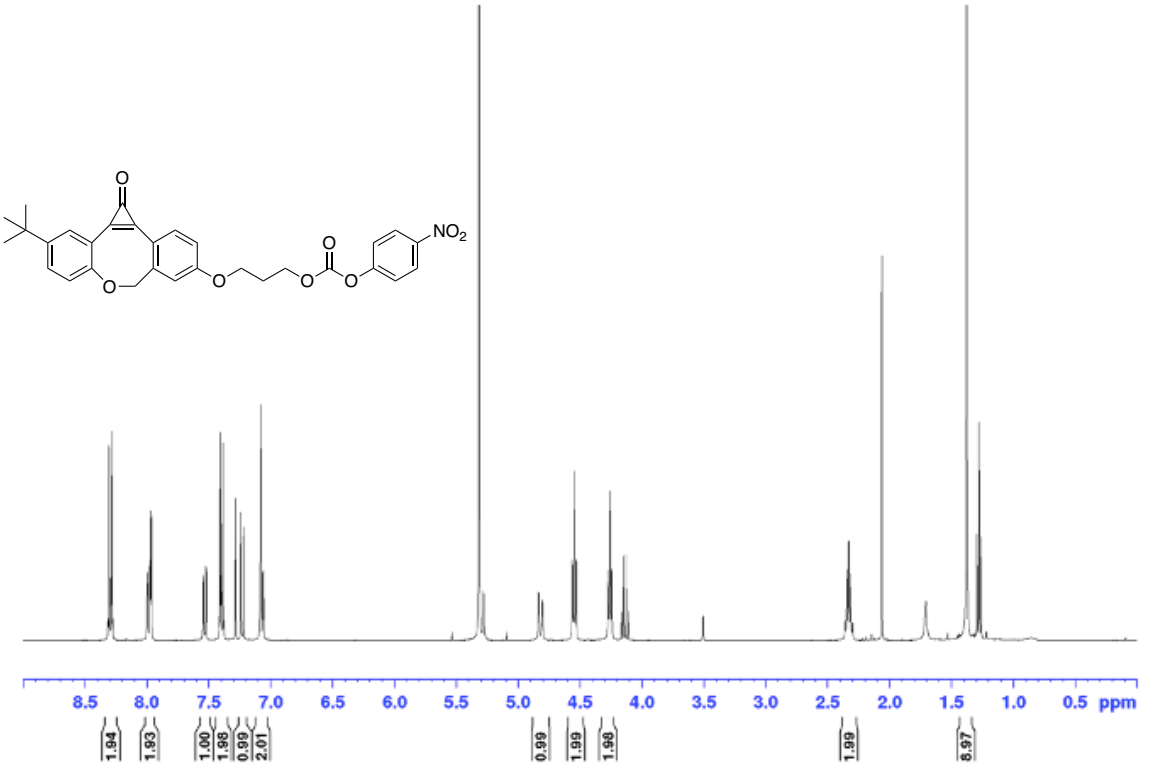
O
O
O
O
O
O
O
NO2
8.5
8.0
7.5
7.0
6.5
6.0
5.5
5.0
4.5
4.0
3.5
3.0
2.5
2.0
1.5
1.0
0.5
ppm
1.94
1.93
1.00
1.98
0.99
2.01
0.99
1.99
1.90
1.99
5.97

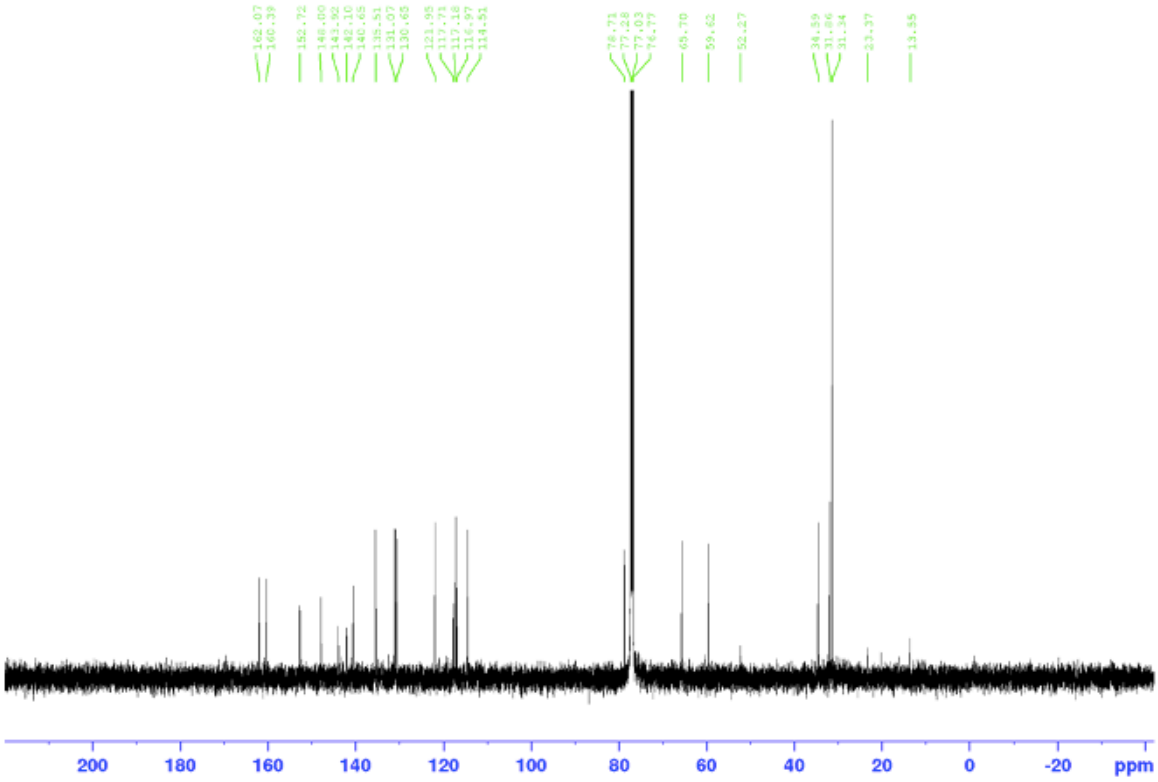
162.07
160.39
152.72
146.00
143.92
142.10
140.65
135.51
131.07
130.63
123.95
119.71
117.18
116.97
114.51
76.71
77.28
77.03
76.77
69.70
59.62
52.27
34.59
31.86
31.34
23.37
13.55
200
180
160
140
120
100
80
60
40
20
0
-20
ppm

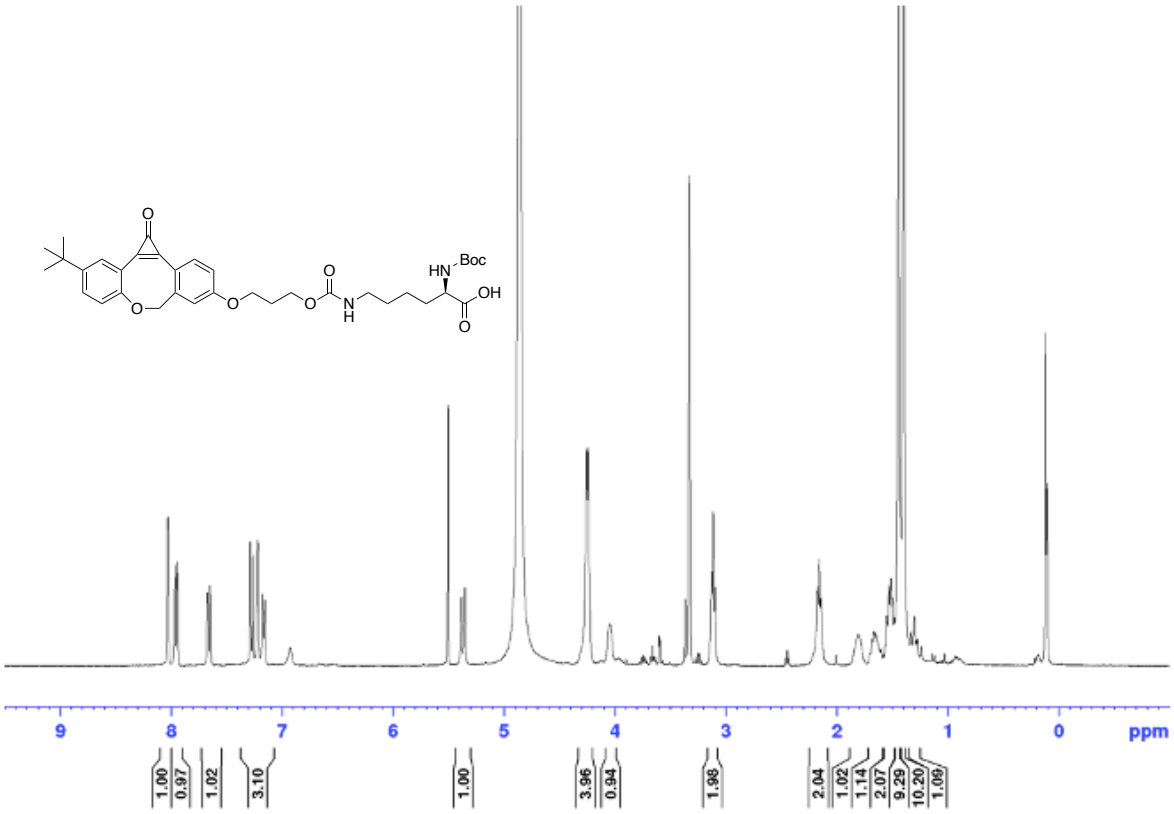
O
O
O
O
O
N
H
HN
Boc
OH
O
9
8
7
6
5
4
3
2
1
0
ppm
1.00
0.97
1.02
3.10
1.00
3.96
0.94
1.98
2.04
1.02
1.14
2.07
9.29
10.20
1.09

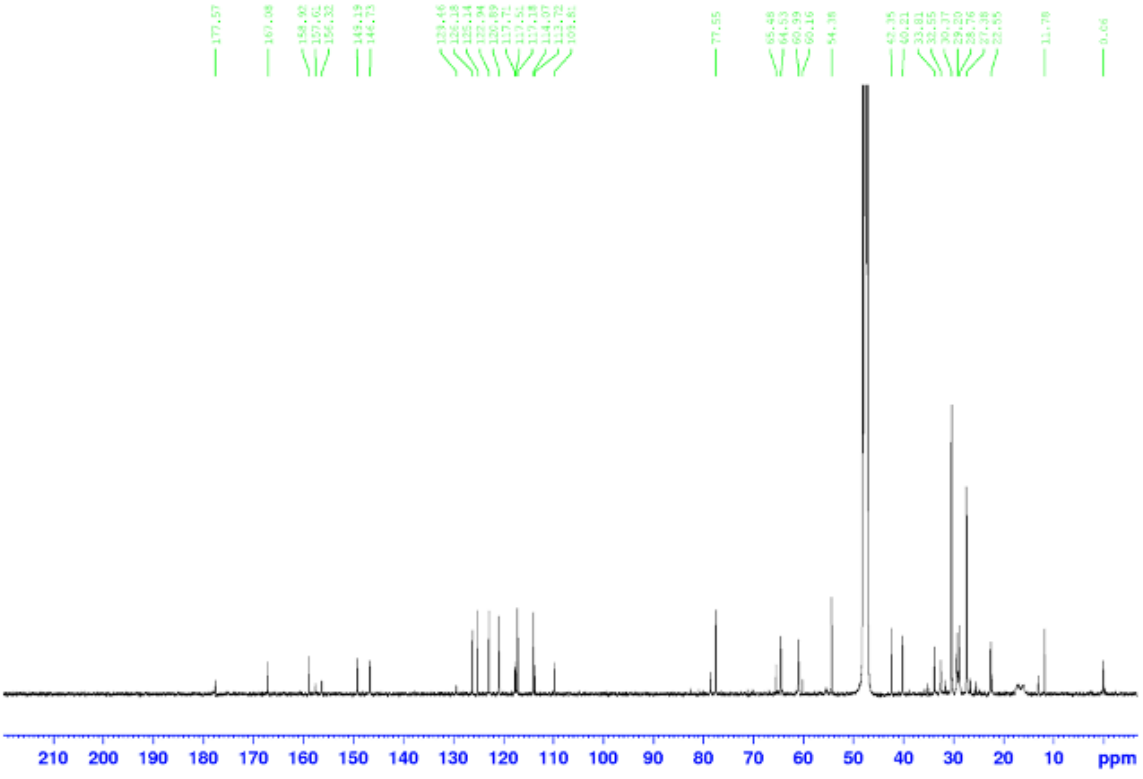
210
200
190
180
170
160
150
140
130
120
110
100
90
80
70
60
50
40
30
20
10
ppm

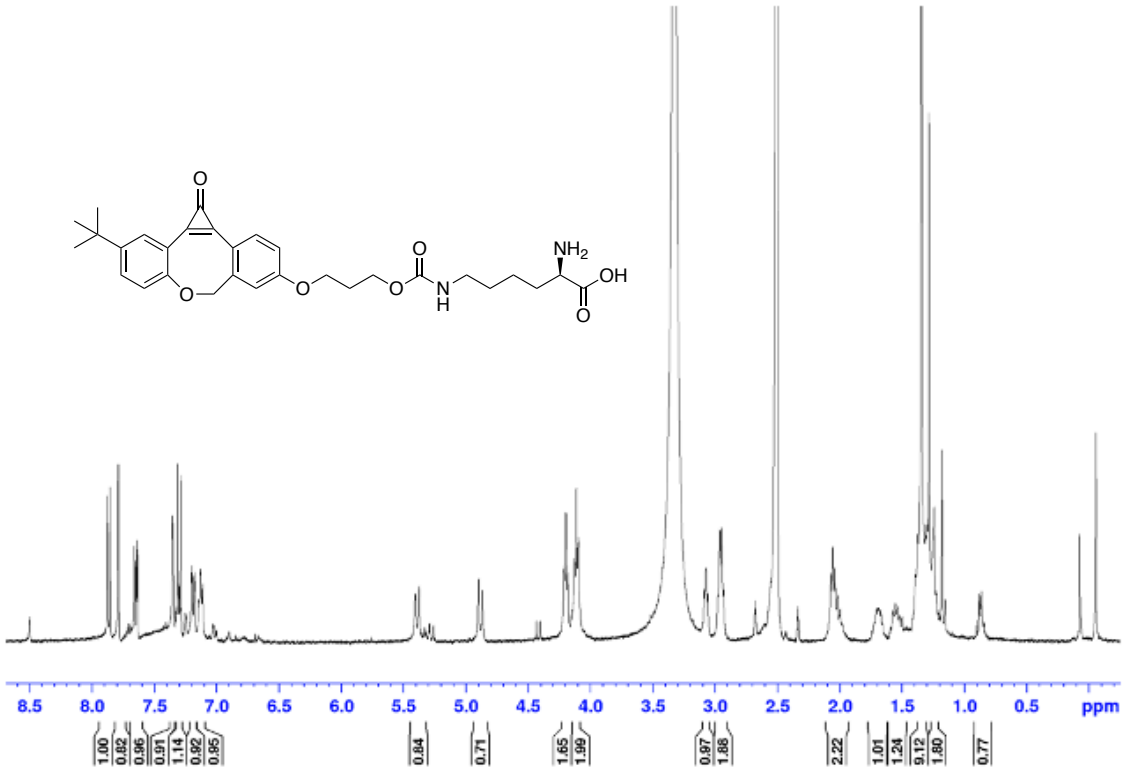
O
O
O
O
O
N
H
NH2
OH
O
8.5 8.0 7.5 7.0 6.5 6.0 5.5 5.0 4.5 4.0 3.5 3.0 2.5 2.0 1.5 1.0 0.5 ppm
1.00 0.82 0.96 0.91 1.14 0.92 0.95 0.84 0.71 1.65 1.99 0.97 1.86 2.22 1.01 1.24 9.12 1.80 0.77

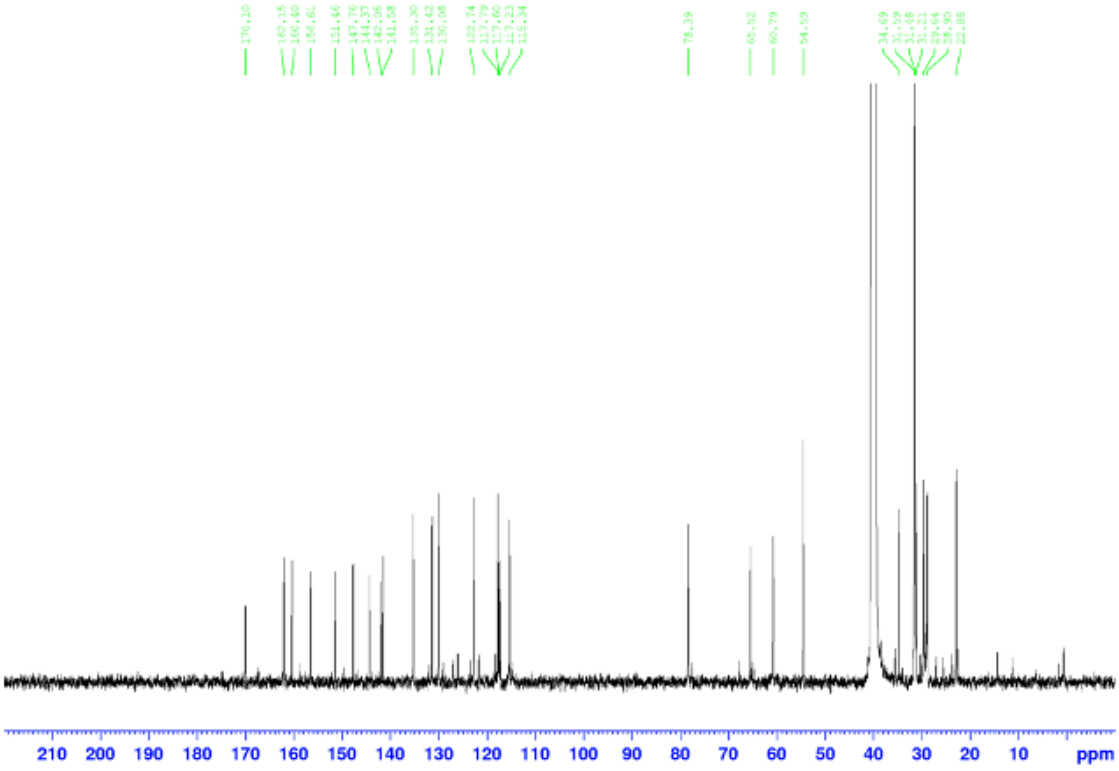
210 200 190 180 170 160 150 140 130 120 110 100 90 80 70 60 50 40 30 20 10 ppm

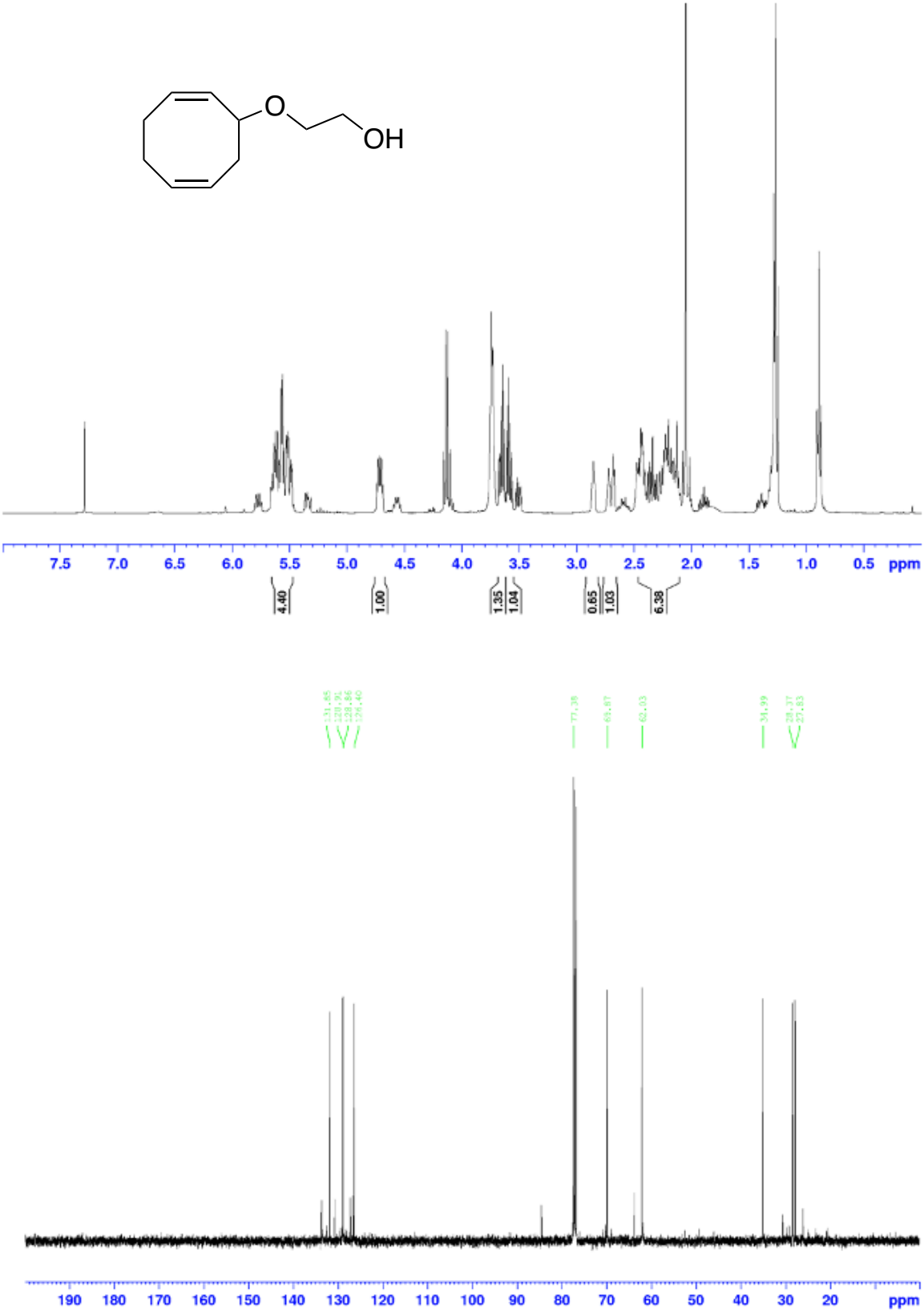
O
OH
7.5 7.0 6.5 6.0 5.5 5.0 4.5 4.0 3.5 3.0 2.5 2.0 1.5 1.0 0.5 ppm
4.40
1.00
1.35
1.04
0.65
1.03
6.38
190 180 170 160 150 140 130 120 110 100 90 80 70 60 50 40 30 20 ppm

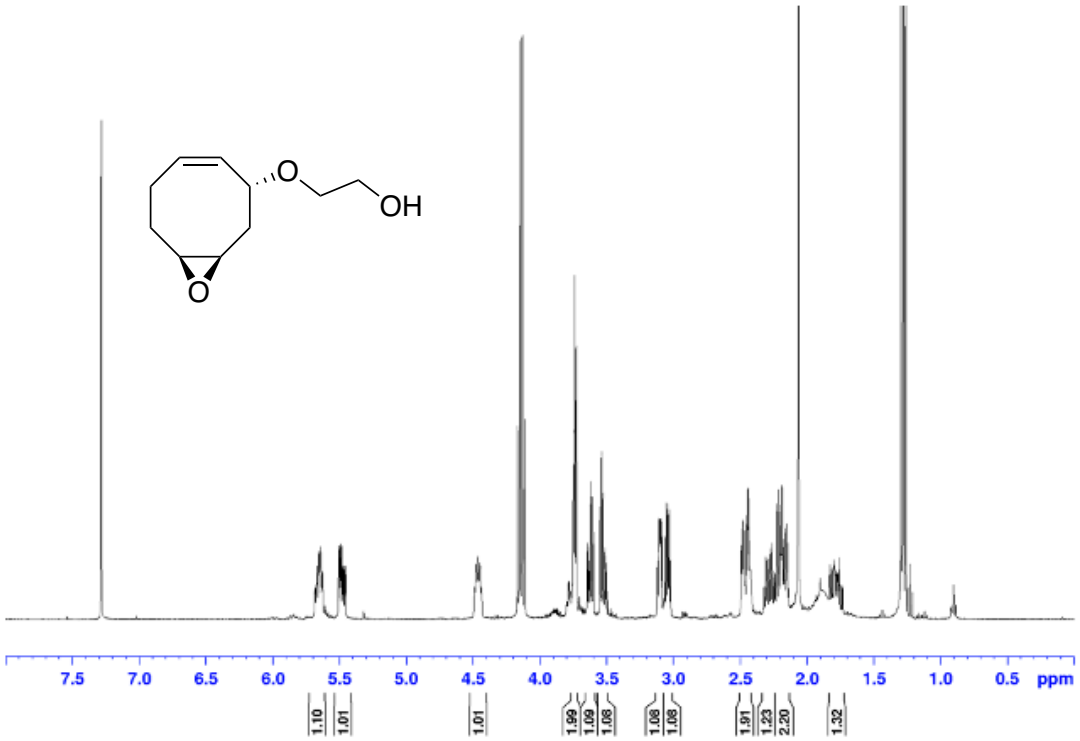
O
OH
O
7.5 7.0 6.5 6.0 5.5 5.0 4.5 4.0 3.5 3.0 2.5 2.0 1.5 1.0 0.5 ppm
1.10 1.01 1.01 1.99 1.09 1.08 1.08 1.08 1.91 1.23 2.20 1.32

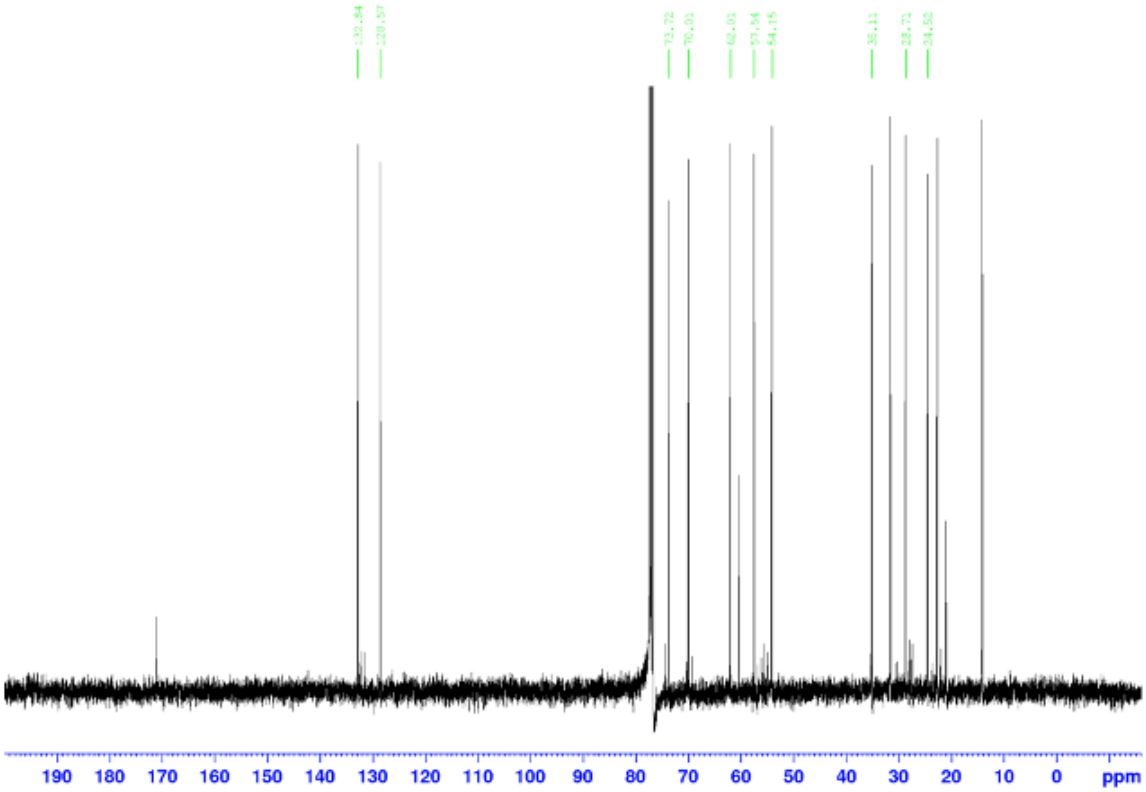
132.84
129.57
73.72
70.01
62.01
57.54
54.15
35.11
28.71
24.52
190 180 170 160 150 140 130 120 110 100 90 80 70 60 50 40 30 20 10 0 ppm

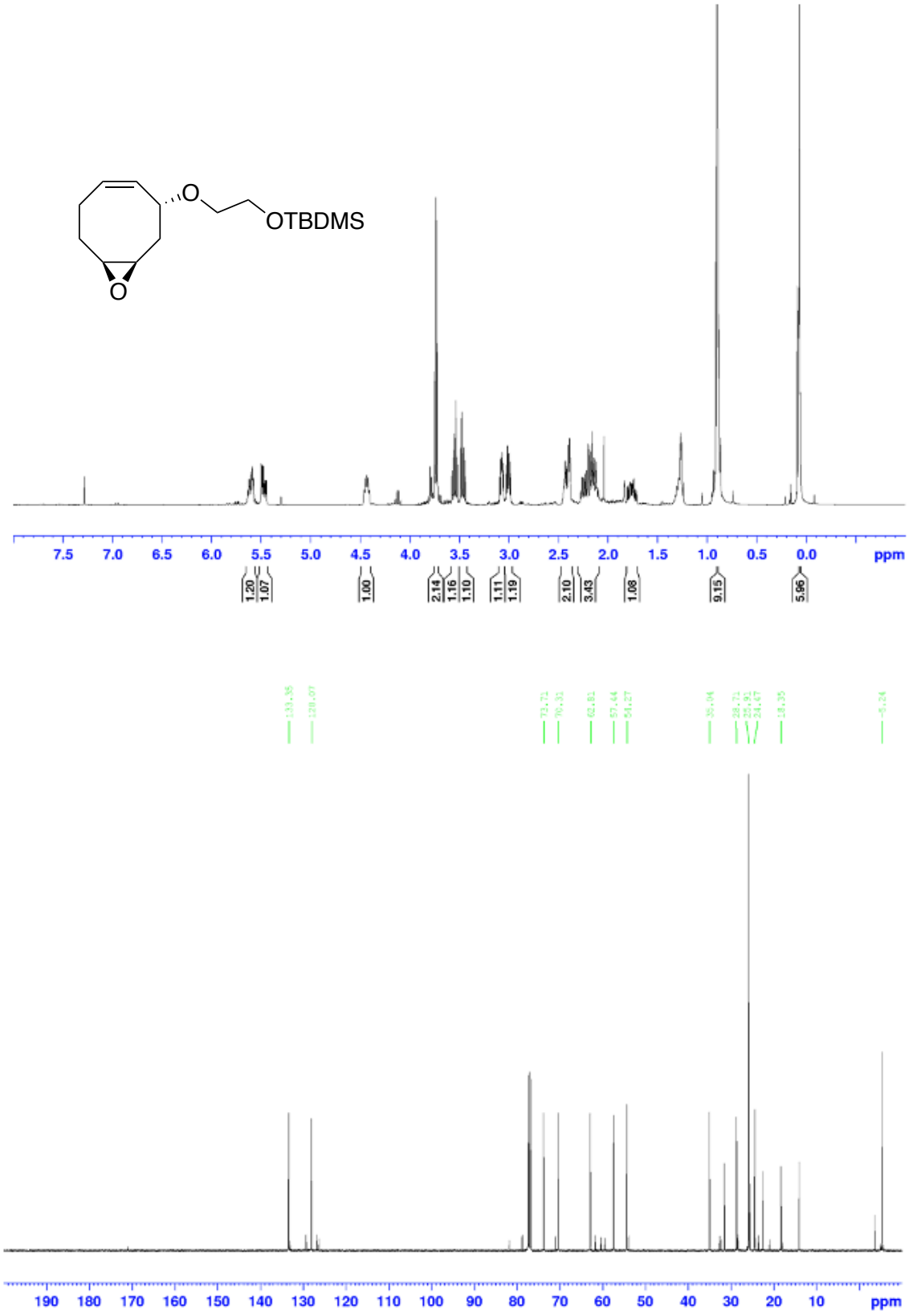
O
OTBDMS
O
7.5 7.0 6.5 6.0 5.5 5.0 4.5 4.0 3.5 3.0 2.5 2.0 1.5 1.0 0.5 0.0 ppm
1.20 1.07 1.00 2.14 1.16 1.10 1.11 1.19 2.10 3.43 1.08 9.15 5.96
190 180 170 160 150 140 130 120 110 100 90 80 70 60 50 40 30 20 10 ppm

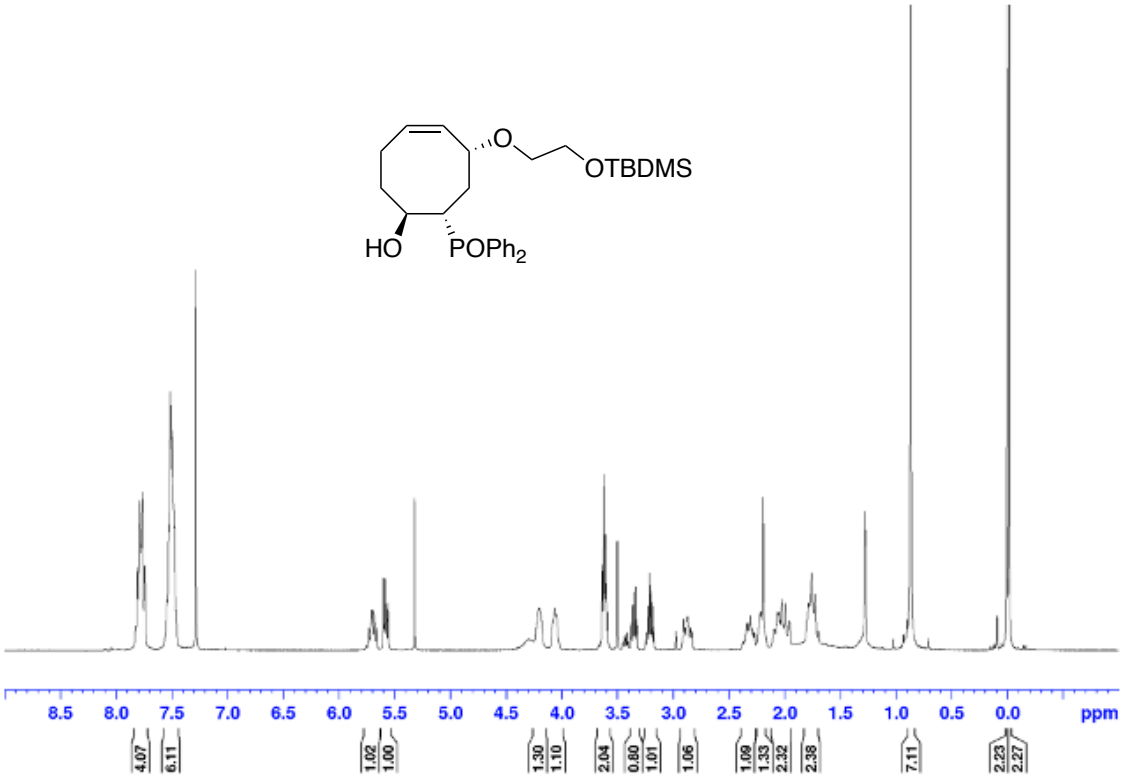
O
OTBDMS
HO
POPh2
8.5 8.0 7.5 7.0 6.5 6.0 5.5 5.0 4.5 4.0 3.5 3.0 2.5 2.0 1.5 1.0 0.5 0.0 ppm
4.07 6.11 1.02 1.00 1.30 1.10 2.04 0.80 1.01 1.06 1.09 1.33 2.32 2.38 7.11 2.23 2.27

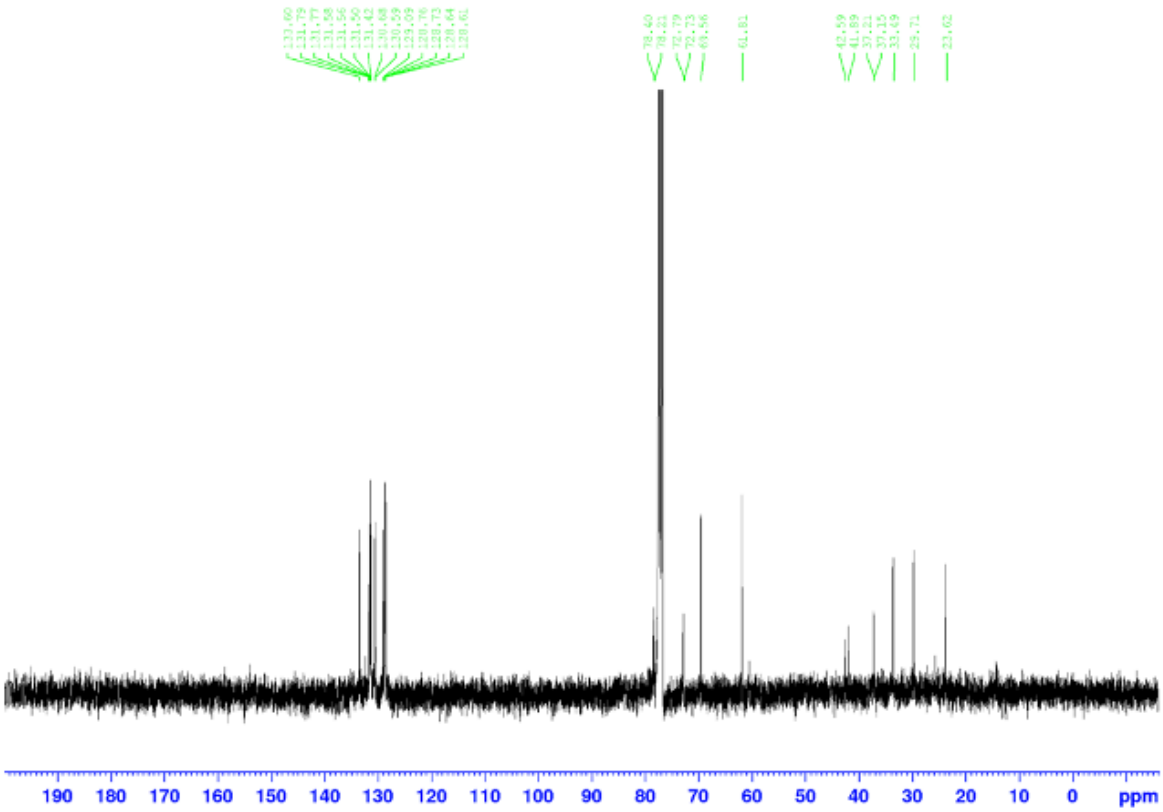
190 180 170 160 150 140 130 120 110 100 90 80 70 60 50 40 30 20 10 0 ppm

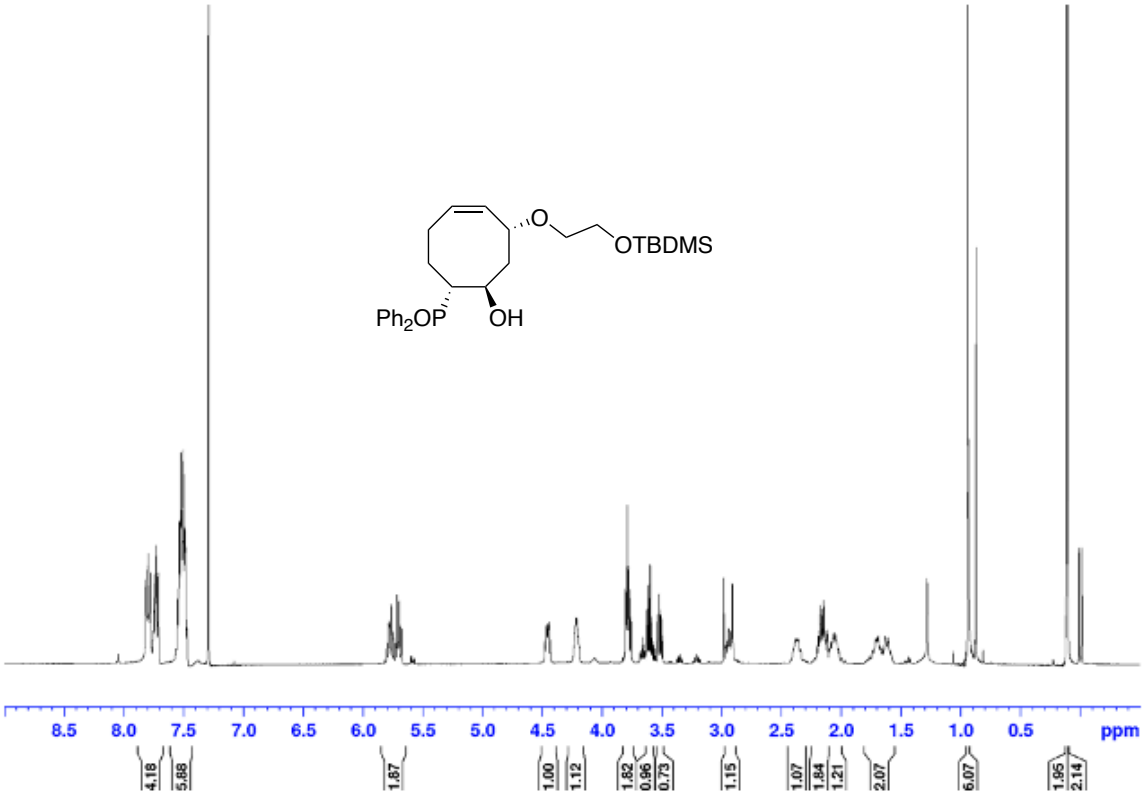
O
OTBDMS
Ph2OP
OH
8.5 8.0 7.5 7.0 6.5 6.0 5.5 5.0 4.5 4.0 3.5 3.0 2.5 2.0 1.5 1.0 0.5 ppm
4.18 5.88 1.87 1.00 1.12 1.82 0.96 0.73 1.15 1.07 1.84 1.21 2.07 6.07 1.95 2.14

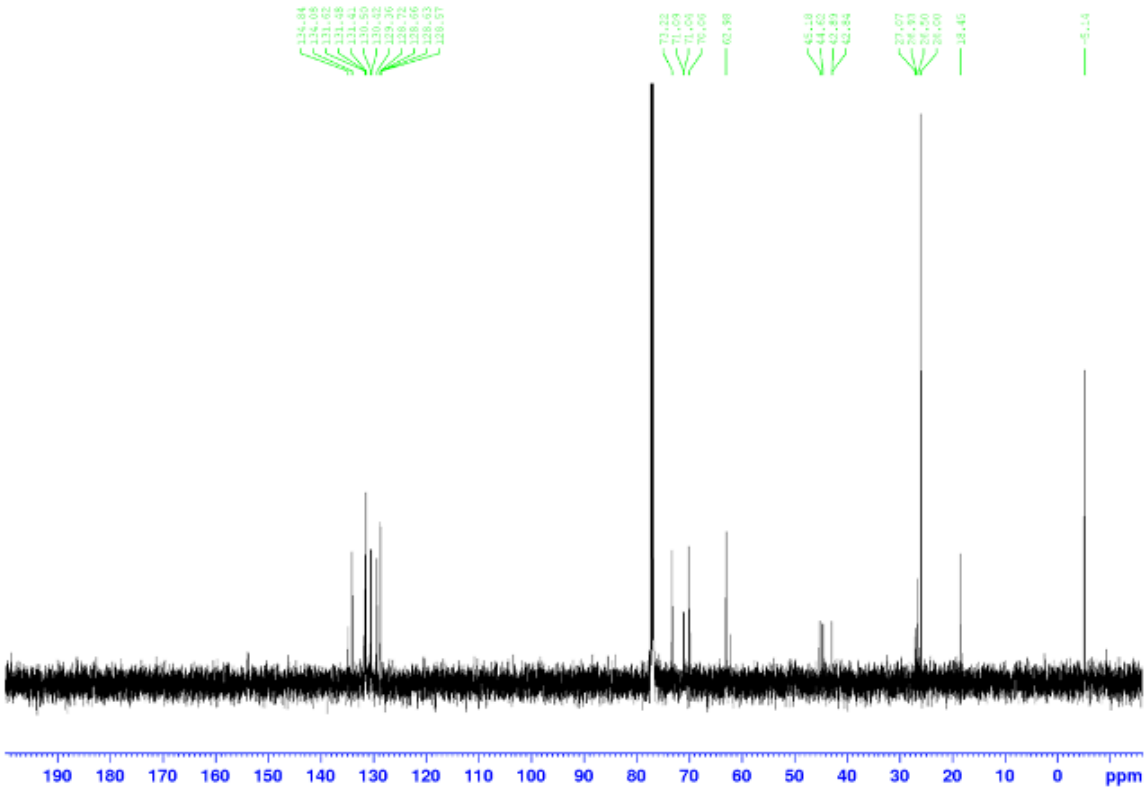
190 180 170 160 150 140 130 120 110 100 90 80 70 60 50 40 30 20 10 0 ppm

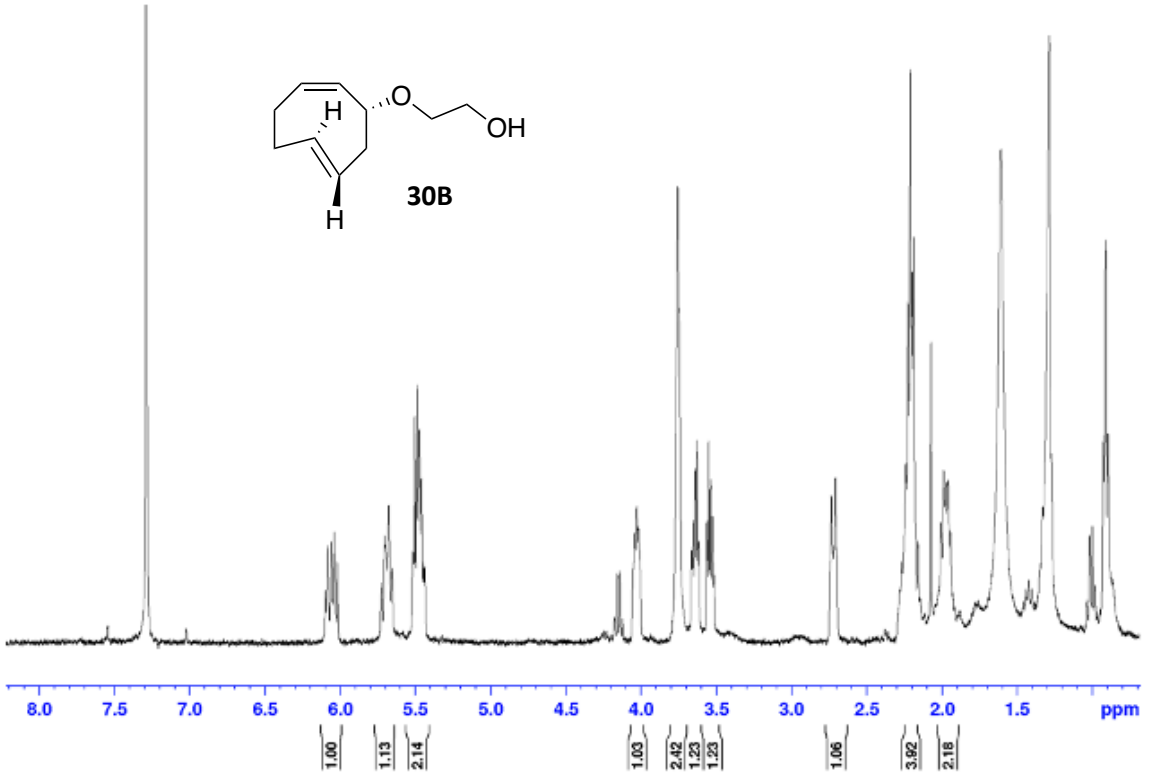
H
O
OH
H
30B
8.0
7.5
7.0
6.5
6.0
5.5
5.0
4.5
4.0
3.5
3.0
2.5
2.0
1.5
ppm
1.00
1.13
2.14
1.03
2.42
1.23
1.23
1.06
3.92
2.18

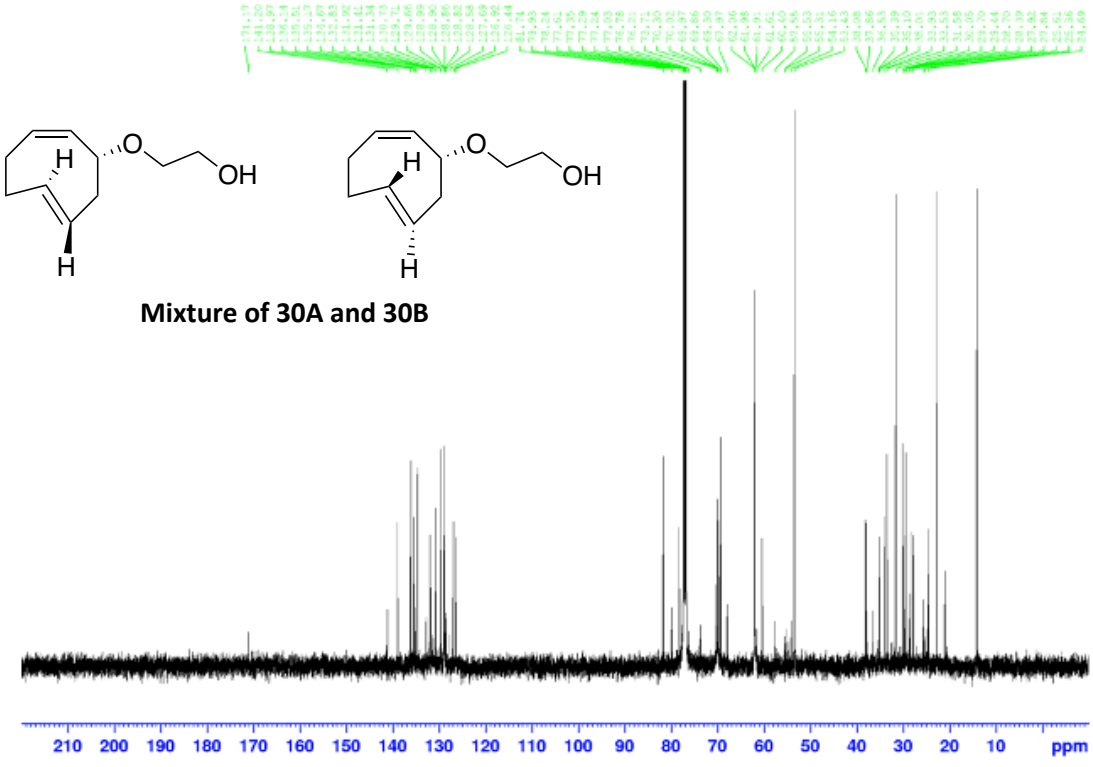
H
O
OH
H
H
O
OH
H
Mixture of 30A and 30B
210
200
190
180
170
160
150
140
130
120
110
100
90
80
70
60
50
40
30
20
10
ppm

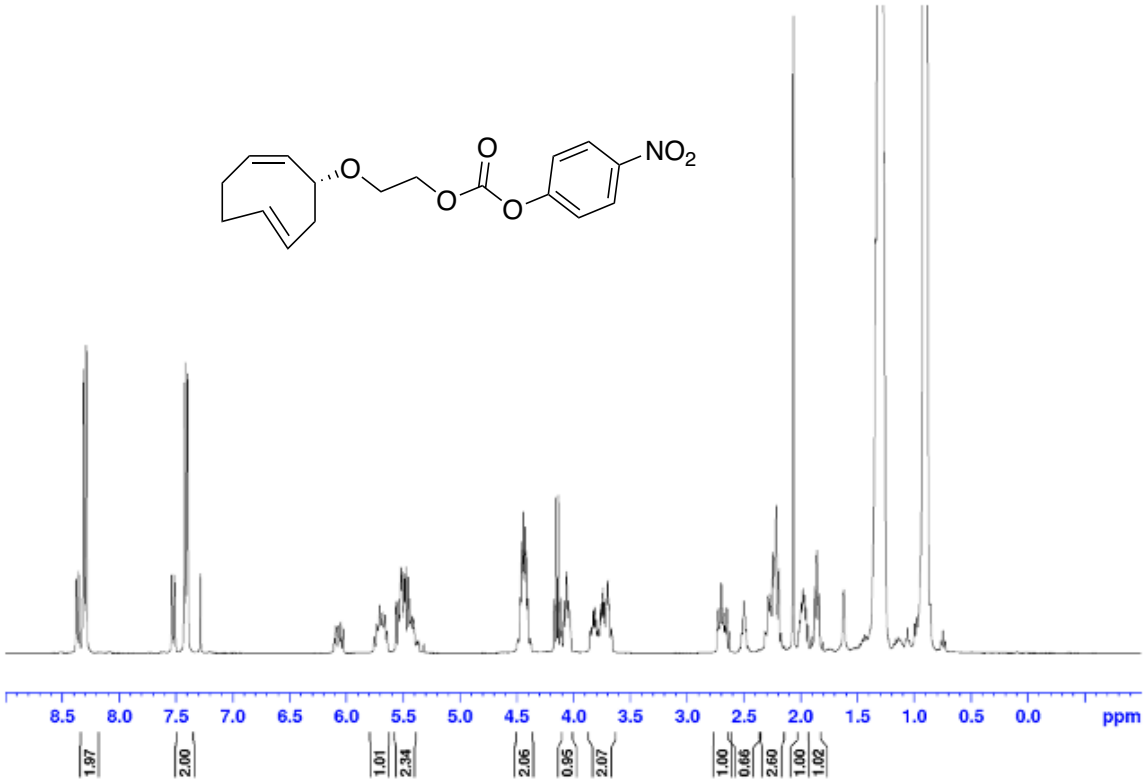
O
O
O
O
NO2
8.5
8.0
7.5
7.0
6.5
6.0
5.5
5.0
4.5
4.0
3.5
3.0
2.5
2.0
1.5
1.0
0.5
0.0
ppm
1.97
2.00
1.01
2.34
2.06
0.95
2.07
1.00
0.66
2.60
1.00
1.02

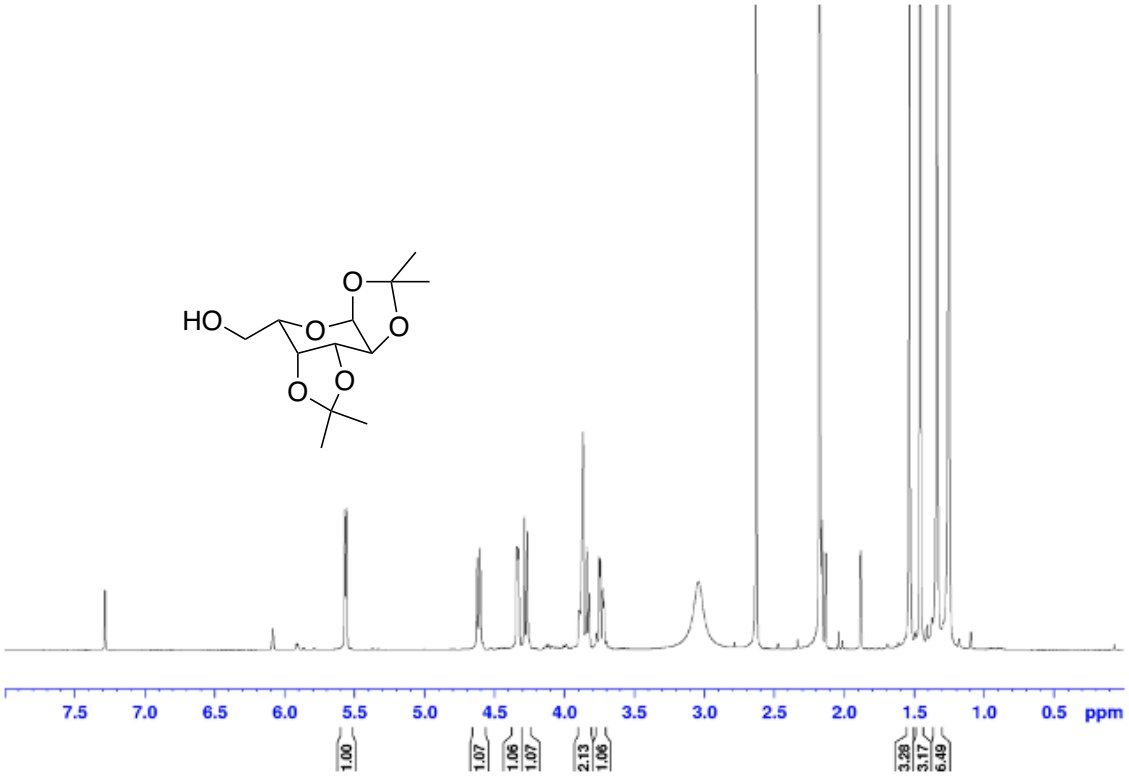
HO
O
O
O
O
O
7.5 7.0 6.5 6.0 5.5 5.0 4.5 4.0 3.5 3.0 2.5 2.0 1.5 1.0 0.5 ppm
1.00
1.07
1.06
1.07
2.13
1.06
3.28
3.17
6.49

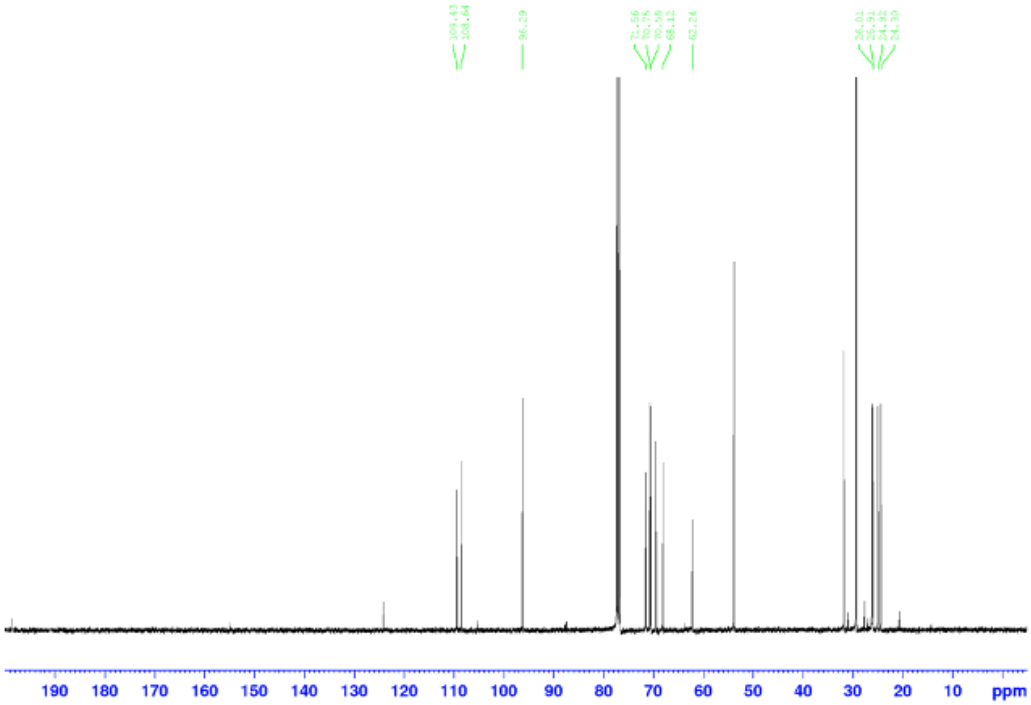
109.43
108.64
96.29
71.56
70.75
70.58
68.12
62.24
26.01
25.91
24.92
24.39
190 180 170 160 150 140 130 120 110 100 90 80 70 60 50 40 30 20 10 ppm

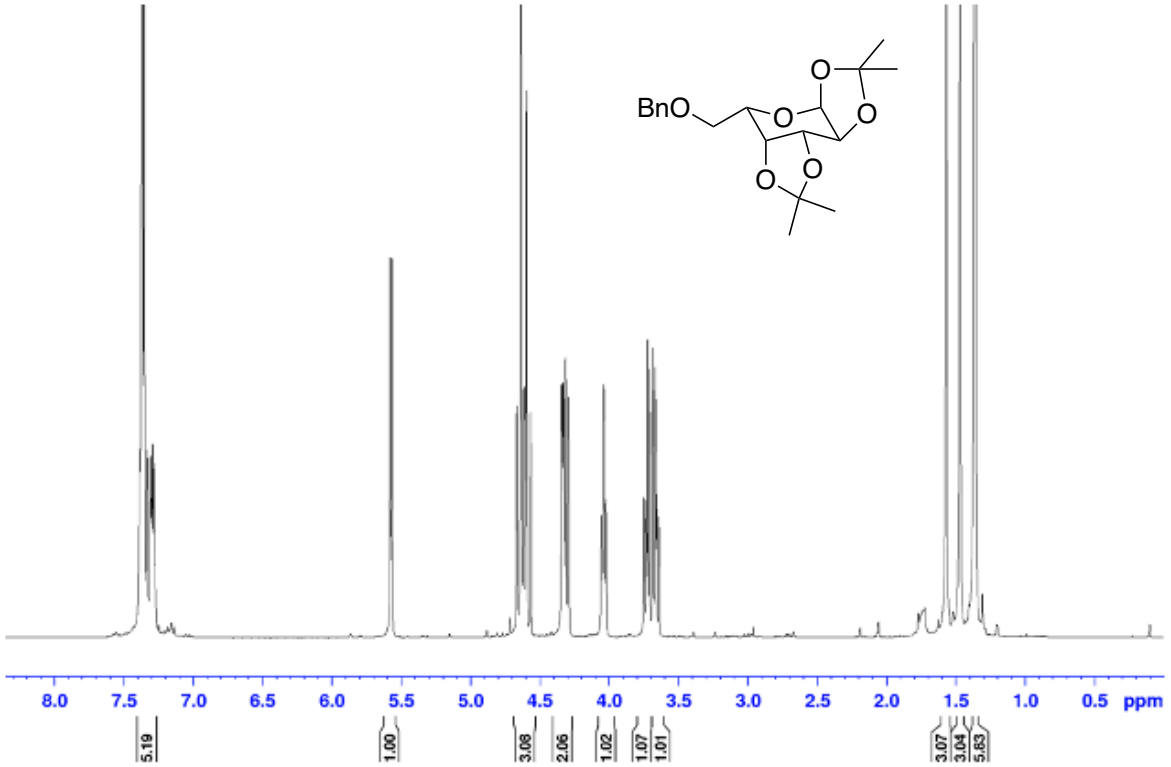
BnO
O
O
O
O
O
8.0
7.5
7.0
6.5
6.0
5.5
5.0
4.5
4.0
3.5
3.0
2.5
2.0
1.5
1.0
0.5
ppm
5.19
1.00
3.08
2.06
1.02
1.07
1.01
3.07
3.04
5.83

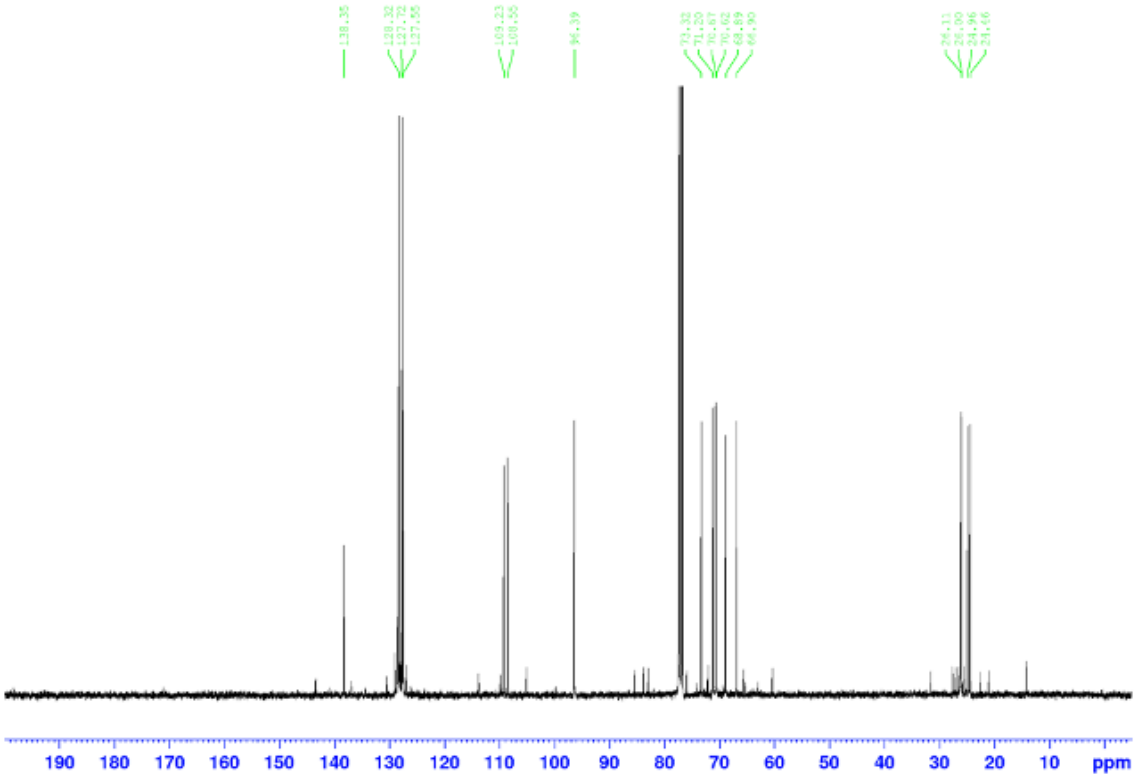
190
180
170
160
150
140
130
120
110
100
90
80
70
60
50
40
30
20
10
ppm

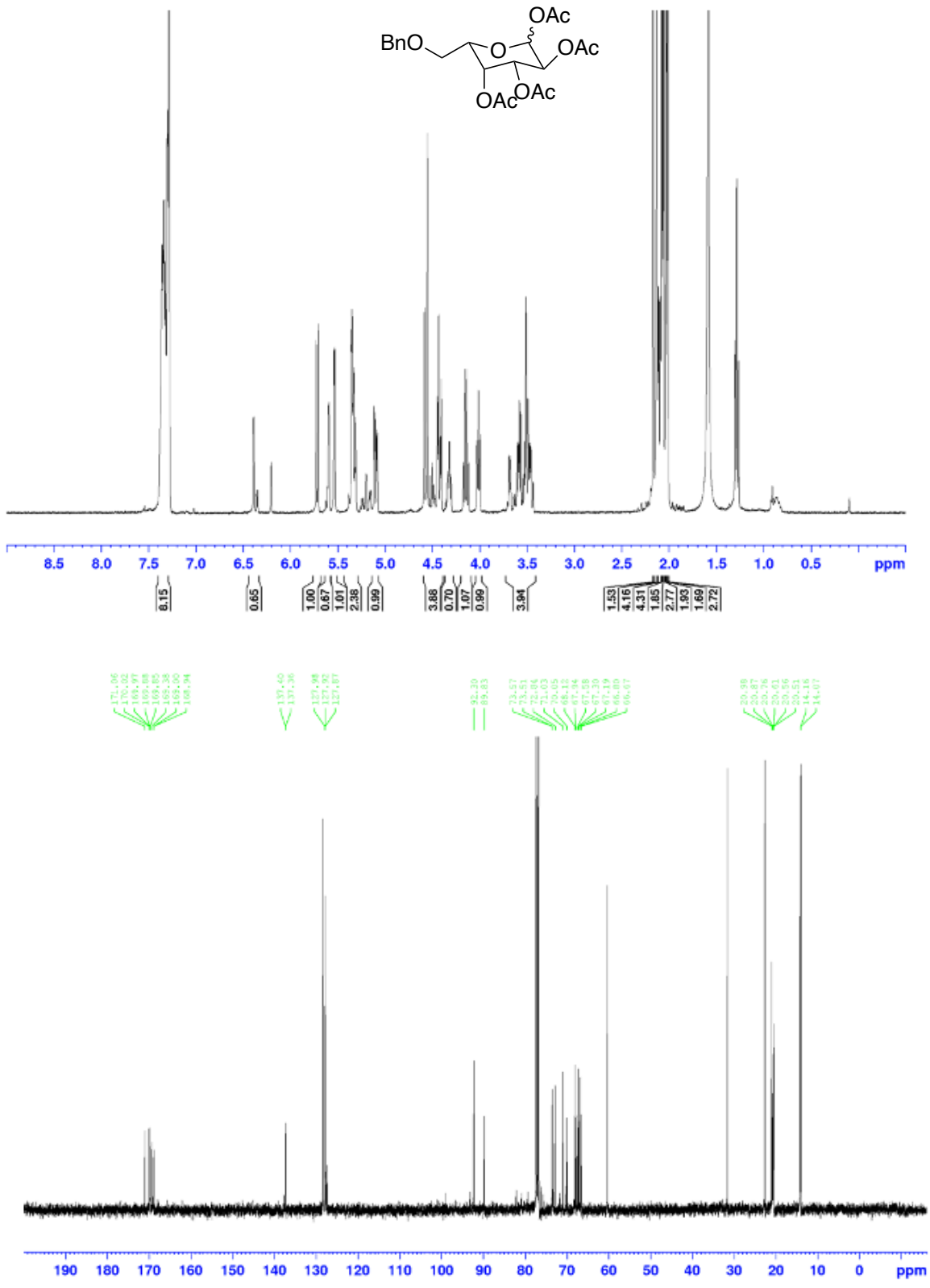
OAc
BnO
O
OAc
OAc
OAc
8.5 8.0 7.5 7.0 6.5 6.0 5.5 5.0 4.5 4.0 3.5 3.0 2.5 2.0 1.5 1.0 0.5 ppm
8.15 0.65 1.00 0.67 1.01 2.38 0.99 3.88 0.70 1.07 0.99 3.84 1.53 4.16 4.31 1.85 2.77 1.93 1.69 2.72
190 180 170 160 150 140 130 120 110 100 90 80 70 60 50 40 30 20 10 0 ppm

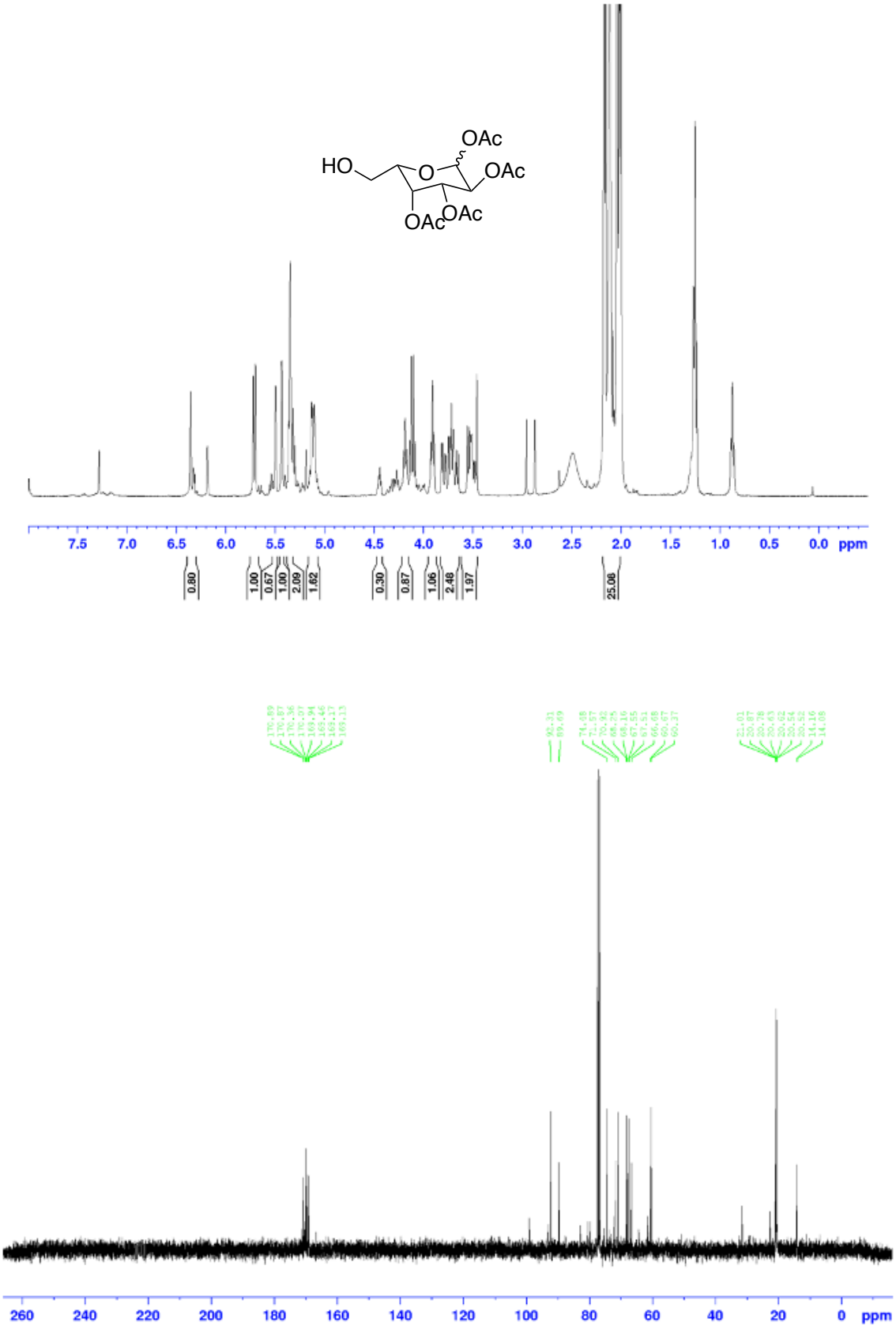
HO
O
OAc
OAc
OAc
OAc
7.5 7.0 6.5 6.0 5.5 5.0 4.5 4.0 3.5 3.0 2.5 2.0 1.5 1.0 0.5 0.0 ppm
0.80 1.00 0.67 1.00 2.09 1.62 0.30 0.87 1.06 2.48 1.97 25.06
260 240 220 200 180 160 140 120 100 80 60 40 20 0 ppm

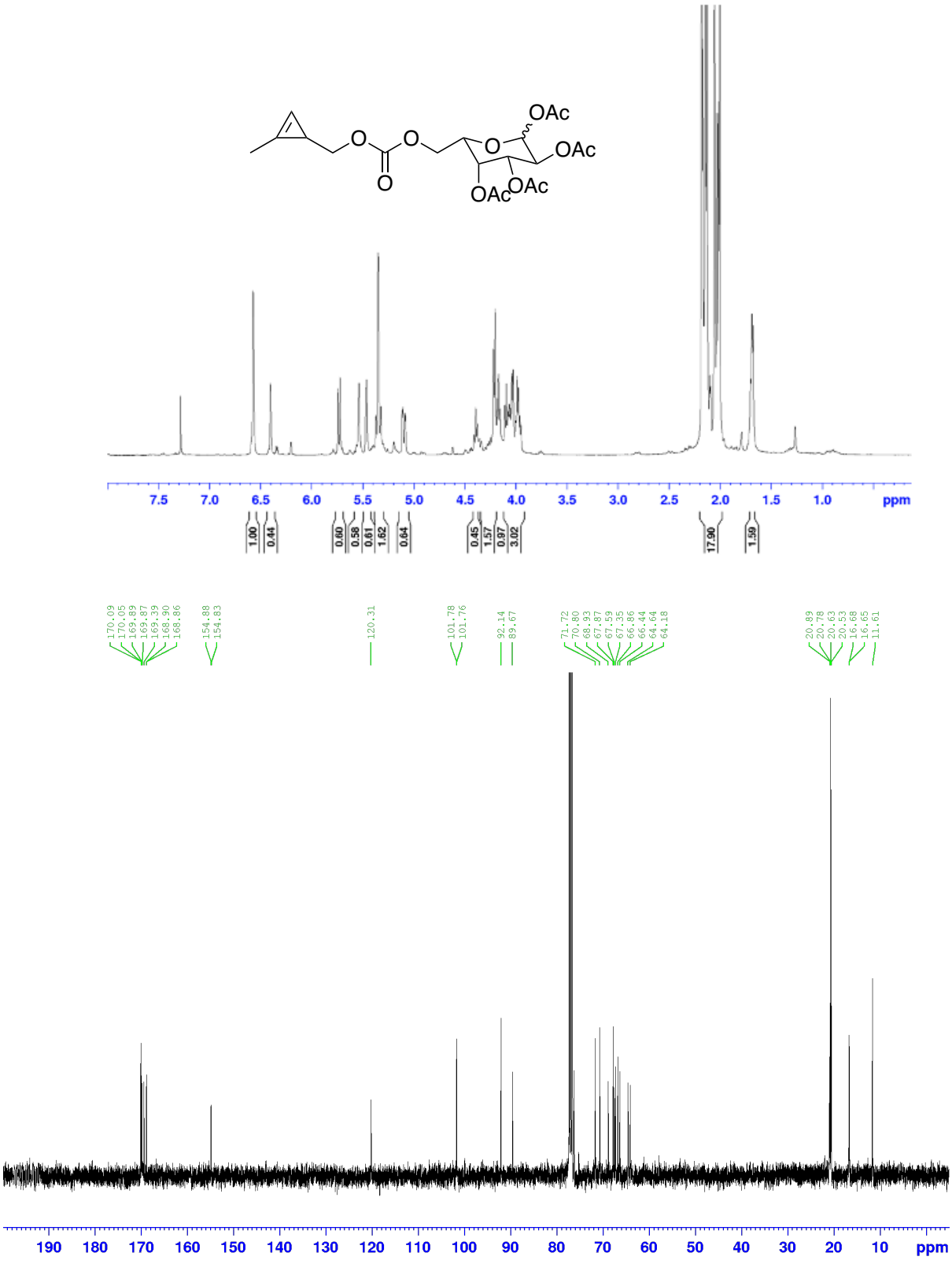
OAc
OAc
OAc
OAc
O
O
O
O
7.5
7.0
6.5
6.0
5.5
5.0
4.5
4.0
3.5
3.0
2.5
2.0
1.5
1.0
ppm
1.00
0.44
0.60
0.58
0.61
1.62
0.64
0.45
1.57
0.97
3.02
17.90
1.59
170.09
170.05
169.89
169.87
169.39
168.90
168.86
154.88
154.83
120.31
101.78
101.76
92.14
89.67
71.72
70.80
68.93
67.87
67.59
67.35
66.86
66.44
64.64
64.18
20.89
20.78
20.63
20.53
16.68
16.65
11.61
190
180
170
160
150
140
130
120
110
100
90
80
70
60
50
40
30
20
10
ppm

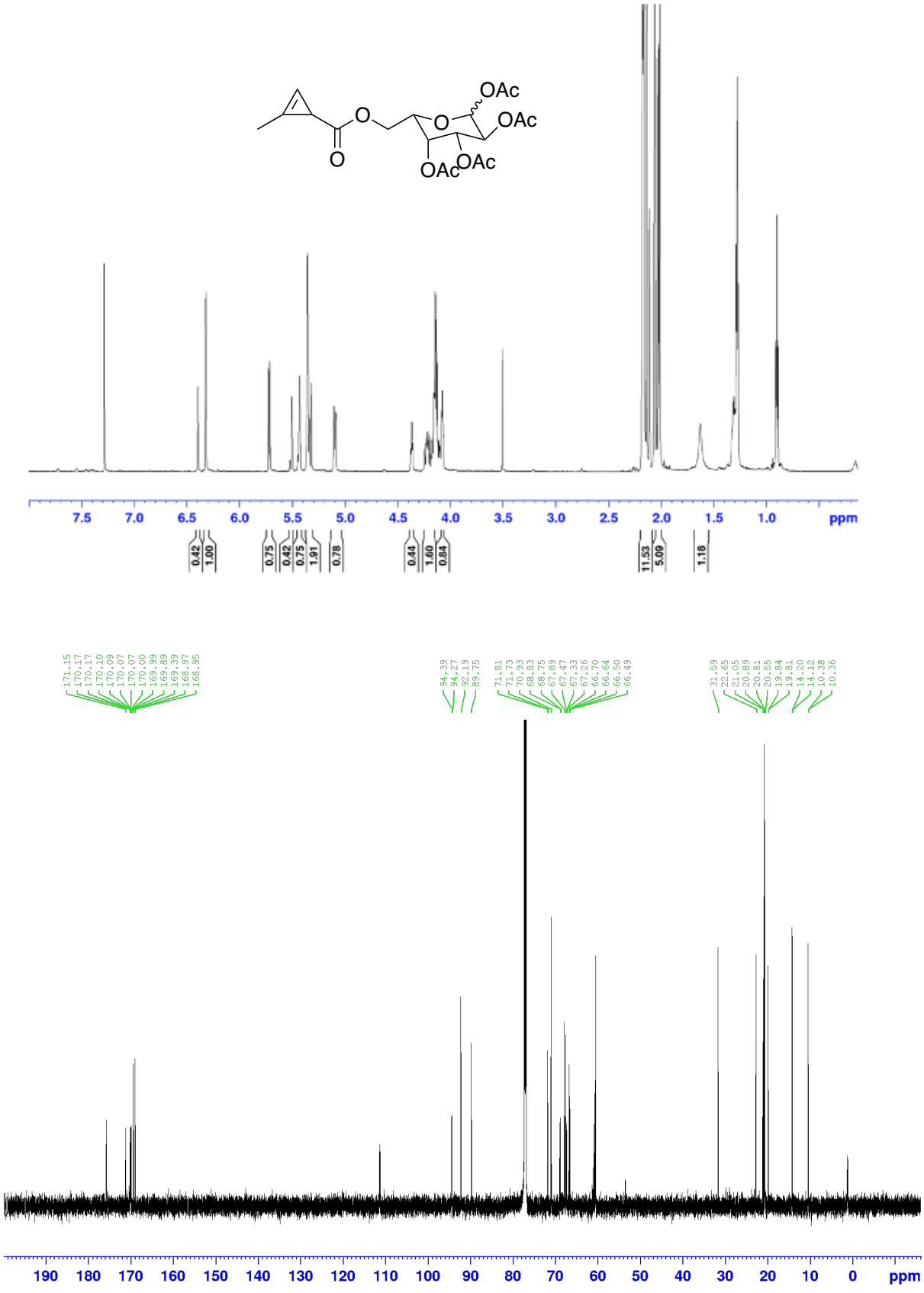
OAc
OAc
OAc
OAc
O
O
O
7.5
7.0
6.5
6.0
5.5
5.0
4.5
4.0
3.5
3.0
2.5
2.0
1.5
1.0
ppm
0.42
1.00
0.75
0.42
0.75
1.91
0.78
0.44
1.60
0.84
11.53
5.09
1.18
171.15
170.17
170.17
170.10
170.09
170.07
170.07
170.00
169.99
169.89
169.39
168.97
168.95
94.39
94.27
92.19
89.75
71.81
71.73
70.93
68.83
68.75
67.89
67.47
67.33
67.26
66.70
66.64
66.50
66.49
31.59
22.65
21.05
20.89
20.81
20.55
19.84
19.81
14.20
14.12
10.38
10.36
190
180
170
160
150
140
130
120
110
100
90
80
70
60
50
40
30
20
10
0
ppm

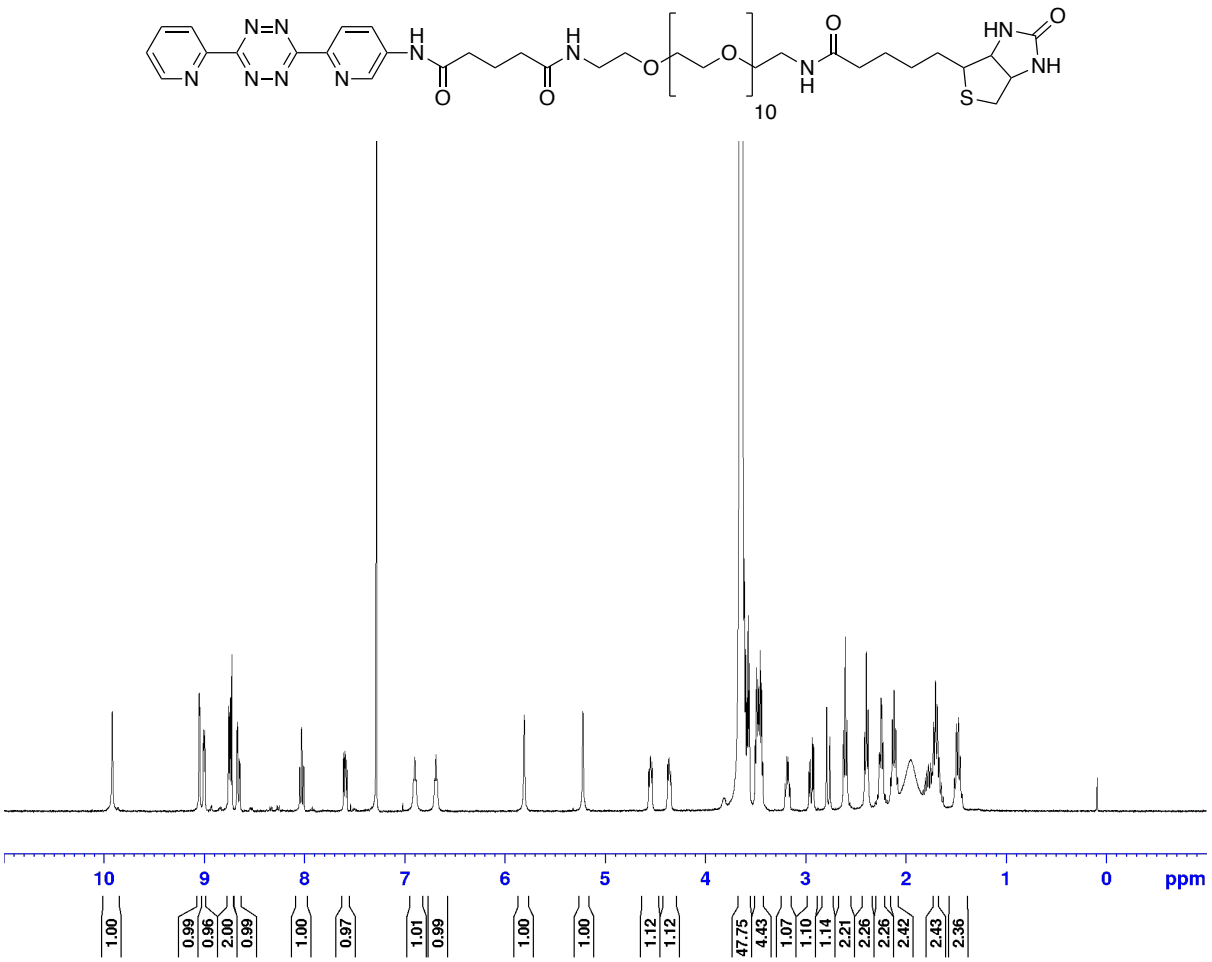
N=N
N
N–N
N
H
N
O
O
H
N
O
O
10
N
H
O
HN
O
NH
S
10
9
8
7
6
5
4
3
2
1
0
ppm
1.00
0.99
0.96
2.00
0.99
1.00
0.97
1.01
0.99
1.00
1.00
1.12
1.12
47.75
4.43
1.07
1.10
1.14
2.21
2.26
2.26
2.42
2.43
2.36